

*FUNCTIONALIZED METAL-ORGANIC  
FRAMEWORKS AS SELECTIVE METAL  
ADSORBENTS*

**De Decker Jeroen**

**Department of Inorganic and Physical Chemistry**

**Faculty of Sciences**

**Ghent University**

**Dissertation submitted in fulfillment of the requirements for the degree of**

**Doctor of Science: Chemistry**

**May 2017**





Promoters	Department
Prof. dr. Pascal Van Der Voort	Inorganic and Physical Chemistry
Prof. dr. Jeriffa De Clercq	Chemical Engineering and Technical Chemistry
Prof. dr. Rik Van Deun	Inorganic and Physical Chemistry

Members of the Jury	Affiliation
Prof. dr. Klaartje De Buysser	Ghent University
Prof. dr. Freddy Kleitz	Universität Wien
Prof. dr. Rob Ameloot	University of Leuven
Prof. dr. Du Laing Gijs	Ghent University
dr. Karen Leus	Ghent University
dr. Anna Kaczmarek	Ghent University

Ghent University

Faculty of Sciences

Department of Inorganic and Physical Chemistry

Krijgslaan 281 S3, B-9000 Ghent, Belgium

Tel.: +32-9-264.44.49

Fax.: +32-9-264.49.83

This research was funded by AUGent/UGent.

Grant Number DEF12/AOP/008-IV1







Alle rechten voorbehouden. Niets uit deze uitgave mag worden gereproduceerd, opgeslagen in een geautomatiseerd gegevensbestand, of openbaar gemaakt, in enige vorm of op enige wijze, hetzij elektronisch, mechanisch, door print-outs, kopieën, of op welke manier dan ook, zonder voorafgaande schriftelijke toestemming van de uitgever.

All rights reserved. No part of this publication may be reproduced, stored in a retrieval system or transmitted in any form or by any means, electronic, mechanical, photocopying, recording or otherwise, without prior permission from the publisher.



## ACKNOWLEDGEMENTS

Nu het hoofdstuk ‘doctoreren’ quasi afgerond is, kan ik bij het neerschrijven van dit dankwoord ook even reflecteren over de vier jaar die erdoor in beslag werden genomen. Wat bij aanvang nog een zee van tijd leek, veranderde naarmate de tijd passeerde toch snel in een ondiepe plas water. Ik heb snel genoeg ondervonden dat doctoraatsonderzoek, en bij uitstek wetenschappelijk onderzoek, geen aaneenschakeling is van geslaagde experimenten en progressie. Men moet rekening houden met zowel successen als tegenslagen, en van die laatste zijn er minstens even veel. Nochtans, filosoof John Dewey zei ooit: “*Failure is instructive*”, en gelukkig maar zijn diens woorden vaak genoeg waarheid gebleken. Er zijn, in mijn ogen, drie zaken die in grote mate bijdragen tot het succesvol afronden van een doctoraat; Een onderzoeksonderwerp dat oprecht interesseert (en blijft interesseren); Het gepast omgaan met tegenslagen en onverwachtheden, en waarschijnlijk nog het belangrijkste: een goeie omringing. Ik mag mij gelukkig prijzen dat al deze zaken aanwezig waren in mijn periode als doctoraatsstudent, en daarom wil ik van dit voorwoord (wat ongetwijfeld het meeste gelezen hoofdstuk van een thesis is) gebruikmaken een hoop mensen uitdrukkelijk te bedanken.

*First and foremost*, wil ik mijn hoofdpromotor, Prof. dr. Pascal Van Der Voort, bedanken voor het aanreiken van dit onderwerp en me zo de kans te geven dit doctoraat te starten. De thematiek rond recuperatie van kritische metalen sprak mij direct aan, en de applicatiegerichtheid van het onderzoek was een extra stimulans. Daarnaast ook mijn dank voor het vertrouwen in mijn wetenschappelijke keuzes en de hulp in het maken ervan.

Verder wil ik ook mijn copromotor, Prof dr. Jeriffa De Clercq, bedanken voor de nauwe opvolging en uitstekende hulp gedurende de hele periode van het doctoraat. Bedankt voor alle goeie raad, de interessante discussies, de vele nieuwe inzichten, enz... Ik ben er dankzij jou zonder twijfel beter uitgekomen als onderzoeker.

Ook wil ik mijn dank uitdrukken aan copromotor, Prof. dr. Rik Van Deun, voor de kennis en inzichten inzake het lanthanideluik van dit onderzoek, wat voor mij toch vrij onbekend terrein was aan het begin van dit doctoraat. Het was een voordeel om te kunnen terugvallen op iemand die zo eigen is in de materie.

Collega’s vormen een enorm belangrijk onderdeel van een goeie omringing, zij het om de uitwisseling van kennis en ideeën, of om het creëren van een goeie werksfeer. Ik wil in de eerste plaats mijn bureaugenoten bedanken voor de fijne momenten, goeie discussies, en alle hulp en samenwerking gedurende de voorbije jaren. Isabelle, Wannes en later ook Hannes. Merci!

Omdat ik verruit het meest op MOF’s gewerkt heb, kon ik ook vaak rekenen op het MOF-team binnen COMOC. In de eerste plaats wil ik Thomas Bogaerts bedanken voor alle hulp en kennis! Ik ben als quasi complete leek het domein van MOF’s binnengewandeld en jouw expertise en

inzichten hebben enorm bijgedragen tot het snel ingewerkt geraken in de materie. Daarnaast wil ik uiteraard ook de andere mensen van het MOF-team bedanken; Kevin Hendrickx, Hannes, Karen, Guangbo.

Met de andere leden van COMOC was de overlap qua onderzoeksthema misschien niet zo groot als met de *MOF'ers*, maar daarom zijn ze niet minder belangrijk in dit verhaal. Ik wil graag Els bedanken voor alle hulp en expertise, de fijne babbels en het organiseren van leuke activiteiten. Daarbij wil ik ook Sander bedanken. Jullie twee stonden zoals gezegd iets verder af van mijn onderzoeksthema, maar dat heeft vaak gezorgd voor een andere kijk het op geheel, wat alleen maar positief bijdroeg aan het *out-of-the-box* denken. Bedankt ook aan Sander om op gevaar van eigen leven in het Gentse een voetbalshirt van *de vijand* (lees: iedereen-FCB) te gaan kopen ;-).

Ik wil ook graag de overige leden van COMOC bedanken, zowel de gevestigde waarden als de nieuwelingen en oudgedienden die ik gedurende mijn doctoraat heb leren kennen: Judith, Funda, Kevin De Vlieger, Norini, Flore, Chidharth, Himanshu, Dolores, Yesid, Xiao, Asamanjoy, Matthias, Fatima, Jeroen, Sara, Yoran, Koen, Mieke, Mei, Shu-na, Shyam.

Overige personen die ik graag wil bedanken: Karel Folens, bedankt voor de vlotte samenwerking in onze projecten! Tom, Bart, Pat & Danny, merci voor alle hulp en ondersteuning omtrent hard- en software uit mijn onderzoek. Verschillende collega's uit andere onderzoeksgroepen binnen S3, zoals Jonas (*JJ*), Hannes Rijckaert, Matthias, Willem, Emile,...

Naast een goeie atmosfeer op de werkvloer, is het ook altijd een meerwaarde als de pauzes en groepsactiviteiten aangenaam verlopen. Alle collega's dragen hier uiteraard toe bij, maar ik wil vooral *zegen en vloek, maar toch vooral zegen* Pierre Van Bockstaele bedanken voor zijn rol als meester-sfeermaker. Uiteraard ook bedankt voor al jouw en Kathleen's hulp op administratief vlak.

Als laatste wil ik de mensen achter de schermen bedanken. Mijn ouders, bedankt voor alle kansen die ik gekregen heb en om altijd klaar te staan wanneer nodig. Het is bovenal dankzij jullie dat ik dit alles heb kunnen verwezenlijken. Ook Matthias, Lennert en Gillian mogen hier niet ontbreken.

Gent, juni 2017

Jeroen De Decker

## ENGLISH SUMMARY

A sustainable future for our world, with the help of renewable energy and green technologies... For a long time, this sounded like an idealism, a concept at best. But now, a little over 250 years since the first industrial revolution, it has become clear that all those decades of mindless resource consumption have left their mark on our planet. Sustainability is no longer a prestigious school project, but a dire necessity, at least if we want to keep our species alive for a few more centuries. However, as the Greek tragedian Euripides once said: “Nothing has more strength than dire necessity”, and thankfully the world is gradually shifting its views. We have developed and optimized technologies to help us achieve such a sustainable future. Electric cars, wind energy, solar and hydropower... The world is ready for its gradual shift towards clean energy, leaving fossil fuels behind.

Sadly, the problems do not end there. While our intentions are noble this time, we have come to the realization that, in order to keep using these clean technologies, a sufficient supply of several important resources is required. Resources such as metals and other elements that are indispensable in the design and operation of ‘clean’ devices and machinery. As it turns out, some of these elements have become increasingly scarce over the past decades, up to a point where complete exhaustion is expected if we do not act in time.

In this context, a group of metals, called the rare earths elements (REEs), play a central role. They are amongst the most critical elements in several sustainable technologies, whilst also being critical with respect to their (future) availability. It is shown throughout this work that it is difficult to mine them in a cost-effective way, and that a lot of geopolitics come into play to acquire them. Moreover, their recycling rate is disappointingly low, mainly because they are present in small quantities in their respective devices, and the current recycling technologies, in most cases, do not allow a cost-effective recovery. It is nonetheless of extreme importance that a steady REE supply is ensured, because in most cases these elements have no worthy replacements.

In the domain of recycling, more and more interest is shown in the concept of urban mining, where the technosphere (i.e., electronic waste) serves as an actual mine, full of valuable resources. This ‘e-waste’ has the potential to supply a significant amount of rare earths to help satisfy an increasing demand. On the other hand, next to urban mining, improved (sustainable) primary mining should also be able to increase our REE supply.

It is in this context that the core of this work resides. Both in primary REE mining and recycling processes, aqueous streams are often generated, containing varying fractions of these metals. It is shown that in the treatment of these solutions, a lot of improvement can be made in terms of applied technologies. While industrial techniques like solvent extraction will remain an obvious

choice for highly concentrated solution processing (e.g., g/L scale), they prove to be cost-ineffective for more dilute streams (e.g., mg/L scale). In addition, when dealing with REE recycling or the processing of secondary deposits (e.g., resources with a typically lower REE content than primary ores), these techniques would face the similar issues.

Therefore, adsorption technology is proposed in this work, as a worthy alternative. The advantages of this technique are discussed, and it is shown that adsorbents are ideal materials for low concentration recovery or removal of certain species of interest. With respect to REE mining and recovery, different domains are proposed where selective adsorption could earn its place as the prevailing technology, and the requirements for such adsorbents are discussed. Whether it is to recover rare earths from process or waste streams, or to purify REE-containing solutions from toxic elements (uranium, thorium...), adsorbents can be tailored readily towards a certain application. Further on, an introduction is given into the world of metal-organic frameworks (MOFs). The concept of using these versatile coordination polymers in aqueous environment as adsorbents is explored and documented with existing literature. The stability of MOFs will play a major role in their possible application as aqueous adsorbents. It was therefore investigated which structural parameters have a significant influence on this stability. In short words; What makes a MOF suitable for water-based applications? In addition, a study was performed on the long-term stability of several popular MOFs, regarding their behavior in different aqueous conditions, i.e., acidic, alkaline, oxidative... With this information a rational choice can be made in the selection of suitable MOFs for aqueous adsorption applications.

This work then describes the application of a specific cage-type MOF, namely MIL-101(Cr), as a potential ideal support for aqueous adsorption. It was chosen based on its incredible stability, high porosity, and ready functionalizability. The MIL-101(Cr) was functionalized via two different routes with a specific ligand and its affinity for certain critical metals (REEs, uranium...) was investigated. In one approach, a carbamoylmethylphosphine oxide-type ligand (CMPO) was covalently anchored onto the surface of MIL-101 via a three-step method. Another approach encapsulates another CPMO-type ligand in-situ in the cages of MIL-101, where it is confined and cannot leach out. Both materials have been subjected to a comprehensive adsorption study, in which their performance in terms of selectivity, stability, uptake, kinetics, recyclability... is investigated.

In conclusion, it is shown that several MOFs do possess the required characteristics to serve as aqueous-phase adsorbents. They can be tailored towards a specific application, via different functionalization methods. This was proven for the ultra-stable MIL-101(Cr), which could be functionalized with selective ligands for critical metals recovery. As there are several stable MOFs to explore, and various strategies to tailor them, it is safe to say that MOF-based adsorption opens up exciting avenues in the field of aqueous-phase metal recovery.

## DUTCH SUMMARY

Een duurzame toekomst voor onze wereld, geholpen door hernieuwbare energie en groene technologieën... Het leek altijd al een idealisme, een mooi concept, echter weinig meer dan dat. Maar nu, ongeveer 250 jaar sinds de eerste industriële revolutie, is gebleken dat al die jaren van achteloze consumptie van natuurlijke rijkdommen, duidelijke sporen hebben achtergelaten op onze planeet. Duurzaamheid is niet langer een prestigieus schoolproject, maar een bittere noodzaak, ten minste als de mensheid het nog een paar eeuwen wil uithouden op deze aarde. De Griekse tragedicus Euripides zei ooit: “Uit bittere noodzaak spruit de grootste kracht”, en dat blijkt, gelukkig, nogmaals de waarheid. Geleidelijk aan past de wereld haar visie aan, en is men volop aan het inzetten op nieuwe en verbeterde technologieën om een dergelijke duurzame toekomst mogelijk te maken. Elektrische wagens, wind-, zonne-, en waterenergie,... De wereld lijkt klaar voor een overgang naar duurzaamheid, zonder fossiele brandstoffen.

Jammer genoeg zijn de problemen nog niet opgelost. Ondanks onze nobele intenties, hebben we vastgesteld dat, om te kunnen blijven gebruik maken van vele schone technologieën, voldoende toevoer van een aantal zeer belangrijke grondstoffen nodig is. Rijkdommen zoals sommige metalen en andere elementen die een cruciale rol spelen in het ontwerp en de werking van allerhande ‘schone’ toestellen en machines. Het is gebleken dat sommige van die grondstoffen over de voorbije decennia bijzonder schaars zijn geworden, in dergelijke mate dat gevreesd wordt voor een complete uitputting als we niet snel handelen.

In deze context speelt één groep metalen, gekend als de zeldzame aarden (*rare earths*, REE's), een zeer belangrijke rol. Ze behoren tot de meest cruciale elementen in verschillende duurzame technologieën, terwijl hun beschikbaarheid meer en meer in gedrang komt. Doorheen dit werk wordt duidelijk dat het mijnen naar zeldzame aarden op een kostenefficiënte wijze geen sinecure is, en dat er verschillende geopolitieke aspecten spelen in de handel ervan. Daarenboven ligt hun recyclagegraad teleurstellend laag, voornamelijk doordat ze slechts in kleine hoeveelheden verwerkt zitten in hun toepassingen. De huidige recyclage processen zijn bijgevolg amper in staat om de zeldzame aarden op een kostenefficiënte wijze terug te winnen. Het is nochtans enorm belangrijk dat voldoende toevoer van de REE's wordt verzekerd, want in de meeste gevallen kennen deze metalen geen waardige vervangers.

In het domein van de recyclage wordt er meer en meer interesse geschonken aan het concept ‘*Urban Mining*’. Kort samengevat doet de technosfeer (waaronder ons elektronisch afval) dienst als een volwaardige mijn, boordevol waardevolle grondstoffen. Dit elektronisch afval bezit het potentieel om een aanzienlijke hoeveelheid zeldzame op te leveren, hetgeen ons kan helpen de toenemende vraag naar deze metalen te bevredigen. Daarnaast kan ook verbeterde, doch duurzame mijnbouw helpen om aan deze vraag te voldoen.

Het is in deze context dat de kern van dit werk is gesitueerd. Zowel in primaire REE mijnbouw als in recyclageprocessen krijgt men vaak te maken met waterige stromen die variërende concentraties aan deze metalen bevatten. Er is gebleken dat er bij het behandelen van deze stromen, veel ruimte voor verbetering is betreffende de toegepaste technologieën. Industriële technieken zoals solvent-extracties blijven waarschijnlijk de meest voor de hand liggende keuze als het de behandeling van geconcentreerde oplossingen betreft (bv. g/L-schaal). Echter, wanneer het om verdunde oplossingen (bv. mg/L-schaal) gaat, schieten deze technieken vaak te kort qua kostenefficiëntie. Verder worden ook meer en meer secundaire bronnen aangewend bij de winning van zeldzame aarden (bronnen waarin deze metalen typisch minder geconcentreerd aanwezig zijn, ook recyclage hoort hier bij). Ook hier zouden dergelijk technieken gelijkaardige limitaties kennen.

Adsorptie wordt in dit werk vooropgesteld als een waardig alternatief. De voordelen van deze technologie worden aangehaald en er wordt aangetoond dat adsorbentia ideale materialen zijn voor de lage-concentratie recuperatie of verwijdering van bepaalde componenten. Met betrekking op zeldzame aarden worden verschillende domeinen voorgesteld waar selectieve adsorptie een belangrijke rol kan spelen. Bovendien worden ook de vereisten voor dergelijk adsorbentia beschreven. Of het nu gaat om terugwinning van zeldzame aarden uit proceswateren of afvalstromen, of om bepaalde REE-bevattende stromen te zuiveren van schadelijke elementen (uranium, thorium,...), adsorbentia kunnen op specifieke wijze worden afgestemd op de applicatie naar keuze.

Verder in dit werk wordt een introductie gegeven in de wereld van metaal-organische roosters (*metal-organic frameworks*, MOF's). Het concept om deze veelzijdige coördinatiepolymeren te gebruiken in waterige toepassingen wordt op genuanceerde wijze besproken, met gepaste terugkoppeling naar de bestaande literatuur. Het is duidelijk dat de stabiliteit van deze MOF's een cruciale rol zal spelen in hun slaagkansen als adsorbentia in waterig milieu. Er werd daarom onderzocht welke structurele parameters een significante invloed hebben op hun stabiliteit. Kort gezegd; Wat maakt een MOF geschikt voor waterige toepassingen? Daarnaast werd een studie uitgevoerd naar de lange-termijn stabiliteit van een aantal populaire MOF's, waarin hun gedrag in verschillende waterige condities werd onderzocht (zuur, basisch, oxidatief,...). Geholpen door deze inzichten kan vervolgens op rationele wijze een selectie gemaakt worden van geschikte MOF's voor waterige adsorptietoepassingen.

Vervolgens wordt beschreven hoe een specifieke kooi-MOF, namelijk MIL-101(Cr), kan aangewend worden als potentiële drager voor waterige adsorptie. Deze MOF werd gekozen op basis van zijn hoge stabiliteit en -porositeit, en gemakkelijke functionaliseerbaarheid. De MIL-101(Cr) werd gefunctionaliseerd op twee verschillende wijzen met een specifiek ligand, waarna de affiniteit voor bepaalde kritieke metalen in kaart werd gebracht (REE's, uranium,...). In een eerste strategie werd een carbamoylmethylphosphine oxide-type ligand (CMPO) op covalente



wijze verankerd op het MIL-101 rooster, via een drie-stap methode. In een andere strategie wordt het CMPO ligand via incapsulatie in-situ opgesloten in de kooien van MIL-101, waaruit het niet kan ontsnappen. Beide materialen werden onderworpen aan een uitvoerige adsorptiestudie, waarin prestaties zoals selectiviteit, stabiliteit, capaciteit, kinetiek en recycleerbaarheid werden onderzocht.

Concluderend is er aangetoond, dat verschillende MOF's weldegelijk de vereiste karakteristieken bezitten die hen geschikt maken als waterige adsorbentia. Ze kunnen naar keuze worden afgestemd op specifieke applicaties, via verschillend strategieën. Dit werd bewezen voor de stabiele MIL-101(Cr), dewelke kan worden gefunctionaliseerd met selectieve liganden voor de recuperatie van kritieke metalen. Omdat er verschillende stabiele MOFs bestaan, net als verschillende manieren om hen te functionaliseren, is het veilig te stellen dat MOF-gebaseerde adsorptie nieuwe, interessante deuren kan openen in het domein van waterige metaalrecuperatie.



## SCIENTIFIC A1 PUBLICATIONS

- CMPO-functionalized MIL-101(Cr) as highly selective uranium adsorbent.  
Jeroen De Decker, Julie Rochette, Jeriffa De Clercq, Justyna Florek, Pascal Van Der Voort, *Analytical Chemistry* (2017) In press.
- Ship-in-a-bottle CMPO in MIL-101(Cr) for selective uranium recovery from aqueous streams through adsorption.  
Jeroen De Decker, Karel Folens, Jeriffa De Clercq, Maria Meledina, Gustaaf Van Tendeloo, Du Laing Gijs, Pascal Van Der Voort, *Journal of Hazardous Materials* 335 (2017) 1 – 9.  
Systematic study of the chemical and hydrothermal stability of selected “stable” Metal Organic Frameworks.  
Karen Leus, Thomas Bogaerts, Jeroen De Decker, Hannes Depauw, Kevin Hendrickx, Henk Vrielinck, Veronique Van Speybroeck, Pascal Van Der Voort, *Microporous and Mesoporous Materials* 226 (2016) 110 – 116.
- Functionalized metal-organic-framework CMPO@MIL-101(Cr) as a stable and selective rare earth adsorbent.  
Jeroen De Decker, Jeriffa De Clercq, Pieter Vermeir, Pascal Van Der Voort, *Journal of Materials Science* 51 (2016) 5019 – 5026.
- Covalent immobilization of the Jacobsen catalyst on mesoporous phenolic polymer: A highly enantioselective and stable asymmetric epoxidation catalyst.  
Jeroen De Decker, Thomas Bogaerts, Ilke Muylaert, Sander Delahaye, Frederic Lynen, Veronique Van Speybroeck, An Verberckmoes, Pascal Van Der Voort, *Materials Chemistry and Physics* 141 (2013) 967 – 972.
- Ordered mesoporous phenolic resins: Highly versatile and ultra-stable support materials.  
Ilke Muylaert, An Verberckmoes, Jeroen De Decker, Pascal Van Der Voort, *Advances in Colloid and Interface Science* 175 (2012) 39 – 51.



## OUTLINE

The core of this dissertation revolves around the application of metal-organic framework based materials (MOFs) as potential aqueous-phase adsorbents for critical metals. The work initially offers a broad view on the importance of these critical metals to our (sustainable) future, with a deep focus on rare earths elements. Gradually, the scope of this work will narrow down, from general mining technologies, to the specific recycling technologies where adsorbents can take their rightful place. Further on, the concept of using MOFs as aqueous adsorbents is approached in a sensible way, discussing both their pros and cons. An overview is given on different state of the art methods to use the MOFs as adsorbents, both pristinely and functionalized. The work is then finalized by discussing the functionalization of the MOF MIL-101(Cr) via different strategies, and its performance in the selective adsorption of critical metals (rare earths, uranium...) from aqueous environments.

Chapter 1 gives an introduction to our gradual evolution towards sustainable energy, and the need for several important resources to achieve such a sustainable future. It is shown that maintaining a continuous supply of several critical resources, will not be without risk.

Chapter 2 discusses the importance of the rare earths metals. Their physical and chemical properties are concisely explained, and their uniqueness as a metals group justified. The difficulties in obtaining these valuable elements are discussed, both from primary sources as from recycling technologies. A conclusion is made that rare earth recycling on an industrial scale, including the urban mining concept, is still of an inadequate level, yet, it offers incredible opportunities to help maintaining the rising demand.

Chapter 3 offers an introduction to the technology of adsorption as an attractive and cost-effective strategy to recover critical elements from aqueous environments. An overview is given on several domains in rare earth or uranium mining/recovery, where selective adsorption would be of high value.

Chapter 4 discusses the concept of MOFs in aqueous-phase applications. A comprehensive overview is given on several important parameters that affect the stability of these coordination polymers in water. As a result, a rational choice can be made in selecting the appropriate MOF-candidates for specific aqueous applications.

Chapter 5 provides a long-term study on the stability of several popular MOFs in different aqueous environments, including acidic, alkaline, and oxidative conditions. The findings are correlated to the existent literature, upon which a reliable assessment per MOF is made.

Chapter 6 offers an overview on various approaches to apply MOFs as adsorbent for organic and inorganic species. The important interactions between the MOF adsorbents and their respective adsorbates are illustrated, and different functionalization strategies are assessed.

Chapter 7 describes the covalent functionalization process of MIL-101(Cr), via a three-step route, to obtain CMPO anchored species on the MIL-101 structure. The material functionalization is thoroughly discussed and a preliminary adsorption experiment is presented, where europium is targeted in a solution containing competing elements, yttrium and zinc.

Chapter 8 expands the adsorption study of Chapter 7 while focusing on the recovery of uranium from acidic solutions. The work presents a selectivity study (rare earths metals), a kinetic study, and recyclability experiments.

Chapter 9 introduces a ship-in-a-bottle type MOF adsorbent, where bulky CMPO species are encapsulated in the cages of MIL-101(Cr). The one-step synthesis is discussed, followed by a thorough adsorption study, targeting uranium in acidic solutions. Selectivity experiments (vs. rare earths, transition metals...), equilibrium studies, kinetic experiments, and recyclability are provided.

Chapter 10 offers a comparison of the developed adsorbents. Their characteristics and performance are evaluated and a correlation is drawn to the theoretic principles from earlier chapters.

Chapter 11 summarizes the important conclusions that were drawn throughout this work, and provides some perspective regarding the future of MOFs as aqueous-phase adsorbents.

# CONTENTS

<b>ACKNOWLEDGEMENTS .....</b>	<b>V</b>
<b>ENGLISH SUMMARY .....</b>	<b>VII</b>
<b>DUTCH SUMMARY .....</b>	<b>IX</b>
<b>SCIENTIFIC A1 PUBLICATIONS .....</b>	<b>XIII</b>
<b>OUTLINE .....</b>	<b>XV</b>
<b>LIST OF TABLES .....</b>	<b>XXI</b>
<b>LIST OF FIGURES .....</b>	<b>XXIII</b>
<b>LIST OF ACRONYMS .....</b>	<b>XXXI</b>
<b>1 INTRODUCTION.....</b>	<b>1</b>
1.1 THE TURNING POINT .....	1
1.2 THE ORE CALLED EARTH .....	2
1.3 RESOURCE NATIONALISM .....	5
<b>2 RARE EARTHS.....</b>	<b>9</b>
2.1 THE RARE EARTH ELEMENTS .....	9
2.1.1 <i>Classification</i> .....	9
2.1.2 <i>Occurrence</i> .....	10
2.1.3 <i>REE Supply in Jeopardy?</i> .....	12
2.2 WHAT MAKES RARE EARTHS SO SPECIAL? .....	13
2.2.1 <i>The 4f-elements</i> .....	13
2.2.2 <i>Physical Properties</i> .....	17
2.3 ONE MAN’S GARBAGE .....	22
2.3.1 <i>Substitution</i> .....	23
2.3.2 <i>Sustainable Mining</i> .....	24
2.3.3 <i>Recycling</i> .....	25
2.4 URBAN MINING.....	26
2.4.1 <i>Benefits and Challenges</i> .....	26
2.4.2 <i>Necessity</i> .....	28
2.4.3 <i>Technology</i> .....	30
2.5 SEPARATING THE RARE EARTHS.....	34
2.6 A REALM OF POSSIBILITIES .....	39
<b>3 ADSORPTION.....</b>	<b>43</b>
3.1 LOW CONCENTRATION RECOVERY.....	43
3.1.1 <i>Shortcomings of the industry</i> .....	43
3.1.2 <i>Areas of potential application</i> .....	44
3.1.3 <i>The role of uranium</i> .....	47
3.1.4 <i>Challenges</i> .....	48


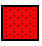
3.2 ADSORPTION OF CRITICAL METALS .....	49
3.2.1 <i>What is adsorption?</i> .....	49
3.2.2 <i>Material porosity</i> .....	50
3.2.3 <i>Supports suitability</i> .....	51
3.3 ADSORPTION OF RARE EARTHS & URANIUM .....	52
3.3.1 <i>Selective ligands</i> .....	54
3.3.2 <i>Choice of supports</i> .....	63
<b>4 MOFS IN AQUEOUS ENVIRONMENT.....</b>	<b>77</b>
4.1 WHAT IS A METAL-ORGANIC FRAMEWORK? .....	77
4.2 WATER STABILITY .....	80
<b>5 SYSTEMATIC STUDY OF THE CHEMICAL &amp; HYDRO-THERMAL STABILITY OF SELECTED STABLE MOFS.....</b>	<b>91</b>
5.1 INTRODUCTION .....	91
5.2 MATERIALS AND METHODS .....	94
GENERAL PROCEDURES .....	94
SYNTHESIS OF THE MOF MATERIALS.....	94
CHEMICAL STABILITY.....	96
HYDROTHERMAL STABILITY .....	96
5.3 RESULTS AND DISCUSSION .....	97
5.3.1 <i>Hydrothermal stability</i> .....	97
5.3.2 <i>Stability towards water and air</i> .....	100
5.3.3 <i>Chemical stability</i> .....	102
5.4 CONCLUSIONS.....	108
<b>6 MOFS IN AQUEOUS ADSORPTION.....</b>	<b>113</b>
6.1 THE SEARCH FOR PROMISING MOF CANDIDATES .....	113
6.2 REMOVAL OF ORGANIC COMPONENTS.....	113
6.2.1 <i>CUS-grafting</i> .....	114
6.2.2 <i>Support charge effects</i> .....	119
6.3 METAL ADSORPTION WITH MOFS .....	121
6.3.1 <i>Inherent functionalities</i> .....	121
6.3.2 <i>Aperture effects</i> .....	122
6.3.3 <i>Open metal sites</i> .....	124
6.3.4 <i>Combined interactions</i> .....	125
6.3.5 <i>Pre-functionalized linkers</i> .....	126
6.3.6 <i>Post-synthetic modification</i> .....	128
6.4 CONCLUDING REMARKS .....	133
6.5 PERSPECTIVE: SHAPING MOFS FOR INDUSTRIAL APPLICATIONS .....	134




<b>7 FUNCTIONALIZED METAL-ORGANIC FRAMEWORK CMPO@MIL-101(CR) AS A STABLE AND SELECTIVE RARE EARTH ADSORBENT .....</b>	<b>137</b>
7.1 INTRODUCTION .....	137
7.2 EXPERIMENTAL SECTION .....	140
7.2.1 Chemicals.....	140
7.2.2 Synthesis of MIL-101(Cr).....	140
7.2.3 CMPO-functionalization of MIL-101(Cr).....	140
7.2.4 Characterization Techniques .....	141
7.2.5 Adsorption experiments.....	142
7.3 RESULTS AND DISCUSSION .....	143
7.3.1 Material characterization .....	143
7.3.2 Adsorbent stability.....	146
7.3.3 Sorption Isotherm.....	146
7.3.4 Selectivity experiments .....	148
7.3.5 Sorption Kinetics.....	148
7.4 CONCLUSION .....	149
<b>8 CMPO-FUNCTIONALIZED MIL-101(CR) AS HIGHLY SELECTIVE URANIUM ADSORBENT.....</b>	<b>153</b>
8.1 INTRODUCTION .....	153
8.2 MATERIALS AND METHODS .....	155
8.3 RESULTS AND DISCUSSION .....	156
<b>9 SHIP-IN-A-BOTTLE CMPO IN MIL-101(CR) FOR SELECTIVE URANIUM RECOVERY FROM AQUEOUS STREAMS THROUGH ADSORPTION .....</b>	<b>163</b>
9.1 INTRODUCTION .....	163
9.2 EXPERIMENTAL .....	166
9.2.1 Chemicals and Reagents .....	166
9.2.2 Synthesis of Ship-in-a-Bottle CMPO in MIL-101(Cr).....	166
9.2.3 Characterization techniques .....	166
9.2.4 Stability .....	167
9.2.5 Adsorption Experiments .....	167
9.3 RESULTS AND DISCUSSION .....	169
9.3.1 Ship-in-a-bottle adsorbent.....	169
9.3.2 Material characterization .....	170
9.3.3 Adsorbent Stability.....	173
9.3.4 Adsorption Studies.....	173
9.4 CONCLUSION .....	180
<b>10 COMPARISON OF THE DEVELOPED ADSORBENTS .....</b>	<b>185</b>
10.1 LIGAND LOADING.....	185

10.2 SELECTIVITY .....	187
10.1 CAPACITY AND KINETICS .....	189
10.2 REUSABILITY .....	190
<b>11 CONCLUSIONS AND OUTLOOK.....</b>	<b>193</b>
<b>12 APPENDICES.....</b>	<b>197</b>

## LIST OF TABLES

TABLE 1.1 TWENTY CRITICAL RAW MATERIALS (CRM) FOR THE EU, ACCORDING TO THE 2014 REPORT ON CRITICAL RAW MATERIALS [4].	3
TABLE 2.1 AVERAGE DISTRIBUTION OF THE INDIVIDUAL REEs <sup>1</sup> .	11
TABLE 2.2 GROUND-STATE ELECTRONIC CONFIGURATIONS OF THE ELEMENTS OF SUBGROUP III-B.	14
TABLE 2.3 APPLICATIONS PER RARE EARTH ELEMENT	20
TABLE 2.4 RARE EARTHS USAGE BY APPLICATION, IN %	22
TABLE 2.5 VARIOUS E-WASTE SOURCES AND THEIR HEALTH EFFECTS.	29
TABLE 2.6 SOME COMMERCIAL EXTRACTANTS FOR RARE EARTH SOLVENT EXTRACTION.	37
TABLE 3.1 SUMMARY OF POSSIBLE SECONDARY RARE EARTH RESOURCES (RETRIEVED FROM [11]).	46
TABLE 3.2 CONCENTRATIONS OF ThO <sub>2</sub> AND U <sub>3</sub> O <sub>8</sub> IN THE MOST IMPORTANT REE-BEARING MINERALS (ACCORDING TO PILLAI[15])	47
TABLE 3.3 COMPLEX FORMATION CONSTANTS (LOGARITHMIC VALUES) OBTAINED WITH CMPO/CALIXARENES-BASED DERIVATES 1 TO 6. (ADAPTED FROM [62]).	61
TABLE 3.4 OVERVIEW ON SEVERAL REPORTED ADSORBENTS FOR CRITICAL METALS (REEs, U). LIST NOT ALL-INCLUSIVE. (ADAPTED FROM [1])	68
TABLE 5.1 STRUCTURAL OVERVIEW OF THE STUDIED MOFs.	93
TABLE 5.2 EFFECT OF THE HYDROTHERMAL TREATMENT, CHEMICAL AND OXIDATIVE TREATMENT AND EXPOSURE TO WATER AND AIR (SHORT-TERM AND LONG-TERM) ON THE LANGMUIR SURFACE AREA (EXPRESSED IN m <sup>2</sup> /g). ALL DATA ARE BASED ON SINGULAR EXPERIMENTS.	99
TABLE 5.3 EFFECT OF THE HYDROTHERMAL STABILITY TEST AND SHORT AND LONG TIME EXPOSURE TO AIR AND WATER ON THE XRPD PATTERN OF THE EXAMINED MOF MATERIALS.	100
TABLE 5.4 EFFECT OF A SHORT AND LONG TIME EXPOSURE TO ACIDS (pH = 0 AND pH = 4), BASES (pH = 12), AND PEROXIDES ON THE XRPD PATTERN OF THE EXAMINED MOF MATERIALS.	105
TABLE 5.5 CONCLUDING OVERVIEW ON THE STABILITY (N <sub>2</sub> AND XRD) OF THE EXAMINED MOFs IN THE VARIOUS MEDIA.  THE XRPD PATTERN AND SURFACE AREA ARE LARGELY PRESERVED,  THE XRPD PATTERN AND SURFACE AREA ARE COMPLETELY	

DESTROYED,  THE XRPD PATTERN AND SURFACE AREA ARE PARTIALLY DECREASED/DEGRADED OR TRANSFORMED).	109
TABLE 7.1 QUANTITATIVE OVERVIEW OF THE MIL-101(Cr) FUNCTIONALIZATION	143
TABLE 7.2 SELECTIVITY RESULTS OF CMPO@MIL-101(Cr), ( $C_{0\text{ EU}} = C_{0\text{ Y}} = C_{0\text{ ZN}} \approx 50$ PPM, PH = 5, T = 24 HRS, L/S = 400 mL/G, T = 25 °C).	148
TABLE 8.1 CHARACTERIZATION RESULTS OF CMPO@MIL-101(Cr) BY N <sub>2</sub> -PHYSISORPTION AND XRF	157
TABLE 9.1 NUMERICAL N <sub>2</sub> -ADSORPTION DATA AND LOADING CALCULATIONS OF MIL-101(Cr) AND MIL-101-SHIP	172
TABLE 9.2 ADSORPTION PARAMETERS OF U(VI) ON MIL-101-SHIP AT PH 3 AND PH 4, FITTED TO LANGMUIR AND FREUNDLICH MODELS	176
TABLE 9.3 OVERVIEW OF REPORTED MOF-BASED U(VI) ADSORBENTS AND THEIR ADSORPTION PERFORMANCE, COMPARED TO MIL-101-SHIP	177
TABLE 9.4 PARAMETERS OF THE PSEUDO-FIRST-ORDER AND PSEUDO-SECOND-ORDER KINETIC MODELS FOR ADSORPTION OF U(VI) ON MIL-101-SHIP. C <sub>0</sub> : 30 MG/L, PH: 3.0, L/S: 1000 mL/G, T = 25 °C	178
TABLE 10.1 OVERVIEW OF THE MATERIAL CHARACTERISTICS FOR BOTH DEVELOPED ADSORBENTS	186
TABLE 10.2 OVERVIEW OF DEVELOPED ADSORBENTS AND THEIR ADSORPTION PERFORMANCE	188

## LIST OF FIGURES

FIGURE 1.1 RAW MATERIALS CRITICALITY ASSESSMENT BY THE AD HOC WORKING GROUP ON DEFINING CRITICAL RAW MATERIALS. THE CRITICAL MATERIALS ARE HIGHLIGHTED IN THE RED BOX. (RETRIEVED FROM [4]).....	4
FIGURE 1.2 WORLDWIDE MAJOR SUPPLIERS OF THE 20 CRM, ACCORDING TO THE 2014 REPORT ON CRITICAL RAW MATERIALS. (RETRIEVED FROM [4]) .....	5
FIGURE 1.3 PRICE EVOLUTION OF SEVERAL RARE EARTH ELEMENTS THROUGHOUT THE YEARS (2008 – 2014). (RETRIEVED FROM [7]).....	7
FIGURE 2.1 SITUATION OF THE RARE EARTH ELEMENTS IN THE PERIODIC TABLE OF ELEMENTS. .....	10
FIGURE 2.2 GROUP III-B OF THE PERIODIC TABLE OF ELEMENTS. (*, † MARKING THE START OF THE LANTHANIDE AND ACTINIDE SERIES, RESPECTIVELY).....	14
FIGURE 2.3 ENERGY LEVELS OF DIFFERENT SUBSHELLS WITHIN AN ATOM.....	15
FIGURE 2.4 IONIC RADII THROUGHOUT THE LANTHANIDE SERIES, DEMONSTRATING LANTHANIDE CONTRACTION. ....	16
FIGURE 2.5 ATOMIC RADII THROUGHOUT THE LANTHANIDE SERIES. ....	17
FIGURE 2.6 WORLD 2015 REE DEMAND BY APPLICATION, AS PROJECTED BY IMCOA. (DATA RETRIEVED FROM [21]).....	19
FIGURE 2.7 COMPREHENSIVE RAW MATERIALS STRATEGY, TARGETING A DIVERSIFIED APPROACH: PRIMARY MINING, SUBSTITUTION, RAW MATERIALS DIPLOMACY AND TECHNOSPHERIC MINING AND RECYCLING. (RETRIEVED FROM [15]) .....	23
FIGURE 2.8 VARIOUS SEGMENTS OF THE TECHNOSPHERIC MINING APPROACH TO IMPROVE THE LIFE CYCLE OF RAW MATERIALS. (RETRIEVED FROM [15]). (MSW: MUNICIPAL SOLID WASTE, MWS: MUNICIPAL WATER SYSTEM, IW: INDUSTRIAL WASTE OR WATER). ....	26
FIGURE 2.9 RHODIA’S URBAN MINING PLANT IN LA ROCHELLE, FRANCE. ....	27
FIGURE 2.10 PRIMITIVE, INFORMAL E-WASTE RECYCLING THROUGH INCINERATION. (©JON SPAULL. RETRIEVED FROM [50]).....	30
FIGURE 2.11 PROCESS FLOW CHART FOR PRECIOUS METALS RECOVERY FROM PCBs AT CSIR- NML, JAMSHEDPUR. (RETRIEVED FROM [42]).....	31
FIGURE 2.12 SIMPLIFIED REPRESENTATION OF A SMELTER (FLASH FURNACE), PRODUCING A MATTE PHASE (BOTTOM LAYER) AND SLAG PHASE (OXIDIZED TOP LAYER). (ADAPTED FROM [34]).....	32

FIGURE 2.13 FLOW SHEET FOR UMICORE’S INTEGRATED METALS SMELTER AND REFINERY. (RETRIEVED FROM [60]) .....	33
FIGURE 2.14 SULFONIC POLYSTYRENE-DIVINYLBENZENE (PS-DVB) TYPE IX RESIN, WHERE SODIUM CATIONS ARE EXCHANGED FOR CALCIUM. (RETRIEVED FROM [62]) .....	34
FIGURE 2.15 SEPARATION OF RARE EARTHS VIA ION EXCHANGE AND ELUTION CHROMATOGRAPHY. (FIGURE ADAPTED FROM [62]) .....	35
FIGURE 2.16 SCHEMATIC REPRESENTATION OF A MIXER-SETTLER SYSTEM FOR CONTINUOUS OPERATION OF SOLVENT EXTRACTION. (RETRIEVED FROM [66]) .....	36
FIGURE 2.17 SIMPLIFIED FLOWSHEET FOR REE REFINERY FROM MONAZITE ORE THROUGH MULTI-STAGE SOLVENT EXTRACTION (SHANGHAI YUE LONG CHEMICAL PLANT). (RETRIEVED FROM [63]) .....	39
FIGURE 3.1 DIFFERENT DESIGNS OF LIGAND SYSTEMS FOR SELECTIVE METAL INTERACTIONS, THROUGH COORDINATION, CHELATION OR INCLUSION. (ADAPTED FROM [2]) .....	48
FIGURE 3.2 (LEFT) ADSORPTION ON AN EXTERNAL SURFACE, (RIGHT) ADSORPTION ON A POROUS MATERIAL, CONTAINING EXTERNAL AND INTERNAL SURFACE. (BLUE DOTS: ADSORBED SPECIES) .....	50
FIGURE 3.3 IRREGULAR PORE STRUCTURE OF ACTIVATED CARBON, AS A RESULT OF ITS ACTIVATION TREATMENT. (ADAPTED FROM [34]) .....	51
FIGURE 3.4 ORBITAL PROBABILITY DISTRIBUTION IN ACTINIDES. (RETRIEVED FROM [41]) .....	53
FIGURE 3.5 STRUCTURE OF THE URANIUM TRICARBONATE COMPLEX $[\text{UO}_2(\text{CO}_3)_3]^{4-}$ . (U: YELLOW, O: RED, C: BLACK) (RETRIEVED FROM [43]) .....	54
FIGURE 3.6 COMMONLY USED LIGANDS FOR RARE EARTH AND ACTINIDE COORDINATION. (RETRIEVED FROM [1] AND [23]) .....	55
FIGURE 3.7 BASIC STRUCTURES OF CMPO (LEFT) AND TBP (RIGHT) .....	56
FIGURE 3.8 SCHEMATIC REPRESENTATION OF THE BIDENTATE $\text{MX}_3\text{L}_N$ (RIGHT) AND OF THE MONODENTATE $\text{MX}_3\text{L}$ COMPLEX ( $\text{O}_p$ COORDINATION) (LEFT). (RETRIEVED FROM [52]) ..	57
FIGURE 3.9 STRUCTURES OF CALCULATED EUROPIUM COMPLEXES. TOP: $\text{EuCl}_3\text{L}$ ; BOTTOM: $\text{Eu}(\text{NO}_3)_3\text{L}$ ; LEFT: BIDENTATE MODE; RIGHT: MONODENTATE MODE. BOND LENGTHS ARE PROVIDED IN ÅNGSTRÖM. (RETRIEVED FROM [52]) .....	58
FIGURE 3.10 STRUCTURE OF THE CALCULATED EUROPIUM COMPLEX $\text{Eu}(\text{NO}_3)_3\text{L}_2$ IN BIDENTATE MODE. BOND LENGTHS ARE PROVIDED IN ÅNGSTRÖM. (RETRIEVED FROM [52]). .....	59
FIGURE 3.11 SCHEMATIC REPRESENTATION OF A CALIX[4]-CMPO LIGAND (CAVITAND) AND OF AN $\text{M}^{3+}$ INCLUSION COMPLEX. (RETRIEVED FROM [52]) .....	59

FIGURE 3.12 DIFFERENT ANALOGUES OF THE CMPO LIGAND. ....	60
FIGURE 3.13 DIFFERENT CMPO ANALOGUES TETHERED ONTO CALIXARENES-BASED MOLECULAR PLATFORMS FOR CATION EXTRACTION. (ADAPTED FROM [62]).....	61
FIGURE 3.14 STRUCTURE OF THE CALCULATED $\text{UO}_2(\text{NO}_3)_2\text{L}$ COMPLEX. BOND LENGTHS ARE PROVIDED IN ÅNGSTRÖM. (RETRIEVED FROM [52]).....	62
FIGURE 3.15 (LEFT) SILICA STRUCTURE AND SURFACE COMPOSITION. (MIDDLE) GRAFTING OF A TYPICAL ORGANOSILANE (APTES), CREATING PRIMARY AMINE FUNCTIONALIZATIONS ON THE SILICA SURFACE, BONDED VIA SILOXANE BRIDGES (RIGHT).....	64
FIGURE 3.16 SCHEMATIC OVERVIEW OF A TYPICAL SELF-ASSEMBLY (SELF-ORGANIZATION) APPROACH FOR ORDERED POROUS MATERIALS. (ADAPTED FROM [67]).....	64
FIGURE 3.17 SCHEMATIC REPRESENTATION OF THE SBA-15 (LEFT) AND KIT-6 (RIGHT) MESOSTRUCTURE, BOTH MESOPOROUS SILICA SUPPORTS. (ADAPTED FROM [1]) .....	65
FIGURE 3.18 SCHEMATIC ILLUSTRATION OF THE NANOCASTING PATHWAY USING MESOPOROUS SILICA HARD TEMPLATES WITH DIFFERENT GEOMETRIES (A: HEXAGONAL AND B: CUBIC). (RETRIEVED FROM [80]).....	66
FIGURE 3.19 SCHEMATIC OVERVIEW OF SOME FUNCTIONALIZATION METHODS OF ORDERED MESOPOROUS PHENOLIC RESINS. (RETRIEVED FROM [82]) .....	67
FIGURE 3.20 LIGAND STRUCTURES, USED IN THE OVERVIEW ON REE/U TARGETING ADSORBENTS. ....	70
FIGURE 4.1 SCHEMATIC BUILD-UP OF A METAL-ORGANIC FRAMEWORK. (ADAPTED FROM [3])	78
FIGURE 4.2 THE MOF-5 STRUCTURE SHOWN AS $\text{ZnO}_4$ TETRAHEDRA (BLUE POLYHEDRA) JOINED BY BENZENE DICARBOXYLATE LINKERS (O, RED AND C, BLACK) TO GIVE AN EXTENDED 3D CUBIC FRAMEWORK. (YELLOW SPHERE REPRESENTS THE LARGEST SPHERE THAT CAN OCCUPY THE PORES WITHOUT COMING WITHIN THE VAN DER WAALS SIZE OF THE FRAMEWORK). (RETRIEVED FROM [2]).....	79
FIGURE 4.3 DIFFERENT LINKERS WITH SELECTED METAL NODES AND SECONDARY BUILDING UNITS IN THEIR CORRESPONDING MOFs (HKUST-1, MIL-101(Cr) AND ZIF-8). ....	80
FIGURE 4.4 CRYSTAL STRUCTURES OF HKUST-1, MIL-101(Cr), AND MOF-5, WITH THEIR RESPECTIVE CHEMICAL FORMULA, ENABLING THE CALCULATION OF RELATIVE METAL CHARGE. (RETRIEVED FROM [32]).....	82
FIGURE 4.5 ELECTRONIC CONFIGURATION OF THREE DIFFERENT <i>D</i> -METAL COMPLEXES IN AN OCTAHEDRAL FIELD. THE <i>D</i> -ORBITAL ENERGIES SPLIT INTO TWO LEVELS, I.E., THE LOWER $T_{2g}$ LEVEL AT $-0.4 \Delta_o$ , AND THE HIGHER $E_g$ LEVEL AT $0.6 \Delta_o$ . ( $\Delta_o$ : LIGAND FIELD SPLITTING	

PARAMETER). LFSE IS CALCULATED BY: $(-0.4N_{T2G} + 0.6N_{EG}).\Delta_o$ WITH $N$ THE AMOUNT OF PRESENT ELECTRONS IN THE RESPECTIVE LEVEL.....	83
FIGURE 4.6 REACTION COORDINATE DIAGRAM HIGHLIGHTING THE IMPORTANCE OF KINETIC FACTORS IN DETERMINING MOF WATER STABILITY. WHILE STRUCTURES 1 (GREEN) AND 2 (RED) HAVE THE SAME THERMODYNAMIC STABILITY, STRUCTURE 1 IS MORE STABLE UNDER HUMID CONDITIONS DUE TO KINETIC FACTORS THAT INCREASE THE ACTIVATION ENERGY BARRIER ( $E_a$ ) FOR HYDROLYSIS. (ADAPTED FROM [29]) .....	84
FIGURE 4.7 SCHEMATIC REPRESENTATION OF MOF-5 (LEFT), AND FUNCTIONALIZED IRMOF-3-AM( $N+1$ ) (RIGHT). (ADAPTED FROM [42]) .....	85
FIGURE 4.8 (A) SBU OF THE UiO-66 FRAMEWORK (SIX-CENTER OCTAHEDRAL METAL CLUSTERS, $M = Zr$ ). (A, RIGHT) BDC LINKERS. (B) UiO-66 NETWORK STRUCTURE. (C) SIMPLIFIED POLYHEDRAL REPRESENTATION OF THE SAME NETWORK STRUCTURE. (RETRIEVED FROM [43]) .....	86
FIGURE 5.1 TGA PLOT OF MIL-101 (Cr) BEFORE AND AFTER THE TREATMENT IN 1 M HCL (HEATING RATE: 2 °C/MIN). .....	104
FIGURE 6.1 CHEMICAL STRUCTURE OF METHYLENE BLUE AND METHYL ORANGE. ....	114
FIGURE 6.2 FORMATION OF COORDINATIVELY UNSATURATED CHROMIUM SITES IN THE $Cr_3O$ -CARBOXYLATE CLUSTER OF THE MIL-101 STRUCTURE. (RETRIEVED FROM [9]).....	115
FIGURE 6.3 ILLUSTRATION OF THE GRAFTED DIAMINE GROUPS ONTO MIL-101 CUS. ED: ETHYLENEDIAMINES, PED: PROTONATED ED. (ADAPTED FROM [3]) .....	115
FIGURE 6.4 CHEMICAL STRUCTURES OF NAPROXEN (LEFT), ETHANOLAMINE (MIDDLE), AND DIETHANOLAMINE (RIGHT). ....	116
FIGURE 6.5 REUSABILITY OF MIL-101-OH IN THE ADSORPTION OF NAPROXEN OVER SUBSEQUENT CYCLES. THE RED AND BLUE HORIZONTAL LINES SHOW THE ADSORBED AMOUNT OF NAPROXEN OVER PRISTINE MIL-101 AND ACTIVATED CARBON, RESPECTIVELY. ADSORPTION TIME PER CYCLE: 12 H, INITIAL CONCENTRATION OF NAPROXEN: 50 MG/L). (RETRIEVED FROM [7]) .....	117
FIGURE 6.6 SCHEMATIC OVERVIEW OF THE DIFFERENT FUNCTIONALIZATION METHODS OF MIL-101 BY SEO <i>ET AL.</i> (ADAPTED FROM [7]).....	118
FIGURE 6.7 (LEFT) EVOLUTION OF NAPROXEN UPTAKE OVER TIME ON MIL-101(Cr) AND ITS FUNCTIONALIZATIONS (ED: ETHYLENE DIAMINE, AMSA: AMINOMETHYLSULFONIC ACID. (RIGHT) pH-DEPENDENCY PLOT OF NAPROXEN UPTAKE BY ED-MIL-101. (RETRIEVED FROM [4]) .....	119



FIGURE 6.8 CHEMICAL STRUCTURE OF MALACHITE GREEN. STRUCTURAL REPRESENTATIONS OF MIL-53, MIL-100, AND MIL-101.....	120
FIGURE 6.9 IMPORTANT MECHANISMS FOR THE ADSORPTION OVER MOFs. (RETRIEVED FROM [1]).....	121
FIGURE 6.10 (A) THE COORDINATION ENVIRONMENT OF THE ZN(II) CENTER; (B) THE 2D LAYERS PILLARED BY THE H <sub>2</sub> BTEC LIGAND GENERATE A 3D PILLAR-LAYER FRAMEWORK; (C) THE (3,4)-CONNECTED AUGMENTED NET AS A NATURAL TILING. (RETRIEVED FROM [16])....	122
FIGURE 6.11 SCHEMATIC OF CAPTURE OF UO <sub>2</sub> <sup>2+</sup> IONS INTO THE ONE-DIMENSIONAL CHANNELS OF MOF-76. (RETRIEVED FROM [17]) .....	123
FIGURE 6.12 (LEFT) EFFECT OF SOLUTION pH ON THE U(VI) ADSORPTION ON THE MOF-76 ADSORBENT. C <sub>0</sub> (U) = 140 MG/L, M/V = 0.4 G/L, AND T = 5 H. (RIGHT) COMPETITIVE ADSORPTION OF COEXISTING IONS BY MOF-76. (RETRIEVED FROM [17]).....	123
FIGURE 6.13 EFFECT OF pH ON As(V) ADSORPTION ON MIL-100(Fe) (C <sub>0</sub> (As(V)): 5 MG/L, M/V = 5.0 G/L, T = 25 °C). .....	124
FIGURE 6.14 pH EFFECT ON ARSENATE SPECIATION, ADSORBENT SURFACE CHARGE, AND As(V) ADSORPTION WITH UiO-66. C <sub>0</sub> (As(V)) = 50 MG/L, M/V = 0.5 G/L. (RETRIEVED FROM [20]) .....	125
FIGURE 6.15 PROPOSED ADSORPTION MECHANISM OF ARSENATE ONTO UiO-66 THROUGH COORDINATION AT THE Zr-O(M3)-Zr HYDROXYL GROUP. (RETRIEVED FROM [20]).....	126
FIGURE 6.16 SCHEMATIC SHOWING THE RESPECTIVE MOF (1-3) PREPARATIONS, INCLUDING A STRUCTURAL MODEL OF THE NEW UiO-BASED MOF, DISPLAYING THE READILY ACCESSIBLE PHOSPHORYLUREA GROUPS. (RETRIEVED FROM [23]).....	127
FIGURE 6.17 SORPTION AND DESORPTION OF URANIUM WITH MOFs 2 AND 3, WITH [U] <sub>0</sub> = 5 MG/L AND pH = 2.5 IN WATER (TOP LEFT), AND SIMULATED SEAWATER (BOTTOM LEFT), AND WITH [U] <sub>0</sub> = 100 MG/L AT pH 2.5 IN SIMULATED SEAWATER, ANALYSED BY UV SPECTROSCOPY (TOP RIGHT) AND ICP-MS (BOTTOM RIGHT). (RETRIEVED FROM [23])..	128
FIGURE 6.18 SCHEMATIC ILLUSTRATION OF THE THIOL-FUNCTIONALIZATION OF MOFs THROUGH COORDINATION BONDING BETWEEN ONE THIOL GROUP OF DITHIOGLYCOL AND COORDINATIVELY UNSATURATED METAL CENTERS (UMCs) IN MOFs. (RETRIEVED FROM [24]).....	129
FIGURE 6.19 U(VI) SPECIES DISTRIBUTION AS A FUNCTION OF pH AT 25 °C. (RETRIEVED FROM [26]).....	130
FIGURE 6.20 (LEFT) EFFECT OF pH ON U(VI) SORPTION ONTO MIL-101, MIL-101-NH <sub>2</sub> , MIL-101-ED, AND MIL-101-DETA; C <sub>0</sub> = 100 MG/L, M/V = 0.4 G/L, T = 25 °C, T = 240 MIN.	

(RIGHT) COMPETITIVE SORPTION OF COEXISTENT IONS BY MIL-101-DETA AT PH 5.5. THE INITIAL CONCENTRATION OF ALL METAL IONS WAS 0.5 MMOL/L. (ADAPTED FROM [13])	131
FIGURE 6.21 STRATEGY FOR THE GENERATION OF MIL-53 PRESENTING ISO(THIO)CYANATE, (THIO)CARBAMATE, AND (THIO)UREA FUNCTIONAL GROUPS. (RETRIEVED FROM [27])	132
FIGURE 6.22 DIFFERENT INTERACTION TYPES OF MOFs (PRISTINE/FUNCTIONALIZED) WITH METALLIC SPECIES. (GREEN ORBS: CATIONIC ADSORBATE, RED ORB: ANIONIC ADSORBATE, GREY ORBS: METAL NODES OF THE MOF).	133
FIGURE 6.23 CROSS-SECTIONAL VIEW OF A FIRED MIL-101 (Cr) MONOLITH. (RETRIEVED FROM [32])	134
FIGURE 7.1 (A) MIL-101 SUPER TETRAHEDRON. (B RESP. C) SMALL AND LARGE SUPER CAGE. (D) MIL-101 STRUCTURE (MTN ZEOTYPE).	138
FIGURE 7.2 CARBAMOYLMETHYLPHOSPHINE OXIDE (CMPO) LIGAND STRUCTURE.	139
FIGURE 7.3 STEPWISE ANCHORING OF CMPO ON MIL-101(Cr). MIL-101: PRISTINE MOF, -Cl: CHLOROMETHYLATED, -NH <sub>2</sub> : AMINATED, MIL-101-LIG: COMPLETED CMPO ON MIL-101.	141
FIGURE 7.4 NITROGEN ADSORPTION ISOTHERM OF THE UNFUNCTIONALIZED MIL-101 (•), AMINATED MIL-101 (--) AND FINALIZED LIGAND MIL-101 (—).	144
FIGURE 7.5 POWDER XRD PATTERNS OF THE (UN)FUNCTIONALIZED MATERIALS.	145
FIGURE 7.6 DRIFTS SPECTRA OF EACH STEP IN THE FUNCTIONALIZATION. INSET: ZOOM ON THE ALIPHATIC STRETCH REGION.	146
FIGURE 7.7 EU(III) ADSORPTION ISOTHERM W/ LANGMUIR FIT (•) OF THE CMPO FUNCTIONALIZED MIL-101 (AVERAGE VALUES OF DUPLICATES). PH = 4, L/S = 1000 mL/G, T = 25 °C. PH 5 INFLUENCE CHECK (°).	147
FIGURE 7.8 EU(III) ADSORPTION KINETICS WITH CMPO@MIL-101(Cr) (C <sub>0</sub> = 50 PPM, PH = 4, L/S = 1000 mL/G, T = 25 °C).	149
FIGURE 8.1 CMPO@MIL-101(Cr) WITH THE MAGNIFIED MIL-101 CAGE STRUCTURE.	155
FIGURE 8.2 SELECTIVITY RESULTS OF CMPO@MIL-101(Cr). ZOOM ON THE COMPETING ELEMENTS: APPENDIX 3.1).	157
FIGURE 8.3 EXPERIMENTAL KINETIC PROFILES FOR U(VI) ADSORPTION WITH CMPO@MIL-101(Cr) USING THREE DIFFERENT URANIUM CONCENTRATIONS.	159
FIGURE 8.4 REGENERATION RESULTS PER CYCLE FOR CMPO@MIL-101, USING 0.1 M OXALATE SOLUTION (PH 4) VIA COLUMN SETUP.	160

FIGURE 9.1 VISUALIZATION OF A CMPO MOLECULE TRAPPED IN AN INDIVIDUAL MIL-101(Cr) CAGE. THREE DIFFERENT ANGLES OF THE CAGE ARE REPRESENTED. THE CMPO LIGAND IS VISUALIZED IN THE BALL-STICK MANNER, WHEREAS THE MIL-101 CAGE IS REPRESENTED AS A WIREFRAME, FOR CLARITY REASONS. (HIGH-RESOLUTION IMAGES ARE PROVIDED IN APPENDIX 4.2).....	170
FIGURE 9.2 DRIFTS SPECTRA OF THE PRISTINE MIL-101(Cr), THE MIL-101-SHIP AND PURE CMPO. (INSET: ZOOM ON THE 650 – 1300 $\text{cm}^{-1}$ REGION).....	171
FIGURE 9.3 NITROGEN ADSORPTION ISOTHERMS (LEFT) AND X-RAY DIFFRACTION PATTERNS (RIGHT) OF PRISTINE MIL-101(Cr) (A) AND MIL-101-SHIP (B). ....	171
FIGURE 9.4 (A)ADF-STEM IMAGE OF A MIL-101 CRYSTALLINE PARTICLE RECORDED ALONG THE [011] ZONE AXIS. (B,C) CHROMIUM (GREEN) AND PHOSPHOROUS (WHITE) EDX MAPPING, SHOWING WELL DISPERSED P THROUGHOUT THE Cr-RICH ENVIRONMENT. ADDITIONAL ADF-STEM IMAGES CAN BE FOUND IN APPENDIX 4.3.....	172
FIGURE 9.5 DISTRIBUTION COEFFICIENTS ( $K_D$ ) FOR THE MIL-101-SHIP (RED) AND PRISTINE MIL-101 (BLUE), PROVIDED WITH STANDARD DEVIATIONS (ERROR BARS). $C_0(\text{M}) = 1 \text{ MG/L}$ EACH, $\text{pH}: 4.0$ , $\text{L/S}: 1000 \text{ mL/G}$ , $T = 25^\circ\text{C}$ , $T = 24 \text{ HRS}$ . ....	174
FIGURE 9.6 U(VI) ADSORPTION CAPACITY IN FUNCTION OF THE pH FOR MIL-101-SHIP (RED) AND THE PRISTINE MIL-101 (BLUE). $C_0(\text{U}) = 30 \text{ MG/L}$ , $\text{L/S}: 1000 \text{ mL/G}$ , $T = 25^\circ\text{C}$ , $T = 24 \text{ HRS}$ . ....	175
FIGURE 9.7 U(VI) ADSORPTION ISOTHERM FOR MIL-101-SHIP, FITTED TO THE LANGMUIR MODEL. $\text{pH}: 3.0$ AND $4.0$ , $\text{L/S}: 1000 \text{ mL/G}$ , $T = 25^\circ\text{C}$ , $T = 24 \text{ HRS}$ . AVERAGE VALUE OF DUPLICATES.....	176
FIGURE 9.8 ADSORPTION KINETICS OF U(VI) ON MIL-101-SHIP, FITTED TO THE PSEUDO-SECOND-ORDER KINETIC MODEL. $C_0(\text{U}) = 30 \text{ MG/L}$ , $\text{L/S}: 1000 \text{ mL/G}$ , $T = 25^\circ\text{C}$ , $\text{pH} = 3$ . AVERAGE VALUE OF DUPLICATES. ....	179
FIGURE 9.9 REUSABILITY RESULTS FOR MIL-101-SHIP OVER THREE CONSECUTIVE CYCLES, USING $0.1 \text{ M HNO}_3$ AS REGENERANT. $\text{L/S}: 1000 \text{ mL/G}$ , $T = 25^\circ\text{C}$ , ADSORPTION $\text{pH} = 4.0$ . ....	180
FIGURE 10.1 DIFFERENCE BETWEEN THE CMPO LIGANDS USED IN THE ANCHORING APPROACH (LEFT) AND ENCAPSULATION APPROACH (RIGHT).....	186



## LIST OF ACRONYMS

### A

AAS Atomic absorption spectroscopy

AES Atomic emission spectroscopy

### B

BDC Benzene-dicarboxylate

BET Brunauer-Emmett-Teller

BTC Benzene-tricarboxylate

### C

CDI Carbonyldiimidazole

CHNS Carbon-hydrogen-nitrogen-sulfur

CN Coordination number

CMPO carbamoylmethylphosphine oxide

CRM Critical raw material

CRT Cathode ray tube

CUS Coordinatively unsaturated site

### D

DEHPA Di-2-ethylhexyl phosphoric acid

DETA Diethylenetriamine

DMF Dimethylformamide

DRIFTS Diffuse reflectance infrared Fourier-transform spectroscopy

### E

ED Ethylene diamine

EOL End-of-life

EU European Union

EXAFS Extended X-ray absorption fine structure

### F

FCC Fluid catalytic cracking

FOB	Free on board
<b>H</b>	
HKUST	Hong-Kong University of Science and Technology
HSAB	Hard-Soft-Acid-Base
<b>I</b>	
ICP	Inductively coupled plasma
IUPAC	International Union of Pure and Applied Chemistry
IX	Ion-exchange
<b>J</b>	
JORC	Joint Ore Reserves Committee
<b>L</b>	
LCD	Liquid crystal display
LED	Light emitting diode
LFSE	Ligand field stabilization energy
L/S	Liquid/solid (ratio)
<b>M</b>	
MB	Methylene blue
MG	Malachite green
MO	Methyl orange
MOF	Metal-organic framework
MIL	Matériaux de l'institut Lavoisier
MRI	Magnetic resonance imaging
MTN	Mobil thirty-nine
<b>N</b>	
NiMH	Nickel-metalhydride
<b>O</b>	
OES	Optical emission spectroscopy

## **P**

PCB	Printed circuit boards
PET	Polyethylene terephthalate
PGM	Platinum group metal
PSM	Post-synthetic modification
PVC	Polyvinyl chloride

## **R**

REE	Rare earth element
REO	Rare earth oxide
RGB	Red-green-blue
ROW	Rest of (the) world

## **S**

SBU	Secondary building unit
SF	Separation factor
SX	Solvent-exchange

## **T**

TEA	Triethylamine
TGA	Thermogravimetric analysis
TPDC	p,p'-Terphenyldicarboxylic acid
TRUEX	Trans-uranium extraction

## **U**

UiO	Universitetet i Oslo
UHT	Ultra-high temperature
UV	Ultra-Violet

## **W**

WTO	World Trade Organization
-----	--------------------------

## **X**

XANES	X-ray absorption near edge structure
-------	--------------------------------------

XR(P)D	X-ray (powder) diffraction
XRF	X-ray fluorescence
<b>Y</b>	
YAG	Yttrium-aluminum garnet
YLF	Yttrium-lithium-fluoride
<b>Z</b>	
ZIF	Zeolitic imidazolate frameworks



# 1 INTRODUCTION

## TOWARDS A SUSTAINABLE FUTURE

### 1.1 The Turning Point

You cannot look past it, there is a revolution going on and sustainability is its name. Electrical cars, wind turbines, solar power, wave energy, bio-filtration... Efforts for clean technologies are finally kicking in. It was never our first choice, though, but it is the right one to make. Far too long have we depended on coal, oil, and other fossil fuels to keep us warm and to facilitate every aspect of our lives. Far too long have we depleted the earth's resources with little to no regard for whoever comes after us. But inevitably, all those centuries of mindless consumption have come with a price to pay. Our species stands at a proverbial precipice, but there is still time to turn things around. Change our ways or leave behind a bleak legacy.

It has taken us over 250 years to realize that most of what we have been doing in the name of progress has been affecting our planet in a slow but tenacious way. Ever since that first industrial revolution, we have been acting in a manner that could be best described through Machiavelli's "*Exitus acta probat*"; The end justifies the means. And now, as we approach the third decade of the 21<sup>st</sup> century, we are reaping the fruits of our actions... Climate change, diminishing ecosystems, devastating floods, environmental pollution, land degradation... On top of that, our population is reaching unsustainable levels. More people requiring more resources, which further exhaust our planet's reserves, like a vicious circle.

Luckily, our ways of thinking are gradually shifting for the better and we have committed ourselves to invest in a sustainable future. The major problems have been identified and strategies to counter them are being devised. Renewable energy is said to be the key for this

planet and perhaps future planets to endure, with the sun, the wind, crust and water as our best allies. Inspiring motto without a doubt, but the realization has come that if we want to *live long and prosper* by these words, we need to handle the earth resources in a rational way.

## 1.2 The Ore Called Earth

The earth's crust is full of riches. Gold, silver, diamonds... Those are most obvious. But it is not just the traditional riches that are in the spotlight here. We have found uses for all possible raw materials we have encountered throughout the ages. There is high strength iron that is used for steel constructions, ductile aluminum for our lightweight cars, conductive copper for electrical wiring, anti-corrosive zinc for various alloys and so on. Then there are the more technical materials, less known to the general public. Platinum is used worldwide in vehicle emission control, neodymium is responsible for lightweight magnets in wind turbines, lithium is an indispensable component in rechargeable batteries for phones, laptops, and other portable devices. Germanium is used in fiber-optics, gadolinium is used in X-ray and MRI scanning systems... The list goes on and on.

Ever since prehistoric times, humanity has mined the earth for its resources. Whether it is flint for primitive weapons or nickel for super alloys in spacecraft, the planet has provided and we accepted graciously. But now, about 200,000 years later, we have realized that some of these resources might not be there anymore in the future. Ironically, some of the raw materials we will need most to achieve our sustainable way of living are facing the risk of complete depletion if we do not act in time.

Whereas supply risks of fossil fuels and their impact on economies have been examined for decades[1, 2] only in the recent years have studies appeared that evaluate the criticality of a broad set of nonfuel minerals, and designate some of them as more critical than others[3]. In its 2014 report on critical raw materials for the EU, the European Commission has identified a list of 20 critical raw materials (CRM) which are prone to a higher risk of supply interruption (Table 1.1)[4]. A total of fifty-four non-energy, non-agricultural materials were analyzed and assessed for their economic importance and supply risk (Figure 1.1). All of these raw materials are important to the European economy, and therefore not being critical does not imply that a given raw material and its availability to the economy should be neglected, and that policy actions should not be limited to CRM exclusively[4].

**Table 1.1 Twenty critical raw materials (CRM) for the EU, according to the 2014 Report on Critical Raw Materials [4].**

Antimony	Beryllium	Borates	Chromium	Cobalt	Coking coal	Fluorspar
Gallium	Germanium	Indium	Magnesite	Magnesium	Natural Graphite	Niobium
Platinum Group metals	Phosphate rock	Heavy Rare Earths	Light Rare Earths	Silicon metal	Tungsten	

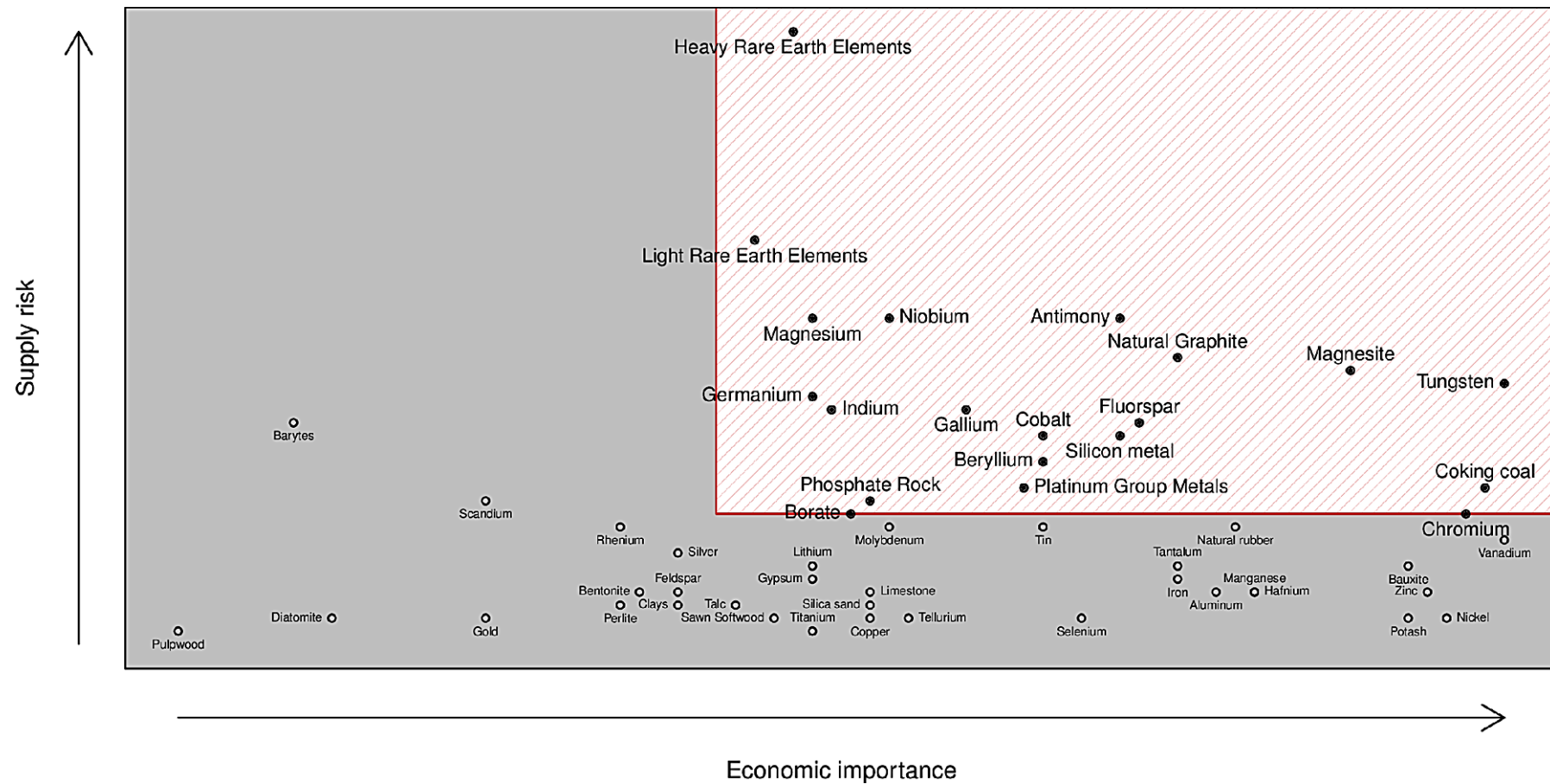
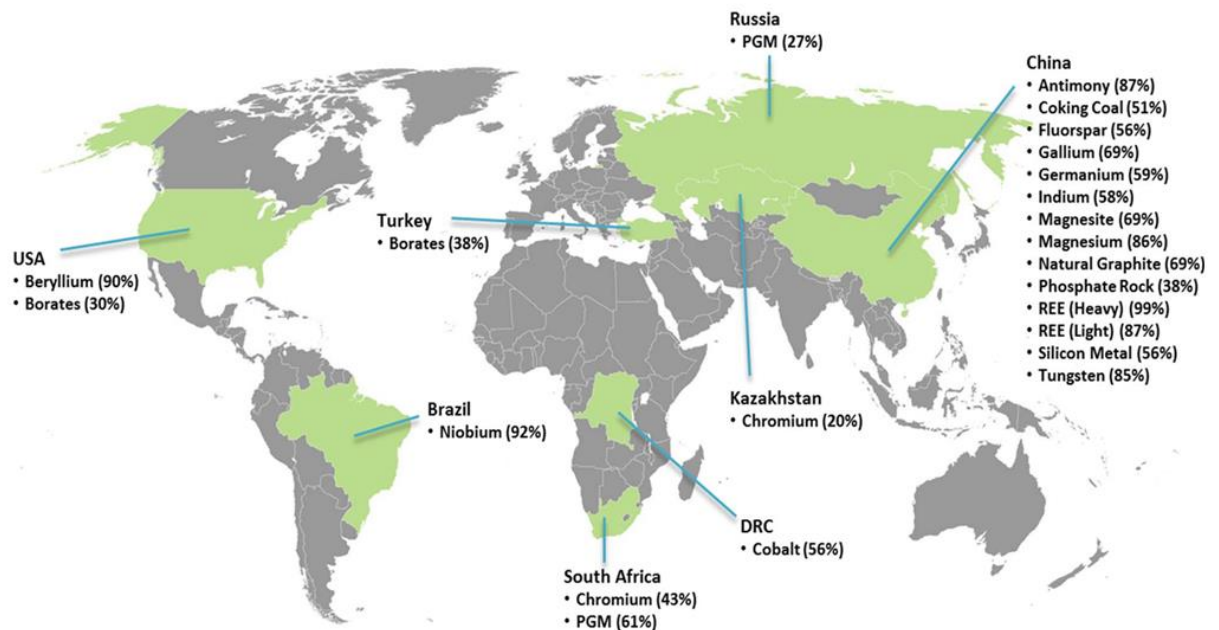


Figure 1.1 Raw materials criticality assessment by the Ad hoc Working Group on defining critical raw materials. The critical materials are highlighted in the red box. (Retrieved from [4])

### 1.3 Resource Nationalism

When defining the criticality of the raw materials, not just the global reserves are taken into account, but geological dispersion as well. Focusing on the 20 CRM from Table 1, the supply from EU sources is very limited[4] and as a result, geopolitics come into play. Of course, trading has been around since the dawn of mankind and will continue to do so, simply because resources are not evenly spread around the globe. It is the backbone of our modern economy. But when supply is at stake, the situation becomes more precarious. An analysis of the world's major suppliers of these critical metals teaches us that China is the most dominant player in the market (Figure 1.2). The country supplies 18 out of 20 CRM and accounts for nearly 50 % of the CRM supply[4].



**Figure 1.2 Worldwide major suppliers of the 20 CRM, according to the 2014 Report on Critical Raw Materials. (Retrieved from [4])**

So not only do we have to deal with gradual resource depletion, but the irregular dispersion of these important materials creates extra tension on their worldwide availability. At the end of the day the simple laws of supply and demand apply, and if valuable resources lie within the borders of your country then you are holding all the cards. It was late Chinese statesman Deng Xiaoping who already in 1987 said: “*The Middle East may have its oil, but we have the rare earths*”, and he could not be more right. When looking at Figure 1.1, the highest supply risk belongs to the rare earth elements (REE). But in addition to these REEs, China is also the main supplier of tungsten, antimony, magnesium, magnesite... each of them with a critical supply

risk and/or high economic importance. So it is safe to say that China is indeed holding all the cards. Luckily there are intergovernmental organizations such as the World Trade Organization (WTO), who regulate international trade and make sure there is a healthy equilibrium between demand and supply. Nonetheless, as recent history has pointed out, a sudden shift in suppliers' trading tactics could have substantial effects on the markets, which forces the requesting parties to review their options.

In 2010, China decided to cut its export quotas for rare earths by 40 %. Although Beijing initially stated that the reduction was a measure to protect the environment and its national resources, the restrictions were widely perceived as China using its control over crucial minerals as a tool of its foreign policy[5]. After a joint complaint by the US, Japan and the EU in 2012, the WTO concluded that China's rare earth policy constituted a violation of international trade law, in which their export quotas were designed to achieve industrial policy goals rather than to mitigate environmental pollution[6]. Despite the intervention of the WTO, the export restrictions had already caused uproar in the markets, resulting in skyrocketing REE prices between 2010 and 2013 (Figure 1.3). In addition, the decision of the WTO has put China under severe pressure. It has to deal with a variety of conflicting interests, such as fulfilling its WTO obligations, satisfying its domestic REE demand, upholding its competitive edge and meeting its own sustainability and environmental protection targets[6].

The above example focuses on rare earths only, but as time passes, other CRM might face the same problems. We can conclude that as resources get scarcer and/or their availability becomes compromised, we need to look for solutions to ensure a steady, sustainable supply.

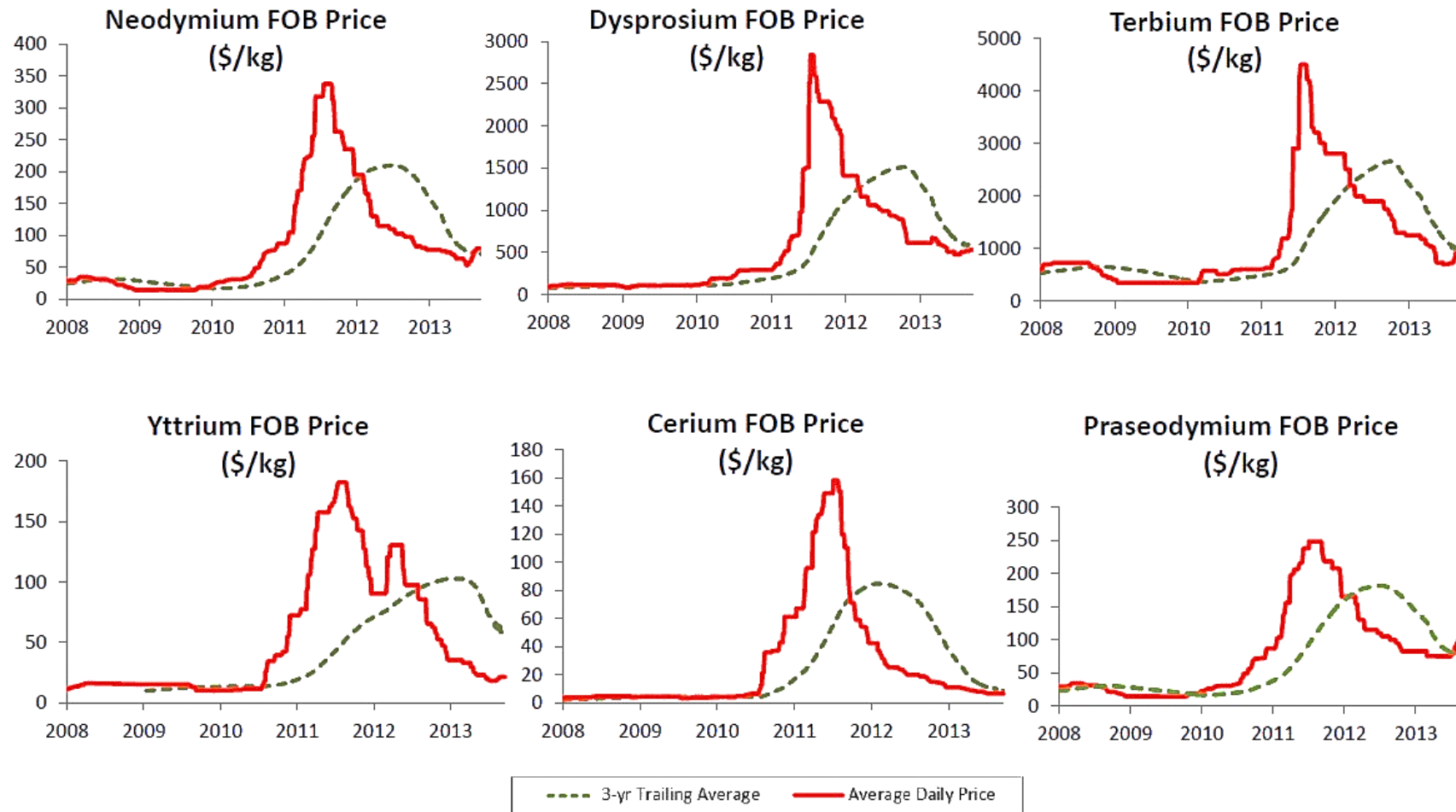


Figure 1.3 Price evolution of several rare earth elements throughout the years (2008 – 2014). (Retrieved from [7])

## REFERENCES

- [1] C.J. Cleveland, An Exploration of Alternative Measures of Natural-Resource Scarcity - the Case of Petroleum Resources in the United-States, *Ecol Econ*, 7 (1993) 123-157.
- [2] R.G. Hubbard, Supply Shocks and Price Adjustment in the World Oil Market, *Q J Econ*, 101 (1986) 85-102.
- [3] L. Erdmann, T.E. Graedel, Criticality of Non-Fuel Minerals: A Review of Major Approaches and Analyses, *Environ Sci Technol*, 45 (2011) 7620-7630.
- [4] Ad hoc Working Group on defining critical raw materials, Report on Critical Raw Materials for the EU (2014).
- [5] J. Ebner, Europe's Rare Earth Dependence on China, European Institute for Asian Studies – Briefing Paper (2014).
- [6] World Trade Organization (WTO), China - Measures related to the Exportation of Rare Earths, Tungsten, and Molybdenum (2014).
- [7] <http://criticalinvestor.eu/rare-earth-elements> (Accessed in 2016).



# 2 RARE EARTHS

## 2.1 The Rare Earth Elements

### 2.1.1 Classification

At the top of the critical elements chart from Figure 1.1, a group of metals is situated called the rare earths elements (REEs). These rare earth elements, or shortly rare earths, are classified by the IUPAC as a group of 17 elements in the third group of the periodic table[1] (Figure 2.1). They include the elements scandium (Sc), yttrium (Y), and the complete lanthanide series, which comprises lanthanum (La), cerium (Ce), praseodymium (Pr), neodymium (Nd), promethium (Pm), samarium (Sm), europium (Eu), gadolinium (Gd), terbium (Tb), dysprosium (Dy), holmium (Ho), erbium (Er), thulium (Tm), ytterbium (Yb), and lutetium (Lu). Rare earths are indispensable in a variety of electronic, magnetic, and optical applications and are key elements to several advanced technologies that are needed in the world's shift to clean and sustainable energy (see Chapter 2.2). Often times, the group of rare earth elements is split into heavy and light REEs, which is also the case in Figure 1.1 from the previous chapter. This is partly based on their respective chemical properties and geological availability, but also upon their market values and respective end-markets[2]. The light REEs are often classified by the elements La to Gd, whereas the heavy rare earths comprise Tb to Lu and Y[3] (Figure 2.1). Yet, the exact transition point between heavy REEs and light REEs is not universally acknowledged and sometimes even an additional medium REE class is created (Pm to Gd)[4].

H																	He		
Li	Be											B	C	N	O	F	Ne		
Na	Mg											Al	Si	P	S	Cl	Ar		
K	Ca	Sc	Ti	V	Cr	Mn	Fe	Co	Ni	Cu	Zn	Ga	Ge	As	Se	Br	Kr		
Rb	Sr	Y	Zr	Nb	Mo	Tc	Ru	Rh	Pd	Ag	Cd	In	Sn	Sb	Te	I	Xe		
Cs	Ba	*	Hf	Ta	W	Re	Os	Ir	Pt	Au	Hg	Tl	Pb	Bi	Po	At	Rn		
Fr	Ra	**	Rf	Db	Sg	Bh	Hs	Mt	Ds	Rg	Cn	Uut	Fl	Uup	Lv	Uus	Uuo		
*			La	Ce	Pr	Nd	Pm	Sm	Eu	Gd	Tb	Dy	Ho	Er	Tm	Yb	Lu		
**			Ac	Th	Pa	U	Np	Pu	Am	Cm	Bk	Cf	Es	Fm	Md	No	Lr		

Light Rare Earth ElementHeavy Rare Earth Element

**Figure 2.1 Situation of the Rare Earth Elements in the periodic table of elements.**

### 2.1.2 Occurrence

Despite the fact that these metals are called *rare* earths, they are actually not that uncommon. Our earth's crust consists of 12 main elements, comprising more than 99% of its mass. These are oxygen (O), silicon (Si), aluminum (Al), iron (Fe), calcium (Ca), magnesium (Mg), sodium (Na), potassium (K), titanium (Ti), hydrogen (H), manganese (Mn), and phosphorous (P)[5]. The REEs are situated in the remaining 1%, but several of them are comparable in abundance to the more commonly regarded elements. For instance, yttrium in the upper continental crust is about as abundant as lithium; cerium's abundance is comparable that of zinc; neodymium and lanthanum are about as abundant as copper, and even dysprosium is about twice as abundant as gold or eight times as abundant as platinum[6]. However, these concentrations are average values, which give a distorted view on REE availability. The problem with rare earths is that they are rather evenly spread throughout the earth's crust, not often forming concentrated deposits[2]. This is in high contrast to elements such as copper or gold which have a higher tendency to aggregate, sometimes to the extent of nugget formation[7]. Moreover, not all rare earths have the same relative occurrence in their deposits, with heavier rare earths being a lot less abundant (on average) than light rare earths[8]. From Table 2.1, it can be seen that cerium is the most abundant REE, while elements such as europium, thulium, and terbium have a relative abundance well under 0.5%. This difference in abundance is significant since the scarcer rare earths are typically in higher demand because of their use in critical applications[2].

**Table 2.1 Average distribution of the individual REEs<sup>1</sup>.**

Lanthanum	24.9%	Europium	0.3%	Erbium	0.5%
Cerium	43.2%	Gadolinium	1.4%	Thulium	0.1%
Praseodymium	4.6%	Terbium	0.2%	Ytterbium	0.4%
Neodymium	16.2%	Dysprosium	0.9%	Lutetium	0.1%
Samarium	2.2%	Holmium	0.2%	Yttrium	4.9%

Rare earths typically occur in a wide range of mineral types including halides, carbonates, oxides, phosphates and silicates. Around 200 minerals are known to contain REEs, but only a small amount of them are commercially interesting[9]. The major minerals for REE production are bastnaesite, monazite, xenotime, and ion adsorption clays[7]. In the former three minerals, the REE content (expressed as percentage rare earth oxide, %REO) can be well over 60%[9]. However, these are figures based upon the minerals themselves. It must be noted that primary REE deposits generally contain only a fraction of these REE rich minerals, and that rare earths are mined from these deposits as a byproduct (~0.1 – 10 % REO) to main elements such as iron, gold, uranium, titanium, and zinc[9, 10]. Besides the conventional ores, the ion-adsorption clays are a relatively new class of REE deposits, but they are highly interesting due to their high relative content of heavy REEs[11]. These clays are the results of lateritic weathering<sup>2</sup> of REE-rich host rocks, forming aluminosilicate clays over time. These fine clay mineral particles have the capability of adsorbing lanthanide ions released/dissolved during weathering[12]. As a surplus, they contain only very small amounts of radioactive elements, which often pose an issue in REE mining (see Chapter 3). In contrast to the primary deposits, the ion-adsorption clays are fairly low graded REE sources (typically 0.03 – 0.35% REO[13]). Despite this limited REE concentration, the clays have the advantage of simpler and more economically attractive mining methods than used in conventional ore processing, making them the current main source of heavy rare earths in the world[12]. An extensive overview on the mineralogy, mining, and processing of rare earths element can be found in the *Commodity Profile on Rare Earth Elements*, by the British Geological Survey[9].

—

<sup>1</sup>Values calculated from REE grades across 51 deposits reported in the resources and reserves by companies that publish these figures according to the JORC, NI-43-101 or comparable reporting standards[2].

<sup>2</sup>Formation of a surface layer onto iron- and aluminum-rich clay minerals, as a result of intensive tropical weathering over a long time span.

### 2.1.3 REE Supply in Jeopardy?

In Chapter 1, China's dominance in the production of rare earths was already portrayed. The country owns the biggest primary deposits in the world[9], as well as several secondary deposits, including all of the adsorption clay deposits, which are situated throughout southern China[13]. These clay deposits account for ~35% of China's total REE production[14]. Yet, despite their quasi-monopoly in REE production, China is estimated to possess less than 40% of the proven global REE reserves[15]. A conclusion could be drawn that mining for rare earths is a business that is often times only feasible if: (a) the rare earths are mined from primary deposits, and (b) they are mined from these deposits as a by-product. The prevailing market value of the rare earths is generally not enough to support the mining and production cost of the current state-of-the-art processes[10]. China has got all the advantages, namely high grade deposits, economically attractive by-product mining (or primary mining from adsorption clays), and rather lenient environmental and labor policies compared to the West[16]. On top of that, no country other than China has enough expertise or manufacturing facilities to refine the rare earth oxides to their respective metals. We have reached a point where it is often times more economical to export the minerals to Chinese factories than to do the REE processing in the country of origin. China aims for the entire supply chain, from mining to the end products, to be based in its country, and it is succeeding in this strategy[7].

In the previous chapter, the panicking effect of the cut in export quotas on rare earth prices was illustrated. However, in essence, higher REE prices would be advantageous, providing that no sudden restrictions on Chinese export would be enforced again. With higher REE prices, there is more incentive for companies (worldwide) to start or restart the mining and processing of rare earths; More money becomes available to invest in environmentally friendly mining techniques; Higher prices may render economical recycling possible[7]. Still, prices for most rare earths markets remain at historical lows, mainly because the panic that was caused by the export cuts in 2010 also lead to large leftover REE stockpiles from the sudden price spike that followed. In addition, China's illegal rare earth production, which is calculated to account for 25-30% of the annual global REE supply[17], has also weighed heavily on market prices in recent years[18].

All things considered, it is difficult to predict what the future of REE supply will look like. The 2016 Roskill - Rare Earth Market Outlook suggests that the following ten years, China will continue to dominate the market, although with a slightly weakened position, as current mining operations in the rest of the world (ROW) will increase production. The continuing low REE prices in the next decade will, however, discourage investments in new projects. On its end, China has committed to tackle the illegal mining problem via the introduction of a raw material tracing system and thorough prosecution laws for illegal practices[17]. At the same time, various sources suggest that the Chinese government should shift from controlling the export to controlling production to improve the pricing power of China's rare earths[19, 20]. Each of

these factors, and many more undiscussed, will have their impact on the future of rare earth supply, and by extension rare earths prices. Assessing this future in a comprehensive manner is a complete study on its own, and is therefore not included in this work. The predominant sentiment is that the demand for rare earths will increase in the distant and/or near future[2, 7, 15, 21]. The EU expects a climbing demand as its 2020 goals on lowering the use of fossil fuels will increase the need for hi-tech devices and green technologies (electric cars, solar panels, windmills...)[22]. The main question will be whether or not the global production can keep supporting the global demand, and if so, for how long?

## 2.2 What Makes Rare Earths So Special?

It is often said that rare earths play a major role in the evolution towards clean, sustainable energy, and that several REEs are indispensable in the design and operation of the devices that are responsible for these new technologies. The following section concisely outlines the characteristics of the rare earths, and more specifically the lanthanides, on a physical and chemical basis and explains why these elements play such a unique role in their applications. A more elaborate overview on rare earth structure and properties can be found in *The Chemistry of Lanthanides* by Moeller[23].

### 2.2.1 The 4f-elements

Rare earths include the lanthanide series, plus the elements yttrium and scandium. The latter two are often grouped with the REEs since they tend to occur in the same ore deposits as the lanthanides and/or have similar chemical properties. The lanthanides, however, are a very peculiar series of metals. Their overall properties suggest that they are members of the III-b subgroup of the periodic table (Figure 2.2)[24]. The elements in this subgroup are usually the first of four *d*-type transition series, which are characterized by a gradual filling of the first available *d*-levels. Indeed, the ground-state electronic configurations throughout subgroup III-b (Sc, Y, La, Ac) seem to follow a logical pattern  $((n-1)d^1(n)s^2)$  (Table 2.2). However, while for scandium and yttrium the transition series are indeed characterized by a gradual filling of the 3*d* (Sc → Cu) and 4*d* (Y → Ag) subshells, respectively, the situation changes for lanthanum (and the actinide actinium).

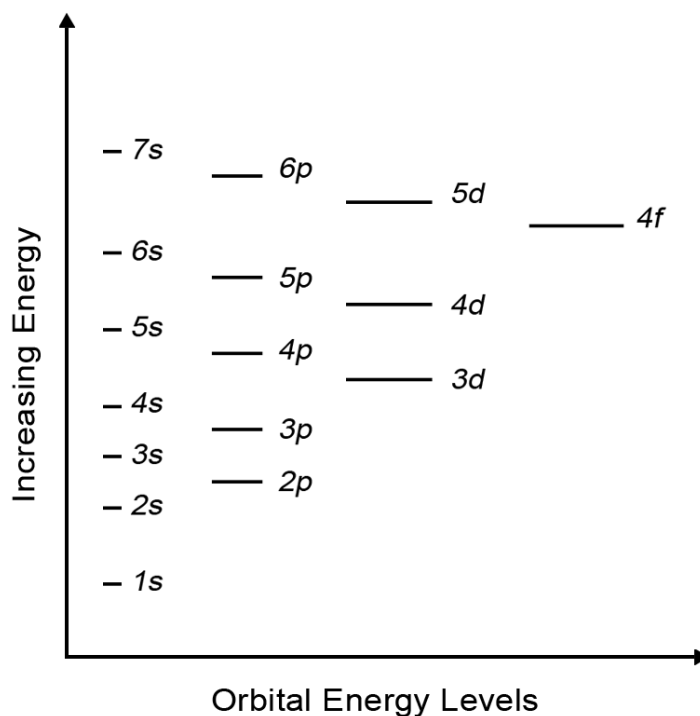
<b>Mg</b>											
24.30	IIIb	IVb	Vb	VIb	VIIb	<-----VIII----->			Ib	IIb	
20	21	22	23	24	25	26	27	28	29	30	
<b>Ca</b>	<b>Sc</b>	<b>Ti</b>	<b>V</b>	<b>Cr</b>	<b>Mn</b>	<b>Fe</b>	<b>Co</b>	<b>Ni</b>	<b>Cu</b>	<b>Zn</b>	
40.08	44.96	47.90	50.94	52.00	54.94	55.85	58.93	58.69	63.55	65.39	
38	39	40	41	42	43	44	45	46	47	48	
<b>Sr</b>	<b>Y</b>	<b>Zr</b>	<b>Nb</b>	<b>Mo</b>	<b>Tc</b>	<b>Ru</b>	<b>Rh</b>	<b>Pd</b>	<b>Ag</b>	<b>Cd</b>	
87.62	88.91	91.22	92.91	95.94	(98)	101.1	102.91	106.42	107.87	112.41	
56	57	72	73	74	75	76	77	78	79	80	
<b>Ba</b>	<b>*La</b>	<b>Hf</b>	<b>Ta</b>	<b>W</b>	<b>Re</b>	<b>Os</b>	<b>Ir</b>	<b>Pt</b>	<b>Au</b>	<b>Hg</b>	
137.33	138.91	178.49	180.95	183.85	186.21	190.2	192.2	195.08	196.97	200.59	
88	89	104	105	106	107	108	109	110	111		
<b>Ra</b>	<b>†Ac</b>	<b>Rf</b>	<b>Db</b>	<b>Sg</b>	<b>Bh</b>	<b>Hs</b>	<b>Mt</b>	<b>Ds</b>	<b>Rg</b>		
226.02	227.03	(261)	(262)	(266)	(264)	(277)	(268)	(271)	(272)		

**Figure 2.2** Group III-b of the periodic table of elements. (\*, † marking the start of the lanthanide and actinide series, respectively)

**Table 2.2** Ground-state electronic configurations of the elements of subgroup III-b.

Element	Z	Configuration
Sc	21	[Ar]3d <sup>1</sup> 4s <sup>2</sup>
Y	39	[Kr]4d <sup>1</sup> 5s <sup>2</sup>
La	57	[Xe]5d <sup>1</sup> 6s <sup>2</sup>
Ac	89	[Rn]6d <sup>1</sup> 7s <sup>2</sup>

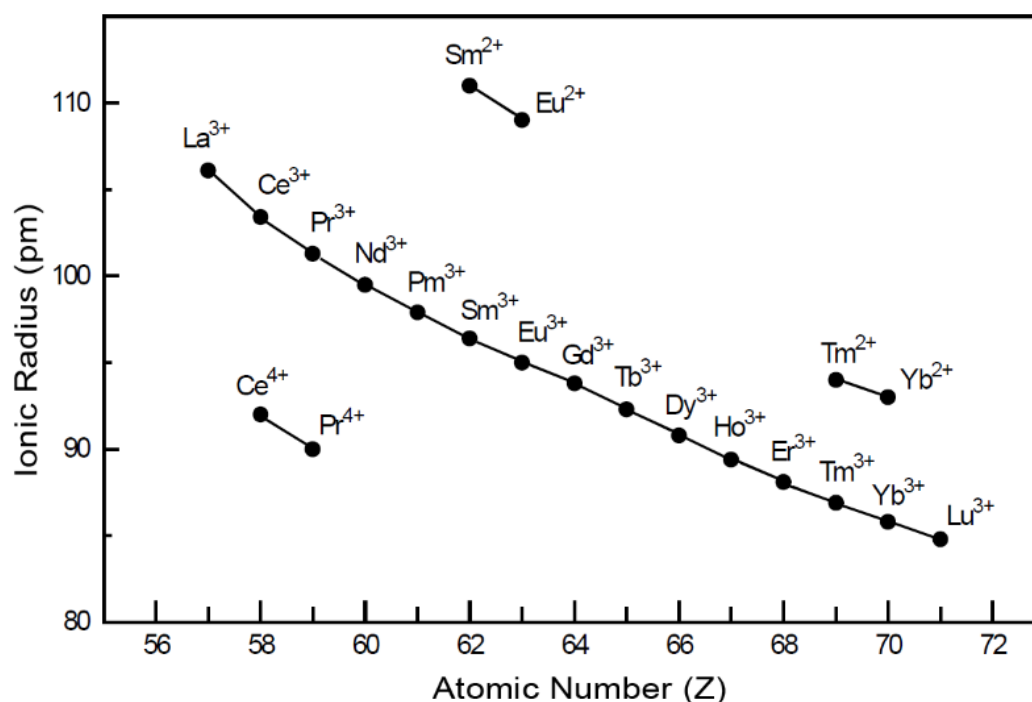
After lanthanum, the energy of the 4*f* subshell falls below that of the 5*d* level (Figure 2.3). As a result, electrons are first added to the 4*f* orbitals, which must be filled completely before the 5*d* orbitals can be used[24]. Hafnium ([Xe]4*f*<sup>14</sup>5*d*<sup>2</sup>6*s*<sup>2</sup>), which comes after lutetium ([Xe]4*f*<sup>14</sup>5*d*<sup>1</sup>6*s*<sup>2</sup>), is therefore a strict analog of zirconium ([Kr]4*d*<sup>2</sup>5*s*<sup>2</sup>), and is thus placed under zirconium in the IV-b subgroup of the periodic table (Figure 2.2). As the 4*f* subshell can hold seven pairs of two electrons, 15 lanthanide elements exist (if we include lanthanum (4*f*<sup>0</sup>)), which are grouped in a separate *f*-type transition series in the periodic system, for clarity reasons. The actinides series are built up analogously and are found below the lanthanides.



**Figure 2.3 Energy levels of different subshells within an atom.**

The lanthanides are therefore known as  $4f$ -elements and the gradual filling of this  $4f$ -subshell is what makes them unique as elements and attributes greatly to their optical and magnetic properties. More importantly, the  $4f$  electrons are well shielded by higher electron shells ( $5s$ ,  $5p$ ...) which makes them generally unhindered by chemical interaction with neighboring atoms or ions. This is in great contrast to the  $d$ -type transition elements, where the  $d$ -electrons are valence electrons which are involved in chemical interaction[24].

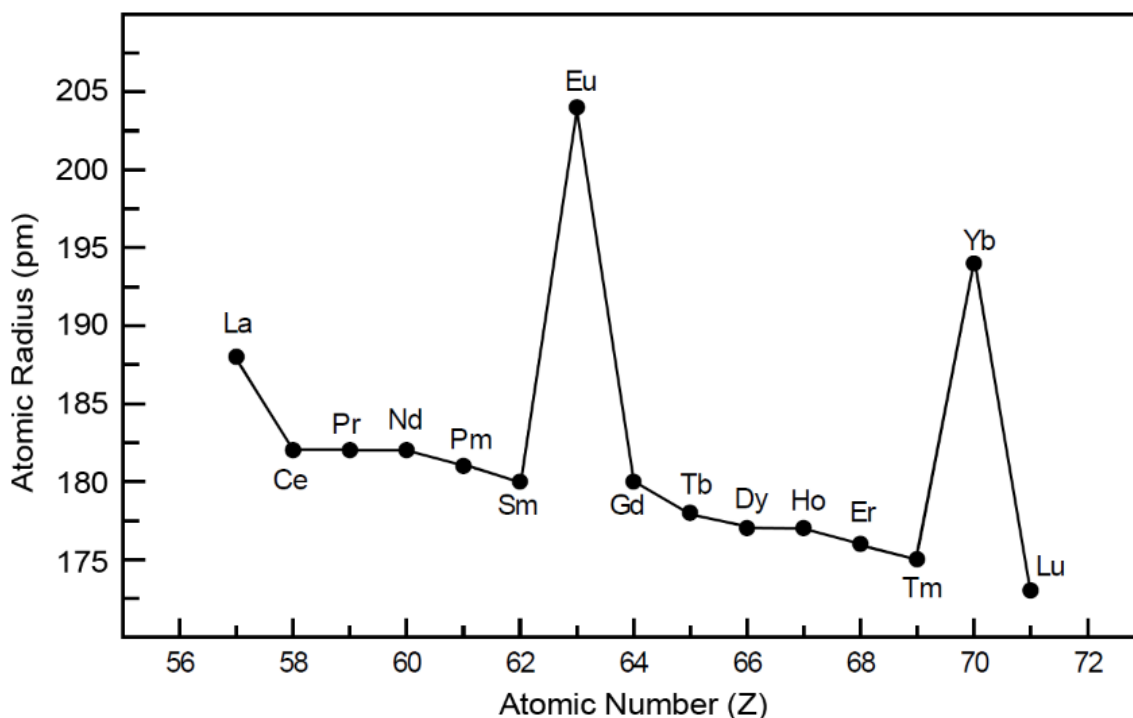
In most common compounds, lanthanides have the trivalent oxidation state. Exceptions with a high enough chemical stability are  $\text{Eu(II)}$ ,  $\text{Yb(II)}$  and  $\text{Ce(IV)}$ . It is concluded that this predominant trivalent state is the result of a somewhat fortunate combination of ionization- and hydration energy (in solution) or ionization- and lattice energy (in solid compounds) rather than to any specific electronic configuration[9, 24]. Another interesting phenomenon is the so-called *Lanthanide Contraction*. A gradual decrease in ionic radii is observed when going through the lanthanide series from La to Lu (Figure 2.4). This is because the electrons in the  $4f$  subshell are unable to properly shield the outer electrons ( $5s$ ,  $5p$ ) from an increasing nuclear charge. This results in a gradually decreasing ionic radius, which is clearly visible for the trivalent ions and, to some extent, for the other valences as well.



**Figure 2.4** Ionic radii throughout the lanthanide series, demonstrating lanthanide contraction.

When looking at the lanthanides' atomic radii, a similar trend can be observed (Figure 2.5) for the same underlying reasons. However, in this series the atomic radii of Eu and Yb are considerably larger than for the other lanthanides. This can be attributed to the metallic state of these elements. In their crystal lattices, the lanthanides are packed together and, while their 4*f* electrons generally remain localized, the outer 5*d* and 6*s* electrons become delocalized, extending throughout the metal as conductive electrons. In Eu and Yb, the intra-atomic interactions make it favorable to (half) fill the 4*f* subshell for extra stability by transferring an electron from the conduction bands to an *f* state. Since the *d* electron is predominantly used to obtain this state, Eu and Yb have a tendency to be divalent in their metallic state (two delocalized 6*s* electrons). The transfer of this *d* electron, whose binding contribution to the electronic pressure is thereby reduced, causes a substantial increase in the atomic volume[25]. In contrast to Eu and Yb, Ce appears to have a slightly smaller radius than expected. This might suggest a preferential tetravalent state, where a 4*f*-electron is delocalized as well, i.e.,  $4f^1 5d^1 6s^2 \rightarrow 4f^0$ .





**Figure 2.5 Atomic radii throughout the lanthanide series.**

Regardless these occasional differences in size and oxidation state, the rare earths (at least the lanthanides and yttrium) are very similar, which means they can substitute for one another in crystal structures. This results in multiple lanthanides occurring within the same minerals[26]. Hence, the challenging separation. Yet, it is due to this small, but notable difference in size (*lanthanide contraction*) that rare earths are in fact able to be separated by fractional means, as small differences in size (with identical trivalent oxidation state) lead to slight differences in acidic (or basic) character, which is reflected in e.g., ion hydrolysis, salt solubility, thermal oxide-stability, and complex formation[27]. As the ionic radii of REEs are typically larger than those of common rock-forming elements (Al, Cr, Fe, S...), the REEs cannot be built into the crystal structures of general rocks[28], which explains why rare earths are not widely available in rich deposits (cfr. Section 2.1.2).

### 2.2.2 Physical Properties

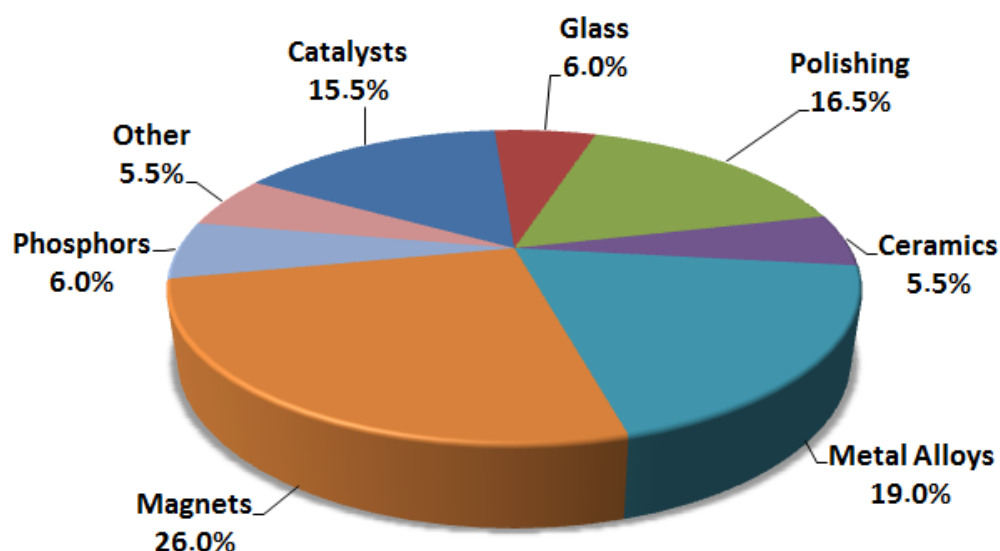
As mentioned before, the well shielded 4f electrons of lanthanides are the foundation of their remarkable magnetic and optical properties. All trivalent rare earth cations, except for  $\text{Sc}^{3+}$ ,  $\text{Y}^{3+}$ ,  $\text{La}^{3+}$ , and  $\text{Lu}^{3+}$ , are paramagnetic, which means they have unpaired electrons. Without going into too much detail on the theoretical physics behind magnetic character, it is important to note that each paramagnetic<sup>1</sup> substance has its own characteristic permanent magnetic moment[24]. The general conception is that the more unpaired electrons a substance possesses, the higher the magnetic moment is, and thus, the stronger the magnetic properties are. This is indeed the case for *d* elements, in which  $d^5$  complexes show the highest magnetic moments (five unpaired

electrons). However, once again, the lanthanides form an exception as their unpaired electrons orbit around the core within the protected  $4f$  subshell. For a typical atom or ion, the magnetic moment consists of two components, namely the orbital-angular moment and spin-angular moment. As mentioned before, the  $d$  electrons of a typical  $d$  element are valence electrons, which means that they take part in bond formation. In a bonded state, e.g., a complex, the orbital contribution of these unpaired  $d$ -electrons is therefore quenched because of the interaction with bonded moieties. As a result, the magnetic moment of such  $d$ -element substances, is mainly the result of electron spin[24]. In the case of lanthanides, the unquenched orbital component of shielded, unpaired  $f$ -electrons adds greatly to their magnetic moments and introduces very interesting anisotropic<sup>2</sup> properties. This has led to several rare earths being of high importance to various hi- and low-tech magnetic applications. In the 1960s it started with the use of powerful samarium-cobalt based permanent magnets, however, throughout the 1980s the neodymium-iron-boron magnets were introduced and have now largely replaced their counterparts[26]. These Nd-Fe-B magnets possess a magnetic energy up to 2.5 times greater than the Sm-Co analogues and are a lot cheaper as they are high in iron content (>60 wt.%) [10]. Because these rare earth based magnets are so powerful, they can be produced in smaller sizes than conventional magnets, which allows for considerable miniaturization of applications. In addition to their widespread use in common consumer goods, such as hard disks, smartphones, speaker systems, and disk drives, the REE magnets are key elements in green, carbon-reducing technologies[9]. For instance, wind turbines have enormous alternators inside them, containing several hundreds of kilograms Nd-based magnets. These magnets are also essential in the motors and generators of hybrid and electrical cars, in addition to many other REE-based components. REE magnets account for over ~20% of the world's rare earth demand, resulting in the biggest market of rare earth applications (Figure 2.6). It is also the fastest growing REE market, to such an extent that the demand for neodymium is beginning to outstrip its supply[17].

—

<sup>1</sup>A paramagnetic material is only magnetic when placed in a magnetic field.

<sup>2</sup>Magnetic anisotropy is the directional dependence of the magnetic properties of a material.



**Figure 2.6** World 2015 REE demand by application, as projected by IMCOA. (Data retrieved from [21])

Another important physical property of trivalent lanthanide ions is their photoluminescence. Upon irradiation with UV-light, several lanthanide ions exhibit luminescence in the visible or near-infrared light[24]. The emissions are due to transitions inside the  $4f$ -shell (intra-configurational  $f-f$  transitions), and because this shell is so well shielded from the environment, bonding groups, e.g., ligands, perturb the electronic configurations of the trivalent lanthanide ions only to a very limited extent[29]. As a consequence, the ions behave more or less as free ions, resulting in very narrow, almost line-like emission spectra. These narrow spectra are characteristic to no other ionic species (except for the related actinides)[24]. Several lanthanides are therefore particularly useful in optical technologies. An important market is the phosphor market. Phosphors are used in various display devices, such as LCD or plasma screens in televisions or computer monitors, but also in fluorescent lamps, LED technology, and solar cells. Basically, these phosphors are luminescent materials which absorb radiation (UV-light, x-rays, electrons...) and emit light of a different wavelength. They are typically solid, inorganic materials consisting of a host lattice (oxide, nitride, silicate...), doped with impurities (such as rare earths or transition metals)[30], for example Eu doped  $Y_2O_3$  ( $Y_2O_3:Eu$ ) or Mn doped  $Zn_2SiO_4$  ( $Zn_2SiO_4:Mn$ ). The emission generally originates from these dopants. In many cases, rare earth phosphors dramatically improved the performance of the devices in which they are applied[31]. For instance, in television screens, europium-yttrium based phosphors are typically used to generate a red color, while terbium-fluoride-zinc sulphide compounds generate a green color and cerium-strontium sulphide have emission of blue light[9]. Each phosphor represents a primary color (RGB) and combined they can emit any desired color. In these display-type applications the phosphors are excited by electron beams. In the case of fluorescent lamps, the

phosphors that cover the glass inner surface are irradiated by UV light, which is typically emitted by an excited mercury source. A combination of several phosphor types in the lamp coating generate an almost perfect copy of daylight upon irradiation. REE-based phosphors are also used in white LEDs, which are 80% more efficient than conventional incandescent lighting[9].

With all these applications in mind, it is clear that the rare earths are a truly unique group of elements of which the properties, both physical and chemical, attribute greatly to the advanced technologies that we use today. Besides the illustrated magnetic and optical applications, REEs also have major applications in several other domains, such as catalysis, glass technology, metal alloys... (Figure 2.6) These will not be further discussed in this work, but a comprehensive list is provided in Table 2.3 as well as the distribution of rare earth use by application in Table 2.4.

**Table 2.3 Applications per rare earth element**

La	<ul style="list-style-type: none"> <li>· Nickel metal hydride batteries</li> <li>· Hydrogen storage alloys <math>\text{LaNi}_3</math></li> <li>· Alloying agent</li> <li>· Optical lenses</li> <li>· Host for phosphors</li> <li>· Petroleum fluid catalytic cracking (FCC)</li> <li>· Cathode material in solid oxide fuel cell</li> </ul>	Dy	<ul style="list-style-type: none"> <li>· Additive to <math>\text{Nd}_2\text{Fe}_{14}\text{B}</math> permanent magnets to improve high-temperature performance, increase coercivity</li> <li>· Phosphors</li> <li>· Nuclear industry - radiation shielding</li> </ul>
Ce	<ul style="list-style-type: none"> <li>· Automotive catalysts</li> <li>· Petroleum fluid catalytic cracking (FCC)</li> <li>· Glass additives</li> <li>· Decolorizer, opacifier</li> <li>· Ultraviolet light absorption</li> <li>· Polishing media for glass, lenses, semiconductors</li> <li>· Phosphors</li> </ul>	Ho	<ul style="list-style-type: none"> <li>· Metal halide lamps</li> <li>· YIG (yttrium-iron-garnet) lasers</li> <li>· YAG and YLF solid-state lasers</li> </ul>
Pr	<ul style="list-style-type: none"> <li>· Additive to <math>\text{Nd}_2\text{Fe}_{14}\text{B}</math></li> <li>· Pr-stabilized <math>\text{ZrO}_2</math></li> <li>· Coloring agents</li> <li>· Glass blower's and welder's goggles (with Nd)</li> <li>· Telecommunication systems as dopant in fluoride fibers</li> </ul>	Er	<ul style="list-style-type: none"> <li>· Fiber optics - signal amplifiers</li> <li>· Lasers (mainly medical/surgical and dental use)</li> <li>· Coloring</li> </ul>
Nd	<ul style="list-style-type: none"> <li>· <math>\text{Nd}_2\text{Fe}_{14}\text{B}</math> permanent magnets</li> </ul>	Tm	<ul style="list-style-type: none"> <li>· X-ray intensifying screens</li> </ul>

	<ul style="list-style-type: none"> <li>· Alloying agent for Mg alloys</li> <li>· Lasers</li> <li>· Metal halide lamps</li> </ul>		<ul style="list-style-type: none"> <li>· Metal halide lamps</li> </ul>
Sm	<ul style="list-style-type: none"> <li>· SmCo permanent magnets</li> <li>· Coloring agent</li> <li>· Phosphors</li> <li>· Nuclear industry radiation shielding</li> </ul>	Yb	<ul style="list-style-type: none"> <li>· Optical lenses</li> <li>· Pressure sensors (metal)</li> </ul>
Eu	<ul style="list-style-type: none"> <li>· Phosphors (red colors)</li> <li>· Nuclear industry radiation shielding</li> </ul>	Lu	<ul style="list-style-type: none"> <li>· Host for scintillator detectors and X-ray phosphors</li> </ul>
Gd	<ul style="list-style-type: none"> <li>· Host for phosphors</li> <li>· MRI contrast agents</li> <li>· X-ray intensifying screen</li> <li>· Laser YGG (yttrium-gadolinium-garnet)</li> </ul>	Sc	<ul style="list-style-type: none"> <li>· High-performance alloys</li> <li>· Lasers</li> <li>· Phosphors</li> <li>· Ceramics</li> </ul>
Tb	<ul style="list-style-type: none"> <li>· Phosphors (green)</li> <li>· X-ray intensifying screens</li> <li>· Magneto-restrictive alloy</li> </ul>	Y	<ul style="list-style-type: none"> <li>· Host for phosphors</li> <li>· YAG laser host material</li> <li>· YBa<sub>2</sub>CuO<sub>2</sub> high-temperature superconductor</li> <li>· Alloying agent</li> </ul>

List not all-inclusive. Retrieved from [7].

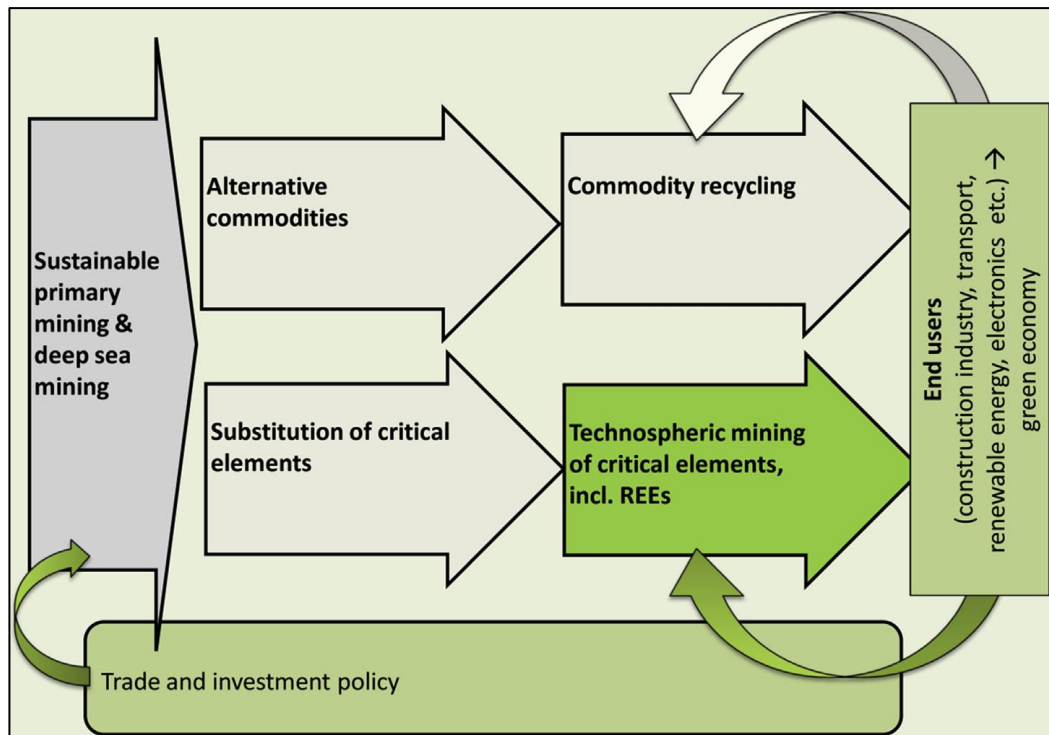
**Table 2.4 Rare earths usage by application, in %**

<b>Application</b>	<b>La</b>	<b>Ce</b>	<b>Pr</b>	<b>Nd</b>	<b>Sm</b>	<b>Eu</b>	<b>Gd</b>	<b>Tb</b>	<b>Dy</b>	<b>Y</b>	<b>Other</b>
Magnets			23.4	69.4			2	0.2	5		
Battery alloys	50	33.4	3.3	10	3.3						
Metallurgy	26	52	5.5	16.5							
Auto catalysts	5	90	2	3							
FCC	90	10									
Polishing powders	31.5	65	3.5								
Glass additives	24	66	1	3						2	4
Phosphors	8.5	11				4.9	1.8	4.6		69.2	
Ceramics	17	12	6	12						53	
Others	19	39	4	15	2		1		19		

Retrieved from [32].

## 2.3 One Man's Garbage...

The uncertainty regarding the future supply of rare earths forces us to explore other methods than primary REE production, to achieve and/or maintain the critical technologies used in our current and future society. To tackle the REE supply challenge, a threefold approach was proposed in the work of Binnemans *et al.*[15], including substitution, sustainable mining, and recycling (*vide infra*). This approach is to be part of a comprehensive raw materials policy, also including thorough commodity recycling and the development of lower eco-impact consumer goods (Figure 2.7).



**Figure 2.7 Comprehensive raw materials strategy, targeting a diversified approach: primary mining, substitution, raw materials diplomacy and technospheric mining and recycling. (Retrieved from [15])**

### 2.3.1 Substitution

A first component of this strategy is to substitute critical rare earths by less critical metals. For most rare earths, no direct substitutes are available, i.e., element for element. However, in several cases systemic substitutes are on the market. In the case of Nd-Fe-B magnets, no direct replacement of Nd or Pr is known. On a systems level other magnet types are available but most do not reach the strength of Nd-Fe-B-type magnets or cannot be miniaturized enough with the same performance[7]. For over 20 years, scientists have been trying to find an alternative for the Nd-Fe-B magnet, with no success[33]. A similar problem is observed in the phosphor industry where no potential substitutes are currently available for phosphors in lighting technologies. However, the invention of the LEDs has at least been able to reduce the required phosphor quantities[7]. In the field of rare earth based batteries, i.e., NiMH-type batteries, there is a worthy competitor, namely the Lithium-ion technology. These batteries have higher energy densities (resulting in smaller sizes), faster recharging, no memory effect, less discharging, and longer power availability[34]. In general, most applications would require a completely new systemic design to achieve technologies that are, at best, competitive to the ones based on REEs. Research on such a scale (from theory to application), requires many years of work, while in most cases, the REE-based applications remain superior. Besides, as in recent years the

REE market has been in over-supply (cfr. Section 2.1.3), the incentive to invest in substitute technologies has been rather limited[9].

### 2.3.2 Sustainable Mining

Substitution, although a viable side path for the future, is not the main solution to tackle the rare earth supply challenge. For the foreseeable time, we will depend on these REEs and therefore, other ways of safeguarding the supply must be introduced. A second component of raw materials policy focuses on sustainable mining of REE deposits[15]. The sustainability aspect makes this a very delicate business, however. It is generally known that mining for precious resources poses an environmental hazard. Toxic tailings can take over ponds and soil can be rendered unfit for farming, because of the concentrated acids that are used to leach ores. Each pound of rare earth mined results in outputs of hundreds or thousands of pounds of waste, experts claim[35]. Another important factor is the radioactivity related to several ores, which will be discussed further in this work. The development and application of sustainable mining techniques could reduce the environmental impact considerably, but the economic factor plays a key role in this. As long as rare earth prices remain low, the viability of sustainable mining projects is limited. Still, noticeable effort is being made to control the impact of the rare earth industry on the environment, even in China. As mentioned before, environmental regulations are rather lax there, and most of the mines still pose significant hazards because of the chemicals used in REE processing. It has been reported that the refinement of one ton of rare earth oxide can produce up to 60,000 m<sup>3</sup> of acidic waste gases, 200 m<sup>3</sup> acidic water, and 1.4 tons of radioactive waste[36]. China is increasingly becoming aware of the impact on its environment and has therefore taken steps to improve overall efficiency and environmental performance of REE production, including the shutdown of several production facilities[9]. Yet, once again, it must be noted that China can afford these kinds of measures, since it controls the REE market. Sustainable mining operations in the ROW continue to be a challenging venture. A fitting example for this is the case of the Mountain Pass mine in California, owned by Molycorp. The mine was once the main supplier of rare earths (1960s – 1980s, the *Mountain Pass Era*), but had to close in 2002 because of environmental restrictions and low REE prices[37]. Following the price spike around 2010 and the resulting global fear for supply risks, Molycorp was one of the companies that revived their REE mining business (around 2012). The use of new mining, separation, and refining technologies allowed an environmentally sound production[7]. Yet today, as prices are once again low, several of these companies struggle with huge financial deficits, to such an extent that Molycorp had to file for Chapter 11 bankruptcy in 2015. It is therefore understandable that when even primary REE mines in the ROW struggle to run a cost-effective operation with sustainable techniques, the incentives to (sustainably) produce rare earths from a lesser grade deposit are very low (remember by-product mining as well).



### 2.3.3 Recycling

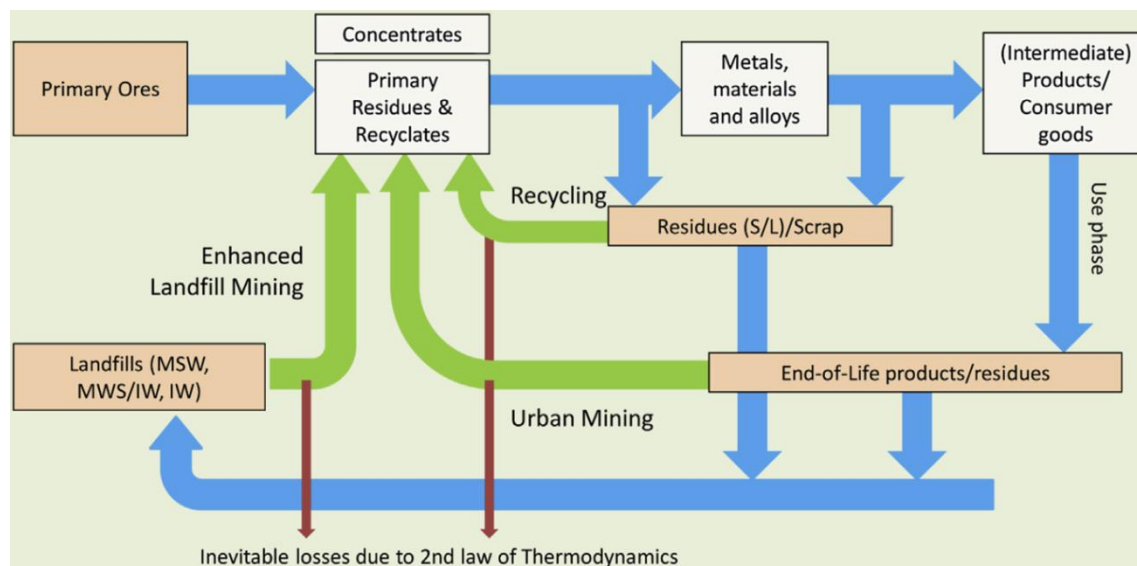
The third segment of the REE supply-tackling approach is recycling. Because of their widespread use, rare earths end up in a vast amount of consumer goods, i.e., cars, lamps, computers, smartphones, televisions... As a result of our consumption oriented society, as well as the high rate of technological improvement, we switch to new devices rather quickly. As a consequence, the replaced consumer goods are disposed of and end up in junkyards, landfills, or simply remain in our drawers and attics. The commodities that do end up in a recycling process are mainly in there to retrieve important base and noble metals (Ni, Cu, Ag, Au...). The REEs usually end up in slags or residues, which are often used as raw construction material, or they get stored in landfills[7]. The reason for this is that rare earth recycling is not as easy as, for instance, recycling soda cans or plastic. For one thing, REEs are present in most of their applications in very small quantities. Also, the continuous miniaturization of electronics, as well as large differences in systemic designs, complicate the situation even further. Specific dismantling techniques and sustainable separation processes come with a high economical cost, and because of the limited prevailing market value of rare earths, there is not a lot of incentive to invest in proper REE recycling. As a result, a lot of commodities, such as electronic waste (e-waste) usually get recycled via conventional crushing, shredding and grinding processes[38], after which the economically interesting metals are recovered from the obtained powders and the remaining fraction goes to waste or storage. Retrieving the (small) rare earth fraction from such powders is often very difficult and uneconomical because of the high variety of elements in the devices. An average smartphone, for instance, can contain up to 62 different types of metals, including most, if not all of the rare earths (except Pm)[39]. Recovering rare earths from such complex powders is said to be more difficult than from raw ore, often requiring more energy and a wider variety of (aggressive) chemicals[9, 38].

In 2013, a critical review on the recycling of rare earths concluded that in 2011 **less than 1%** of the REEs were commercially recycled, despite a vast existence of literature dealing with the subject (mostly lab scale research)[15]. This was attributed to the above mentioned complications, i.e., inefficient collection, technological difficulties, and lack of incentives. Yet, there is a huge potential hidden inside the recycling of REE containing commodities, especially from the so called End-of-Life (EOL) electronic waste. According to the United Nations, the world produced approximately 50 million tons of e-waste in 2012 and this is expected to increase on a yearly basis by 3 – 5 %[40, 41]. It is the most rapidly growing segment of the municipal waste system[42]. This enormous amount of ‘waste’ offers incredible opportunities as a secondary source of raw materials, including rare earths. As a result, the concept of Urban Mining was born, in which our e-waste is no longer regarded as waste, but as an ample ore, full of added benefits.

## 2.4 Urban Mining

### 2.4.1 Benefits and Challenges

Urban mining is one of three major segments of the so called technospheric mining, as discerned by Jones *et al.*[43]. The other two segments are direct recycling of pre-consumer manufacturing scrap or residues, and landfill mining of historic and future urban or industrial waste residues (Figure 2.8). The recovery of valuable metals, and more specifically rare earths, through urban (and technospheric) mining, offers a lot of advantages. For one thing, EOL products contain much lower levels of harmful elements, which are common to primary ores (see Chapter 3). Also, the mining of primary ore results in the production of enormous amounts of uneconomic minerals (gangue), which is not the case in technospheric mining. This provides large energy and water savings[44]. In addition, the elemental content and concentrations in EOL material are usually known, which facilitates the design of separation processes. Furthermore, a lot of these devices are a lot higher in REE content than what is retrieved from the respective primary ores[44]. Besides, not all REEs are typically present (together) in their devices, which further eases their separation. If these ‘urban riches’ are recycled in a sensible way, a significant percentage of the rare earth demand could be met. Especially for parts of the world without domestic primary REE production, this could considerably decrease dependency on foreign resources[9].



**Figure 2.8 Various segments of the technospheric mining approach to improve the life cycle of raw materials. (Retrieved from [15]). (MSW: municipal solid waste, MWS: municipal water system, IW: industrial waste or water).**

Yet, as mentioned before, there are a lot of challenges to overcome in order to achieve sustainable recycling of the technosphere. The additional problem of a limited current market value of rare earths discourages a lot of companies to invest in such ventures. Still, there are

several companies trying to make REE recycling work. The French chemical company Rhodia, part of the Belgian Solvay group, is working on multiple rare earth recycling projects[45]. Solvay focusses on existing concentrated deposits, such as tailings and recycle loops, and aims to recycle REEs from low energy lamps and NiMH batteries (in cooperation with Belgium's Umicore for the nickel recovery), but also from production losses in the magnet industry. They possess a historical stockpile site in La Rochelle, as a prime example of an urban mine, with a large and complex spectrum of components. Recycling started already in 2010. Furthermore, the La Rochelle plant (Figure 2.9) is the sole facility outside of China able to separate all rare earths, including the heavy ones[45]. Other companies with a shift to REE recycling are, for instance, Mitsubishi Electric (Japan), who reported in 2012 the recycling of rare earth magnets from air conditioners. Hitachi (Japan) invested in the development of a magnet recovery machine for hard disk drives and air conditioners, with the intent to bring the technology into commercial operation. Honda (Japan) announced in 2013 that it was starting the recovery of the rare earth elements from its hybrid car batteries[38].



**Figure 2.9 Rhodia's Urban Mining plant in La Rochelle, France.**

All things considered, rare earth recycling is still in its infancy, but a thorough recycling culture could provide about 20 % of the global yearly demand, as stated by Binnemans [46]. Recycling alone is of course not enough to tackle the supply challenge, nor could it replace primary mining. The REE consumption market is simply growing too fast for that[47]. Urban mining, as well as REE recycling in general, should be seen as one of several key aspects of the path towards the sustainable REE production, next to improved primary mining, and the quest for enhanced and/or alternative (green) technologies (cfr. substitution). It must, however, be noted that the success of REE recycling is not solely determined by the availability of the proper recovery techniques. A shift in thinking is needed at virtually each level (industrial, political, public...), more specifically to improve the collection rate of e-waste. Even if the collected commodities could be recycled 90 %, if only 10 % of the waste gets collected properly, the ultimate recycling rate would still only be 9 %. In 2012, the European Union updated its directive on recycling e-waste, issuing new rules stating that, from 2016 on, all EU members are

to ensure that 45 % of the electrical and electronic equipment sold in each country is collected for recycling. By 2019, this percentage needs to rise to 85 % [48]. While this updated directive is primarily designed to help revive the declining REE supplies (and other CRM supplies), there is a secondary objective to reduce the outflow of e-waste from Europe to other continents, e.g., (West) Africa, where it is illegally dumped and processed, causing environmental hazards [48] (see below).

### 2.4.2 Necessity

Although urban e-waste contains much lower levels of harmful elements, it does not imply that storing or processing e-waste is without risk. Most of these EOL electrical commodities comprise numerous components, many of which are inherently hazardous and/or toxic in nature (Table 2.5). If these are not dealt with through sound sustainable recycling and disposal, their introduction into the environment can have dangerous effects on our earth and its inhabitants [42].

The portion of e-waste that is not properly recycled (by developed countries) is usually stockpiled, shipped overseas, or gets disposed in landfills, deposited in waste dumps, or incinerated [49]. When shipped out of the continent (often illegally), e-waste is typically recycled informally, which means it is treated by untrained, cheap workers in (mostly) developing countries, using primitive, hazardous extraction- and recovery techniques [42, 44] (open air burning, acid baths) (Figure 2.10). The resulting dispersion of hazardous metals, liquids and gasses causes severe damage to the environment and the workers. Even untreated e-waste in landfills can already be harmful. As it typically concerns open spaces, the precipitation percolating through the landfill can form leachates full of toxic elements [42].

Once again, the conclusion could be drawn that in order to improve the e-waste management, change is needed, not only at the technical level, but mainly in our way of thinking. As long as the money side prevails, cheap, hazardous, informal recycling will remain widespread, constituting a vital part of the economies of many nations, both those which provide e-waste and those which process it [44]. Disrupting the trade would, in many cases, have severe economic repercussions, but will in time enable a sustainable, environmentally sound recycling culture.

**Table 2.5 Various e-waste sources and their health effects.**

<b>E-waste sources</b>	<b>Constituents</b>	<b>Health effects</b>
Solder in PCBs, glass panels, and gaskets in computer monitors	Lead	Damage to nervous system, circulatory system, kidneys. Affects brain development in children.
Chip resistors and semiconductors	Cadmium	Neural damage.
Relays and switches, PCBs	Mercury	Chronic damage to brain and respiratory and skin disorders.
Corrosion protection of untreated galvanized steel plates, decorator, or hardener for steel housing	Hexavalent chromium	Bronchitis and DNA damage.
Cabling and computer housing	Plastics incl. PVC	Affects reproductive system and immune system, and leads to hormonal disorder.
Plastic housing of electronic equipments and circuit boards	Brominated flame retardants	Disrupts endocrine system functions.
Front panel of CRTs	Barium, phosphor, and heavy metals	Muscle weakness and damage to heart, liver, and spleen.
Motherboard	Beryllium	Carcinogenic in nature, causing skin diseases.

PCB: printed circuit board, CRT: cathode ray tube. (Retrieved from [42])



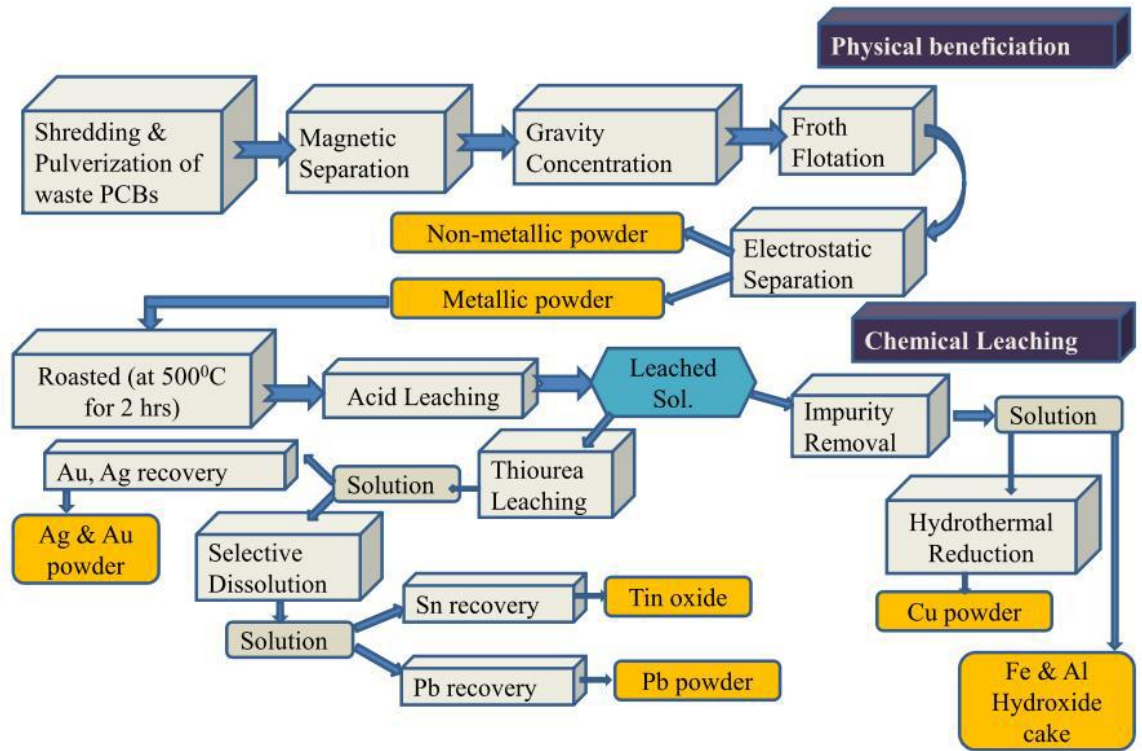
**Figure 2.10 Primitive, informal e-waste recycling through incineration. (©Jon Spaul. Retrieved from [50])**

### 2.4.3 Technology

Covering the complete gamma of possible e-waste recycling technologies would be a work of Sisyphean proportions. Not futile, of course, but many elaborate studies have already been published in this field[15, 44, 51, 52], and the scope of this work is of a more specified nature than just recycling as a whole. Ideally, a formal recycling process for e-waste comprises three phases, i.e., collection, pre-processing, and end-processing. So far, it has been illustrated that the collection phase can be improved dramatically. It is possibly the most critical phase in the whole recycling process[52], especially with respect to rare earths. The second phase is pre-processing, where the e-waste undergoes a series of sorting steps, followed by dismantling, and physical and chemical separation[53, 54]. Here, there is a lot of room for improvement as well. The biggest drawback is that, in most cases, state-of-the-art pre-processing facilities are still optimized for mass recovery, at the expense of low concentrated precious and specialty metals[52]. In this phase, better targeted dismantling approaches could increase the recycle rate of specialty metals[55, 56]. In Section 2.3.3 it was already explained that simple shredding and pulverization processes, without adequate dismantling, result in very complex powders that dramatically complicate further processing (cfr. smartphones). To illustrate this, a flow chart is provided (Figure 2.11), which depicts a metal recovery process on PCBs[42]. In this process, seven metals are targeted (Ag, Au, Sn, Pb, Cu, Fe, Al). The recycling chain (after collection), consists of 14 steps, 9 of which happen after the electrostatic separation (right before the metal separations). Imagine the number of steps (incl. water, solvents, energy, chemicals...) needed to separate mixtures of 20 metals or more, including several chemically similar rare earths. It becomes clear that a thorough metal recovery from such powders is simply not economical, and as a result only the elements with a high enough monetary value are recovered. Optimized



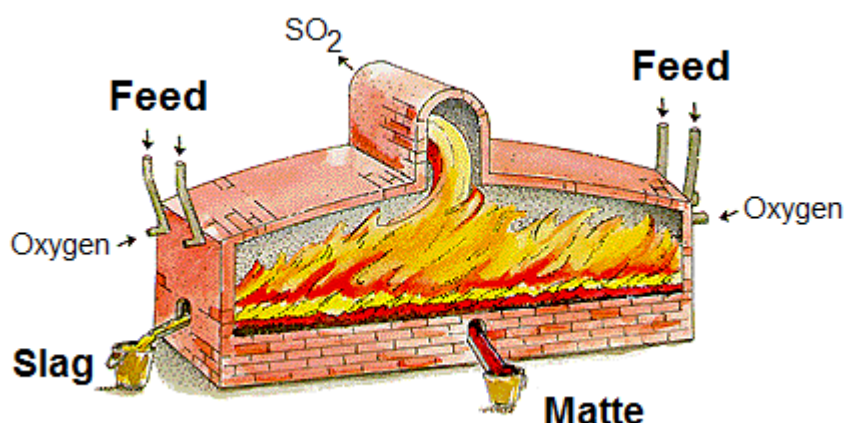
disassembly techniques could prevent such difficult separations, by limiting the amount of different metals in the obtained pre-processed fractions. However, the continuous miniaturization of technology, and the resulting high dissipation of metals in electronics does not help this cause. Ideally, an information loop between materials scientists and designers should exist, so that facile, yet efficient recycling is kept in mind when designing new devices[52].



**Figure 2.11 Process flow chart for precious metals recovery from PCBs at CSIR-NML, Jamshedpur. (Retrieved from [42]).**

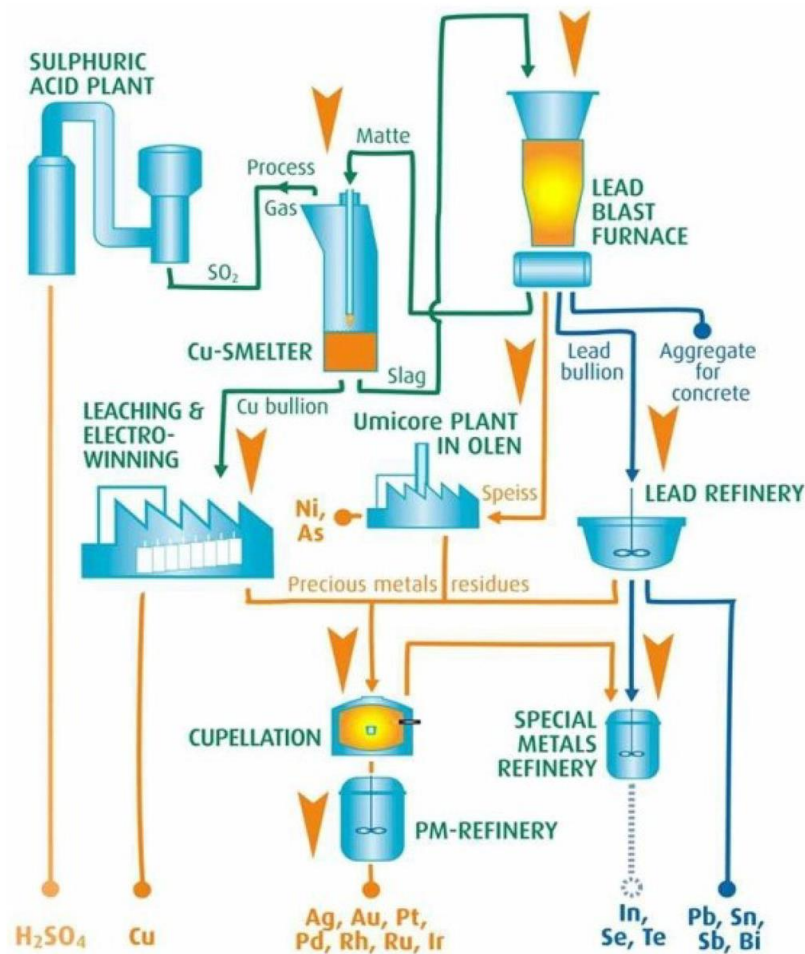
During the final stage of e-waste recycling, i.e., end-processing, the obtained fractions are purified into their respective metals, oxides or salts. Once again, the development and application of industrial methods to recover specific metals is driven by their market value. As a result, the main focus lies on the recovery of ‘paying metals’, such as precious metals (gold, silver, palladium...) and important base metals (copper, lead...)[57]. Co-recovery of other base and specialty metals is possible if the overall operation remains cost-effective. Opposed to collection and pre-processing, which take place at a local/regional or regional/national level, respectively, the end-processing of e-waste is a globalized service[57], with only a handful major companies in the world[58]. Currently, the state of the art on industrial end-processing of e-waste is mainly based on integrated smelter facilities[57]. They combine pyrometallurgical, hydrometallurgical, and electrometallurgical processes to recover precious metals, copper and other non-ferrous metals (including certain critical metals), while isolating hazardous substances. At Belgium’s Umicore, the largest e-waste recycling facility in the world, the

overall refinery process is driven by base elements copper, lead, and nickel. In addition, precious metals, Platinum groups metals (PGMs) and other secondary metals are recovered with high efficiency. Their smelting process (pyrometallurgy) isolates precious metals into a molten copper phase (called *matte*) from mostly all other metals which are concentrated in a lead slag (Figure 2.12). The copper is leached out from this matte phase and is then purified by electro-winning. The residue of the electro-winning process is hydrometallurgically treated to recover the precious metals. The lead slag is refined as well, eventually producing pure lead, nickel, and several base and specialty metals. The overall process is illustrated in Figure 2.13. More detailed information on this and other similar processes can be found in [59, 60].



**Figure 2.12** Simplified representation of a smelter (flash furnace), producing a matte phase (bottom layer) and slag phase (oxidized top layer). (Adapted from [34]).





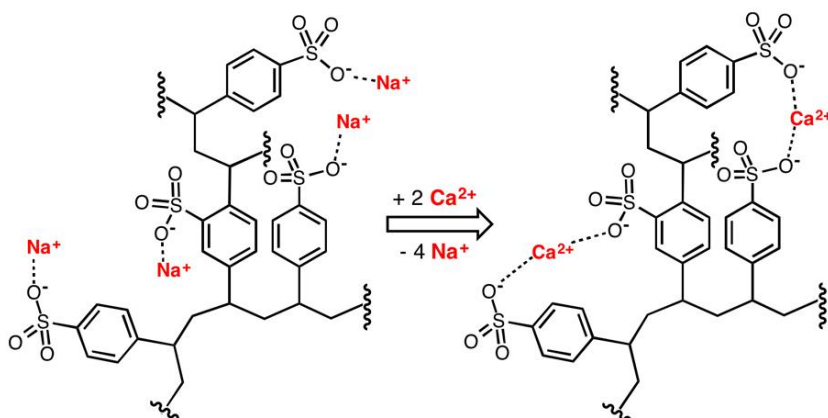
**Figure 2.13** Flow sheet for Umicore’s integrated metals smelter and refinery. (Retrieved from [60])

The rare earths in e-waste typically end up as oxides in the slag phases of the smelting process. If thermodynamically and economically viable, they can be recovered[57], but often times they are ignored and slags that still contain various valuable metals are landfilled or used as a whole in construction materials[60] (cement, bricks, tiles...). However, industrial projects have been realized to efficiently recover the rare earths from these secondary resources. For instance, in 2011, Umicore started up the first ever industrial size processing plant for REE-containing NiMH (and Li-ion) batteries. These batteries are fed into an ultra-high temperature (UHT) oven, where the rare earths end up in the slag, which is further processed to obtain a REE concentrate. These concentrates are sent to the earlier mentioned La Rochelle facility from Rhodia (Solvay), who refine them into individual REOs[61]. This facility also treats REE-containing powder concentrates from processed lamp phosphors. Other notable examples are the earlier mentioned recycling facilities of Hitachi (magnets) and Honda (NiMH batteries).

## 2.5 Separating the Rare Earths

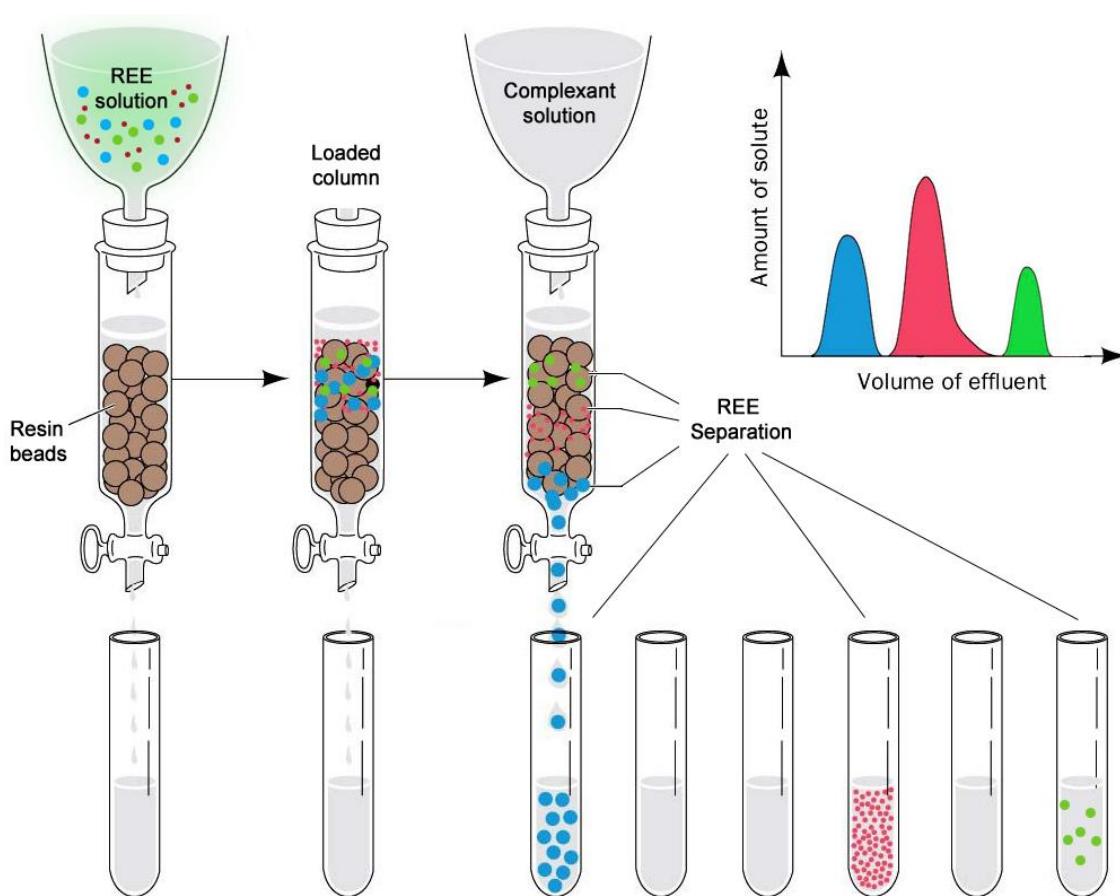
Perhaps the most intricate step in the process to obtain pure rare earths (both from primary mining concentrates and from e-waste) is their individual separation. Due to their chemically similar nature, separating these elements is no easy business. Yet, over the past decades many techniques have been developed. At the heart of these methods lie two important properties of the rare earths, namely the lanthanide contraction (see Section 2.2.1), which influences their basicity and therefore solubility, ionic hydrolysis, and complexation, and secondly, the fact that some REEs can have stable oxidation states other than +3, so that e.g. divalent Eu and tetravalent Ce can be separated from the other trivalent lanthanides via selective oxidation/reduction[27, 61].

Nowadays, the main industrial technique of REE separation is solvent extraction. Other methods, such as fractional crystallization and fractional precipitation have been applied as well, but are mostly out of focus due to being too inefficient and labor intensive[9]. An alternative efficient method is ion-exchange (IX), in which a solid (often resinous) material is used to capture REEs from a solution via an ion exchange process. A conventional IX resin, e.g., a sulfonic polystyrene-based cation exchanger (Figure 2.14) exchanges its cations ( $H^+$ ,  $Na^+$ ,  $NH_4^+$ ...) with the encountered metals from the solution. The affinity for the resin is greatly determined by the charge, size, and degree of hydration of the exchanged ions[51]. Due to the similar nature of rare earth cations, however, this approach is not very suitable for REE separation. Therefore, more advanced methods are applied, combining a REE-loading phase through IX, followed by an elution phase (ion-chromatography), where eluting solutions containing specific complexants are used to selectively interact with the rare earth cations (Figure 2.15). As these complexing agents form REE-complexes with different stability constants, a separation can be achieved.



**Figure 2.14 Sulfonic polystyrene-divinylbenzene (PS-DVB) type IX resin, where sodium cations are exchanged for calcium. (Retrieved from [62])**

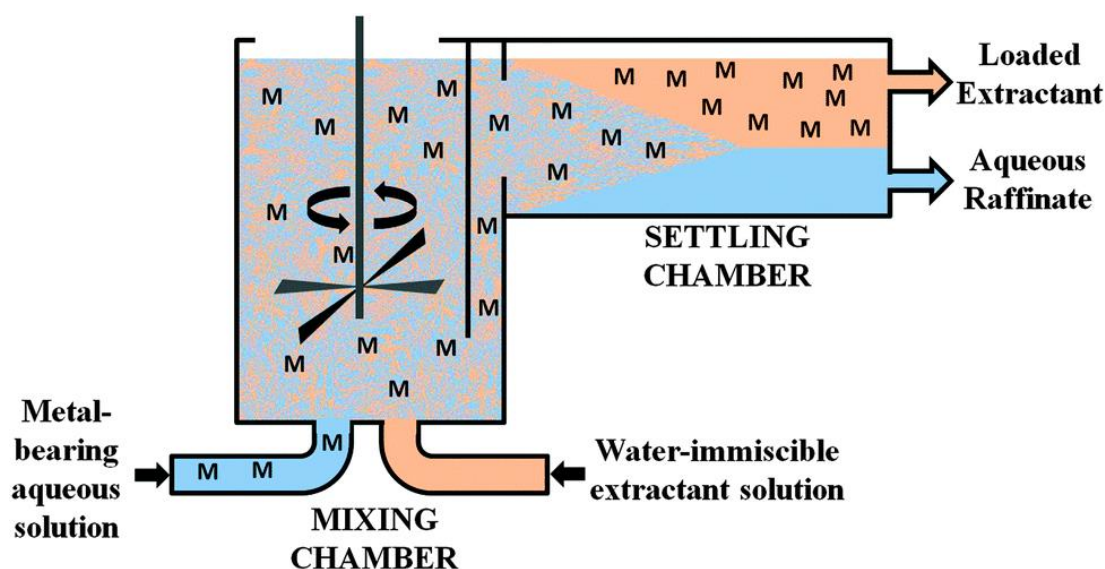
A broad spectrum of such complexants exist, including aminopolycarboxylic acids, carboxylic acids, hydroxy-acids, keto-acids, thio-acids, phosphonic acids, and aminophosphonic acids[51]. Ion-exchange produces highly pure rare earths, albeit in small quantities. Before the advent of industrial scale solvent extraction in the 1960s, IX technology was the only practical way to separate the rare earths in large quantities[63]. The method is, however, described as time consuming and nowadays it is only used to produce a few of the heavy REEs on a smaller scale[9, 61]. Detailed information on rare earths separation though IX (cationic, anionic, chelators...), as well as historic separation techniques (fractional crystallization, precipitation) can be found in [23, 51].



**Figure 2.15 Separation of rare earths via ion exchange and elution chromatography. (Figure adapted from [62])**

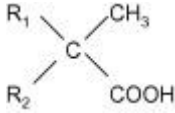
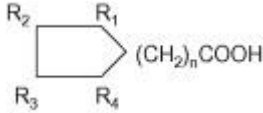
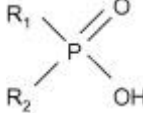
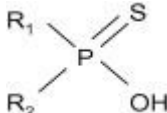
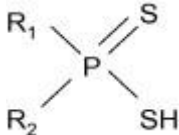
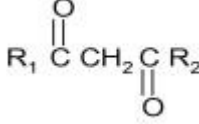
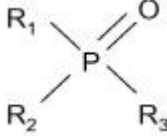
Solvent extraction (SX), or liquid-liquid extraction is a process where a certain solute of interest is recovered/removed from a feed solution by enabling thorough contact with a (partially) immiscible solvent. This leads to a transfer of solute from the feed to the solvent, resulting in a two-phase distribution. The technique is often carried out in a continuous multi-stage setup, consisting of repetitive fractionation in a group of mixer-settlers, called *batteries*[9] (Figure

2.16). Another widely used extraction setup is via a mechanically agitated/stirred column, which is rather similar to the stripping section of a distillation column, i.e., the solvent flow (extract) is similar to the vapor flow, and the raffinate resembles the liquid flow in the stripping column[64]. When dealing with rare earths separation, the REE-containing aqueous feed is mixed with an organic solvent phase. This organic phase contains specific complexing/extracting agents with varying affinities for the different rare earths[65]. The extractants are rather similar to the ones used in REE IX-chromatography, but typically contain bulky organic moieties (alkyl tails) to enable solution into the organic phase. A popular extractant for rare earths is the organophosphorus acid type, e.g., di-2-ethylhexyl phosphoric acid (DEHPA). The organic phase is usually a mixture of inert hydrocarbons (kerosene). Some notable examples of commercial extractants are shown in Table 2.6.



**Figure 2.16** Schematic representation of a mixer-settler system for continuous operation of solvent extraction. (Retrieved from [66])

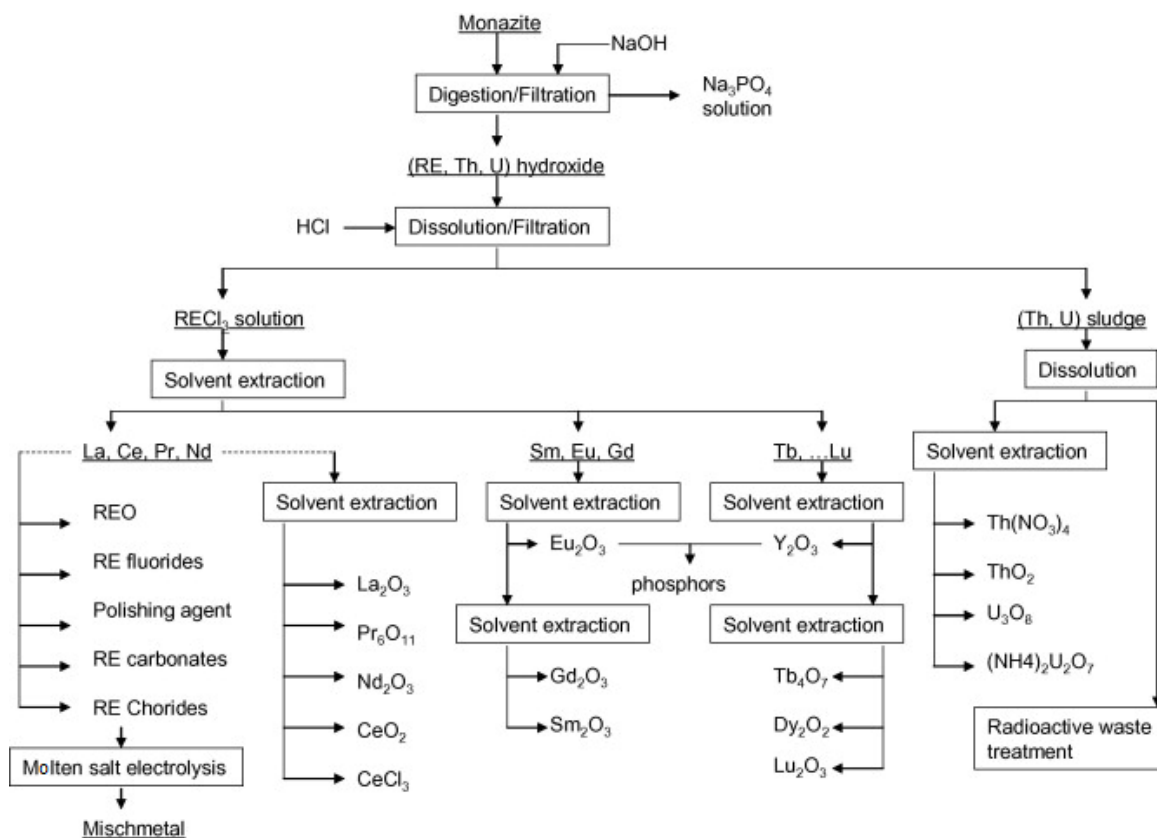
**Table 2.6 Some commercial extractants for rare earth solvent extraction.**

Extractant class	Structure	Extractants
1.Cation extractants		
Carboxylic acids		Versatic acids: $R_1 + R_2 = C_7$ , Versatic 10; $R_1 + R_2 = C_6-C_8$ , Versatic 911
		Naphthenic acids: $R_1-R_4$ : varied alkyl groups
Phosphorous acids		Phosphoric acids: $R_1 = R_2 = C_4H_9CH(C_2H_5)CH_2O-$ , di-2-ethylhexylphosphoric acid (D2EHPA, DEHPA)
		Phosphonic acids: $R_1 = C_4H_9CH(C_2H_5)CH_2O-$ , $R_2 = C_4H_9CH(C_2H_5)CH_2-$ , 2-ethylhexylphosphonic acid mono-2-ethylhexyl ester (EHEHPA, HEHEHP, P507, PC88A)
		Phosphinic acids: $R_1 = R_2 = C_4H_9CH(C_2H_5)CH_2-$ , di-2-ethylhexylphosphinic acid (P229) $R_1 = R_2 = CH_3(CH_2)_3CH_2CH(CH_3)CH_2-$ , di-2,4,4-trimethylpentylphosphinic acid (Cyanex 272)
		Monothiophosphorous acids $R_1 = R_2 = CH_3(CH_2)_3CH_2CH(CH_3)CH_2-$ , di-2,4,4-trimethylpentyl-monothiophosphinic acid (Cyanex 302)
		Dithiophosphorous acids $R_1 = R_2 = CH_3(CH_2)_3CH_2CH(CH_3)CH_2-$ , di-2,4,4-trimethylpentyl-dithiophosphinic acid (Cyanex 301)
2.Chelating extractants		$\beta$ -diketones: $R_1 = R-C_6H_5$ , $R_2 = CH_3(CH_2)_5-$ , R: unknown side alkyl, (LIX 54)
3.Solvating extractants		Phosphorous ester: $R_1 = R_2 = R_3 = CH_2(CH_2)_2CH_2O-$ , tri-n-butyl-phosphate (TBP) $R_1 = R_2 = CH_2(CH_2)_2CH_2O-$ , $R_3 = CH_2(CH_2)_2CH_2-$ , dibutylbutylphosphonate (DBBP)

		Phosphine oxides: $R_1 = R_2 = R_3 = \text{CH}_2(\text{CH}_2)_6\text{CH}_2-$ , tri-n-octylphosphine oxide (TOPO, Cyanex 921)
4. Anion extractants	$\text{RNH}_2$	Primary amines $R = (\text{CH}_3)_3\text{C}(\text{CH}_2)_2\text{C}(\text{CH}_3)_2$ (Primene JMT, N1923)
	$\text{RNH}_2$ 	Quaternary amines: $R_1 = R_2 = R_3 = \text{C}_8\text{--C}_{10}$ mixture (Aliquat 336, Adogen 464)

(Retrieved from [63])

Due to the small differences between the rare earths, one mixer-settler battery will not suffice to obtain an adequate separation of these elements. The process must be repeated many times to be effective, yet it is able to produce REE compounds of  $> 99.99\%$  purity[61]. A typical plant producing multiple single rare earth products may contain hundreds of stages of mixers and settlers[63]. Often times, the rare earths are first split into major groups in one SX stage (e.g., heavy REEs in the organic phase, light REEs in the aqueous raffinate), after which each group is further separated into individual REEs in additional SX stages (Figure 2.17). Enriched organic phases are usually ‘stripped’ with (acidic) aqueous solutions (e.g.,  $\text{HCl}$ ,  $\text{HNO}_3$ ), where the ions have higher solubility[61]. To obtain the pure solid REE compounds, the cations are precipitated from these solutions by forming insoluble salts or hydroxides. The obtained solids are then separated, dried or calcined at high temperatures and subsequently ground into powders[9]. An extensive review on the state of the art on industrial solvent extractions of rare earths (as well as the complete route from ore to REE product) was performed by Xie *et al.*[63].



**Figure 2.17 Simplified flowsheet for REE refinery from monazite ore through multi-stage solvent extraction (Shanghai Yue Long Chemical Plant). (Retrieved from [63])**

## 2.6 A realm of possibilities

Up to this point, this work has offered a concise view on the importance of rare earth elements to our modern society. Their advantages, as well as their necessity in several technologies has been illustrated, and the theory behind their main physical and chemical properties has been discussed. We can conclude that in many stages of rare earth processing, from primary mining to commodity recycling, a lot of improvement can be made in terms of applied technologies. Not only to help safeguard the supply of these critical metals, but also to better protect our environment in doing so. It was also established that, in addition to technological prowess, the economic and political situation, as well as the mind-set of the people, plays a major role in this quest.

It is undeniable that a topic such as sustainable rare earth (and critical metal) winning offers incredible opportunities for new research and development ventures, both from an industrial viewpoint and an academic one. The core of this work focuses on the development of a technology that can help achieving a more thorough winning/recovery of critical metals, as well as enabling a zero-waste management in the currently applied processing methods.

## REFERENCES

- [1] IUPAC, Nomenclature of Inorganic Chemistry, RSC Publishing, Cambridge, 2005.
- [2] European Commission, Report on Critical Raw Materials for the EU - Critical Raw Materials Profiles (2015).
- [3] B.S. Van Gosen, P.L. Verplanck, K.R. Long, J. Gambogi, R.R. Seal, II The rare-earth elements - Vital to modern technologies and lifestyles: U.S. Geological Survey Fact Sheet (2014).
- [4] D.J. Kingsnorth, Rare Earths: Facing New Challenges in the New Decade, in: SME Annual Meeting, Phoenix, Arizona, 2010.
- [5] B.J. Skinner, Chapter 10 - A Second Iron Age Ahead?, in: P.A. Trudinger, D.J. Swaine (Eds.) Studies in Environmental Science, Elsevier, 1979, pp. 559-575.
- [6] R.L. Rudnick, S. Gao, 3.01 - Composition of the Continental Crust A2 - Holland, Heinrich D, in: K.K. Turekian (Ed.) Treatise on Geochemistry, Pergamon, Oxford, 2003, pp. 1-64.
- [7] V. Zepf, Chapter 1 - An Overview of the Usefulness and Strategic Value of Rare Earth Metals A2 - Lima, Ismar Borges De, in: W.L. Filho (Ed.) Rare Earths Industry, Elsevier, Boston, 2016, pp. 3-17.
- [8] A. Tsamis, M. Coyne, Recovery of Rare Earths from Electronic wastes: An opportunity for High-Tech SMEs, European Parliament, Brussels (2015).
- [9] Rare Earth Elements, British Geological Survey, United Kingdom (2011).
- [10] N. Krishnamurthi, C.K. Gupta, Extractive Metallurgy of Rare Earths, CRC Press, 2005.
- [11] R. Chi, J. Tian, Weathered Crust Elution-deposited Rare Earth Ores, Nova Science Publishers, 2008.
- [12] V.G. Papangelakis, G. Moldoveanu, Recovery of Rare Earth Element from Clay Minerals, in: ERES2014: 1st European Rare Earth Resources Conference, Milos, Greece, 2014.
- [13] R. Grauch, A. Mariano, Ion-Absorption Type Lanthanide Deposits, in: Abstract Annual SME Conference, Salt Lake City, 2008.
- [14] X.J. Yang, A. Lin, X.-L. Li, Y. Wu, W. Zhou, Z. Chen, China's ion-adsorption rare earth resources, mining consequences and preservation, Environmental Development, 8 (2013) 131-136.
- [15] K. Binnemans, P.T. Jones, B. Blanpain, T. Van Gerven, Y.X. Yang, A. Walton, M. Buchert, Recycling of rare earths: a critical review, J Clean Prod, 51 (2013) 1-22.
- [16] C. Blakely, J. Cooter, A. Khaitan, I. Sincer, R. Williams Rare Earth Metals & China (2012).
- [17] Roskill, Rare Earths: Global Industry, Markets & Outlook - 16th edition (2016).
- [18] Argus Consulting Services, Argus Rare Earths Monthly Outlook, A.M. Group (2016).
- [19] A.P. Han, J.P. Ge, Y.L. Lei, An adjustment in regulation policies and its effects on market supply: Game analysis for China's rare earths, Resour Policy, 46 (2015) 30-42.
- [20] L. Zhang, Q. Guo, J.B. Zhang, Y. Huang, T. Xiong, Did China's rare earth export policies work? - Empirical evidence from USA and Japan, Resour Policy, 43 (2015) 82-90.
- [21] M. Humphries, Rare Earth Elements: The Global Supply Chain, Congressional Research Service (2013).
- [22] J. Ebner (European Institute for Asian Studies), Europe's Rare Earth Dependence on China (2014).
- [23] T. Moeller, The Chemistry of Lanthanides, Chapman and Hall, London, 1965.



- [24] T. Moeller, 2 - Atomic Structure and its Consequences: The Dawn of Understanding, in: The Chemistry of Lanthanides, Chapman and Hall, 1965.
- [25] J. Jensen, A.R. Mackintosh, Rare Earth Magnetism: Structures and Excitations - 1st Edition, Clarendon Press, Oxford, 1991.
- [26] S.B. Castor, J.B. Hedrick, Rare Earth Elements, in: J.E. Kogel, N.C. Trivedi, J.M. Barker, S.T. Krukowski (Eds.) Industrial Minerals and Rocks - Commodities, Markets, and Uses (7th Edition), Society for Mining, Metallurgy, and Exploration (SME), 2006.
- [27] T. Moeller, 3 - The Oxidation States - A Combination of the Commonplace and the Unusual, in: The Chemistry of Lanthanides, Chapman and Hall, 1965.
- [28] V. Zepf, Rare Earth Elements, Springer-Verlag Berlin Heidelberg, 2013.
- [29] Handbook on the Physics and Chemistry of Rare Earths, Elsevier, 2005.
- [30] W.M. Yen, M.J. Weber, Inorganic Phosphors: Compositions, Preparation and Optical Properties, CRC Press, 2004.
- [31] C.R. Ronda, T. Jüstel, H. Nikol, Rare earth phosphors: fundamentals and applications, Journal of Alloys and Compounds, 275–277 (1998) 669-676.
- [32] N. Curtis, Rare Earths, We Can Touch Them Everyday, in: Lynas Presentation at the JP Morgan Australia Corporate Access Days, New York, 2010.
- [33] Why Rare Earth Metals Matter, interview with M. Smith by T. Vulcan (2009).
- [34] <http://www.asarco.com/about-us/our-locations/asarco-mineral-discovery-center/making-copper/smelting/> (Accessed in 2016)
- [35] N. Rudarakanchana, China Rare Earth Export Restrictions Found Unfair By WTO, China Objects And Says Rules Needed To Protect Environment, International Business Times (2014).
- [36] L. Jiabao, L. Jie, Rare Earth Industry Adjusts to Slow Market, China Daily (2009).
- [37] R.J. Weber, D.J. Reisman, Rare Earth Elements: A Review of Production, Processing, Recycling, and Associated Environmental Issues, United States Environmental Protection Agency, Washington, DC (2012).
- [38] J. Marshall, Why Rare Earth Recycling Is Rare (And What We Can Do About It), Ensia (2014).
- [39] B. Rohrig, Smartphones, Smart Chemistry, ChemMatters, (2015) 10 - 12.
- [40] Global E-Waste Management Market (Types, Sources and Geography) - Size, Global Trends, Company Profiles, Segmentation and Forecast, 2013 - 2020, A.M. Research (2015).
- [41] J.R. Cui, E. Forssberg, Mechanical recycling of waste electric and electronic equipment: a review, J Hazard Mater, 99 (2003) 243-263.
- [42] A. Vidyadhar, Chapter 6 - A Review of Technology of Metal Recovery from Electronic Waste, in: F.-C. Mihai (Ed.) E-Waste in Transition - From Pollution to Resource, InTech, 2016.
- [43] P.T. Jones, T. Van Gerven, K. Van Acker, D. Geysen, K. Binnemans, J. Fransaer, B. Blanpain, B. Mishra, D. Apelian, CR3: Cornerstone to the sustainable inorganic materials management (SIM2) research program at K.U.Leuven, Jom-Us, 63 (2011) 14-15.
- [44] R.M. Izatt, S.R. Izatt, R.L. Bruening, N.E. Izatt, B.A. Moyer, Challenges to achievement of metal sustainability in our high-tech society, Chem Soc Rev, 43 (2014) 2451-2475.
- [45] Solvay, Latest Developments in Rare Earth Recovery from Urban Mines, in: Exchange of Good Practices on Metal By-Products Recovery, Brussels, 2015.
- [46] I. Farrell, Recycling Rare Earth Elements using Ionic Liquids, Chemistry World (2013).
- [47] F. Grosse, Is Recycling “Part of the Solution”? The Role of Recycling in an Expanding Society and a World of Finite Resources, S.A.P.I.E.N.S., (2010) 1 - 17.

- [48] EU activates new e-waste recycling rules, United Press International (UPI) (2012).
- [49] F.O. Ongondo, I.D. Williams, T.J. Cherrett, How are WEEE doing? A global review of the management of electrical and electronic wastes, *Waste Manage*, 31 (2011) 714-730.
- [50] A. Minter, The Burning Truth Behind an E-Waste Dump in Africa, *Smithsonian* (2016).
- [51] D. Kołodyńska, Z. Hubicki, Chapter 6 - Investigation of Sorption and Separation of Lanthanides on the Ion Exchangers of Various Types, in: A. Kilislioğlu (Ed.) *Ion Exchange Technologies*, InTech, 2012.
- [52] B.K. Reck, T.E. Graedel, Challenges in Metal Recycling, *Science*, 337 (2012) 690-695.
- [53] T.G. Gutowski, Materials Separation and Recycling, in: B.R. Bakshi, T.G. Gutowski, D.P. Sekulic (Eds.) *Thermodynamics and the Destruction of Resources*, Cambridge University Press, Cambridge, 2011, pp. 113-132.
- [54] M. Renter, A. van Schaik, Thermodynamic metrics for measuring the "sustainability" of design for recycling, *Jom-Us*, 60 (2008) 39-46.
- [55] P. Chancerel, C.E.M. Meskers, C. Hageluen, V.S. Rotter, Assessment of Precious Metal Flows During Preprocessing of Waste Electrical and Electronic Equipment, *J Ind Ecol*, 13 (2009) 791-810.
- [56] J.G. Johansson, A.E. Bjorklund, Reducing Life Cycle Environmental Impacts of Waste Electrical and Electronic Equipment Recycling, *J Ind Ecol*, 14 (2010) 258-269.
- [57] I. Bakas, C. Fischer, S. Haselsteiner, D. McKinnon, L. Milios, A. Harding, J. Kosmol, A. Plepys, N. Tojo, H. Wilts, Present and potential future recycling of critical metals in WEEE, *Copenhagen Resource Institute* (2014).
- [58] S. Art, Recycling van edelmetalen en andere uit elektronica - Visie van een eindverwerker, in: *RTA Symposium, Umicore, Leusden, The Netherlands*, 2014.
- [59] F. Vanbellen, The Hoboken Recycling Plant, in: *Capital Markets Event on Recycling, Umicore*, 2010.
- [60] A. Khaliq, M.A. Rhamdhani, G. Brooks, S. Masood, Metal extraction processes for electronic waste and existing industrial routes: a review and Australian perspective, *Resources*, 3 (2014) 152-179.
- [61] H. Royen, U. Fortkamp, Rare Earth Elements-Purification, Separation and Recycling, *IVL* (2016).
- [62] [http://upendratts.blogspot.be/2013\\_05\\_01\\_archive.html](http://upendratts.blogspot.be/2013_05_01_archive.html) (Accessed in 2017)
- [63] F. Xie, T.A. Zhang, D. Dreisinger, F. Doyle, A critical review on solvent extraction of rare earths from aqueous solutions, *Miner Eng*, 56 (2014) 10-28.
- [64] G.D. Saravacos, A.E. Kostaropoulos, Mass Transfer Equipment, in: *Handbook of Food Processing Equipment*, Springer US, Boston, MA, 2002, pp. 494-541.
- [65] P. Enghag, Scandium, Yttrium, Lanthanum and the 14 Lanthanides – Rare Earth Metals (REMs), in: *Encyclopedia of the Elements*, Wiley-VCH Verlag GmbH & Co. KGaA, 2007, pp. 373-492.
- [66] A.M. Wilson, P.J. Bailey, P.A. Tasker, J.R. Turkington, R.A. Grant, J.B. Love, Solvent extraction: the coordination chemistry behind extractive metallurgy, *Chem Soc Rev*, 43 (2014) 123-134.

# 3 ADSORPTION

## 3.1 Low concentration recovery

### 3.1.1 Shortcomings of the industry

It has been shown in Chapter 2 that conventional technologies for rare earth recovery (and metal recovery in general) are typically of a pyro- or hydrometallurgical nature. They include, but are not limited to, solvent extraction (SX), smelting, leaching, ion exchange (IX), and precipitation processes[1-3]. These technologies are designed for high concentration recovery, such as found in primary REE mining operations. When rich ores are treated (leached) with certain acidic or alkaline solutions to release their elements of interest, the obtained highly concentrated leachates could be fed to a SX installation, which can effectively separate the target elements from the unwanted ones. Such feeds are typically in the g/L scale, with >100 g/L being no exception (cfr. Molycorp process[3]). In the case of rare earth refinery, SX is the main technology to separate individual REEs or to produce mixed rare earths, with several processes being able to obtain purities over 99 %, even 99.99 % [4].

There are, however, a few concerns that need addressing. First of all, while the SX processes are very effective, they are not perfect, i.e., even a 99.9 % recovery, results in leftover (waste) streams of 0.1 %. This might not seem like a lot, but with feeds of 100 g/L, the waste streams still contain 100 mg/L. In the longer run, this would result in a high loss of resources, especially if it concerns critical metals. Secondly, in order to reach such high recovery percentages in SX, a high amount of sequential extraction steps are typically required[1, 4], especially in REE refinery, because of their highly similar nature (cfr. Chapter 2). Although SX (and other hydrometallurgical separation technologies) offer a lot of advantages over pyrometallurgical processes, such as diminished or eliminated air pollution, shortened treatment cycles, and higher metal recoveries[5, 6], hydrometallurgical technologies (SX, IX, precipitation) can have a high

environmental impact due to general use of solvents (often toxic or flammable) and other chemicals, as well high water usage[2]. This is rather contradictive to the green and clean potential of the technologies relying on the elements that need recovering (i.e., REEs)[1].

Moreover, deposits full of rich ores are limited, especially outside China. Gradually we will have to shift towards rare earth winning from lower-grade ores, and such ores increasingly complicate the conventional separation methods, and increase their energy input and water usage[2]. Also, in terms of commodity recycling, the low relative concentration of critical metals in e-waste results in similar difficulties. Eventually, selective recovery or removal of critical elements from dilute aqueous streams will become an important topic and a key factor in improving metal sustainability. However, the conventional hydro- and pyrometallurgical technologies prove to be inadequate to selectively recover metals from dilute solutions in the mg/L concentration range, especially as matrices become more complex[2]. In addition, in some cases the metal concentration can be of such a low level, that even the costs to pump the aqueous streams for processing can surpass the value of the recoverable metals. Therefore, the domain of alternative, passive recovery techniques must be explored for industrial application.

### 3.1.2 Areas of potential application

The occurrence of dilute REE-containing aqueous streams has been illustrated in the previous sections: waste streams from current SX processes in primary mining; process streams in e-waste recycling... There is a lot of potential for low concentration recovery. It was also mentioned that gradually we will have to explore other REE sources than rich primary ores, in order to keep up with the demand. A lot of secondary sources contain a significant amount of REEs, but cannot be processed cost-effectively by the current industrial methods. An example is the phosphoric acid industry, where the main resource for phosphorous is the mineral apatite  $\text{Ca}_5(\text{PO}_4)_3(\text{Cl}, \text{F}, \text{OH})$ . Apatite contains about 0.1 to 1 % REEs[7], present as either  $\text{REE}^{3+}$  ions substituted on the apatite lattice or as REE mineral inclusions[8]. Even though the apatite is dissolved with sulphuric acid, thereby also releasing the REEs into solution, the calcium is also precipitated as sulphate (gypsum), which causes a loss of ~80 % of the REEs[8]. Nevertheless, the REEs can still be recovered from this gypsum[9], as well as from the remaining waste streams from the phosphoric acid process (i.e., the remaining ~20 % REEs). Moreover, some phosphoric acid industries have completely redesigned their apatite processing, e.g., by using nitric acid instead of sulphuric acid, which yields calcium nitrate instead of the sulphate[10]. The nitrate's solubility is easier to control, so REEs can be recovered from the solution before they are co-precipitated[8].

Another potential secondary REE source is red mud. It is a waste product of the Bayer process, where bauxite ore is converted into alumina. Although being a hazardous waste product, it draws a lot of interest to the industry due to its high metal content (especially iron, up to 60 %). It was also found that red mud contains a significant amount of rare earths, ranging from 500 to 1700 parts per million (ppm)[11]. The recovery of REEs from this mud is investigated, but the efficiencies are currently too low and/or the consumption of chemicals too high[12].

There are a lot of interesting secondary resources for REE winning, both naturally occurring and anthropogenic (e.g., e-waste). An overview of some notable examples is presented in Table 3.1. More detailed information on their current processing technologies can be found in Peelman *et al.*[11].

**Table 3.1 Summary of Possible Secondary Rare Earth Resources (Retrieved from [11])**

Secondary resource	REE content	Extraction technology	Yield	Remarks
Apatite rock	0.1 – 1 wt. %	Conventional $\text{H}_3\text{PO}_4$ process	20 % at best	Can be done with no changes to process
		Hemihydrate process	80 – 85 %	Implementable using standard equipment
		$\text{HNO}_3/\text{HCl}$ process	80 %	In development
Phosphogypsum	0.3 – 0.4 wt. %	$\text{H}_2\text{SO}_4$ leaching	50 %	Does not decompose gypsum
		$(\text{NH}_4)_2\text{CO}_3$ process	-	Valuable byproduct
Red mud	0.05 – 0.17 wt. %	Physical upgrading followed by leaching	< 20 %	Low yield, low chemical consumption
		Direct leaching	Heavy REE: 80 - 90% Light REE: 30 - 50%	Many impurities, a lot of waste
Lamp phosphors	10 – 28 wt. %	Sequential leaching	-	Extraction efficiency varies between steps and compound
SmCo magnets	23 – 33 wt. %	Total dissolution	100 %	Yield after solvent extraction: 70 - 95%
FeNdB magnets	26.7 wt. %	Total dissolution	100 %	Yield after solvent extraction: 96 - 99%
		Selective dissolution	96 – 99 %	Yield depends on tolerance on Fe dissolution

### 3.1.3 The role of uranium

In addition to being closely associated to one another in nature, the rare earths also have a close relation to actinides, in particular, uranium and thorium[13]. These actinides are often present in the rare earth minerals via lattice substitution, resulting in radiation issues in rare earth processing[14]. According to Pillai[15], the uranium content within typical rare earth minerals varies from insignificant concentrations to 0.8 wt.%, whereas the thorium content varies from 0.1 to 10 wt.% or even higher (Table 3.2). Some mineral studies even report contents up to 20 wt.% uranium and 16 wt.% thorium (as oxides) in certain monazites[16]. Also, the ion-adsorption clays, which are the main source of heavy REEs to the world (see Chapter 2), contain a considerable amount of uranium (ppm range). Yet, no measures are taken in controlling the uranium radiation due to its low concentrations in the clays[14].

**Table 3.2 Concentrations of ThO<sub>2</sub> and U<sub>3</sub>O<sub>8</sub> in the Most Important REE-Bearing Minerals (according to Pillai[15])**

	<b>Thorium (ThO<sub>2</sub>)</b>	<b>Uranium (U<sub>3</sub>O<sub>8</sub>)</b>
Bastnaesite	0.1 - 0.2 wt.%	Negligible
Monazite	4.5 - 9.5 wt.%	0.2 - 0.4 wt.%
Xenotime	0.83 wt.%	0.81 wt.%

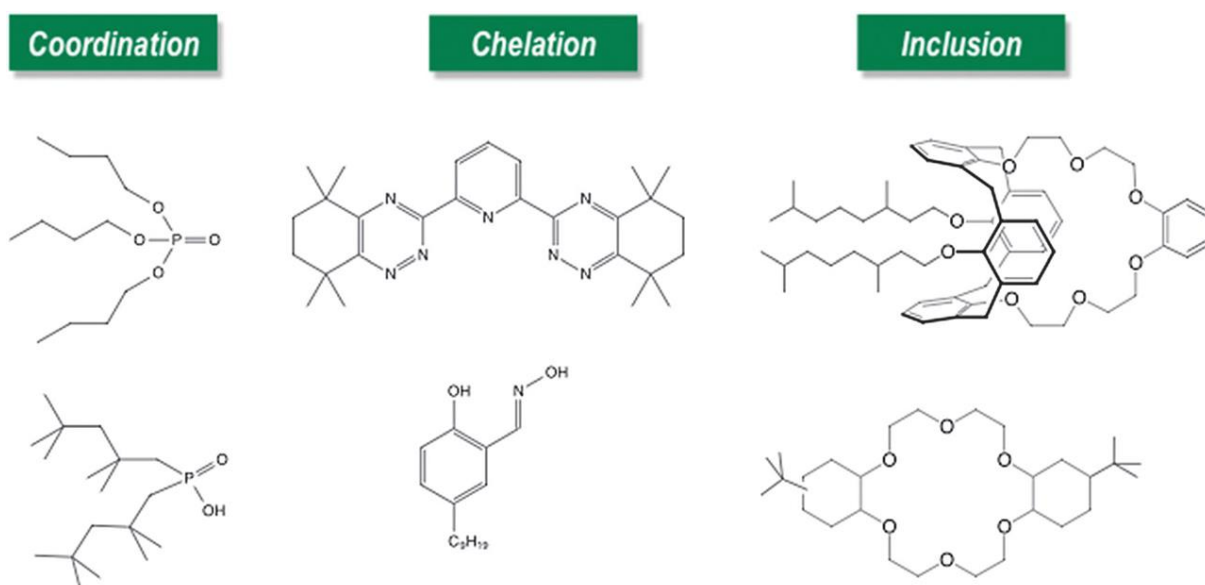
In several conventional rare earth ores, the considerable amount of uranium present is deemed high enough to invest in uranium recovery as a by-product for uses in nuclear fuel[14]. That makes the role of uranium (and by extension thorium) bifold. From an environmental viewpoint, they are to be removed in the mining of rare earths, due to radiation issues, and from an energy viewpoint, they are recovered from rare earth minerals as a byproduct, to help meet the demand for nuclear energy. In our quest to be less dependent on fossil fuels, uranium fuel (next to solar power and wind energy) will remain to play a key role in energy production for the foreseeable time[17] (thorium can be applied in this field as well[18]). Yet, as the demand for nuclear fuel rises, equal effort should be made to close the nuclear fuel cycles (recyclability) or to optimize current processes with clear and effective waste management strategies. In addition, a similar trend to rare earth production is also observed in uranium recovery, where secondary resources are now gaining a lot of interest (e.g., phosphate rocks, seawater, carbonatite, black shale, lignite[19-21]). Regardless of the viewpoint, actinide/rare earth separation is of high importance, even at the level of low concentration processing.

These developments open up interesting avenues for selective adsorbents. In the case of rare earth mining, actinide-targeting techniques could be applied to pretreat leachates and purify them from these radioactive elements. The opposite situation counts as well, where e.g.,

uranium is the resource in focus (energy viewpoint) and the rare earths are recovered as traces from the uranium-rich processing streams. In any case, a high product grade is required, no matter the element in focus. As stated by Florek *et al.*[1]: While both REEs and actinides can be found naturally in mineral deposits worldwide and are not as rare as their name implies, the true economic value of these elements as vectors for technological applications and energy sources is only reached when they are isolated and thoroughly purified from the mineral matrix and from each other.

### 3.1.4 Challenges

Dilute, metal containing aqueous streams can originate from various sources, e.g., processing solutions from primary mining or recycling technologies, polluted waters, even the ocean is full of interesting metals[1, 2, 6, 22]. The metals can be regarded as valuable or harmful (sometimes both), yet, in any case, their selective recovery/removal is necessary. In addition to being selective, an adequate separation technology needs to be energy efficient and show a good yield as well[2]. The introduction of the so-called molecular recognition approach has been an important step in the quest for selective recovery techniques. Specific functionalities are designed to selectively interact with target species, such as selective ligands for metal binding. These functionalities are described by Izatt *et al.* as ion receptors or hosts[2]. Examples are, for instance, the selective ligands that are used in SX or IX chromatography, as described in Chapter 2 (e.g., DEHPAA). Their binding with target metals occurs via various donor-acceptor interactions, e.g., coordination, chelation or inclusion (Figure 3.1).



**Figure 3.1** Different designs of ligand systems for selective metal interactions, through coordination, chelation or inclusion. (Adapted from [2])



By immobilizing such receptors onto a solid phase matrix, one could effectively create a heterogeneous system for the recovery/removal of target metals. Being a passive technique, this approach sounds very appealing for the treatment of dilute metal streams.

## 3.2 Adsorption of critical metals

To overcome the limitations of homogeneous liquid-based separation technologies, the development of solid-phase extraction strategies has emerged over the past few years[1, 22-28]. Various materials have been, and are investigated as potential solids to use as selective adsorbents, either pristinely or functionalized (*vide infra*) [1, 29].

### 3.2.1 What is adsorption?

In general, adsorption can be understood as the binding, either reversible or irreversible, of molecules and/or atoms (the adsorbate) from the gaseous or liquid phase onto a surface (the adsorbent)[30]. The reverse process is called desorption. Depending on the type of bonding involved, adsorption can be classified as follows (according to Inglezakis *et al.*[31]).

(a) *Physical adsorption*. In physical adsorption (or physisorption), no exchange of electrons is observed. The interaction is based on intermolecular attractions between favorable energy sites, where the interaction energies are comparable to heats of vaporization (condensation). The adsorbate is held to the surface by relatively weak van der Waals forces and multiple layers may often be formed with approximately the same heat of adsorption (a few kJ/mol).

(b) *Chemical adsorption*. Chemical adsorption (or chemisorption) involves an exchange of electrons between the specific surface sites and solute molecules, resulting in a chemical bond. This interaction is a lot stronger than physisorption, with energies comparable to the strength of chemical bonds (tens of kJ/mol). Generally, only a single molecular layer can be adsorbed.

(c) *Electrostatic adsorption (ion exchange)*. This interaction is a result of Coulomb attractive forces between ions and charged functional groups and is commonly classified as ion exchange.

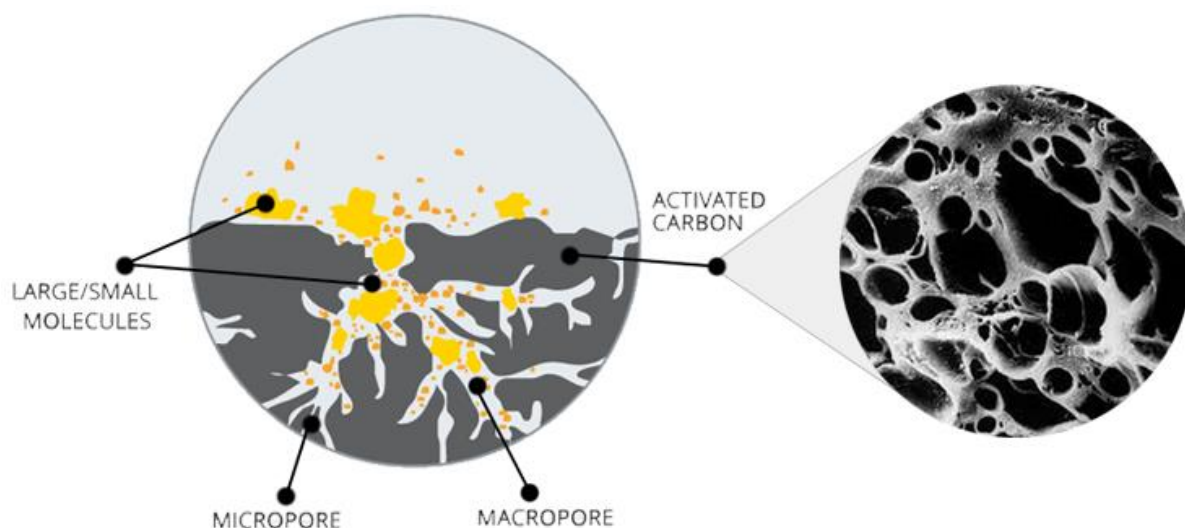
The surface of a solid plays an important role in adsorption. It can be characterized as external when it involves bulges or cavities with width greater than the depth, or as internal when it involves pores and cavities that have depth greater than the width[32] (Figure 3.2). The introduction of porosity to a solid is very advantageous for adsorption purposes (and other applications), as the available surface area for interaction increases dramatically.



**Figure 3.2 (Left) Adsorption on an external surface, (Right) Adsorption on a porous material, containing external and internal surface. (Blue dots: adsorbed species)**

### 3.2.2 Material porosity

Porosity is said to be decisive for an adsorbent's usage. Its pore structure, total number of pores, their shape and size determine the adsorption capacity and even the adsorption rate of the material[31]. In terms of size (diameter), pores are generally classified as either macroporous ( $> 50$  nm), mesoporous ( $2 - 50$  nm) or microporous ( $< 2$  nm)[33]. Porosity is not considered an intrinsic property of solids; therefore pores are created by a certain treatment. This could be an aggregation of particles into a certain porous system, or a detachment/destruction of a part of the mass of the solid, leaving pores behind[31]. These are typically treatments that result in an irregular pore system, i.e., one has limited control over the pore-creation process. A well-known example is activated carbon (or charcoal). It makes use of various kinds of carbonaceous raw materials, such as coal, wood, coconut shells or lignite, which are treated, either thermally or chemically, to obtain an active (micro) porous material. Thermal treatments generally involve carbonization and oxidation (steaming), while chemical methods impregnate certain solutions (acidic, alkaline) as activators, prior to carbonization. The obtained adsorbents have surface areas up to several thousand  $\text{m}^2/\text{g}$  and are used in a variety of adsorption processes for the removal of organics from liquid or gaseous media[34]. Their pore structure and size distribution are very irregular, however (Figure 3.3), and for certain applications, a more uniform pore structure might be desired.



**Figure 3.3 Irregular pore structure of activated carbon, as a result of its activation treatment. (Adapted from [34])**

With the concept of molecular recognition in mind (i.e., selective ligands), it is important to have a pore system that both facilitates the immobilization of the desired functionalities, and enables an unhindered transport of solute-containing fluid throughout the material. It is therefore recommended to opt for controlled porosity, for instance by using structure directing agents (*vide infra*) during the material synthesis or by pursuing a reticular synthetic approach (see Chapter 4). This results in materials with a more uniform structure, and thus more constant performance.

### 3.2.3 Supports suitability

There are several parameters that define the quality of a (porous) solid as a potential adsorbent support. The ideal support meets as many as possible of these standards.

(a) Porosity is, as mentioned, a crucial parameter. A high surface area results in higher uptakes; larger pores enable the immobilization of bulky ligands; and a well-interconnected pore system facilitates fluid transport. Mesoporous materials (pores: 2 – 50 nm) are suggested to be ideal materials for liquid-phase adsorption, as they are an excellent compromise between large pores and high surface areas[1].

(b) Functionalizability of the support is an obvious requirement in order to obtain a selective adsorbent. These functionalization processes are preferably straightforward, involving but a few steps (e.g., pre-functionalization and/or post-functionalization), as well as cost/time-effective. Moreover, the linkage between support and functionality needs to be strong enough to survive the intended environment. A ligand-functionalized adsorbent may be extremely selective towards a certain metal, yet, if for instance its acidic environment causes cleavage of the support-ligand link, the material is useless for continuous application.

(c) Support stability is, in addition to linkage-stability, another important requirement. A porous solid must be resistant to the applied sorption environments. This includes both adsorption and desorption conditions. While many metal adsorption processes can take place in neutral, or moderately acidic or alkaline solutions, desorption (regeneration) often takes place in highly acidic conditions[35]. An ideal support survives the repetitive adsorption/desorption cycles, resulting in a reusable adsorbent (providing that the linkage is stable enough).

(d) The selectivity of an ideal metal adsorbent predominantly results from the embedded ligands. However, in some cases, functionalization is not necessary to obtain a selective material (i.e., inherently selective solids, see Chapter 6). It is also important to consider the affinity of a support for certain (unwanted) species, e.g., while the embedded ligand targets a specific metal, the support itself could adsorb competing metals. Ideally, the support shows no affinity towards any species, making the embedded ligands the sole active sites of the adsorbent.

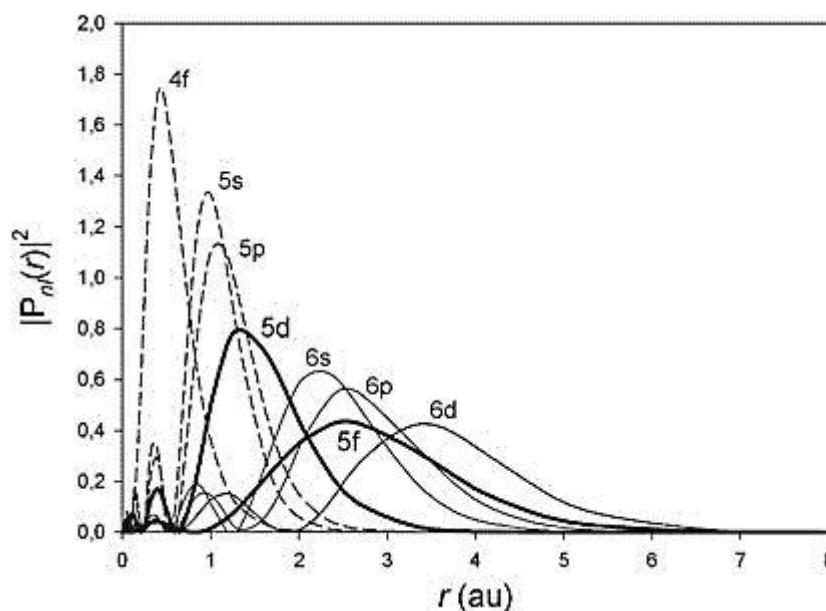
As a general trend, a higher selectivity requires more sophisticated (and costly) ligands. With the processing of dilute metal streams (mg/L) in mind, it may seem counterintuitive to employ such costly ligands when the return per unit-volume of feed decreases. However, the combination of a high selectivity and reusability of an adsorbent makes the process economical[2]. According to Izatt *et al.*, robust molecular recognition materials (such as selective metal adsorbents) in which the receptor is covalently bound to a solid support, thereby preventing its loss, can provide the needed recyclability to treat metal-containing streams at < 100 mg/L[2].

### 3.3 Adsorption of rare earths & uranium

In order to develop rare earth selective adsorbents, it is important to look at their chemistry. The remarkable character of these elements was already illustrated in Chapter 2. Due to the restricted extension of the rare earths' 4*f* orbitals, they cannot overlap with surrounding orbitals of other components (e.g., ligands). This means that covalent bonding for the lanthanides in their normal oxidation states virtually does not occur. As a result, the lanthanides are predominantly bonded by ionic/electrostatic interactions[36], and there is little preference in terms of bond-direction. Ligands are therefore coordinating around the rare earth cation with minimal repulsion between them[37]. The large size of lanthanides (1,06 - 0,85 Å) allows for high coordination numbers, typically varying between 6 and 9, although exceptions are not uncommon[37]. In addition, rare earths cations are typically hard Lewis acids and preferentially bind with hard Lewis bases (cfr. Pearson's *Hard Soft Acid Base* theory, HSAB)[38]. These properties should be kept in mind when designing/investigating ligands for REE coordination.

When uranium is considered, the situation slightly changes. Being part of the actinides, uranium is a 5*f* element with the [Rn]5*f*<sup>3</sup>6*d*<sup>1</sup>7*s*<sup>2</sup> configuration. The actinide group as a whole is not

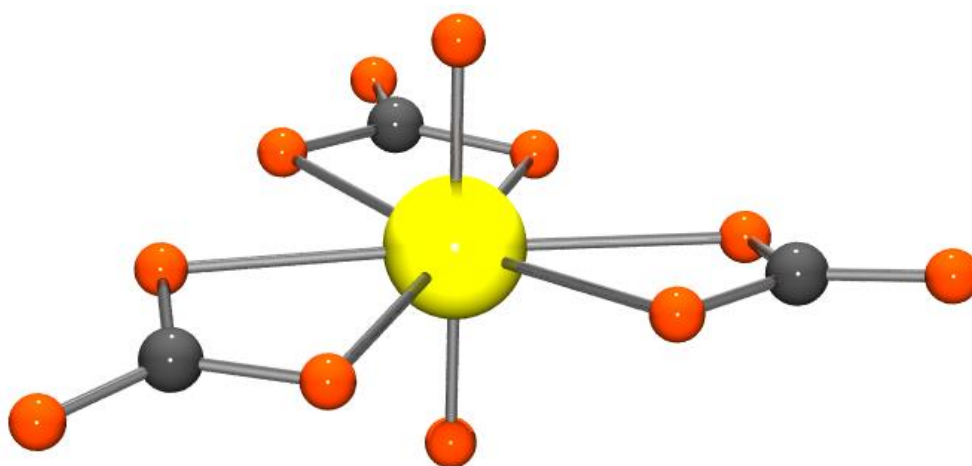
discussed in this work, but it should be noted that there are a lot of similarities with the lanthanides. For instance, both groups involve the filling of *f*-orbitals, and both experience a contraction phenomenon, where the element radius gradually decreases with increasing atomic number, because of improper shielding from the increasing nuclear charge by the 4*f* (lanthanides) or 5*f* (actinides) electrons (cfr. Section 2.2.1). However, while the 4*f* subshell in lanthanides is well protected from the environment by the higher 5*s*, 5*p* subshells, the 5*f* subshell in actinides is not shielded by the filled 6*s* and 6*p* subshells (Figure 3.4). In addition, the 5*f* subshell has a very small energy difference with its higher shells. As a result, the 5*f* electrons can become active in bonding, which leads to a higher variety of oxidation states in actinides, typically ranging from +3 to +7 [39]. For instance, for uranium, its [Rn]5*f*<sup>3</sup>6*d*<sup>1</sup>7*s*<sup>2</sup> configuration readily gives rise to a +6 oxidation state. Overall, the ionic character predominates in actinide bonding, just like for lanthanides, but because of the mentioned poor shielding of the 5*f* subshell by the higher shells, the radial extension of the 5*f* orbitals allows for overlap with ligand orbitals, which results in some covalent bonding contribution[40].



**Figure 3.4 Orbital probability distribution in actinides. (Retrieved from [41])**

Uranium is a very hard Lewis acid and therefore a strong electron acceptor in all its different oxidation states[40]. Its ionic size highly depends on its oxidation state and coordination mode, and commonly varies between 1.02 and 0.73 Å [42]. In natural environments, its most important oxidation states are +4 and +6 [39]. Compounds containing tetravalent uranium are insoluble in mildly acidic to alkaline conditions, whereas, those containing the linear uranyl moiety  $\text{UO}_2^{2+}$  are highly soluble and mobile[40]. These linear “-yl” species in aqueous solutions are somewhat unique for the actinides. In the case of uranyl, the short U(VI)–O<sub>yl</sub> bond distance, approximately 1.75 Å, indicates a strong multiple uranium–oxygen bonding, one of  $\sigma$  and two of  $\pi$  character. The uranyl(VI) ion can therefore be described as  $^{-2}\text{O}\equiv\text{U}^{+6}\equiv\text{O}^{-2}$  [39, 40].

When it comes to coordination chemistry, the structure of uranyl complexes can generally be summarized as a uranyl ion surrounded by a ‘girdle’ of 4, 5, or 6 donor atoms around its waist. In general, if there are 4 or 5 donor atoms around the waist, they are reasonably coplanar, but some distortion can sometimes occur when there are six[39]. Figure 3.5 shows an example of a mononuclear uranium tricarbonate complex  $[\text{UO}_2(\text{CO}_3)_3]^{4-}$  where three carbonates are coordinating in a plane perpendicular to the uranyl O-U-O axis, effectively forming a hexagonal bipyramid. Similarly, the uranyl aqua-complex  $[\text{UO}_2(\text{OH}_2)_5]^{2+}$  is established as a pentagonal bipyramid[39]. More information on the chemistry and coordination of uranium and other actinides can be consulted in *Lanthanide and Actinide Chemistry*, by S. Cotton[39] and *The Chemistry of the Actinide and Trans-actinide Elements* by J. Katz, L. Morss, N. Edelstein, and J. Fuger[40].

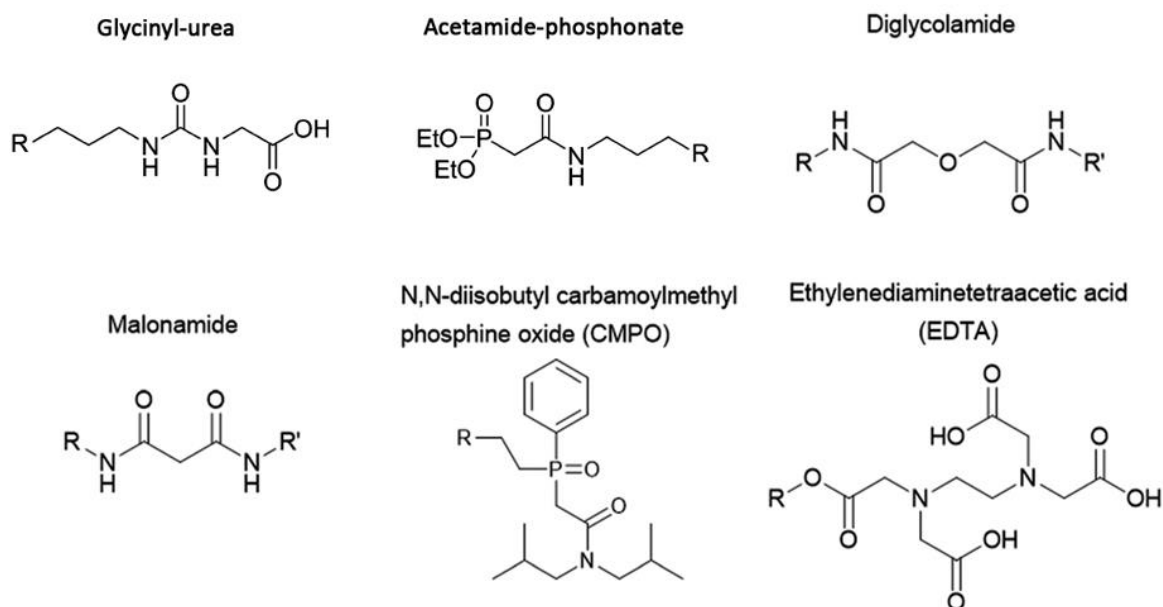


**Figure 3.5 Structure of the uranium tricarbonate complex  $[\text{UO}_2(\text{CO}_3)_3]^{4-}$ . (U: yellow, O: red, C: black) (Retrieved from [43])**

### 3.3.1 Selective ligands

When looking at REE and U extractions, hard oxygen-containing ligands are probably the most widely applied for rare earth coordination[1, 23, 27, 39, 44, 45]. Typical ligands are based on alkoxides, carboxylates, phosphonates, amides...[23]. In addition, it has been found in SX processes that by combining different ligand types, a certain advantageous effect can be obtained on the extraction performance. This phenomenon is called ligand synergism, and the idea behind it is to increase the lipophilicity of the metal-complex (i.e., higher affinity for the organic phase in SX), via an optimal surrounding of the cation by different ligand types. The effect arises from the replacement of residual water in the inner coordination sphere or by occupation of open coordination sites by neutral electron donors, called synergists[46]. For adsorption purposes, the coupling of hard anionic ligands with a synergistic ligand, makes it possible to create a chelating ligand with a very high affinity for *f*-element coordination[23, 47-50]. In addition to a desired combination of ligands into a chelate, its resulting selectivity can

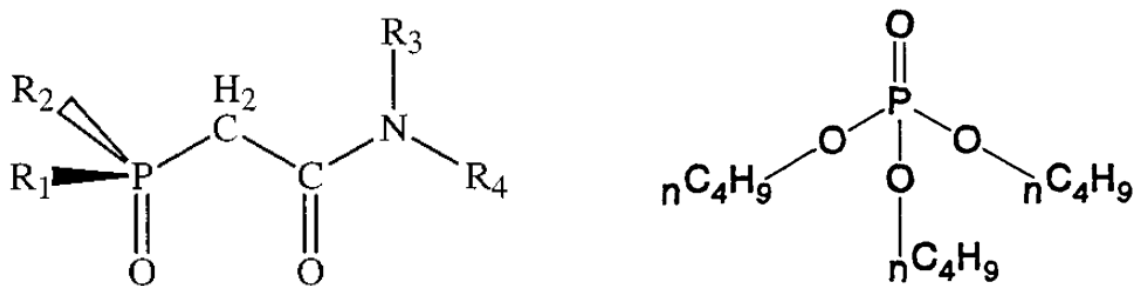
also be determined by its ‘bite’[2], i.e., a certain ‘pocket’ or ‘cavity’[23] is formed which can influence the affinity for certain species. A few typical chelating ligands for rare earth and actinide coordination are depicted in Figure 3.6.



**Figure 3.6 Commonly used ligands for rare earth and actinide coordination. (Retrieved from [1] and [23])**

As a consequence of the described characteristics of these *f*-elements (*vide supra*), it appears that the most thermodynamically stable ligand/metal coordination conditions should contain multidentate O-donors, efficiently packed around the cation in such a way as to provide maximum numbers of ligand/donor interactions with a minimum of steric strain[51].

Bidentate ligands, such as diphosphine oxides,  $\beta$ -diketones, and diamides are widely applied to bind both lanthanides and actinides[52]. They are generally preferred over monodentate analogues[53]. A prominent example of a selective bidentate ligand is carbamoylmethylphosphine oxide (CMPO), which combines a phosphine oxide-type donor with an amide (Figure 3.7). CMPO is widely applied in industrial nuclear fuel reprocessing[54], and can be used to target actinides and lanthanides, depending on the respective feeds solutions. For instance, CMPO is used to treat aqueous raffinates from a solvent extraction process called PUREX (*Plutonium Uranium Refining by Extraction*), in which tri-*n*-butyl phosphate (TBP, Figure 3.7) is applied to extract most of the uranium (and plutonium). These aqueous raffinates contain other trivalent actinides and lanthanides[52], but also residual uranium, and their processing with a combination of TBP and CMPO is what is known as the TRUEX process (TRans-Uranium Extraction)[54].

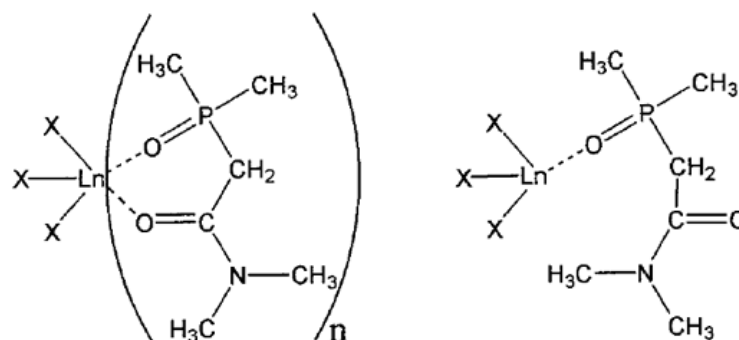


**Figure 3.7 Basic structures of CMPO (left) and TBP (right).**

Regardless of its high efficiency for *f*-element extraction, the basis of CMPO selectivity is very intricate. Even its binding mode with cations is not definite and depends on a lot of parameters. Solid-state structures show that CMPO and its derivatives (e.g., analogues with phosphine oxide or phosphonate groups, *vide infra*) generally coordinate with lanthanide or uranyl cations in a bidentate mode, however, monodentate binding by the phosphoryl  $O_P$  oxygen is also observed[55, 56] (Figure 3.8). The work of Boehme and Wipff[52] has offered a lot of insight in the coordination behavior of CMPO, by performing a quantum mechanical study and taking various factors into account that influence the ligand's coordination behavior. Some of the authors' main findings are given below. In their work, a tetramethyl CMPO-derivate, denoted **L**, was used for the modeling (Figure 3.8), and the trivalent lanthanides La, Eu, and Yb were investigated, as well as uranyl.

When comparing binding modes (monodentate vs. bidentate) in gas phase, they found that **L** always prefers bidentate binding mode, but that the difference to monodentate binding is surprisingly small, e.g., metal-ligand (M-L) binding energy in  $EuCl_3L$ : -255 kJ/mol (bidentate) vs. -229 kJ/mol (monodentate). One would expect a larger difference in stability between bidentate and monodentate modes, due to the energy gain from the additional  $M-O_C$  interaction. Yet, it appears that steric interactions (repulsions) within the first coordination sphere of the metal play an important role in the thermodynamic complex stability. As the bidentate binding mode enforces a *cis*-conformation on the ligand, this leads to some intraligand repulsion between the carbonyl and phosphoryl dipoles. Such interactions partially counteract the gain of an additional M-O bond. Moreover, this intraligand repulsion is further enhanced by the polarizing effect of the cation charge, which adds an induced dipole moment to their permanent dipole moments[52].

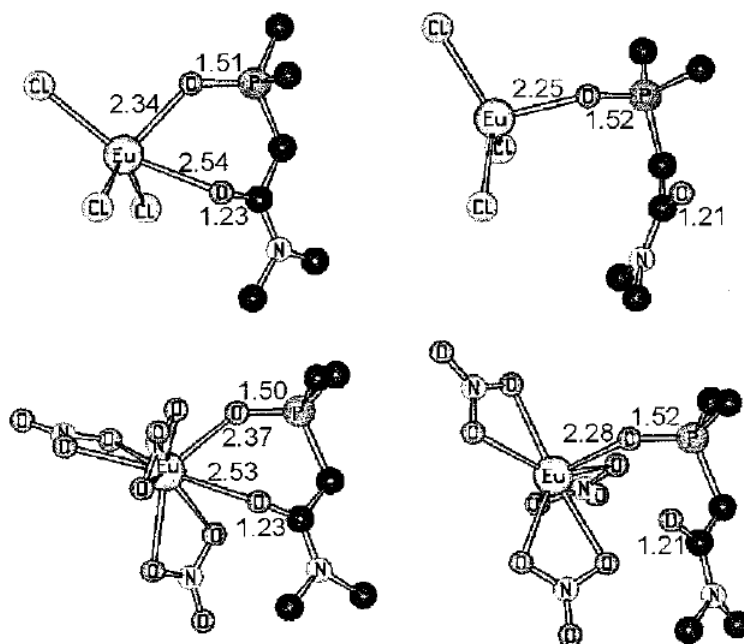




**Figure 3.8** Schematic representation of the bidentate  $\text{MX}_3\text{Ln}$  (right) and of the monodentate  $\text{MX}_3\text{L}$  complex ( $\text{O}_\text{P}$  coordination) (left). (Retrieved from [52])

These repulsions also affect the selectivity between cations. Overall, the authors observed that CMPO formed stronger (shorter) bonds as the lanthanides got smaller (cfr. *lanthanide contraction*), as can be expected from their increasing charge density and thus increasing affinity with the hard oxygen donors. This was also observed from the M-L binding energies, which increased upon cation size reduction, e.g.,  $\text{LaCl}_3\text{L}$  (-247 kJ/mol) <  $\text{EuCl}_3\text{L}$  (-255 kJ/mol) <  $\text{YbCl}_3\text{L}$  (-260 kJ/mol) (all bidentate mode, but similar effect for monodentate). However, as can be seen, the difference in binding energies is very small. The reason for this is that while the charge density of the cation increases, it also strengthens the induced dipole moment on the CMPO ligand, which causes stronger intraligand repulsions. As a result, a basic coordinating CMPO (**L**) in bidentate mode experiences little selectivity between the lanthanides. In monodentate binding mode, the intraligand repulsions are more or less negligible, causing larger differences in M-L interaction energies. So, even though the monodentate binding mode leads to a decrease in binding energy compared to the bidentate mode, it does result in a slight increase in metal cation selectivity.

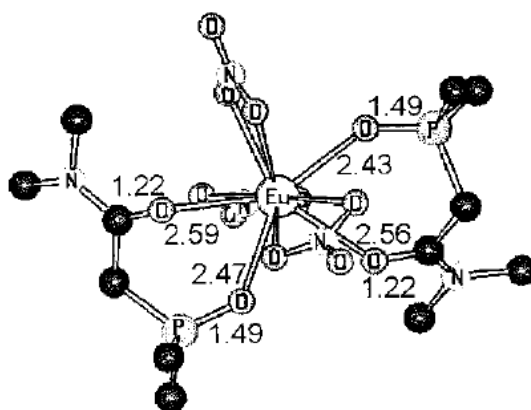
Another important influence on the coordination are the counter ions (X) in the complex. These ions also cause steric effects in the first coordination sphere, i.e., interligand repulsions. When comparing nitrate anions to chlorine ones in  $\text{MX}_3\text{L}$  complexes, the authors observed an increase in M- $\text{O}_\text{P}$  bond lengths in the nitrate complex (both in monodentate and bidentate mode), which they attributed to more steric hindrance of the nitrates in the first coordination sphere (Figure 3.9). The increase in bond length is very small, however, and once again this is the result of a counteracting effect. Because the nitrate anion is less polarizable than the chlorine, a lower charge transfer between nitrate and metal is achieved. As a result, a higher netto-charge remains on the metal cation, which can then attract the CMPO donor atom(s) in a stronger fashion. Nonetheless, following the observed M-L binding energies, the complex with chlorine anions appears more stable than the nitrate one, both in bidentate mode ( $\text{EuCl}_3\text{L}$ : -255 kJ/mol vs.  $\text{Eu}(\text{NO}_3)_3\text{L}$ : -219 kJ/mol) and in monodentate mode ( $\text{EuCl}_3\text{L}$ : -229 kJ/mol vs.  $\text{Eu}(\text{NO}_3)_3\text{L}$ : -186 kJ/mol)[52].



**Figure 3.9** Structures of calculated europium complexes. Top:  $\text{EuCl}_3\text{L}$ ; Bottom:  $\text{Eu}(\text{NO}_3)_3\text{L}$ ; Left: bidentate mode; Right: monodentate mode. Bond lengths are provided in Ångström. (Retrieved from [52])

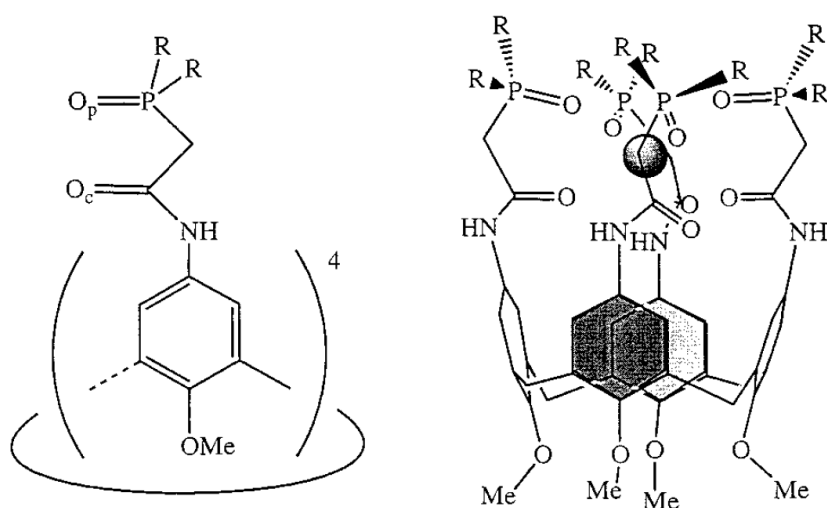
Counter ions can also greatly influence the selectivity of the CMPO ligand. As mentioned, **L** as such shows very little selectivity between the tested cations, but the situation changes when steric crowding is introduced in the form of counter ions (or other ligands, for that matter). While the authors observed an increasing selectivity in the order of  $\text{La}^{3+} < \text{Eu}^{3+} < \text{Yb}^{3+}$  for the bidentate  $\text{MCl}_3\text{L}$  complexes (i.e., following the decreasing cation size), a selectivity order of  $\text{La}^{3+} < \text{Yb}^{3+} < \text{Eu}^{3+}$  was observed in the bidentate nitrate complex,  $\text{M}(\text{NO}_3)_3\text{L}$ , ascribed to the more spatially demanding nitrate counter ion influencing the conformation of CMPO[52].

The coordination of more than one CMPO ligand was taken into account as well by Boehme and Wipff. When two CMPOs are taken into consideration instead of one, e.g.,  $\text{Eu}(\text{NO}_3)_3\text{L}_2$ , which form bidentate bonds to the cation (Figure 3.10), all M-O bond distances increase as a result of an increased steric strain in the first coordination sphere. It was also found that the addition of the second bidentate ligand **L** results in less than half of the binding energy that is obtained by the addition of the first one, i.e., -89 kJ/mol for  $\text{Eu}(\text{NO}_3)_3\text{L}_2$  vs. -218 kJ/mol for  $\text{Eu}(\text{NO}_3)_3\text{L}$  [52].



**Figure 3.10** Structure of the calculated europium complex  $\text{Eu}(\text{NO}_3)_3\text{L}_2$  in bidentate mode. Bond lengths are provided in Ångström. (Retrieved from [52]).

Despite the loss in binding energy, the addition of multiple ligands to the cation can result in a different selectivity pattern for metal coordination, by influencing the steric crowding around the cation (similar to the steric effect of counter ions). An example is the organization of multiple CMPO units (or other ligands) onto molecular platforms such as calixarenes<sup>1</sup> (Figure 3.11) or analogues. The use of such molecular platforms to position ligating sites for actinide/lanthanide complexation was first reported by Böhmer *et al.*[57]. Their approach was based on the fact that three CMPOs are involved in the (solvent) extraction of actinides/lanthanides[58]. They found that attachment of four CMPOs to a calix[4]arene could result in a considerable enhancement of the extraction efficiency toward actinides and lanthanides compared to single CMPO[59, 60].

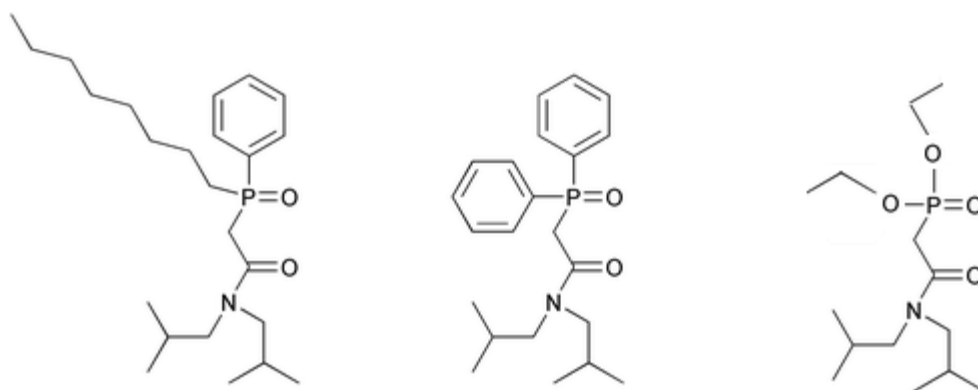


**Figure 3.11** Schematic representation of a calix[4]-CMPO ligand (cavitand) and of an  $\text{M}^{3+}$  inclusion complex. (Retrieved from [52])

<sup>1</sup>A calixarene is a cyclic oligomer formed by hydroxyalkylation of a phenolic compound (phenol, resorcinol...) and an aldehyde (formaldehyde, acetaldehyde...).

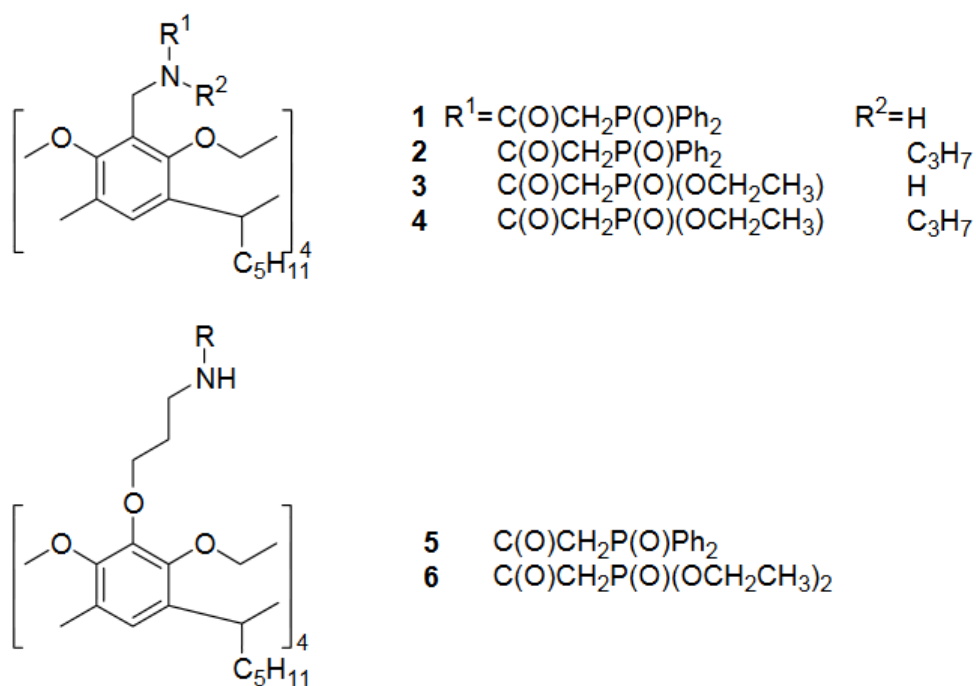
Also within the series of lanthanides and actinides, large differences in selectivity could be obtained by investigating different analogues of these molecular platforms and/or by tailoring their so called upper or lower rim. In Figure 3.11, the calix[4]arene has its upper rim functionalized by the CMPO units, while the lower rims contains methoxy groups. Such upper rim CMPO-functionalized calix[4]arenes have been reported to exhibit selectivity in the trivalent lanthanides series ( $\text{La} \gg \text{Yb}$ ) and can discriminate between trivalent lanthanides and actinides ( $\text{Am} > \text{Eu}$ )[61]. Different lower rim functions can also influence this selectivity by enforcing a different conformation on the platform[62].

When considering the CMPO ligand itself, either in free form or tethered onto a molecular platform, the presence of various substituents can also greatly influence extraction efficiencies and selectivity. In the earlier described study of Boehme and Wipff[52], calculations were performed with the tetramethyl-CMPO, but analogues with aliphatic and/or aromatic substituents or substituted phosphonates instead of phosphine oxides exist as well (Figure 3.12). In addition to a sterical effect on the conformation of the CMPO itself (intraligand effects), as well as on the ligand crowding in the first coordination sphere (interligand effects), these substituents can also affect the electron density on the donor atoms (cfr. electron donating/withdrawing properties), overall influencing the stability as well as the selectivity of the formed M-L complexes.



**Figure 3.12 Different analogues of the CMPO ligand.**

In order to illustrate the effect of substituents, a comparison is made of various CMPO/calixarene-based extractants ('cavitands'), based on a study in [62]. The cavitands (Figure 3.13) were used in solvent extractions to investigate their coordination behavior towards different metals. As can be seen from Figure 3.13, each cavitand differs in substituents on the CMPO ligand (phenyl, alkyl, alkoxy groups). Table 3.3 gives an overview of their complex formation constants (logarithmic values) for a variety of cations.



**Figure 3.13** Different CMPO analogues tethered onto calixarenes-based molecular platforms for cation extraction. (Adapted from [62])

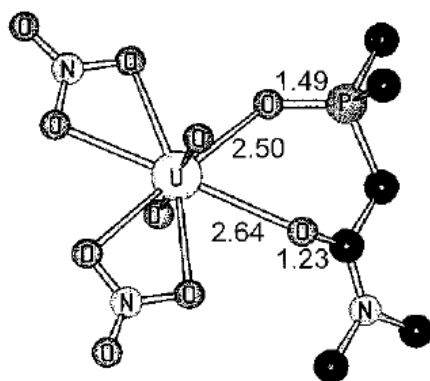
**Table 3.3** Complex formation constants (logarithmic values) obtained with CMPO/calixarenes-based derivatives 1 to 6. (Adapted from [62]).

Ionophore Cation	CMP(O)					
	1	2	3	4	5	6
Eu <sup>3+</sup>	27.6	24.7	31.0	28.1	27.7	22.5
UO <sub>2</sub> <sup>2+</sup>	22.4	18.7	25.5	20.3	22.6	17.7
Pb <sup>2+</sup>	18.8	16.0	22.5	18.2	18.3	12.7
Cd <sup>2+</sup>	18.1	15.6	22.7	16.7	16.8	13.4
Sr <sup>2+</sup>	18.5	13.7	21.4	n.d. <sup>a</sup>	15.2	n.d. <sup>a</sup>
Cu <sup>2+</sup>	17.4	15.9	21.7	17.7	17.0	13.8
Ag <sup>+</sup>	6.4	5.3	8.9	7.5	7.4	5.5
Ca <sup>2+</sup>	14.0	12.7	16.9	n.d. <sup>a</sup>	16.6	n.d. <sup>a</sup>
Mg <sup>2+</sup>	14.4	11.4	16.5	n.d. <sup>a</sup>	14.4	n.d. <sup>a</sup>
K <sup>+</sup>	6.7	5.6	10.2	n.d. <sup>a</sup>	5.6	n.d. <sup>a</sup>
Na <sup>+</sup>	7.2	7.2	12.0	8.0	7.6	6.1

a) Not determined.

It can be seen that the complex formation constants in Table 3.3, essentially follow the order of  $\text{Eu}^{3+} > \text{UO}_2^{2+} > \text{Pb}^{2+}$ ,  $\text{Cu}^{2+}$ ,  $\text{Cd}^{2+}$ ,  $\text{Sr}^{2+} > \text{Ca}^{2+}$ ,  $\text{Mg}^{2+} \gg \text{Ag}^+$ ,  $\text{K}^+$ ,  $\text{Na}^+$ . The high values of the complex stability constants for  $\text{Eu}^{3+}$  and  $\text{UO}_2^{2+}$  confirm that these CMPO-cavitands are strong receptors for these cations[62]. In addition, it is clear that the presence of different substituents causes significant variations in complexation properties. It appears, for instance, that the phosphonate derivatives (**3**, **4**) show stronger interactions than the phosphine oxide ones (**1**, **2**), although it has been shown that complexation properties of P-containing compounds differ in the order of phosphonate < phosphate < phosphine oxide, when alkyl chains are present at those groups[62]. But since in **1** and **2**, phenyl groups are present, it might explain the lower formation constants vs. **3** and **4**, as it has been shown that phenyl groups can lower the basicity of the phosphine oxide, as well as influence the conformation of the CMPO[62].

As to explain the difference between actinides (e.g., uranyl) and lanthanides (e.g., europium), it becomes clear that all of the described factors will influence the complexing behavior of a certain CMPO-type ligand (and by extension other ligands). A certain combination of ligands, their substituents, and organization will result in more favorable actinide receptors, while other combinations could shift the preference to lanthanides. When looking at the basic CMPO itself, as Boehme and Wipff did[52], it was found that in the basic CMPO (**L**) complex with uranyl, i.e.,  $\text{UO}_2(\text{NO}_3)_2\text{L}$  (Figure 3.14), the M-O bond distances are comparable to those in the  $\text{La}^{3+}$  complexes, with the U-O<sub>P</sub> bond being slightly longer than the La-O<sub>P</sub> bonds and the U-O<sub>C</sub> and La-O<sub>C</sub> bonds having similar lengths. This means that the difference in phosphoryl vs. amide binding contributions is smaller in the uranyl than in the lanthanum complexes, although the M-O<sub>P</sub> bond remains the more important one. The lengthening of the U-O<sub>P</sub> bond compared to La-O<sub>P</sub> suggests a slightly weaker interaction with the uranyl, which the authors saw confirmed in the M-L binding energies (-189 kJ/mol for  $\text{UO}_2(\text{NO}_3)_2\text{L}$  vs. -215 kJ/mol for  $\text{La}(\text{NO}_3)_3\text{L}$  (bidentate).



**Figure 3.14** Structure of the calculated  $\text{UO}_2(\text{NO}_3)_2\text{L}$  complex. Bond lengths are provided in Ångström. (Retrieved from [52])

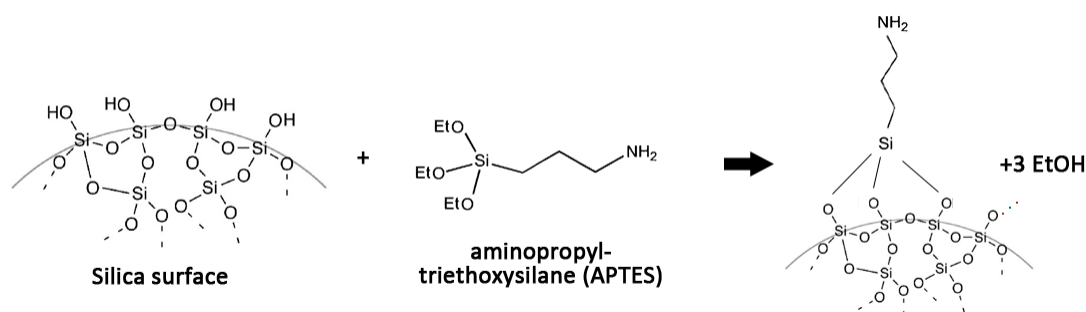
Taking all factors into account, ligand design is a very versatile, yet, intricate business. Calculations can give a lot of insight, but experimental data will teach us the most, as there are a

lot of influencing parameters. Coordination behavior is determined by cation size and charge density, amount of ligands, their organization, the presence of substituents, counter ions affecting the coordination spheres... The shift from gas-phase calculations to real-life aqueous environments dramatically complicates the situation. In such conditions, the first coordination shell is filled with different ligands, anions, and/or solvent molecules, each influencing the stability and selectivity of the complex. Furthermore, when dealing with bidentate ligands like CMPO, the differences between monodentate and bidentate binding (*vide supra*) may be easily compensated in favor of the former, as a result of second shell environment effects, like hydrogen bonding interactions with the uncoordinated carbonyl group of CMPO (e.g. with co-extracted nitric acid or water), thereby once again influencing the coordination sphere sterics and ultimately the selectivity. Finally, it must also be stressed that both enthalpy and entropy effects need to be considered to assess complex stability and selectivity. For instance, binding water molecules or additional ligands to monodentate CMPO complexes to compensate for a binding site of the ligand could easily result in an entropy penalty, as a result of reduced freedom[52].

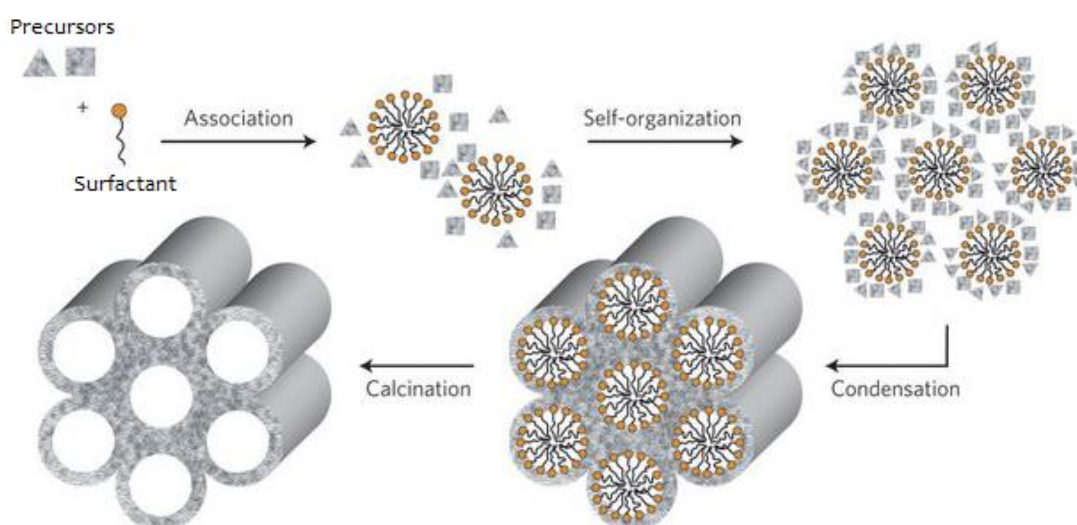
Despite our insight in the matter, it is often times difficult to give a proper theoretical explanation of observed extraction results, which makes the design and synthesis of improved multicoordinate ligands essentially a matter of trial and error[63].

### 3.3.2 Choice of supports

With the requirements for ligand and support in mind (*vide supra*), a selection of a suitable porous materials can be made. One of the most widely applied (inorganic) solids is silica ( $\text{SiO}_2$ ). Traditionally, it is used as silica gel (bare or modified) as a common porous solid in solid-phase separation processes[64]. As the surface of this material has an abundance of silanol groups ( $\text{Si-OH}$ ), an easy and efficient functionalization can be realized via a condensation process of (organo) silanes, creating siloxane bonds (grafting) (Figure 3.15)[64, 65]. These grafted organosilanes can be used as active sites for metal adsorption or serve as primary anchoring points for the functionalization into selective (chelating) ligands (or catalytic complexes)[23, 64, 66]. In addition, the silicas can be synthesized around so-called structure directing agents (a.k.a. templates or surfactants). These are typically micelles of amphiphilic block-copolymers of which the morphology in solution can be tailored. After the silica bulk is formed (condensed) around these micelle networks, they can be removed (thermally or chemically), and ordered porous silica is obtained. Such a self-assembly process is illustrated in Figure 3.16, and can be applied for other material syntheses as well (e.g., mesoporous carbons, *vide infra*). It allows a specific formation of pores with well-defined size and shape[1].



**Figure 3.15 (Left) Silica structure and surface composition. (Middle) grafting of a typical organosilane (APTES), creating primary amine functionalizations on the silica surface, bonded via siloxane bridges (Right).**

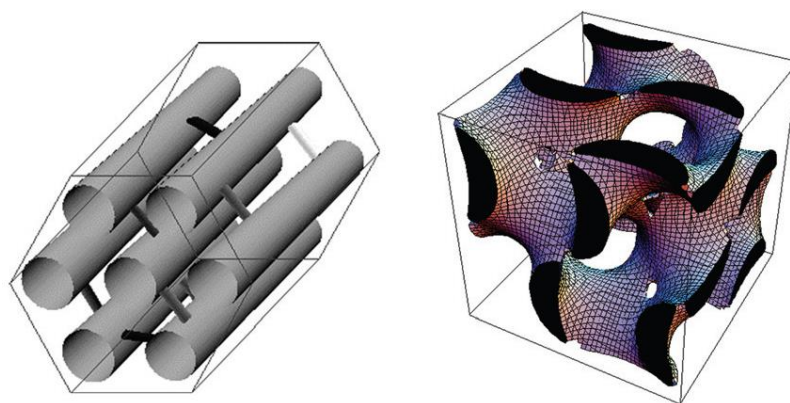


**Figure 3.16 Schematic overview of a typical self-assembly (self-organization) approach for ordered porous materials. (Adapted from [67])**

By adapting process parameters, such as precursor/surfactant ratios, surfactant type, solvents, temperature and contact times, the self-assembly process can be tailored towards very specific nanoporous silicas[1, 68], which can differ in pore structure, pore size, specific surface area, etc. SBA-15 [69] and KIT-6 [70] (Figure 3.17) are two typical examples of ordered mesoporous silicas, with high surface areas ( $> 800$  or  $1000 \text{ m}^2/\text{g}$ ), high pore volumes ( $> 1 \text{ cm}^3/\text{g}$ ), and large pore diameters ( $6 - 13 \text{ nm}$ )[1]. The combination of these characteristics, with the inherent thermal and chemical stability (as well as non-toxicity) and facile functionalization of silica[1], makes this material class very interesting for heterogeneous applications (sorption, catalysis...). As a result, various reports have been published on the application of nanoporous silica as (selective) metal adsorbents[1, 23, 64, 71-73]. However, in certain metal recovery fields, the concept of functionalized silicas is considerably flawed for long-term application. While it is generally known that silica has a poor resistance to alkaline conditions, with dissolution already

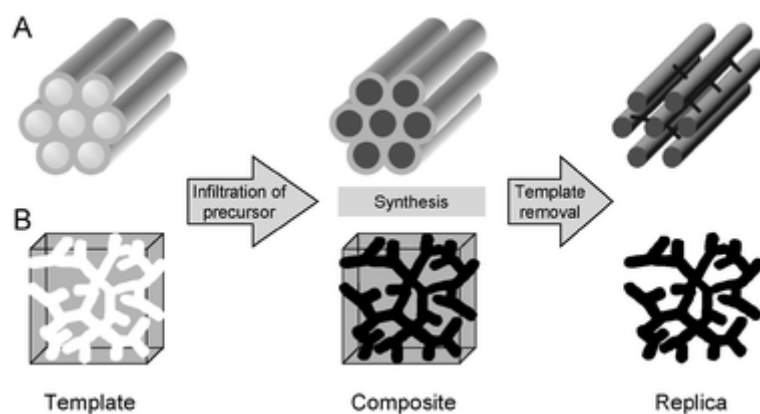


taking place at  $\text{pH} > \sim 8$  [74-76], it is also reported that acidic conditions can have a detrimental impact on the material and its functionalizations (organosilanes). For example, under  $\text{pH} \sim 2$ , surface-grafted siloxane bonds are prone to cleavage [75, 77] which could cause ligand leaching. At the same time, stronger acidic conditions can gradually dissolve the material itself, even at room temperature [76]. It is therefore important to consider the applied environment, before selecting a support material. Nonetheless, several silica-based adsorbents for critical metals (REEs, U) have been reported. An overview is given further in this chapter (Table 3.4).



**Figure 3.17 Schematic representation of the SBA-15 (left) and KIT-6 (right) mesostructure, both mesoporous silica supports. (Adapted from [1])**

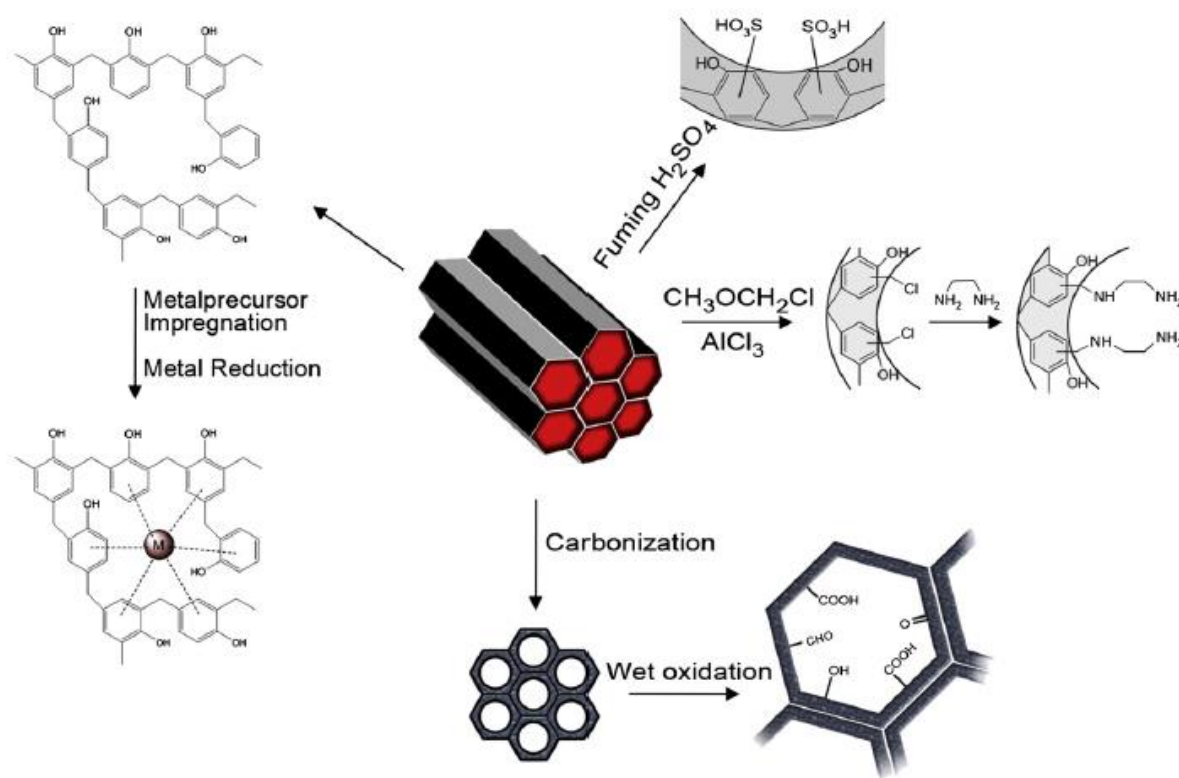
In the organic family of solids, nanoporous carbon equivalents of nanoporous silica are expected to better tolerate harsh acidic or alkaline conditions [1]. Here as well, the evolution from common activated carbon towards ordered nanoporous analogues was achieved through the templating route. One could distinguish two approaches, i.e., (a) nanocasting (hard-template), where premade nanoporous silica is used as a template, and (b) a soft-template method, similar to the one for nanoporous silicas, illustrated earlier (Figure 3.6). In nanocasting, the carbon precursors (e.g., furfuryl alcohol, sucrose [78]) polycondense inside the pores of the silica, followed by carbonization. The silica template is then chemically removed via a washing step, and a carbon-based ‘negative’ or ‘replica’ of the nanoporous silica is obtained [78, 79] (Figure 3.18). As a result, the morphology and porosity of the used silica material determine those of the obtained carbon. Nanocasting can also be applied to obtain other types of nanoporous materials (e.g., metal-oxides [80]). The method is, however, rather tedious and rather difficult to apply on a larger scale [1], due to the inclusion of many steps and the ‘waste’ of the nanoporous silica template. Nonetheless, it is an effective way to obtain nanoporous carbons with similar porosity features as for the analogue silicas.



**Figure 3.18** Schematic illustration of the nanocasting pathway using mesoporous silica hard templates with different geometries (A: hexagonal and B: cubic). (Retrieved from [80])

A popular type of ordered nanoporous carbons are phenol/formaldehyde-based carbons. As the name implies, these are synthesized by polycondensation of a phenolic-type precursor with formaldehyde, typically via the soft-template (self-assembly) approach, i.e., around a network of micelles. Upon carbonization, highly stable nanoporous solids are obtained, with high specific surface areas (several 100s, even over 1000 m<sup>2</sup>/g), large mesopores, and high pore volumes[1, 81, 82]. Just as with the nanoporous silicas, the soft-template process for carbons is highly tunable, giving rise to different porosity features and morphologies[81, 82]. Moreover, it is also possible to apply them as nanoporous polymers (phenolic resins), by performing the calcination at temperatures that do not trigger carbonization ( $\leq 400$  °C)[82]. A similar approach can also be applied in the nanocasting method. As a polymer, these phenolic resins still have their abundant surface (phenolic) hydroxyl groups, which could serve as possible anchoring points. It also makes them very hydrophilic, which is beneficial for aqueous applications.

Ordered mesoporous carbons (and phenolic resins) are less explored for metal adsorption purposes than their silica analogues, although several reports have been published[83-86]. Yet, they offer a lot of potential for functionalization. A few basic functionalization methods are illustrated in Figure 3.19. A particularly interesting one is the chloromethylation approach (also depicted in the figure), which introduces reactive chloromethyl-species onto the surface. These can be used as ideal covalent anchoring points for the immobilization of selective ligands. Another widely selected approach, especially for selective ligand functionalization on carbons, is via a two-step sequence, i.e., a first oxidation step, followed by proper ligand anchoring[87, 88].



**Figure 3.19** Schematic overview of some functionalization methods of ordered mesoporous phenolic resins. (Retrieved from [82])

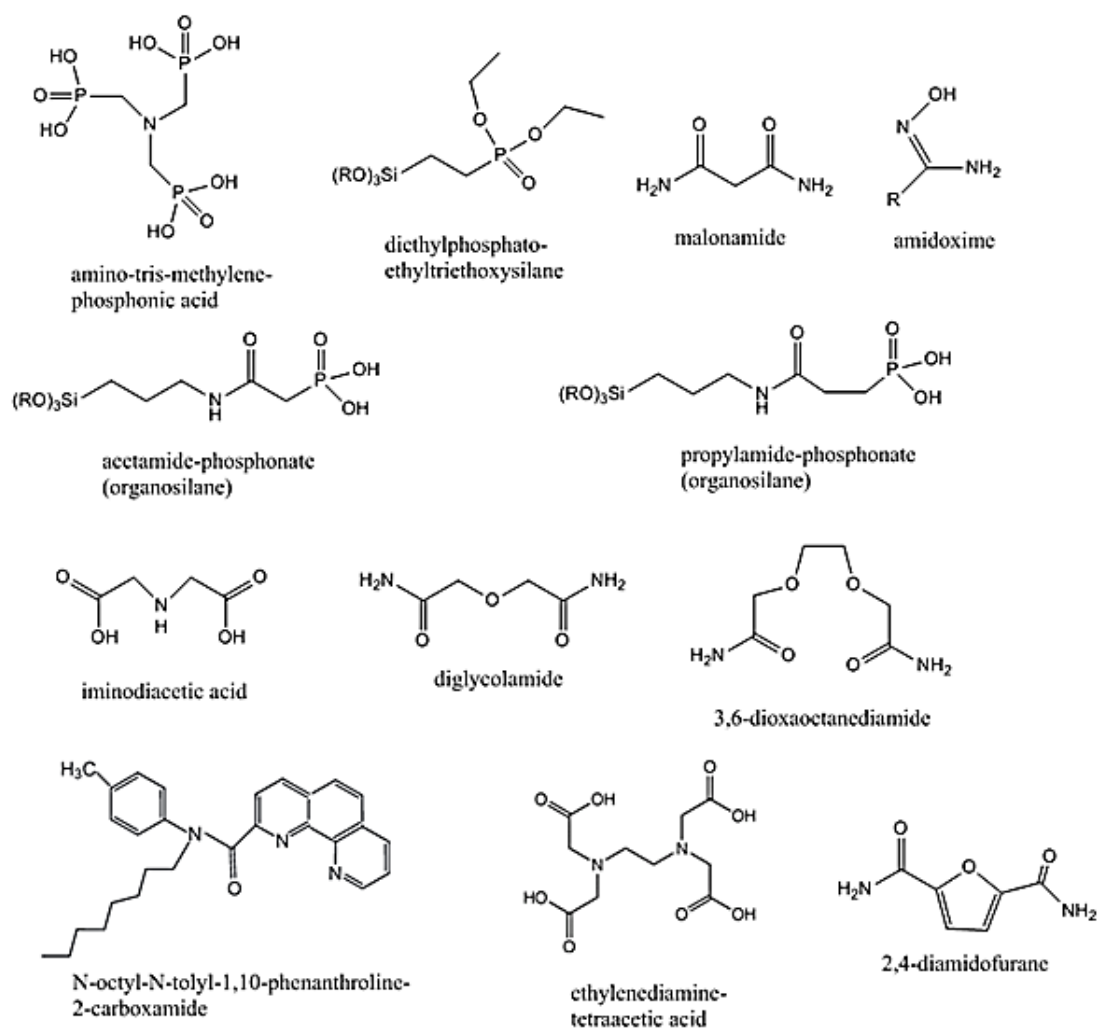
Table 3.4 gives an overview (not all-inclusive) of several REE/U targeting adsorbents, based on nanoporous silica, carbon, or different types of supports. For each adsorbent, important information regarding adsorption conditions (pH, competing elements...) and adsorbent performance (capacity, affinity, recycling) is provided. Several of the used ligands in these adsorbents are given in Figure 3.20.

**Table 3.4 Overview on several reported adsorbents for critical metals (REEs, U). List not all-inclusive. (Adapted from [1])**

			Adsorption conditions				Performance			
Ligand type	Support	Extracted element	pH	Time (h)	Competing elements	Liquid/ Solid-ratio (L/S; mL/g)	$K_d$ (mL/g)	Capacity (mg/g)	Reuse (amount of cycles)	Ref.
ATMP <sup>a</sup>	Zr-organophosphonates	La, Nd, Eu, Ho, Yb	0.1 M HNO <sub>3</sub>	24	Co, Cs, Sr	100	n.a.	30 – 60 (Eu)	n.a.	[89]
	Zr-titanate	Gd	0 – 3 M HNO <sub>3</sub>	0 – 24	n.a.	80	10145	0.83	n.a.	[24]
DPETE <sup>b</sup>	Silica microspheres	Nd, Dy	5.8 Nd 4.8 Dy	1	n.a.	400	n.a.	45 (Nd) 46 (Dy)	2	[26]
Ac-Phos	Silica-SAMMS	La, Nd, Eu, Lu	1 – 6.5	2	Fe, Ni, Cu, Zn, K, Ca	200	0 - 400000	n.a.	1 – 10	[23]
Prop-Phos										
H <sub>2</sub> IDA <sup>c</sup>	Core-shell $\gamma$ -Fe <sub>2</sub> O <sub>3</sub> @SiO <sub>2</sub>	La, Nd, Dy	n.a.	0 – 50	n.a.	100	n.a.	28 (La) 34 (Nd) 40 (Dy)	n.a.	[90]
DGA <sup>d</sup>	KIT-6	REEs	4	0.5	Al, Fe, U, Th	500	7000 (Eu)	n.a.	5	[72]
FDGA <sup>e</sup>	KIT-6	REEs	4	0.5	Al, Fe, U, Th	500	5000 (Sc)	75 (Eu)	10	[91]
DOODA <sup>f</sup>	KIT-6	REEs	4	0.5	Al, Fe, U, Th	500	11000 (Er-Lu)	151 (Eu)	10	[91]
OcTolPTA <sup>g</sup>	Silica monolith	Nd, Eu, Yb	1 – 5.4	0 –	Na, K, Ca, Mg,	1000	n.a.	162 (Nd)	8	[92]

				1.3	Al			163 (Eu) 176 (Yb)		
MA <sup>h</sup>	Silica NP	Sm - Er	4	0 – 4.2	Al, Fe	1000	2673 (Gd)	85 (Gd)	5	[93]
EDTA	Chitosan-silica	La, Nd, Eu, Dy, Lu	1 – 7	0 – 6	n.a.	400	n.a.	36 (Nd)	4	[45]
DTPA	Chitosan-silica	La, Nd, Eu, Dy, Lu	1 – 7	0 – 6	n.a.	400	0 – 350	43 (Nd)	4	[45]
Alkyl phosphine oxides	Vinyl co-condensed mesoporous silica	U	0.5 – 6	24	n.a.	1000	n.a.	100	n.a.	[94]
Amidoxime	Magnetic mesoporous silica	U	5	24	Zn, Ni, Co, Pb, Cr, Eu, Ce	5000	n.a.	277	5	[95]
	Hydrothermal carbon	U	1 – 4.5	2	Multi-element	2500	5000	269	n.a.	[88]
	Magnetic mesoporous silica	U	5	24	Zn, Ni, Co, Pb, Cr, Eu, Ce	5000	n.a.	277	5	[95]
	Hydrothermal carbon	U	1 – 4.5	2	Multi-element	2500	5000	269	n.a.	[88]

n.a. – not analyzed, <sup>a</sup>amino-tris-methylenephosphonic acid. <sup>b</sup>diethylphosphatoethyltriethoxysilane. <sup>c</sup>iminodiacetic acid. <sup>d</sup>diglycolamide. <sup>e</sup>2,4-diamidofurane. <sup>f</sup>3,6-dioxaoctanediamide. <sup>g</sup>N-octyl-N-tolyl-1,10-phenanthroline-2-carboxamide. <sup>h</sup>Malonamide.  $K_d$ : distribution coefficient; affinity for a specific metal (see Chapter 7). Ligand structures are given in Figure 3.20 for clarity.



**Figure 3.20** Ligand structures, used in the overview on REE/U targeting adsorbents.

There is no doubt on the potential of these ordered nanoporous solids (silicas, carbons) as adsorbents in aqueous metal recovery. They meet many of the required material standards for ideal supports, and a lot of (successful) research has already been performed on them. For applications in (highly) acidic environments (e.g., recycling process waters or mining leachates), silica-based adsorbents might not be the optimal choice if a long-term stability is desired. In such cases, carbon-based adsorbents might take the upper hand. However, if target streams have a more moderate pH (either naturally or by adaptation), the silica pathway might be preferred, as their functionalization is so attractive (organosilanes).

Nonetheless, neither of both solids are in focus in this work. As mentioned before, when treating dilute metal streams, it is important to keep the process cost-effective. The aspects of stability (reusability) and selectivity were brought forward as crucial parameters to achieve such a cost-effectiveness. While in theory, this should be sufficient, there might be additional room for improvement. Another aspect of cost-effectiveness can be found in the ease with which an ordered nanoporous material can be produced. The introduction of ordered porosity in the

described silicas and carbons was the result of structure directing agents (templates). This means that for the synthesis of these supports, one requires solvent(s), precursors, and a template, followed by the chemicals or the (thermal) energy to remove the template (as was illustrated in Figure 3.16). Then the material still needs to be functionalized via one or more steps to become a selective adsorbent. Further in this work, we explore a material class which does not require a template to obtain porosity, and it is probably one of the most ordered and uniform classes known to date... The metal-organic frameworks.

## REFERENCES

- [1] J. Florek, S. Giret, E. Juere, D. Lariviere, F. Kleitz, Functionalization of mesoporous materials for lanthanide and actinide extraction, *Dalton Trans*, 45 (2016) 14832-14854.
- [2] R.M. Izatt, S.R. Izatt, R.L. Bruening, N.E. Izatta, B.A. Moyer, Challenges to achievement of metal sustainability in our high-tech society, *Chem Soc Rev*, 43 (2014) 2451-2475.
- [3] C.K. Gupta, N. Krishnamurthy, Extractive Metallurgy of Rare-Earths, *Int Mater Rev*, 37 (1992) 197-248.
- [4] F. Xie, T.A. Zhang, D. Dreisinger, F. Doyle, A critical review on solvent extraction of rare earths from aqueous solutions, *Miner Eng*, 56 (2014) 10-28.
- [5] S.R. Izatt, R.L. Bruening, N.E. Izatt, Metal Separations and Recovery in the Mining Industry, *Jom-Us*, 64 (2012) 1279-1284.
- [6] S.R. Ramachandra Rao, Resource recovery and recycling from metallurgical wastes: Waste management series 7, Elsevier BV, The Netherlands, 2006.
- [7] F. Habashi, F.T. Awadalla, M. Zailaf, The Recovery of Uranium and the Lanthanides from Phosphate Rock, *J Chem Technol Biot*, 36 (1986) 259-266.
- [8] S. Peelman, Z.H.I. Sun, J. Sietsma, Y. Yang, Leaching of rare earth elements: past and present, in: *ERES2014: 1st European Rare Earth Resources Conference*, Milos Greece, 2014, pp. 446-456.
- [9] A. Jarosiński, J. Kowalczyk, C. Mazanek, Development of the Polish wasteless technology of apatite phosphogypsum utilization with recovery of rare earths, *Journal of Alloys and Compounds*, 200 (1993) 147-150.
- [10] H. Li, F. Guo, Z. Zhang, D. Li, Z. Wang, A new hydrometallurgical process for extracting rare earths from apatite using solvent extraction with P350, *Journal of Alloys and Compounds*, 408-412 (2006) 995-998.
- [11] S. Peelman, Z.H.I. Sun, J. Sietsma, Y. Yang, Chapter 21 - Leaching of Rare Earth Elements: Review of Past and Present Technologies A2 - Lima, Ismar Borges De, in: W.L. Filho (Ed.) *Rare Earths Industry*, Elsevier, Boston, 2016, pp. 319-334.
- [12] K. Binnemans, Y. Pontikes, P.T. Jones, T. Van Gerven, B. Blanpain, Recovery of rare earths from industrial waste residues: a concise review, in: *Proceedings of the 3rd International Slag Valorisation Symposium: the Transition to Sustainable Materials Management*, 2013, pp. 191-205.
- [13] D.M. Hoatson, S. Jaireth, Y. Mieztis, The major rare-earth-element deposits of Australia: geological setting, exploration, and resources, *Geoscience Australia*, 2011.
- [14] Z. Zhu, Y. Pranolo, C.Y. Cheng, Separation of uranium and thorium from rare earths for rare earth production - A review, *Miner Eng*, 77 (2015) 185-196.

- [15] P.M.B. Pillai, Naturally occurring radioactive material (NORM) in the extraction and processing of rare earths, in: *Proceedings of an International Symposium on NORM*, International Atomic Energy Agency, Vienna, Austria, 2007, pp. 197-221.
- [16] A. Jordens, Y.P. Cheng, K.E. Waters, A review of the beneficiation of rare earth element bearing minerals, *Miner Eng*, 41 (2013) 97-114.
- [17] M. Salvatores, G. Palmiotti, Radioactive waste partitioning and transmutation within advanced fuel cycles: Achievements and challenges, *Prog Part Nucl Phys*, 66 (2011) 144-166.
- [18] N. Cooper, D. Minakata, M. Begovic, J. Crittenden, Should We Consider Using Liquid Fluoride Thorium Reactors for Power Generation?, *Environ Sci Technol*, 45 (2011) 6237-6238.
- [19] Uranium 2014: Resources, Production and Demand, (2014).
- [20] E.H.Y. AbowSlama, E. Ebraheem, A.K. Sam, Precipitation and purification of uranium from rock phosphate, *J Radioanal Nucl Ch*, 299 (2014) 815-818.
- [21] J. Kim, C. Tsouris, R.T. Mayes, Y. Oyola, T. Saito, C.J. Janke, S. Dai, E. Schneider, D. Sachde, Recovery of Uranium from Seawater: A Review of Current Status and Future Research Needs, *Separ Sci Technol*, 48 (2013) 367-387.
- [22] M. Carboni, C.W. Abney, S. Liu, W. Lin, Highly porous and stable metal-organic frameworks for uranium extraction, *Chem Sci*, 4 (2013) 2396-2402.
- [23] G.E. Fryxell, H. Wu, Y.H. Lin, W.J. Shaw, J.C. Birnbaum, J.C. Linehan, Z.M. Nie, K. Kemner, S. Kelly, Lanthanide selective sorbents: self-assembled monolayers on mesoporous supports (SAMMS), *J Mater Chem*, 14 (2004) 3356-3363.
- [24] C.S. Griffith, M. De Los Reyes, N. Scales, J.V. Hanna, V. Luca, Hybrid Inorganic-Organic Adsorbents Part 1: Synthesis and Characterization of Mesoporous Zirconium Titanate Frameworks Containing Coordinating Organic Functionalities, *Acs Appl Mater Inter*, 2 (2010) 3436-3446.
- [25] S.E. Matthews, P. Parzuchowski, A. Garcia-Carrera, C. Gruttner, J.F. Dozol, V. Bohmer, Extraction of lanthanides and actinides by a magnetically assisted chemical separation technique based on CMPO-calix[4]arenes, *Chem Commun*, (2001) 417-418.
- [26] I.V. Melnyk, V.P. Goncharyk, L.I. Kozhara, G.R. Yurchenko, A.K. Matkovsky, Y.L. Zub, B. Alonso, Sorption properties of porous spray-dried microspheres functionalized by phosphonic acid groups, *Micropor Mesopor Mat*, 153 (2012) 171-177.
- [27] M.M. Reinoso-Garcia, D. Janczewski, D.N. Reinhoudt, W. Verboom, E. Malinowska, M. Pietrzak, C. Hill, J. Baca, B. Gruner, P. Selucky, C. Gruttner, CMP(O) tripodands: synthesis, potentiometric studies and extractions, *New J Chem*, 30 (2006) 1480-1492.
- [28] A. Walcarius, L. Mercier, Mesoporous organosilica adsorbents: nanoengineered materials for removal of organic and inorganic pollutants, *J Mater Chem*, 20 (2010) 4478-4511.
- [29] *Environmental applications of nanomaterials: synthesis, sorbents and sensors*, Imperial College Press, London, UK, 2007.
- [30] H.-J. Bart, U. von Gemmingen, Adsorption, in: *Ullmann's Encyclopedia of Industrial Chemistry*, Wiley-VCH Verlag GmbH & Co. KGaA, 2000.
- [31] V.J. Inglezakis, S.G. Pouloupoulos, 2 - Adsorption, Ion Exchange, and Catalysis, in: *Adsorption, Ion Exchange and Catalysis*, Elsevier, Amsterdam, 2006, pp. 31-56.
- [32] S.J. Gregg, S.K.S. W, Adsorption, Surface Area and Porosity, Wiley-VCH Verlag GmbH & Co. KGaA, 1967.
- [33] L.B. McCusker, F. Liebau, G. Engelhardt, Nomenclature of structural and compositional characteristics of ordered microporous and mesoporous materials with inorganic hosts - (IUPAC recommendations 2001), *Pure Appl Chem*, 73 (2001) 381-394.
- [34] S. Liu Activated Carbon Basics, (2016).



- [35] F. Ke, L.G. Qiu, Y.P. Yuan, F.M. Peng, X. Jiang, A.J. Xie, Y.H. Shen, J.F. Zhu, Thiol-functionalization of metal-organic framework by a facile coordination-based postsynthetic strategy and enhanced removal of  $\text{Hg}^{2+}$  from water, *J Hazard Mater*, 196 (2011) 36-43.
- [36] A.W.G. Platt, Group Trends, in: D.A. Atwood (Ed.) *The Rare Earth Elements: Fundamentals and Applications*, 2012.
- [37] K. Binnemans, *Coördinatiechemie*, Course notes (KU Leuven), (2004).
- [38] R.B. Martin, Hard & Soft Acids and Bases, in: *Encyclopedia of Inorganic and Bioinorganic Chemistry*, John Wiley & Sons, Ltd, 2011.
- [39] S. Cotton, *Lanthanide and actinide chemistry*, John Wiley & Sons, 2013.
- [40] J.J. Katz, L.R. Morss, N. Edelstein, J. Fuger, *The Chemistry of the Actinide and Transactinide Elements (Volumes 1-5)*, Springer Science & Business Media, 2007.
- [41] Radial wave functions from <http://ej.iop.org/images>. [http://ej.iop.org/images/0953-4075/45/3/035002/Full/jpb413213f2\\_online.jpg](http://ej.iop.org/images/0953-4075/45/3/035002/Full/jpb413213f2_online.jpg) (Accessed in 2017)
- [42] Database of Ionic Radii. <http://abulafia.mt.ic.ac.uk/shannon/ptable.php> (Accessed in 2017)
- [43] Structure of the uranium tricarbonate complex. <https://markforeman.wordpress.com/2011/12/26/mononuclear-uranium-carbonate-complexes/> (Accessed in 2017)
- [44] F.W. Lewis, M.J. Hudson, L.M. Harwood, Development of Highly Selective Ligands for Separations of Actinides from Lanthanides in the Nuclear Fuel Cycle, *Synlett*, (2011) 2609-2632.
- [45] J. Roosen, K. Binnemans, Adsorption and chromatographic separation of rare earths with EDTA- and DTPA-functionalized chitosan biopolymers, *J Mater Chem A*, 2 (2014) 1530-1540.
- [46] P. Dey, S. Basu, Synergistic Extraction of Copper from Nitrate Solutions Using beta-Hydroxy-Naphthaldoxime and Organophosphorus Compounds into Carbon-Tetrachloride, *Metall Mater Trans B*, 42 (2011) 1136-1143.
- [47] E.P. Horwitz, R. Chiarizia, M.L. Dietz, DIPEX: A new extraction chromatographic material for the separation and preconcentration of actinides from aqueous solution, *React Funct Polym*, 33 (1997) 25-36.
- [48] M.L.P. Reddy, J.R. Bosco Bharathi, S. Peter, T.R. Ramamohan, Synergistic extraction of rare earths with bis(2,4,4-trimethyl pentyl) dithiophosphinic acid and trialkyl phosphine oxide, *Talanta*, 50 (1999) 79-85.
- [49] M.L.P. Reddy, S. Sujatha, R.L. Varma, T.R. Ramamohan, T.P. Rao, C.S.P. Iyer, A.D. Damodaran, Mixed-ligand chelate extraction of trivalent lanthanides with 4,4,4-trifluoro-1-phenyl-1,3-butanedione and neutral oxo-donors, *Talanta*, 44 (1997) 97-103.
- [50] W. Yantasee, T. Sangvanich, J.A. Creim, K. Pattamakomsan, R.J. Wiacek, G.E. Fryxell, R.S. Addleman, C. Timchalk, Functional Sorbents for Selective Capture of Plutonium, Americium, Uranium, and Thorium in Blood, *Health Phys*, 99 (2010) 413-419.
- [51] R. Paine, Design and Synthesis of F-Element Selective Ligands, in: *Separations of f Elements*, Springer, 1995, pp. 63-75.
- [52] C. Boehme, G. Wipff, Carbamoylphosphine oxide complexes of trivalent lanthanide cations: Role of counterions, ligand binding mode, and protonation investigated by quantum mechanical calculations, *Inorg Chem*, 41 (2002) 727-737.
- [53] B.P. Hay, D.A. Dixon, R. Vargas, J. Garza, K.N. Raymond, Structural Criteria for the Rational Design of Selective Ligands, *Inorg Chem*, 40 (2001) 3922-3935.
- [54] R. Taylor, *Reprocessing and recycling of spent nuclear fuel*, Elsevier, 2015.

- [55] S.M. Bowen, E.N. Duesler, R.T. Paine, Synthesis and Crystal and Molecular-Structure of Bis(Nitrato)[Diisopropyl (N,N-Diethylcarbamyl)Methylenephosphonate]Dioxouranium(Vi), *Inorg Chem*, 22 (1983) 286-290.
- [56] L.J. Caudle, E.N. Duesler, R.T. Paine, Preparation and Structure of a Neodymium Complex Containing Bidentate (Carbamoylmethyl)Phosphine Oxide Ligands, *Inorg Chem*, 24 (1985) 4441-4444.
- [57] F. ArnaudNeu, V. Bohmer, J.F. Dozol, C. Gruttner, R.A. Jakobi, D. Kraft, O. Mauprivez, H. Rouquette, M.J. SchwingWeill, N. Simon, W. Vogt, Calixarenes with diphenylphosphoryl acetamide functions at the upper rim. A new class of highly efficient extractants for lanthanides and actinides, *J Chem Soc Perk T 2*, (1996) 1175-1182.
- [58] E.P. Horwitz, H. Diamond, D.G. Kalina, Carbamoylmethylphosphoryl Derivatives as Actinide Extractants - Their Significance in the Processing and Recovery of Plutonium and Other Actinides, *Acs Sym Ser*, 216 (1983) 433-450.
- [59] S. Barbosa, A.G. Carrera, S.E. Matthews, F. Arnaud-Neu, V. Bohmer, J.F. Dozol, H. Rouquette, M.J. Schwing-Weill, Calix[4]arenes with CMPO functions at the narrow-rim. Synthesis and extraction properties, *J Chem Soc Perk T 2*, (1999) 719-723.
- [60] T.N. Lambert, G.D. Jarvinen, A.S. Gopalan, Syntheses of some new polyaminocarboxylate and CMPO calix[4]arene chelators for the selective extraction of actinide ions, *Tetrahedron Lett*, 40 (1999) 1613-1616.
- [61] L.H. Delmau, N. Simon, M.J. Schwing-Weill, F. Arnaud-Neu, J.F. Dozol, S. Eymard, B. Tournois, V. Bohmer, C. Gruttner, C. Musigmann, A. Tunayar, 'CMPO-substituted' calix[4]arenes, extractants with selectivity among trivalent lanthanides and between trivalent actinides and lanthanides, *Chem Commun*, (1998) 1627-1628.
- [62] M.M. Reinoso-Garcia, Chelating agents for actinide/lanthanide separation, University of Twente, 2004, and references therein.
- [63] H.H. Dam, D.N. Reinhoudt, W. Verboom, Multicoordinate ligands for actinide/lanthanide separations, *Chem Soc Rev*, 36 (2007) 367-377.
- [64] P.K. Jal, S. Patel, B. Mishra, Chemical modification of silica surface by immobilization of functional groups for extractive concentration of metal ions, *Talanta*, 62 (2004) 1005-1028.
- [65] A.P. Wight, M.E. Davis, Design and Preparation of Organic-Inorganic Hybrid Catalysts, *Chem Rev*, 102 (2002) 3589-3614.
- [66] G.R. Reddy, S. Balasubramanian, Synthesis, characterization and photocatalytic studies of mesoporous silica grafted Ni(II) and Cu(II) complexes, *Rsc Adv*, 5 (2015) 53979-53987.
- [67] S.H. Tolbert, Mesoporous Silica Holey Quasicrystals, *Nat Mater*, 11 (2012) 749-751.
- [68] D.A. Doshi, A. Gibaud, V. Goletto, M.C. Lu, H. Gerung, B. Ocko, S.M. Han, C.J. Brinker, Peering into the self-assembly of surfactant templated thin-film silica mesophases, *J Am Chem Soc*, 125 (2003) 11646-11655.
- [69] D.Y. Zhao, J.L. Feng, Q.S. Huo, N. Melosh, G.H. Fredrickson, B.F. Chmelka, G.D. Stucky, Triblock copolymer syntheses of mesoporous silica with periodic 50 to 300 angstrom pores, *Science*, 279 (1998) 548-552.
- [70] F. Kleitz, S.H. Choi, R. Ryoo, Cubic Ia3d large mesoporous silica: synthesis and replication to platinum nanowires, carbon nanorods and carbon nanotubes, *Chem Commun*, (2003) 2136-2137.
- [71] J. Aguado, J.M. Arsuaga, A. Arencibia, M. Lindo, V. Gascon, Aqueous heavy metals removal by adsorption on amine-functionalized mesoporous silica, *J Hazard Mater*, 163 (2009) 213-221.

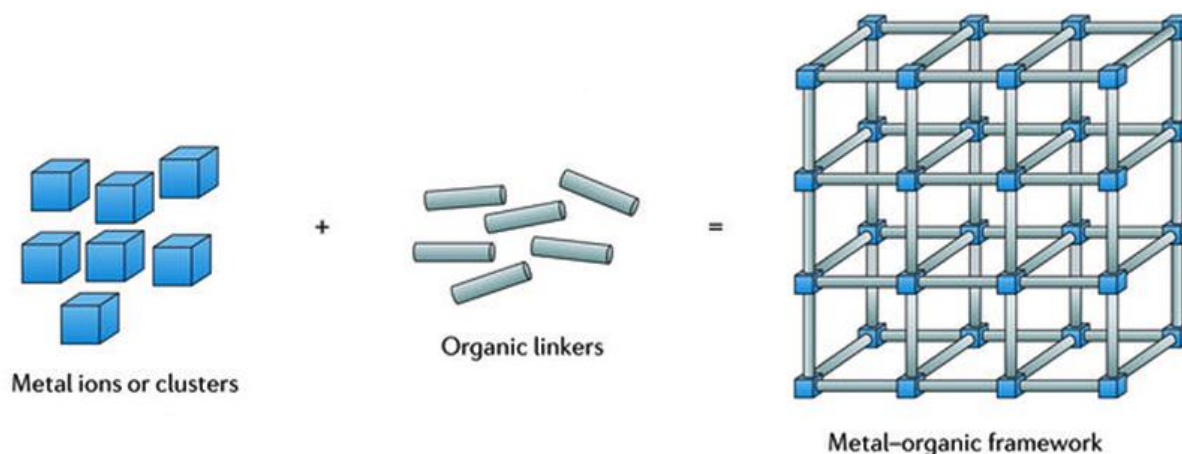
- [72] J. Florek, F. Chalifour, F. Bilodeau, D. Lariviere, F. Kleitz, Nanostructured Hybrid Materials for the Selective Recovery and Enrichment of Rare Earth Elements, *Adv Funct Mater*, 24 (2014) 2668-2676.
- [73] A.M. Liu, K. Hidajat, S. Kawi, D.Y. Zhao, A new class of hybrid mesoporous materials with functionalized organic monolayers for selective adsorption of heavy metal ions, *Chem Commun*, (2000) 1145-1146.
- [74] B. Çelebi, A simple synthetic route for the preparation of a reversed-phase stationary phase based on monosized-porous hydrogel beads and its chromatographic use for separation of small molecules, *Acta Chromatogr*, (2016) 1-17.
- [75] H. Luo, A Silica-based Hydrophobic Cation Exchange Phase for Water Soluble Pharmaceuticals and Bioactive Analytes, ProQuest, 2006.
- [76] V.R. Choudhary, S.D. Sansare, Thermal, hydrothermal and acid-base stability of highly siliceous MCM-41 mesoporous material, *P Indian as-Chem Sci*, 109 (1997) 229-233.
- [77] R.A. Sheldon, H. Van Bekkum, Solid-acid Catalysts-General, in: *Fine Chemicals through Heterogeneous Catalysis*, Wiley-VCH Verlag GmbH, 2007, pp. 61-121.
- [78] K.P. Gierszal, M. Jaroniec, T.W. Kim, J. Kim, R. Ryoo, High temperature treatment of ordered mesoporous carbons prepared by using various carbon precursors and ordered mesoporous silica templates, *New J Chem*, 32 (2008) 981-993.
- [79] A.H. Lu, F. Schuth, Nanocasting: A versatile strategy for creating nanostructured porous materials, *Adv Mater*, 18 (2006) 1793-1805.
- [80] A. Walcarius, Mesoporous materials and electrochemistry, *Chem Soc Rev*, 42 (2013) 4098-4140.
- [81] W. Libbrecht, F. Deruyck, H. Poelman, A. Verberckmoes, J. Thybaut, J. De Clercq, P. Van der Voort, Optimization of soft templated mesoporous carbon synthesis using Definitive Screening Design, *Chem Eng J*, 259 (2015) 126-134.
- [82] I. Muylaert, A. Verberckmoes, J. De Decker, P. Van der Voort, Ordered mesoporous phenolic resins: Highly versatile and ultra stable support materials, *Adv Colloid Interfac*, 175 (2012) 39-51.
- [83] M.J. Baniamerian, S.E. Moradi, A. Noori, H. Salahi, The effect of surface modification on heavy metal ion removal from water by carbon nanoporous adsorbent, *Appl Surf Sci*, 256 (2009) 1347-1354.
- [84] W. Chouyyok, Y. Shin, J. Davidson, W.D. Samuels, N.H. Lafemina, R.D. Rutledge, G.E. Fryxell, T. Sangvanich, W. Yantasee, Selective Removal of Copper(II) from Natural Waters by Nanoporous Sorbents Functionalized with Chelating Diamines, *Environ Sci Technol*, 44 (2010) 6390-6395.
- [85] Y.S. Shin, G. Fryxell, W.Y. Um, K. Parker, S.V. Mattigod, R. Skaggs, Sulfur-functionalized mesoporous carbon, *Adv Funct Mater*, 17 (2007) 2897-2901.
- [86] X. Zhuang, Q.F. Zhao, Y. Wan, Multi-constituent co-assembling ordered mesoporous thiol-functionalized hybrid materials: synthesis and adsorption properties, *J Mater Chem*, 20 (2010) 4715-4724.
- [87] M. Carboni, C.W. Abney, K.M.L. Taylor-Pashow, J.L. Vivero-Escoto, W.B. Lin, Uranium Sorption with Functionalized Mesoporous Carbon Materials, *Ind Eng Chem Res*, 52 (2013) 15187-15197.
- [88] X.D. Yang, J. Li, J. Liu, Y. Tian, B. Li, K.C. Cao, S.B. Liu, M. Hou, S.J. Li, L.J. Ma, Simple small molecule carbon source strategy for synthesis of functional hydrothermal carbon: preparation of highly efficient uranium selective solid phase extractant, *J Mater Chem A*, 2 (2014) 1550-1559.

- [89] J. Veliscek-Carolan, T.L. Hanley, V. Luca, Zirconium organophosphonates as high capacity, selective lanthanide sorbents, *Sep Purif Technol*, 129 (2014) 150-158.
- [90] E.P. Legaria, S.D. Topel, V.G. Kessler, G.A. Seisenbaeva, Molecular insights into the selective action of a magnetically removable complexone-grafted adsorbent, *Dalton T*, 44 (2015) 1273-1282.
- [91] J. Florek, A. Mushtaq, D. Lariviere, G. Cantin, F.G. Fontaine, F. Kleitz, Selective recovery of rare earth elements using chelating ligands grafted on mesoporous surfaces, *RSC Advances*, 5 (2015) 103782-103789.
- [92] M.R. Awual, T. Kobayashi, H. Shiwaku, Y. Miyazaki, R. Motokawa, S. Suzuki, Y. Okamoto, T. Yaita, Evaluation of lanthanide sorption and their coordination mechanism by EXAFS measurement using novel hybrid adsorbent, *Chem Eng J*, 225 (2013) 558-566.
- [93] X.D. Zheng, C. Wang, J.D. Dai, W.D. Shi, Y.S. Yan, Design of mesoporous silica hybrid materials as sorbents for the selective recovery of rare earth metals, *J Mater Chem A*, 3 (2015) 10327-10335.
- [94] W. Zhang, G. Ye, J. Chen, Novel mesoporous silicas bearing phosphine oxide ligands with different alkyl chains for the binding of uranium in strong HNO<sub>3</sub> media, *J Mater Chem A*, 1 (2013) 12706-12709.
- [95] Y.G. Zhao, J.X. Li, S.W. Zhang, X.K. Wang, Amidoxime-functionalized magnetic mesoporous silica for selective sorption of U(VI), *Rsc Adv*, 4 (2014) 32710-32717.

# 4 MOFs IN AQUEOUS ENVIRONMENT

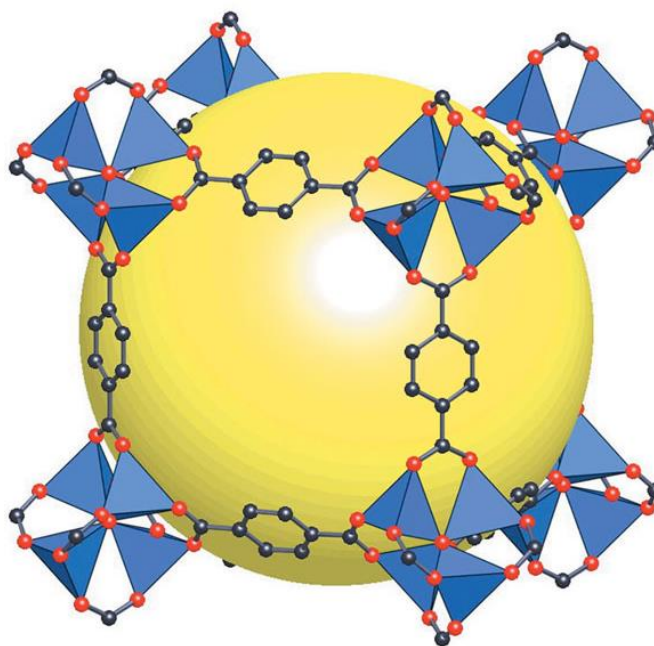
## 4.1 What is a Metal-Organic Framework?

Metal-organic frameworks, or MOFs, are a class of hybrid coordination polymers. They are made up of organic and inorganic constituents, forming a network of repetitive building blocks in one or more dimensions. A typical MOF is constructed by joining metal nodes (ions or clusters) with polytopic organic linkers, using strong coordination bonds to create open crystalline frameworks with permanent porosity[1] (Figure 4.1). The design of MOFs is somewhat unique in materials science, because it implies reticular synthesis. Such a synthesis can be described as the process of assembling well-chosen rigid molecular building blocks into predetermined ordered structures, which are held together by strong bonding[2]. As a result, materials are produced in which the structural integrity and rigidity of the building blocks remain unaltered. This differs greatly from traditional methods, where the starting entities do not maintain their structure during the reaction, which leads to poor correlation between reactants and products, and therefore to a general lack of control over the character of the solids[2].



**Figure 4.1 Schematic build-up of a metal-organic framework. (Adapted from [3])**

MOFs are, much like classical inorganic porous solids (e.g., zeolites), constructed by the association of secondary building units (SBUs). However, whereas in zeolites, the inorganic SBU contains only inorganic parts (e.g.,  $\text{SiO}_4$ ,  $\text{PO}_4$ ,  $\text{SO}_4$ ) associated with metallic cations, the hybrid SBUs of MOFs have their anionic species replaced by organic linkers[4]. A fitting illustration is MOF-5 (Figure 4.2), which is made up of  $\text{Zn}_4\text{O}(\text{CO}_2)_6$  units, containing four  $\text{ZnO}_4$  tetrahedra with a common vertex, and six carboxylate carbon atoms that define an octahedral SBU. These SBUs are joined together by benzene links, leading to a cubic network in which the vertices (nodes) are the octahedral SBUs and the edges are the benzene struts (linkers)[2]. The ‘node-strut’ connection is ensured by using polytopic linkers (ligands), containing oxygen or nitrogen donors. When oxygen is concerned, they are mainly carboxylates and phosphonates. All of them can provide different possibilities of linkage with the inorganic cations (chelating, single bond...). The nitrogen derivatives (cyanides, pyridine, imidazoles...) are fixed directly to the cation[4]. In the case of MOF-5, a benzene-dicarboxylate (BDC) is used to obtain the benzene strut of the framework.

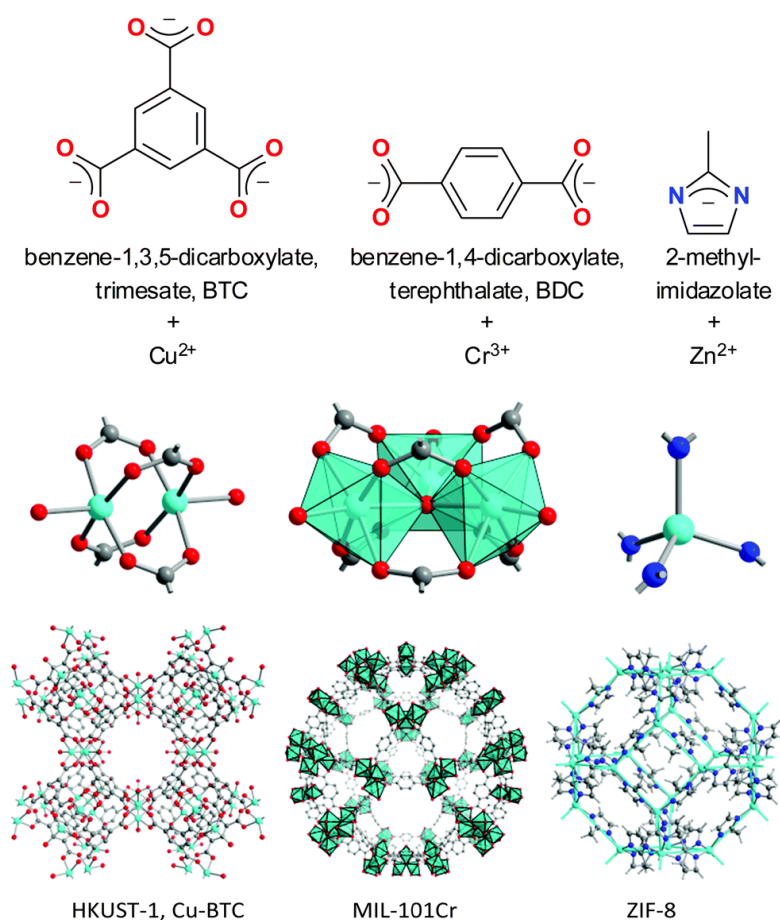


**Figure 4.2** The MOF-5 structure shown as  $\text{ZnO}_4$  tetrahedra (blue polyhedra) joined by benzene dicarboxylate linkers (O, red and C, black) to give an extended 3D cubic framework. (Yellow sphere represents the largest sphere that can occupy the pores without coming within the van der Waals size of the framework). (Retrieved from [2])

Over the past decade, the study and preparation of MOFs has been given an enormous amount of attention in the materials science. With application in mind, MOFs possess a lot of advantages over their commonly used porous (synthetic) counterparts. From a structural viewpoint, they have an incredible uniformity, as their specific ordered geometry and porosity is repeated throughout the whole framework. In addition, no real pore walls are present, since the organic linkers and metal (cluster) centers make up the whole structure. Therefore, no material is lost in the bulk. This leads to frameworks with incredibly high specific surface areas[5-7]. Typical surface areas range between 1000 and 4000  $\text{m}^2/\text{g}$  (BET). The materials are micro- or mesoporous with pore apertures or channel diameters ranging from 0.3 to 3.4 nm, and pore volumes up to 1.5 or 2  $\text{cm}^3/\text{g}$ [8]. (Exceptions to these estimates are not uncommon.)

Often compared to zeolites, MOFs have the advantage of not needing any (organic or inorganic) template to form the framework during synthesis, as this role is taken up by a solvent[4]. This avoids the use of surfactants or other structure directing agents (and their subsequent removal), which yields a time- and/or cost-effective material synthesis. In addition, most of the metal cations, di-, tri-, or tetravalent, can participate in MOF formation[4], opposed to most inorganic materials which mainly make use of a few cations such as Si, Al, and P [9]. This adds greatly to the tunability of MOFs, ranking them amongst the most versatile porous material classes known to date. Furthermore, both the organic linker and the metal center can be varied or altered, which leads to a very broad spectrum of structures (Figure 4.3), pore dimensions, and

topologies, each with their specific physicochemical properties. Moreover, a lot of MOFs are subjected to post-synthetic modification (PSM) to further fine-tune their interactions with guest species[10]. As a result, MOFs can be tailored accurately towards a desired application, which has enabled their use in a large variety of research fields such as gas storage and separation[11-14], catalysis[15, 16], separation of chemicals[17, 18], drug delivery[19, 20], magnetism[21], luminescence[22]... In particular, applications in energy technologies such as fuel cells, supercapacitors, and catalytic conversions have made them objects of extensive study, and industrial-scale production and application[23-25]. Extensive reviewing work on the design, properties, and applications of MOFs can be found in Ferey [4] and Yaghi *et al.*[1].



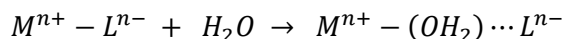
**Figure 4.3** Different linkers with selected metal nodes and secondary building units in their corresponding MOFs (HKUST-1, MIL-101(Cr) and ZIF-8).

## 4.2 Water Stability

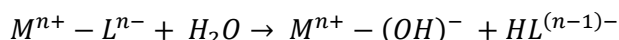
One of the emerging fields of MOF applications comprises use in aqueous environments as potential adsorbents or sensors. Opposed to their many advantages, however, MOFs also have the prejudice of being unstable, water-sensitive materials, because of the presence of metal-ligand coordination bonds, and indeed, the greater part of them is not suitable for uses in moist conditions, let alone (long-term) applications in aqueous media[26-28]. Damage inflicted to a sorbent by moisture at process conditions or during regeneration will evidently limit its



usefulness. The hydration reaction of water with the MOF's metal clusters could involve ligand displacement and/or hydrolysis, as reported by Low *et al.*[28]. The ligand displacement reaction comprises the insertion of water molecules into the metal–ligand (M – L) bonds of the framework. This leads to the formation of hydrated cations and to the release of free ligands:



During the hydrolysis reaction, the M – L bonds are broken and water dissociates to form a hydroxylated cation and a free protonated ligand:

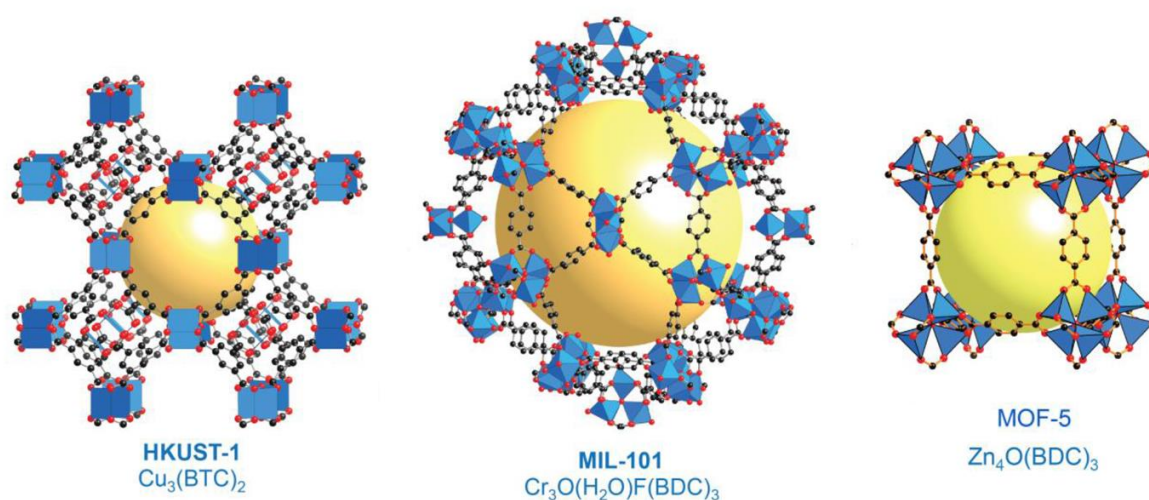


The key requirement for thermodynamically stable MOFs is an inert metal cluster that renders it unfavorable for an irreversible hydrolysis reaction to occur. If the electrophilic metal center is not sufficiently inert, nucleophilic water can coordinate with the metal cluster and distort or destroy the MOF's crystal lattice[29]. On the other hand, even if a certain structure does not fully meet the thermodynamic requirements to yield an inert metal center, the presence of kinetically influencing factors, such as hydrophobicity and ligand sterics, can increase the activation energy to a high enough level to avoid hydrolysis, thus rendering the structure stable under humid conditions[29].

Overall, the water-stability of a MOF can be attributed to both the electronic and steric effects of the ligand on the metal node. The strength of metal–donor bonds[28], combined with the shielding ability of the ligand to protect the inorganic node against water coordination, drives the water resistance of the material[30]. Because MOFs are governed by Lewis acid–base coordination chemistry, the pKa of the coordinating ligand can be used as a first-order approximation of the metal–ligand bond strength. As a general rule, utilizing ligands with higher pKa values is a useful strategy for targeting novel structures with higher water tolerances[29].

The properties of the metal species will also play an important role, and factors such as the metal oxidation state and ionic radius also need to be taken into account[29]. Moreover, the metal-ligand combination and the affinity between them has a high impact on the structural stability as well (cfr. Pearson's *Hard Soft Acid Base* theory, HSAB). So far, carboxylates are the most commonly used ligands in MOF synthesis. Utilization of high-valence metals as hard acids appears to be the most straightforward approach for the construction of stable MOFs. However, the interaction between softer nitrogen containing ligands (such as imidazoles, triazoles, pyrazoles...) with softer metal ions (such as  $Zn^{2+}$  and  $Co^{2+}$ ) can also be exploited in stable MOF synthesis[27]. As a matter of fact, it is reported that MOFs constructed with nitrogen containing ligands (pyrazoles, pyridines...) tend to exhibit better stability than MOFs assembled from carboxylic acid functionalities[29]. This is due to the increased pKa of the ligands, e.g., terephthalate (pKa: 3.51 – 4.82) vs. imidazole (pKa: 7.0) vs. pyrazolate (pKa: 14.3)[31].

Several additional phenomena are described to have a significant impact on improved water stability. For example, it is observed that MOFs containing 6-coordinate (usually octahedral) metal ions tend to be more stable than those containing 4-coordinate (usually tetrahedral) metal ions (*vide infra*). An explanation to this is that more space is available for a water molecule to coordinate to a tetrahedrally coordinated metal than a metal with octahedral coordination[28]. According to Low *et al.*, it is also expected that higher oxidation state metal clusters yield relatively more stability versus water hydration, and thus degradation. This suggests, for example, that the SBUs of HKUST-1 and Cr-MIL-101 (relative Cu, resp. Cr charge = +2) form more stable bonds with their respective carboxylate linkers than, for instance, MOF-5 (relative Zn charge = +1.5) does with its linker (BDC) (Figure 4.4).

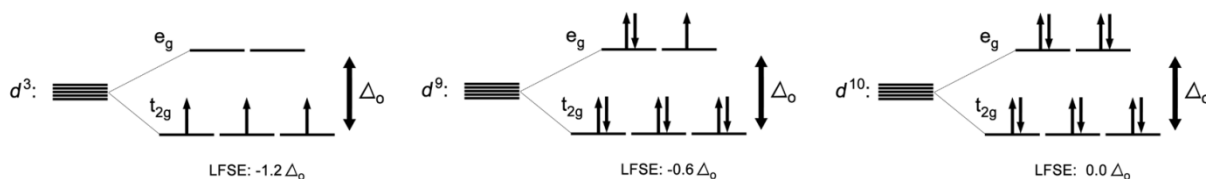


**Figure 4.4 Crystal structures of HKUST-1, MIL-101(Cr), and MOF-5, with their respective chemical formula, enabling the calculation of relative metal charge. (Retrieved from [32])**

Research on the effect of the central metal on MOF stability was performed by Kang *et al.*[33], by using a series of isotopic metal-benzenedicarboxylates as target MOFs, i.e., MIL-53-Al (Al-BDC), MIL-53-Cr (Cr-BDC) and MIL-47-V (V-BDC), and testing them in water, acidic, and alkaline conditions. It was found, based on changes in surface areas and XRD signal intensities, that the stability of the M-BDCs, decreases in the order of Cr-BDC > Al-BDC > V-BDC. Particularly V-BDC degrades very fast, and Al-BDC shows continuous degradation in time as well. Cr-BDC was found to perfectly maintain its structure, with no apparent changes observed. These trends were found in either water, as well as alkaline and acidic conditions. As mentioned earlier, phenomena such as bond strength, coordination type, and oxidation state attribute to the stability of MOFs. However in this case, none of these can provide a valid explanation for the observed stability pattern of the M-BDCs, since: (1) the average bond strength of the respective MOFs decreases as V-O (637 kJ/mol) > Al-O (502 kJ/mol) > Cr-O (461 kJ/mol)[34], which is completely opposite to the stability pattern, (2) all three M-BDCs possess the same octahedral

coordination, and (3) the oxidation states of the respective cations in their framework are more or less the same ( $\text{Al}^{\text{III}}$ ,  $\text{Cr}^{\text{III}}$ ,  $\text{V}^{\text{IV}}$ ), with V-BDC being the least stable structure, regardless of its higher oxidation state (+IV after purification)[33].

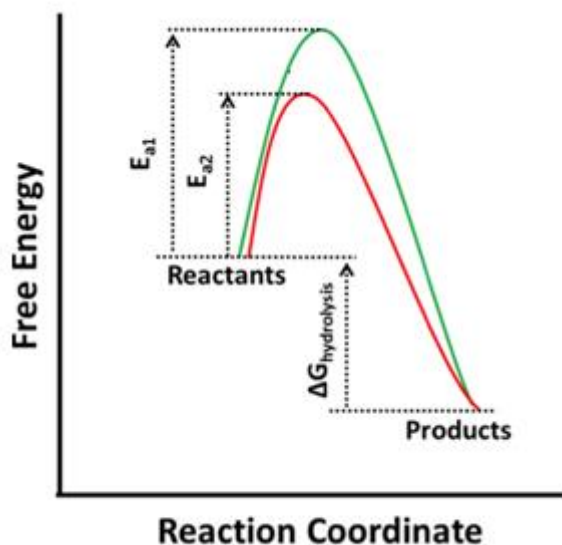
The authors attribute the relative stability of the M-BDCs to the lability of the metal ions, where in this case, the ion inertness follows the increasing order of  $\text{V}^{\text{IV}} < \text{V}^{\text{III}} < \text{Al}^{\text{III}} < \text{Cr}^{\text{III}}$  [35]. Indeed, high lability results in facile ligand displacement and therefore a higher chance of water coordination and ultimately structural collapse. Parameters influencing the lability of a metal cation include ion charge density (low linker exchange rates are generally observed with increasing charge-to-size ratio of metal ions[36]), but also the electronic configuration of  $d$ -orbitals (in the case of transition metals), determining the ligand field stabilization energy (LFSE)[27, 36]. A fitting example is that of UiO-66, made up of zirconium and BDC (*vide infra*, Figure 4.8).  $\text{Zr}^{4+}$  may exchange a ligand more easily than, for example,  $\text{Cr}^{3+}$  despite chromium's lower charge. This is because  $d^3$  chromium has a favorable LFSE (Figure 4.5), which increases the activation energy for ligand displacement or removal (which would disrupt the ligand field). Since  $\text{Zr}^{4+}$  ( $d^0$ ) has no LFSE, facile Zr-carboxylate displacement is plausible[37]. On the other hand, a full  $d$ -orbital, such as  $d^{10}$   $\text{Zn}^{2+}$  in MOF-5, or nearly full  $d$ -orbital (e.g.  $d^9$   $\text{Cu}^{2+}$  in HKUST-1), experiences no or a very low LFSE, respectively (Figure 4.5), and such MOFs prove to be highly moisture sensitive (as the ligands are more prone to displacement)[27, 36]. Generally, an increased LFSE should make ligand replacing less favorable, and thus realize more inertness to the structure. Note, however, that several important factors need to be considered to fully assess and calculate the LFSE effect of a certain configuration, including pairing energy (and overall stabilization energy), different geometries (octahedral, tetrahedral), high-spin/low-spin configurations... These will not be further discussed in this work.



**Figure 4.5 Electronic configuration of three different  $d$ -metal complexes in an octahedral field. The  $d$ -orbital energies split into two levels, i.e., the lower  $t_{2g}$  level at  $-0.4 \Delta_o$ , and the higher  $e_g$  level at  $0.6 \Delta_o$ . ( $\Delta_o$ : ligand field splitting parameter). LFSE is calculated by:  $(-0.4n_{t_{2g}} + 0.6n_{e_g}) \cdot \Delta_o$  with  $n$  the amount of present electrons in the respective level.**

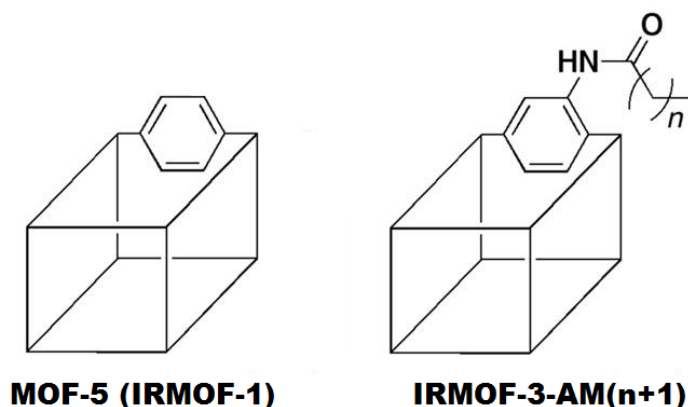
As mentioned, in addition to thermodynamics, kinetic factors can also greatly influence the water-resistance of a MOF. Simply put, even if it is thermodynamically more favorable to go from the intact MOF to a hydrolyzed product, if the energy barrier to get there is too high,

hydrolysis will happen less likely. This is illustrated in Figure 4.6 for two MOFs with identical thermodynamic stability.



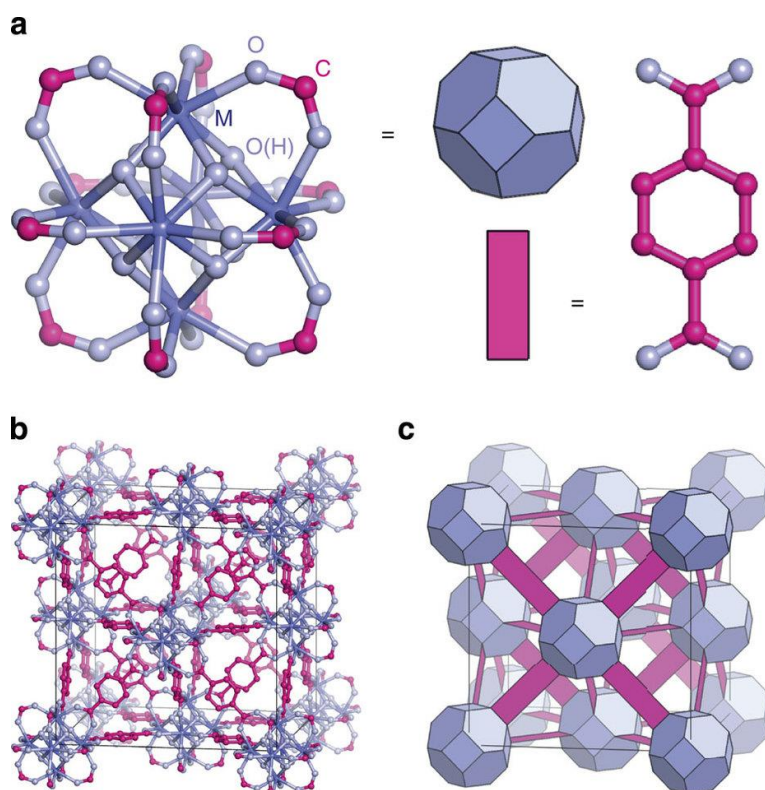
**Figure 4.6** Reaction coordinate diagram highlighting the importance of kinetic factors in determining MOF water stability. While structures 1 (green) and 2 (red) have the same thermodynamic stability, structure 1 is more stable under humid conditions due to kinetic factors that increase the activation energy barrier ( $E_a$ ) for hydrolysis. (Adapted from [29])

One way to achieve a higher stability through kinetic factors is by introducing hydrophobicity into the material. This can prevent water molecules from reaching the metal clusters of the framework. Two cases of hydrophobicity mechanisms are distinguished, namely pore hydrophobicity and internal hydrophobicity[29]. The former can prevent water from adsorbing into the pores altogether[38, 39], while the latter implies localized hydrophobicity, i.e., water can still adsorb into the pores, but cannot cluster around the metal centers and react[40, 41]. In practice, the incorporation of hydrophobic alkyl and fluorinated functional groups on the ligand has been widely reported to improve MOF stability under humid conditions, by either full or localized hydrophobization (references in [29]). A prominent example is the functionalization of MOF-5 with extended alkyl-amide chains, by Nguyen *et al.*[42]. Opposed to the extremely poor water-stability of MOF-5 (even to ambient air), an analogue structure containing polyalkylamide chains on the benzene struts (denoted IRMOF-3-AM( $n+1$ ), Figure 4.7) can result in a stable, hydrophobic material. It is important to note, however, that with aqueous adsorption in mind, pore hydrophobization is not desired, as water will not be able to enter the pores of the adsorbent.



**Figure 4.7** Schematic representation of MOF-5 (left), and functionalized IRMOF-3-AM(n+1) (right). (Adapted from [42])

In addition to hydrophobicity, steric effects can also help preventing structure degradation through hydrolysis. While hydrophobization tries to shield the metal clusters from contact with water as much as possible, the presence of steric factors can reduce the reaction kinetics by providing a significant activation energy barrier. One example concerning high coordination numbers (CN) (e.g., octahedral vs. tetrahedral) was already briefly mentioned in this chapter. The increased stability as a result of high CN is due a crowding effect from the many ligands around the metal cluster, which prevents the formation of water clusters near the metal center. Additionally, even if bond breakage were to occur in these structures, their higher metal CN can result in a greater tolerance for hydrolysis before lattice collapse will occur, by having a number of other bound ligands still available as support[29]. The earlier mentioned UiO-66 (Figure 4.8) is a fitting example. Despite the relatively low pK<sub>a</sub> of its ligand (BDC) and the lack of LFSE from Zr<sup>4+</sup>, the UiO-66 (in its defect-free form) contains zirconium-oxo clusters ([Zr<sub>6</sub>O<sub>4</sub>(OH)<sub>4</sub>]) surrounded by 12 BDC ligands, resulting in a high degree of topological connectivity. This design is considered the basis for the material's high thermal, chemical, and water stability[29, 43, 44]. In addition, there is a high affinity between the hard Lewis acid, Zr<sup>4+</sup>, and hard base, BDC.



**Figure 4.8 (a) SBU of the UiO-66 framework (six-center octahedral metal clusters, M = Zr). (a, right) BDC linkers. (b) UiO-66 network structure. (c) Simplified polyhedral representation of the same network structure. (Retrieved from [43])**

Another steric factor includes rotational effects on linkers, for instance, a biphenyldicarboxylate-type linker is reported to yield less stable structures than a single phenyldicarboxylate analogue, because of the greater torsional strain that the biphenyl linker creates around the metal cluster[45]. For the biphenyldicarboxylate linker, it is calculated that the most stable configuration is achieved when both aromatic units are rotationally shifted about  $40^\circ$  from each other. In UiO-67, this linker cannot satisfy its most stable configuration without causing a distortion on the Zr-O bonds, thereby weakening them[45]. Other steric factors include breathing behavior of certain MOFs, and ligand functionalization, where bulky functional groups can also sterically lock the labile ligands in place to prevent their irreversible displacement[29].

Conclusively, there are several factors that influence the water stability of a MOF (thermodynamically and kinetically), and taking each of them into account can help us to better predict the behavior of a certain MOF in water-based applications. On the other hand, a poor result at any of these parameters, e.g., a metal with high lability or a low relative cation charge, does not necessarily mean the MOF is unfit as a water-stable material. The overall stability can still be guaranteed by a favorable dimensionality or connectivity of the SBU within the framework, or optimized by functionalities embedded into the ligand that promote local hydrophobicity or sterical locking of labile ligands[28, 29].

The work of Burtch *et al.* offers an extensive view on the water stability of MOFs, including a comprehensive review on the thermodynamic and kinetic stability of a high variety (>200) of MOFs[29]. An elaborate study on the effects of water adsorption on MOFs has been performed by Low *et al.*, by combining molecular modeling and experimental research[28]. Additionally, comprehensive reviewing work on this topic has been performed by Farrusseng *et al.*, including stability in both gaseous and aqueous media, mechanisms of water adsorption and structure degradation/altering, as well as adsorption properties of several MOFs[30]. One of the main conclusions of the latter work was that even though several water stable MOFs may exist, most applications in which MOFs are promising candidates deal with much more demanding media such as acid or alkaline environments. Indeed, regardless of the tremendous amount of published research on water stability of MOFs, few studies deal with the effects of these particular media (acidic, alkaline...), especially on the long term. In order to consider certain MOFs as viable materials for adsorption in various aqueous environments, these studies are of vital importance.

In addition, it is important to use of a combination of analysis techniques to properly investigate the impact of specific conditions on the stability of MOFs. A first method is to perform post-exposure powder X-ray diffraction measurements, and compare the obtained diffraction pattern to the pristine one. This method works well as an initial stability-evaluation, but regardless of an unchanged PXRD pattern, a sample can still show a considerable loss in porosity and surface area. It is important to follow this up with a nitrogen adsorption analysis, to verify the impact on the MOF's porosity characteristics[29]. The combination of PXRD en N<sub>2</sub>-adsorption is one of the most used approaches to investigate the stability of MOFs[28-30], yet, it could be very useful to also apply techniques that don't yield a structurally averaged result[29]. For instance, microscopic analyses (SEM, TEM) could give insight in surface cracks and fractures (defects), of which it is shown they can have an impact on MOF moisture stability[46]. However, such techniques are not always suitable for MOF analysis, as these solids are often electrical insulators, which creates the problem of sample charging, or they can be electron beam sensitive [47]. Other interesting techniques are infrared and Raman spectroscopy, which can be used to observe vibrational modes that correspond to hydrolysis events in MOFs[29]. If real-time information on the kinetics of a certain degradation mechanism is desired, one can include in-situ techniques such as NMR [48] or X-ray absorption techniques (XANES, EXAFS)[49]. Evidently, the more techniques can be combined in a study, the more thorough the resulting stability assessment will be.

## REFERENCES

- [1] H. Furukawa, K.E. Cordova, M. O'Keeffe, O.M. Yaghi, *The Chemistry and Applications of Metal-Organic Frameworks*, Science, 341 (2013) 1230444.
- [2] O.M. Yaghi, M. O'Keeffe, N.W. Ockwig, H.K. Chae, M. Eddaoudi, J. Kim, *Reticular synthesis and the design of new materials*, Nature, 423 (2003) 705-714.
- [3] A.J. Howarth, Y.Y. Liu, P. Li, Z.Y. Li, T.C. Wang, J. Hupp, O.K. Farha, *Chemical, thermal and mechanical stabilities of metal-organic frameworks*, Nat Rev Mater, 1 (2016).
- [4] G. Ferey, *Hybrid porous solids: past, present, future*, Chem Soc Rev, 37 (2008) 191-214.
- [5] O.K. Farha, I. Eryazici, N.C. Jeong, B.G. Hauser, C.E. Wilmer, A.A. Sarjeant, R.Q. Snurr, S.T. Nguyen, A.O. Yazaydin, J.T. Hupp, *Metal-Organic Framework Materials with Ultrahigh Surface Areas: Is the Sky the Limit?*, J Am Chem Soc, 134 (2012) 15016-15021.
- [6] G. Ferey, C. Mellot-Draznieks, C. Serre, F. Millange, J. Dutour, S. Surble, I. Margiolaki, *A chromium terephthalate-based solid with unusually large pore volumes and surface area*, Science, 309 (2005) 2040-2042.
- [7] T.C. Wang, W. Bury, D.A. Gomez-Gualdrón, N.A. Vermeulen, J.E. Mondloch, P. Deria, K.N. Zhang, P.Z. Moghadam, A.A. Sarjeant, R.Q. Snurr, J.F. Stoddart, J.T. Hupp, O.K. Farha, *Ultrahigh Surface Area Zirconium MOFs and Insights into the Applicability of the BET Theory*, J Am Chem Soc, 137 (2015) 3585-3591.
- [8] F. Jeremias, D. Frohlich, C. Janiak, S.K. Henninger, *Water and methanol adsorption on MOFs for cycling heat transformation processes*, New J Chem, 38 (2014) 1846-1852.
- [9] N.A. Khan, Z. Hasan, S.H. Jung, *Adsorptive removal of hazardous materials using metal-organic frameworks (MOFs): A review*, J Hazard Mater, 244 (2013) 444-456.
- [10] Z.Q. Wang, S.M. Cohen, *Postsynthetic modification of metal-organic frameworks*, Chem Soc Rev, 38 (2009) 1315-1329.
- [11] J.R. Li, R.J. Kuppler, H.C. Zhou, *Selective gas adsorption and separation in metal-organic frameworks*, Chem Soc Rev, 38 (2009) 1477-1504.
- [12] J.R. Li, Y.G. Ma, M.C. McCarthy, J. Sculley, J.M. Yu, H.K. Jeong, P.B. Balbuena, H.C. Zhou, *Carbon dioxide capture-related gas adsorption and separation in metal-organic frameworks*, Coordin Chem Rev, 255 (2011) 1791-1823.
- [13] J. Liu, P.K. Thallapally, B.P. McGrail, D.R. Brown, J. Liu, *Progress in adsorption-based CO<sub>2</sub> capture by metal-organic frameworks*, Chem Soc Rev, 41 (2012) 2308-2322.
- [14] M.P. Suh, H.J. Park, T.K. Prasad, D.W. Lim, *Hydrogen Storage in Metal-Organic Frameworks*, Chem Rev, 112 (2012) 782-835.
- [15] J. Lee, O.K. Farha, J. Roberts, K.A. Scheidt, S.T. Nguyen, J.T. Hupp, *Metal-organic framework materials as catalysts*, Chem Soc Rev, 38 (2009) 1450-1459.
- [16] J.W. Liu, L.F. Chen, H. Cui, J.Y. Zhang, L. Zhang, C.Y. Su, *Applications of metal-organic frameworks in heterogeneous supramolecular catalysis*, Chem Soc Rev, 43 (2014) 6011-6061.
- [17] B. Chen, S. Xiang, G. Qian, *Metal-Organic Frameworks with Functional Pores for Recognition of Small Molecules*, Accounts Chem Res, 43 (2010) 1115-1124.
- [18] J.R. Li, J. Sculley, H.C. Zhou, *Metal-Organic Frameworks for Separations*, Chem Rev, 112 (2012) 869-932.
- [19] P. Horcajada, R. Gref, T. Baati, P.K. Allan, G. Maurin, P. Couvreur, G. Ferey, R.E. Morris, C. Serre, *Metal-Organic Frameworks in Biomedicine*, Chem Rev, 112 (2012) 1232-1268.
- [20] R.C. Huxford, J. Della Rocca, W. Lin, *Metal-organic frameworks as potential drug carriers*, Curr Opin Chem Biol, 14 (2010) 262-268.



- [21] M. Kurmoo, Magnetic metal-organic frameworks, *Chem Soc Rev*, 38 (2009) 1353-1379.
- [22] J. Rocha, L.D. Carlos, F.A. Almeida Paz, D. Ananias, Luminescent multifunctional lanthanides-based metal-organic frameworks, *Chem Soc Rev*, 40 (2011) 926-940.
- [23] M. Jacoby, Heading to market with MOFS, *Chem Eng News*, 86 (2008) 13-16.
- [24] U. Mueller, M. Schubert, F. Teich, H. Puetter, K. Schierle-Arndt, J. Pastre, Metal-organic frameworks - prospective industrial applications, *J Mater Chem*, 16 (2006) 626-636.
- [25] Metal-Organic Frameworks Issue, *Chem Rev*, 112 (2012) 673-1268.
- [26] C.H. Wang, X.L. Liu, N.K. Demir, J.P. Chen, K. Li, Applications of water stable metal-organic frameworks, *Chem Soc Rev*, 45 (2016) 5107-5134.
- [27] M. Bosch, M. Zhang, H.-C. Zhou, Increasing the Stability of Metal-Organic Frameworks, *Advances in Chemistry*, 2014 (2014) 8.
- [28] J.J. Low, A.I. Benin, P. Jakubczak, J.F. Abrahamian, S.A. Faheem, R.R. Willis, Virtual High Throughput Screening Confirmed Experimentally: Porous Coordination Polymer Hydration, *J Am Chem Soc*, 131 (2009) 15834-15842.
- [29] N.C. Burtch, H. Jasuja, K.S. Walton, Water Stability and Adsorption in Metal-Organic Frameworks, *Chem Rev*, 114 (2014) 10575-10612.
- [30] J. Canivet, A. Fateeva, Y.M. Guo, B. Coasne, D. Farrusseng, Water adsorption in MOFs: fundamentals and applications, *Chem Soc Rev*, 43 (2014) 5594-5617.
- [31] K.S. Park, Design, Synthesis and Control of Topology and Properties of Zeolitic Imidazolate Frameworks and Metal-organic Frameworks Based on Pyrazolate, Dissertation (Adviser: O. M. Yaghi), University of California (2008).
- [32] A. Alshammari, Z. Jiang, K.E. Cordova, Metal Organic Frameworks as Emerging Photocatalysts, 2016.
- [33] I.J. Kang, N.A. Khan, E. Haque, S.H. Jhung, Chemical and Thermal Stability of Isotypic Metal-Organic Frameworks: Effect of Metal Ions, *Chem-Eur J*, 17 (2011) 6437-6442.
- [34] Y.-R. Luo, Comprehensive handbook of chemical bond energies, CRC press, 2007.
- [35] J.E. Huheey, Inorganic chemistry: principles of structure and reactivity, 3rd ed., Harper International, New York, 1983.
- [36] T. Wittmann, R. Siegel, N. Reimer, W. Milius, N. Stock, J. Senker, Enhancing the Water Stability of Al-MIL-101-NH<sub>2</sub> via Postsynthetic Modification, *Chem-Eur J*, 21 (2015) 314-323.
- [37] M. Bosch, Y. Shuai, H.-C. Zhou, Group 4 metals as secondary building units: Ti, Zr, and Hf based MOFs, in: S. Kaskel (Ed.) *The chemistry of metal-organic frameworks: synthesis, characterization, and applications*, Wiley, VCH, Germany, 2016, pp. 904.
- [38] T.H. Chen, I. Popov, O. Zenasni, O. Daugulis, O.S. Miljanic, Superhydrophobic perfluorinated metal-organic frameworks, *Chem Commun*, 49 (2013) 6846-6848.
- [39] C. Yang, U. Kaipa, Q.Z. Mather, X.P. Wang, V. Nesterov, A.F. Venero, M.A. Omary, Fluorous Metal-Organic Frameworks with Superior Adsorption and Hydrophobic Properties toward Oil Spill Cleanup and Hydrocarbon Storage, *J Am Chem Soc*, 133 (2011) 18094-18097.
- [40] L. Bellarosa, J.J. Gutierrez-Sevillano, S. Calero, N. Lopez, How ligands improve the hydrothermal stability and affect the adsorption in the IRMOF family, *Phys Chem Chem Phys*, 15 (2013) 17696-17704.
- [41] J.B. Decoste, G.W. Peterson, M.W. Smith, C.A. Stone, C.R. Willis, Enhanced Stability of Cu-BTC MOF via Perfluorohexane Plasma-Enhanced Chemical Vapor Deposition, *J Am Chem Soc*, 134 (2012) 1486-1489.
- [42] J.G. Nguyen, S.M. Cohen, Moisture-Resistant and Superhydrophobic Metal-Organic Frameworks Obtained via Postsynthetic Modification, *J Am Chem Soc*, 132 (2010) 4560-4561.

- [43] M.J. Cliffe, W. Wan, X.D. Zou, P.A. Chater, A.K. Kleppe, M.G. Tucker, H. Wilhelm, N.P. Funnell, F.X. Coudert, A.L. Goodwin, Correlated defect nanoregions in a metal-organic framework, *Nat Commun*, 5 (2014).
- [44] J.B. DeCoste, G.W. Peterson, B.J. Schindler, K.L. Killops, M.A. Browe, J.J. Mahle, The effect of water adsorption on the structure of the carboxylate containing metal-organic frameworks Cu-BTC, Mg-MOF-74, and UiO-66, *J Mater Chem A*, 1 (2013) 11922-11932.
- [45] J.B. DeCoste, G.W. Peterson, H. Jasuja, T.G. Glover, Y.G. Huang, K.S. Walton, Stability and degradation mechanisms of metal-organic frameworks containing the  $\text{Zr}_6\text{O}_4(\text{OH})_4$  secondary building unit, *J Mater Chem A*, 1 (2013) 5642-5650.
- [46] Y. Yoo, V. Varela-Guerrero, H.K. Jeong, Isoreticular Metal-Organic Frameworks and Their Membranes with Enhanced Crack Resistance and Moisture Stability by Surfactant-Assisted Drying, *Langmuir*, 27 (2011) 2652-2657.
- [47] Z. Liu, N. Fujita, K. Miyasaka, L. Han, S.M. Stevens, M. Suga, S. Asahina, B. Slater, C.H. Xiao, Y. Sakamoto, M.W. Anderson, R. Ryoo, O. Terasaki, A review of fine structures of nanoporous materials as evidenced by microscopic methods, *Microscopy-Jpn*, 62 (2013) 109-146.
- [48] D.I. Kolokolov, A.G. Stepanov, V. Guillerm, C. Serre, B. Frick, H. Jobic, Probing the Dynamics of the Porous Zr Terephthalate UiO-66 Framework Using H-2 NMR and Neutron Scattering, *J Phys Chem C*, 116 (2012) 12131-12136.
- [49] S. Bordiga, F. Bonino, K.P. Lillerud, C. Lamberti, X-ray absorption spectroscopies: useful tools to understand metallorganic frameworks structure and reactivity, *Chem Soc Rev*, 39 (2010) 4885-4927.

# 5 SYSTEMATIC STUDY OF THE CHEMICAL & HYDRO- THERMAL STABILITY OF SELECTED STABLE MOFs

**Based on:** Leus, K., Bogaerts, T., De Decker, J., Depauw, H., Hendrickx, K., Vrielinck, H., Van Speybroeck, V., and Van Der Voort, P. **Microporous and Mesoporous Materials** 226 (2016) 110-116. **Contribution:** Synthesis, stability experiments and analyses on MIL-101(Cr).

## 5.1 Introduction

Metal-Organic frameworks (MOFs) are a class of inorganic-organic hybrid materials that have received great interest over the past decades. While initial research on MOFs was focused on their synthesis and structural characterization, an increasing number of MOFs are now being examined for their interesting optical, magnetic, and electronic properties, as well as for their various potential applications in catalysis, ion exchange, gas storage and separation, sensing, polymerization, and drug delivery [1-3]. However, one of the major problems that limit the use of MOFs is their relatively poor stability. Besides their low thermal stability (limited to 350 - 400 °C), few MOFs are known to be stable in the presence of water. This is due to the hydrophilic properties of the metal nodes which results in a strong interaction with water molecules and therefore leads to the cleavage of coordination bonds, hence, destroying the framework [4]. Since the pioneering study of Low *et al.* many other studies have been carried out on the water sensitivity of MOFs [5-7]. Very few MOFs showed no structural integrity loss in the presence of water. However, there are several types of MOFs that demonstrate promising

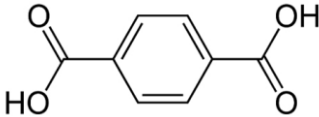
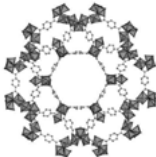
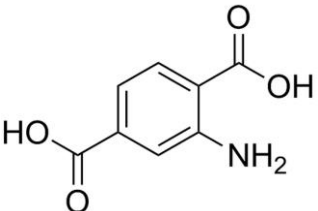
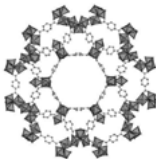
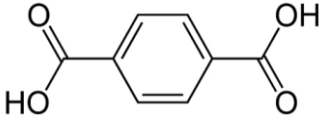
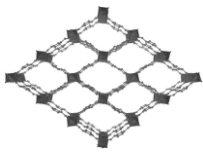
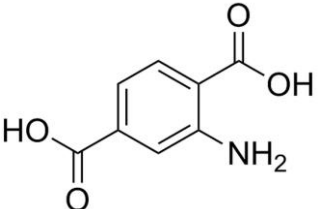
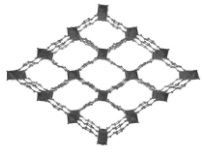
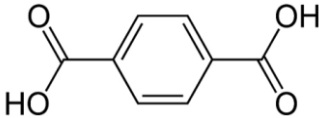
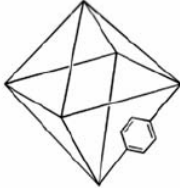
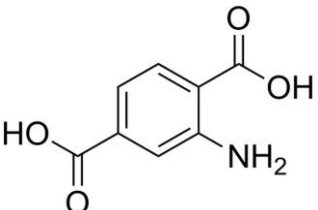
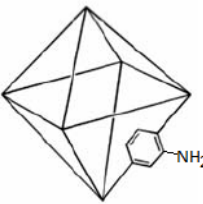
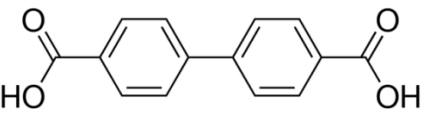
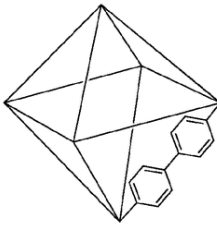
results. For instance, the pyrazolate based frameworks show remarkable stability after exposure to boiling water and other solvents, which is attributed to the high pK<sub>a</sub> value of the imidazole ligands [8]. Besides the pyrazolate based frameworks, the hydrothermally synthesized MIL series constructed from octahedrally coordinated aluminium or chromium metal clusters (MIL-53, respectively, MIL-101) and zeolitic imidazolate frameworks (ZIFs) have been reported to be stable in water [9, 10]. In particular the ZIF-8 material, in which the zinc atoms are coordinated to methylimidazolate ligands via Zn-N bonds possess a very high stability, not only under mechanical pressure but also in aqueous solutions [11, 12]. The higher basicity of the imidazolate linker, in comparison to the carboxylate linkers, results in stronger metal-ligands bonds with the zinc and therefore in an enhanced stability towards water [8].

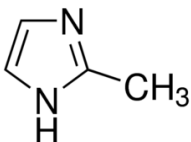
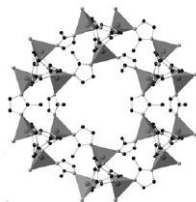
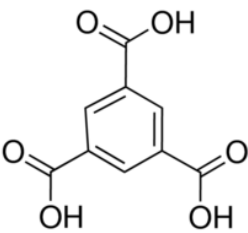
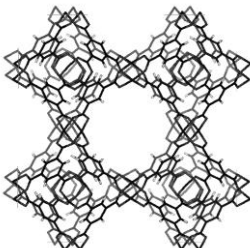
Interesting work on the water-stability of MIL-101(Cr) was performed in a study on dehumidification over hierarchically porous MOFs and the use as advanced water adsorbents, by Chang *et al.* [13]. Furthermore, MOFs constructed from Zr<sub>6</sub>-based nodes also show a remarkably high stability (mechanical, hydrolytical, and chemical). The stability of these Zr-based MOFs, of which UiO-66 is a prototypical example, is due to the strong Coulombic interaction of the highly oxophilic Zr<sup>IV</sup> metal sites with the negatively charged termini of the carboxylate linkers [14].

For the evaluation of MOFs towards processes in industry, the long-term chemical, thermal, and hydrothermal stability are important factors, as many processes are performed in the presence of acids or bases (liquid phase reactions) or at elevated temperature (gas phase reactions) for an extended period of time. Furthermore, the stability of MOFs towards commonly used oxidants is also very crucial in oxidative processes. Although there have already been studies on the chemical, thermal, and hydrothermal stability of MOFs, to the best of our knowledge no systematic or long-term stability investigations have been carried out [15].

Here, we present for the first time a systematic comparative study of reportedly stable metal-organic frameworks, i.e., MIL-101(Cr), NH<sub>2</sub>-MIL-101(Al), MIL-53(Al), NH<sub>2</sub>-MIL-53, UiO-66, NH<sub>2</sub>-UiO-66, UiO-67, ZIF-8 and Cu-BTC. More specifically, their hydrothermal and chemical stability to aqueous acids (pH = 0 and pH = 4), bases (pH = 12), and oxidative environment (5 wt. % H<sub>2</sub>O<sub>2</sub>) is studied on short-term (3 days) and long-term (60 days). Additionally, their short and long-term exposure to water and air has been evaluated as well. A structural overview of the studied MOFs is given in Table 5.1. As several of them have similar central metals and/or linkers, it is interesting to study the effect of these constituents (and their combination) on the stability of the framework.

**Table 5.1 Structural overview of the studied MOFs**

	Metal	Linker	Structure
MIL-101(Cr)	Cr		
NH <sub>2</sub> -MIL-101 (Al)	Al		
MIL-53(Al)	Al		
NH <sub>2</sub> -MIL-53	Al		
UiO-66	Zr		
NH <sub>2</sub> -UiO-66	Zr		
UiO-67	Zr		

ZIF-8	Zn		
Cu-BTC	Cu		

## 5.2 Materials and Methods

### *General procedures*

All chemicals were purchased from Sigma Aldrich or TCI Europe and used without further purification. Nitrogen adsorption experiments were carried out at  $-196\text{ }^{\circ}\text{C}$  using a Belsorp mini II gas analyzer. Prior to analysis, the samples were dried under vacuum at  $120\text{ }^{\circ}\text{C}$  to remove adsorbed water. X-Ray powder diffraction (XRPD) patterns were collected on an ARL X'TRA X-ray diffractometer with Cu  $K\alpha$  radiation of  $0.15418\text{ nm}$  wavelength and a solid state detector. Thermogravimetric Analysis (TGA) was performed on an SDT 2960 from TA Instruments.

### *Synthesis of the MOF materials*

#### *MIL-101 (Cr)*

MIL-101(Cr) was synthesized according to an adapted recipe from Edler *et al.*[16]. In a typical experiment,  $0.665\text{ g}$  terephthalic acid ( $4\text{ mmol}$ ) and  $1.608\text{ g}$   $\text{Cr}(\text{NO}_3)_3 \cdot 9\text{H}_2\text{O}$  ( $4\text{ mmol}$ ) were added to  $20\text{ mL}$  deionized water. The resulting suspension was placed in a Teflon-lined autoclave at  $210\text{ }^{\circ}\text{C}$  during 8 hours under autogenous pressure (2 hours warm-up). After cooling down to room temperature, the mixture was filtered and the green solid was collected and washed thoroughly with dimethylformamide (DMF) and water in order to purify the material by removing any unreacted reagents. The material was not subjected to any additional activation steps.

#### *NH<sub>2</sub>-MIL-101(Al)*

The  $\text{NH}_2$ -MIL-101(Al) material was prepared in a few smaller batches as proposed by Fischer *et al.* [17].  $270\text{ mg}$  ( $1.49\text{ mmol}$ ) of 2-aminoterephthalic acid was dissolved in  $60\text{ mL}$  of DMF. This

solution was heated to 110 °C and 730 mg (3.0 mmol)  $\text{AlCl}_3 \cdot 6\text{H}_2\text{O}$  was added in 6 equal portions, one per 15 minutes. The solid material began to form after approximately 30 minutes of reaction. After adding the last portion, the mixture was stirred for an additional 3 hours. In a final step the mixture was kept under heat without stirring for 16 hours. Afterwards, the solid was filtered off and washed several times with DMF, followed by soxhlet extraction with acetone for 6 hours, in order to remove any free linkers and  $\text{AlCl}_3$ .

#### *Cu-BTC*

For the synthesis of Cu-BTC, 2g (9.52 mmol) of benzene-1,3,5-tricarboxylic acid (BTC) was added to 50 mL of a 1:1:1 mixture of DMF/EtOH/ $\text{H}_2\text{O}$ . 3.4 g (17.24 mmol) of  $\text{Cu}(\text{OAc})_2 \cdot \text{H}_2\text{O}$  was added to 50 mL of the same solvent mixture and both mixtures were combined under stirring. Finally, triethylamine (TEA, 2 mL) was added, after which the resulting mixture was stirred for 23 hours at room temperature. The product was collected by filtration and washed 2 times with 25 mL of DMF [18].

#### *UiO-66-X (X=H, $\text{NH}_2$ )*

The UiO-66-X materials were synthesized according to a slightly modified procedure of Van Der Voort *et al.* [19]. Typically, 0.3g (0.89 mmol)  $\text{ZrO}_2\text{Cl}_2 \cdot 8\text{H}_2\text{O}$  and 0.1545g (0.93 mmol) terephthalic acid or 0.168g (0.93 mmol) 2-aminoterephthalic acid were added to 3.6 mL formic acid and 9 mL dimethyl acetamide. After 20 minutes of sonication, the solution was transferred to a Teflon-lined autoclave and placed in an oven at 150°C for 12 hours. When cooled down, the solid was filtered off and subsequently stirred in DMF (12 hours) and methanol (24 hours) to remove any free linker and DMF from the pores. The resulting materials were dried under dynamic vacuum at 65° (X=H) and 220° (X= $\text{NH}_2$ ) for 24 hours.

#### *UiO-67*

The synthetic procedure of UiO-67 was based on the recipe of Farha *et al.* [20]. 0.27 mmol  $\text{ZrCl}_4$  and 0.38 mmol 4,4'-diphenyldicarboxylic acid (BPDC) were dissolved in 15 mL DMF and 0.5 mL concentrated HCl. The resulting solution was sonicated for 20 minutes and subsequently transferred to a thermoblock at 80° for 12 hours. After filtration and washing with DMF and ethanol, the samples were dried under dynamic vacuum at 90°C, and activated at 150°C (3 hours).

#### *MIL-53 (Al)*

MIL-53 (Al) was synthesized according to a slightly modified procedure of Ferey *et al.* [21]. A mixture of  $\text{AlCl}_3 \cdot 6\text{H}_2\text{O}$  (2.90 g, 12.0 mmol), terephthalic acid (2.00 g, 12.0 mmol), and deionized water (60 mL) is placed in a Teflon-lined autoclave at 210 °C for 24 hours.

Afterwards, the MIL-53 (Al) (*as synthesized*) is collected by filtration and washed with acetone, followed by calcination at 300 °C for 72 hours to obtain MIL-53 (Al).

### *NH<sub>2</sub>-MIL-53*

The NH<sub>2</sub>-MIL-53 was synthesized by the recipe of Stock *et al.* [22]. 1.48 g (6.13 mmol) of AlCl<sub>3</sub>·6H<sub>2</sub>O was mixed with 1.13 g (6.24 mmol) of 2-aminoterephthalic acid in 15 mL of deionized water. The resulting solution was placed in a Teflon-lined autoclave at 150 °C (warm-up: 1 hour) for 5 hours. Afterwards, the solid material was filtered off and suspended in DMF in an autoclave for an additional 15 hours at 150 °C, to remove unreacted linker. The DMF molecules were removed by a thermal treatment in air at 130 °C in a muffle furnace.

### *ZIF-8*

For the synthesis of ZIF-8, 0.733 g Zn(NO<sub>3</sub>)<sub>2</sub>·6H<sub>2</sub>O (2.46 mmol) was dissolved in 50 mL deionized water. A second solution of 1.622 g 2-methylimidazole (HMe-Im, 19.75 mmol) and 2.00 g triethylamine (TEA, 19.76 mmol) in 50 mL deionized water was prepared. The Zn solution was added to the second solution under stirring, which resulted immediately in an opaque white solution. After stirring for an additional 10 minutes at room temperature, the solid was separated through centrifugation and placed in water for 12 hours. This procedure was repeated 2 times. Hereafter the solid was collected and dried in air at 110 °C. Finally, the sample was dried under vacuum at 150 °C for 1 hour [23].

### *Chemical stability*

The chemical stability tests were performed by exposing the MOFs for 3 or 60 days to acidic conditions (HCl, pH=0 and pH=4), basic conditions (NaOH, pH=12) or under oxidizing conditions (5 wt. % H<sub>2</sub>O<sub>2</sub>). Additionally, the stability of the MOFs was examined by exposing them to air and water for respectively 3 or 60 days. All the tests were carried out at room temperature (RT) without stirring. It was important to only assess the pH effect. Therefore, a simple acid (HCl) and base (NaOH) were selected for the tests, rather than, for instance, an oxidizing acid such as HNO<sub>3</sub>.

### *Hydrothermal stability*

The hydrothermal stability study was conducted by exposing the MOF samples to saturated steam for 5 hours at 200 °C.



## 5.3 Results and Discussion

### 5.3.1 Hydrothermal stability

In Table 5.2, the Langmuir surface area is presented of all the pristine MOF materials and after exposing them to water, air, acidic-, basic-, oxidative-, and a hydrothermal environment. In Table 5.3, the results of the hydrothermal treatment as well as those of the short and long-term exposure to air and water are illustrated (based on XRPD spectra). As can be seen from Table 5.3 and Appendix 1.1, MIL-101 (Cr) preserved its crystalline structure after the steaming test. This observation is in agreement with the earlier report of Ferey *et al.*, in which the high moisture-stability of MIL-101 (Cr) was already stated [24]. Furthermore, the hydrothermal stability of this chromium-based MOF was confirmed in the work of Kang *et al.* in which they observed that the MIL-101 (Cr) was structurally stable after exposure to water at 80°C for 5 days. It was also observed in the work of Chang *et al.*, who demonstrated that the MIL-101 (Cr) preserved its crystalline structure after exposure to boiling water for 1 week [25, 26].

In contrast to the high hydrothermal stability of the MIL-101 (Cr), it is known that the MIL-101 analogues of  $\text{Fe}^{3+}$  and  $\text{Al}^{3+}$  show a much lower resistance to hydrolysis. This last conclusion was also confirmed by our study, demonstrating that the  $\text{NH}_2$ -MIL-101 (Al) is highly sensitive to water, which leads to transformation into the thermodynamically more stable  $\text{NH}_2$ -MIL-53 (Al). The latter observation is in agreement with the recent report of Senker *et al.*, demonstrating that the  $\text{NH}_2$ -MIL-101 (Al) already transforms into  $\text{NH}_2$ -MIL-53 (Al) after only 5 minutes exposure to water [27].

Besides the MIL-101 (Cr), the  $\text{NH}_2$ -MIL-53 is also stable under the examined steaming conditions (see Table 5.3 and Appendix 1.1), as no changes are observed in the XRPD pattern in comparison to the pristine  $\text{NH}_2$ -MIL-53. In contrast to the  $\text{NH}_2$ -MIL-53, the MIL-53 (Al) exhibits a partial transformation towards a new crystalline phase, as new diffraction signals arise at  $2\theta = 11^\circ$  and  $21^\circ$ . Furthermore, as can be seen from Table 5.2, the Langmuir surface area of the MIL-53 (Al) is reduced from 1531  $\text{m}^2/\text{g}$ , to 792  $\text{m}^2/\text{g}$ , which suggests a partial hydrolysis of the MOF framework. This observation was also noted in the work of Bellat *et al.*, and Jung *et al.*, who attributed this effect to the production of free organic linker  $\text{H}_2\text{BDC}$  and to the formation of  $\gamma$ - $\text{AlO}(\text{OH})$  species under reflux conditions in water [15, 28].

The copper paddle-wheeled framework, Cu-BTC, is known to be unstable under steaming conditions [29]. As can be seen from Appendix 1.1 and Table 5.2, not only was the framework converted into another structure, the porosity was completely lost after the hydrothermal treatment. Based on literature, the structure of the green phase obtained after the hydrothermal treatment could be assigned to  $[\text{Cu}_2\text{OH}(\text{BTC})(\text{H}_2\text{O})]n.2n\text{H}_2\text{O}$  [30]. While the Cu-BTC material is completely destroyed, the ZIF-8 framework can withstand the hydrothermal treatment, as no changes are observed in the crystal structure and only a minor decrease in the Langmuir surface

area is noted (from 772 m<sup>2</sup>/g, to 660 m<sup>2</sup>/g). This observation is in agreement with previous studies showing that ZIF-8 is resistant to steam for hours and to boiling water for at least a week [6, 12].

The UiO-66 and NH<sub>2</sub>-UiO-66 frameworks are stable after 5 hours at 200 °C under autogenous pressure, while the UiO-67 material is completely destroyed. The lack of stability of the UiO-67 material to H<sub>2</sub>O exposure was recently assigned to the linker hydrolysis engineered by clustering of H<sub>2</sub>O molecules near the Zr<sub>6</sub> nodes and to rotational effects of the extended organic linker [31].

**Table 5.2 Effect of the hydrothermal treatment, chemical and oxidative treatment and exposure to water and air (short-term and long-term) on the Langmuir Surface Area (expressed in m<sup>2</sup>/g). All data are based on singular experiments.**

	Treatment conditions	UiO-66	NH <sub>2</sub> -UiO-66	UiO-67	MIL-53 (Al)	NH <sub>2</sub> -MIL-53 (Al)	MIL-101 (Cr)	NH <sub>2</sub> -MIL-101 (Al)	Cu-BTC	ZIF-8
	pristine material	1008	885	2395	1531	NP	2001 <sup>a</sup>	2026	846	772
<b>3 days</b>	pH=0, RT	549	712	35	D	NP	3180	D	D	D
	pH=4, RT	1063	994	2182	1068	NP	3200	182	1103	673
	pH=12, RT	1051	590	1395	76	NP	3109	187	153	652
	water, RT	1018	632	2436	1380	NP	2227	1060	823	656
	steam, 5 h	886	548	33	792	NP	2200	253	4	660
	Air	651	492	172	1385	NP	2005	244	701	801
	5% H <sub>2</sub> O <sub>2</sub> , RT	979	686	19	607	NP	2040	430	402	502
<b>2 months</b>	pH=0, RT	534	591	29	D	NP	3787	D	D	D
	pH=4, RT	973	729	16	136	NP	3470	173	266	160
	pH=12, RT	866	646	2042	740	NP	3250	191	289	139
	water, RT	1145	740	2320	1165	NP	2322	183	469	673
	Air	738	562	523	1530	NP	1998	119	284	755
	5% H <sub>2</sub> O <sub>2</sub> , RT	1142	486	77	241	NP	<20	377	41	107

NP: Narrow Pore, Langmuir surface area is <50 m<sup>2</sup>/g, D = dissolved. <sup>a</sup>Specific surface area as obtained after synthesis, without additional purification steps.

**Table 5.3 Effect of the hydrothermal stability test and short and long time exposure to air and water on the XRPD pattern of the examined MOF materials.**

	3 Days		2 Months		Hydrothermal Stability
	Air	Water	Air	Water	
MIL-101 (Cr)	+	+	+	+	+
NH <sub>2</sub> -MIL-101 (Al)	-	PT	-	T (NH <sub>2</sub> -MIL-53)	T (NH <sub>2</sub> -MIL-53)
MIL-53 (Al)	+	+	+	+	PT
NH <sub>2</sub> -MIL-53	+	+	+	+	+
UiO-66	PD	+	PD	+	+
NH <sub>2</sub> -UiO-66	+	+	+	+	+
UiO-67	+	+	+	+	D
Cu-BTC	+	PT	+	PT	T([Cu <sub>2</sub> OH(BTC)(H <sub>2</sub> O)] <sub>n</sub> .2nH <sub>2</sub> O)
ZIF-8	+	+	+	PT	+

+: crystallinity preserved, -: MOF is destroyed, PT: partial transformation, PD: partial destruction, T: transformation, D: dissolved.

### 5.3.2 Stability towards water and air

As can be seen from Table 5.3 and Appendix 1.2, the MIL-101 (Cr) perfectly preserved its crystalline structure after 3 days in air or water, which is in agreement with earlier literature reports on this Cr-based MOF [25,32]. Moreover, even after exposure for 2 months to air or water, no changes are observed its Langmuir surface area and XRPD pattern, confirming the remarkable stability of this framework. Noteworthy is the starting value of the Langmuir surface area of MIL-101(Cr) (~2000 m<sup>2</sup>/g), which is considerably lower than the value reported by Ferey *et al.* [24]. This is due to the fact that the material was not subjected to an activation step after synthesis (e.g., purification with hot ethanol and/or NH<sub>4</sub>F for several hours [16]) in order to check if the applied stability conditions could also serve as purification solvents.

In contrast to the MIL-101 (Cr), the NH<sub>2</sub>-MIL-101 (Al) is already completely destroyed after exposure to air for 3 days. Additionally, slight changes are observed in the XRPD pattern of the NH<sub>2</sub>-MIL-101 (Al) after exposure for 3 days to water, and a decrease in the Langmuir surface area is observed (from 2026 m<sup>2</sup>/g, to 1060 m<sup>2</sup>/g), suggesting a partial transformation of the

framework into NH<sub>2</sub>-MIL-53. In contrast to the report of Senker *et al.*, who observed this transformation after only 5 minutes in water, we observed this framework transformation after 2 months [27]. Besides the MIL-101 (Cr), also the MIL-53 (Al) and NH<sub>2</sub>-MIL-53 exhibit a good stability to air and water after a contact time of 3 days. Even after 2 months in air or water no significant changes are observed in the XRPD patterns for both materials. The high stability of MIL-53 (Al) could be due to the strong chemical bond between the Al sites in the secondary building unit (SBU) and the oxygen atoms. Additionally, Huang *et al.* stated that the hydrophobic aromatic walls can prevent the attack of the AlO<sub>4</sub>(OH)<sub>4</sub> units by water molecules [33]. Nevertheless, it should be noted that a small degradation of the framework will not be visible in the XRPD pattern due to the high intensities. As the Langmuir surface area of the MIL-53 (Al) decreases from 1531 m<sup>2</sup>/g, to 1165 m<sup>2</sup>/g, a partial hydrolysis/transformation, similar to the one observed during the hydrothermal treatment (*vide supra*) is suggested.

In contrast to the MIL-53 (Al) framework, which shows a good stability in water, the Cu-BTC material is known to be unstable in the presence of water. This observation was confirmed by our experiments. From the XRPD data in Appendix 1.2, it can be seen that even after a contact time of 3 days with water, characteristic Cu-BTC diffraction peaks are present, next to new diffractions. Many groups have examined the degradation of this framework and the assumption was made that water molecules can coordinate along the Cu–Cu axis and therefore can distort the secondary building unit (SBU) along that axis. However, this distortion is not able to break the Cu–carboxylate bonds, and water clusters need to be formed around the SBU before degradation will take place [34,35].

In comparison to the Cu-BTC material, which has free metal sites, a defect-free zirconium based MOF, i.e., UiO-66, should have fully saturated sites which makes it impossible for water molecules to coordinate with the framework, leading to a higher water stability. Indeed, no changes are observed in the XRPD pattern and in the Langmuir surface, even after exposure for 2 months to water. Furthermore, the incorporation of functional groups into this framework resulted in a similar stability to water and even a higher stability in air. As can be seen from Appendix 1.2, the UiO-66 already starts to degrade after 3 days of air exposure, while the NH<sub>2</sub>-UiO-66 shows no structural changes based on the XRPD data. This similar or better stability in comparison to the parent framework was already observed by Lillerud *et al.* [36].

The extended UiO-66 framework, denoted as UiO-67, shows a good stability towards linker hydrolysis in water, which was also noted in the study of Farha *et al.*, and Maurin *et al.* [14,37]. Although, no changes are observed in the XRPD pattern of the UiO-67 after exposure for 2 months to air, there is a significant decrease in the Langmuir surface (from 2395 m<sup>2</sup>/g for the pristine material, to 172 m<sup>2</sup>/g after 3 days and 523 m<sup>2</sup>/g after 2 months exposure to air). The lower surface area value for 3 days exposure, compared to 2 months exposure, could be due to differences between the batches used for these individual tests. Perhaps some structural defects

in the 3-day test caused this high degradation. The remarkable difference between XRD and N<sub>2</sub>-adsorption results once again proves that it is highly important to use more than one analysis technique to assess the material's stability (*vide supra*).

Considering the stability of ZIF-8, there is a lot of debate whether the material is stable in water or not, as conflicting results have been published. From our hydrothermal stability tests (*vide supra*), it was clear that the ZIF-8 showed no structural degradation. However, after storage at room temperature for 2 months, new diffraction peaks appear in the XRPD pattern, which were also observed in the work of Kaskel *et al.* [5] (see Appendix 1.2). In a recent report of Friscic *et al.*, these diffraction peaks have been assigned to complex carbonates, the hydrolytic degradation products of ZIF-8, which are formed due to the chemical reaction of the framework with CO<sub>2</sub> in the presence of water or moisture [38].

### 5.3.3 Chemical stability

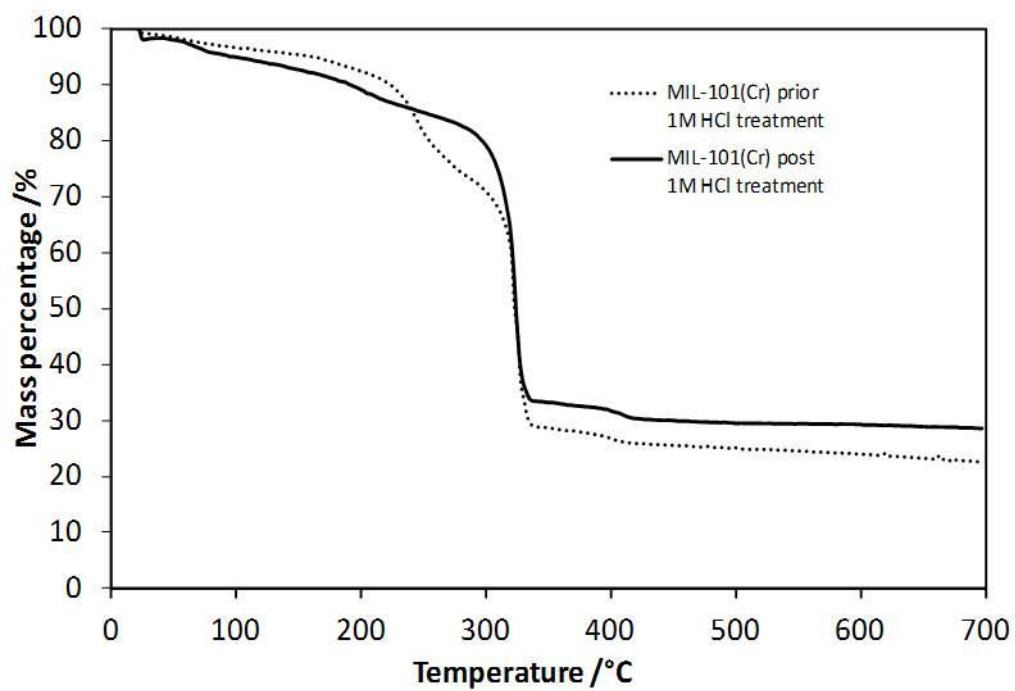
#### *Stability towards acids*

In Table 5.4, the effects of exposing the MOFs for 3 days or 2 months to acidic solutions (pH = 0 and pH = 4), basic conditions (pH = 12), and peroxides (5% H<sub>2</sub>O<sub>2</sub>) are reported. From this table and Appendix 1.3, it can be seen that the MIL-101 (Cr) exhibits an extremely high stability under acidic conditions, as no changes can be observed in the XRPD patterns even after exposing the material for 2 months in a pH = 0 solution. Moreover, from Table 5.2, it is clear that the Langmuir surface area increased drastically after treating the MOF with acidic solutions (from 2001 m<sup>2</sup>/g, to 3180 m<sup>2</sup>/g or higher). To determine if this increase in surface area is due to the removal of left-over starting reagents (e.g., terephthalic acid), TGA experiments were carried out. Figure 5.1 shows the TGA plot of the pristine MIL-101(Cr) and after a 1 M HCl treatment for 3 days. From this figure, it is clear that the pristine MIL-101(Cr) exhibits an initial weight loss at approximately 250-260 °C, which can be assigned to free terephthalic acid molecules that are still clogged in the pores, as this temperature corresponds to the flash-point of terephthalic acid. In a second weight loss step at 320 °C, the MIL-101 (Cr) starts to decompose. The thermal stability is in agreement with the earlier reports on MIL-101 (Cr) [39]. After acid exposure, the first weight loss step at 250 °C is absent, indicating that the acid treatment removes the free organic linker from the pores.

In contrast to MIL-101 (Cr), NH<sub>2</sub>-MIL-101 (Al) shows a very low stability towards acids. The NH<sub>2</sub>-MIL-101 (Al) structure is completely converted into the thermodynamically more stable NH<sub>2</sub>-MIL-53 after 3 days in a pH = 4 solution, whereas in a pH = 0 solution, the MOF was completely dissolved after a few minutes. Next to NH<sub>2</sub>-MIL-101 (Al), the ZIF-8 and Cu-BTC structures were also immediately dissolved after exposure to a solution of pH = 0. However, ZIF-8 still possesses a good crystallinity after 3 days in a pH = 4 solution, whereas Cu-BTC already starts to form a new crystalline phase, which was also observed after exposing it to water (*vide supra*). After 2 months in pH = 4, the ZIF-8 shows a significant degradation. Although part of the MOF's diffraction peaks are still present in XRPD, new diffraction peaks can be observed as well, which were also noted after storage for 2 months in water and can be assigned to carbonates (*vide supra*) [38].

Next to the MIL-101 (Cr), both UiO-66 and NH<sub>2</sub>-UiO-66 exhibit a good stability in acidic conditions, even after exposure for 2 months in pH = 0 solutions. The short-term stability of both materials was already observed by the group of Lillerud, who reported that no loss in crystallinity was observed after 2 h in HCl (pH = 1) [36]. In the recent report of Zhong *et al.*, it was shown that UiO-66 can be kept intact in solutions of pH = 2 to pH = 6 for at least 24 h, in the absence of fluorine [40]. However, although both materials show no loss in crystallinity, one can clearly see from Table 5.2 that the Langmuir surface area decreases significantly for both MOFs after exposure for 3 days at pH = 0. The Langmuir surface areas of the pristine UiO-66 and NH<sub>2</sub>-UiO-66 are respectively 1008 m<sup>2</sup>/g, and 885 m<sup>2</sup>/g, whereas afterwards they dropped to 549 m<sup>2</sup>/g and 712 m<sup>2</sup>/g, respectively.

In contrast to UiO-66, UiO-67 shows a much lower stability towards acids. In a pH = 4 solution, the framework is still well preserved as can be seen from the XRPD pattern in Appendix 1.3. Also, no significant loss in the Langmuir surface area is observed (see Table 5.2). However, after immersing the material for 2 months in this solution, the framework shows a significant decrease in crystallinity and in surface area. Moreover, the MOF is completely destroyed after 3 days at pH = 0, as only the diffraction peaks from the free organic linker, (4,4'-diphenyldicarboxylic acid), can be observed in the XRPD pattern (Appendix 1.3).



**Figure 5.1** TGA plot of MIL-101 (Cr) before and after the treatment in 1 M HCl (heating rate: 2 °C/min).



**Table 5.4 Effect of a short and long time exposure to acids (pH = 0 and pH = 4), bases (pH = 12), and peroxides on the XRPD pattern of the examined MOF materials.**

	3 days				2 months			
	pH=0	pH=4	pH=12	H <sub>2</sub> O <sub>2</sub>	pH=0	pH=4	pH=12	H <sub>2</sub> O <sub>2</sub>
MIL-101 (Cr)	+	+	+	+	+	+	+	T(MIL-53 <i>a.s.</i> )
NH <sub>2</sub> -MIL-101 (Al)	D	T(NH <sub>2</sub> -MIL-53)	T(NH <sub>2</sub> -MIL-53)	T(NH <sub>2</sub> -MIL-53)	D	T(NH <sub>2</sub> -MIL-53)	T(NH <sub>2</sub> -MIL-53)	T(NH <sub>2</sub> -MIL-53)
MIL-53 (Al)	D	+	+	PT	D	PT	+	PT
NH <sub>2</sub> -MIL-53	PD	+	+	+	D	+	+	PT
UiO-66	+	+	+	+	+	+	+	+
NH <sub>2</sub> -UiO-66	+	+	+	+	+	+	+	+
UiO-67	D	+	+	D	D	PD	+	D
Cu-BTC	D	PT	T (several phases)	+	D	PT	T (several phases)	D
ZIF-8	D	+	+	PD	D	PD	PT	D

+: crystallinity preserved, PT: partial transformation, PD: partial destruction, T: transformation, D: dissolved

MIL-53 (Al) material exhibits a rather good stability at pH = 4 for 3 days (Appendix 1.3). No changes in the crystallinity are observed, which is consistent with the report of Huang *et al.*, who demonstrated that the MIL-53 (Al) structure is highly resistant to hydrolysis in acidic solutions (pH = 2) after immersing the material for 7 days at room temperature or even at 100 °C [33]. However, although no changes are observed in the XRPD pattern, a significant decrease is noted in the Langmuir surface area in comparison to the pristine material. After exposure for 3 days in a pH = 4 solution, the Langmuir surface area is decreased to 1068 m<sup>2</sup>/g, whereas the pristine MOF started out at 1531 m<sup>2</sup>/g. Furthermore, after exposure for 2 months to a solution of pH = 4, the Langmuir surface area decreased to 136 m<sup>2</sup>/g, which shows that the MIL-53 (Al) gradually decomposes. Also, after 2 months at pH = 4, a new crystalline phase starts to appear, which can be assigned to  $\gamma$ -AlO(OH) and terephthalic acid intercalated into the pores [28]. As expected, after immersing the material for a period of 3 days in a solution of pH = 0, the structure is completely destroyed and only the diffraction peaks of the terephthalic acid linkers can be observed in the XRPD pattern. In comparison to MIL-53 (Al), the functionalized NH<sub>2</sub>-MIL-53 exhibits an enhanced stability under acidic conditions, as even exposure for 2 months at pH = 4 shows no difference in the crystallinity of this MOF. However, in stronger acidic conditions (pH = 0), the material experiences a gradual decomposition. After suspending the material for 2 months at pH = 0 the structure of NH<sub>2</sub>-MIL-53 is almost completely destroyed and only the diffraction peaks of the free 2-aminoterephthalic acid are observed.

#### *Stability towards bases*

In addition to the very high stability of MIL-101 (Cr) in acidic media, it can be seen from Table 5.4 and Appendix 1.4 that it also possesses a high stability towards alkaline environment. No changes in the crystallinity are observed after 2 months in a pH = 12 solution. Additionally, the Langmuir surface area increases significantly, an effect which was also observed after the treatment with acid. The Langmuir surface area of the MIL-101 (Cr) after 2 months is increased to 3250 m<sup>2</sup>/g, whereas the parent MOF (*a.s.*) had a Langmuir surface area of 2001 m<sup>2</sup>/g.

In contrast to the very high stability of the MIL-101 (Cr), the NH<sub>2</sub>-MIL-101 (Al) and Cu-BTC framework show an exceptionally low stability towards bases, as can be seen from Appendix 1.4. After contact for only 3 days at pH = 12, a complete structure transformation of NH<sub>2</sub>-MIL-101 (Al) into NH<sub>2</sub>-MIL-53 is observed, whereas the Cu-BTC framework is converted into other crystalline phases, which were also observed after contact in water and acidic media. These formed phases can probably be assigned to free organic linker, benzene-1,3,5-tricarboxylic acid (BTC), [Cu<sub>2</sub>OH(BTC) (H<sub>2</sub>O)]<sub>n</sub> · 2nH<sub>2</sub>O and the original Cu-BTC framework [30].

MIL-53 (Al) and NH<sub>2</sub>-MIL-53 exhibit a good stability in alkaline media. No loss of crystallinity is observed from the XRPD patterns (Appendix 1.4). However, there is a significant decrease in the Langmuir surface area of the MIL-53 (Al), in comparison to the pristine MOF. This result is

in agreement with the report of Jhung *et al.*, who noticed a decrease in the surface area and XRD intensities as a function of contact time, after stirring the MIL-53 (Al) in a  $7.0 \times 10^{-2}$  M NaOH solution at room temperature [15]. Also, the group of Huang observed no significant changes in the degree of crystallinity after uninterrupted exposure to pH = 14, up to 7 days at room temperature or 50 °C [33]. However, after increasing the temperature to 100 °C, the framework shows limited structure stability in a pH = 14 solution and structural transformations start to occur after 2 days.

ZIF-8 shows proper stability in alkaline solutions, as can be seen in Appendix 1.4. After 3 days in a pH = 12 solution, no changes are observed in the XRPD pattern and only a minor decrease in Langmuir surface area is noted. This is in agreement with the report of Yaghi *et al.*, demonstrating that the ZIF-8 stays unchanged for up to 24 hours in 0.1 M and 8 M aqueous NaOH at 100 °C [12]. However, after contact for 2 months in a pH = 12 solution, extra diffraction peaks are observed, which can be assigned to the formation of carbonates [38]. Next to the ZIF-8 material, the UiO-66, NH<sub>2</sub>-UiO-66 and UiO-67 also reveal a high resistance towards bases. No changes are observed in their XRPD patterns and only a slight decrease is observed in the Langmuir surface areas. However at higher pHs, Lillerud *et al.* have noticed that the UiO-66 framework starts to transform in a less crystalline material within 2 hours, whereas the treatment of NH<sub>2</sub>-UiO-66 with NaOH led to a total decomposition of the MOF into an amorphous phase [36].

#### *Stability towards peroxides*




In contrast to the previous examined media, in which the MIL-101 (Cr) showed an exceptionally high stability, it can be seen from Table 5.4 and Appendix 1.5, that after 2 months of exposure to the H<sub>2</sub>O<sub>2</sub> solution, the MIL-101 (Cr) is completely converted into another crystalline phase, i.e., the MIL-53 (*a.s.*) structure. The ZIF-8 material is almost fully amorphized after 2 months in said solution, whereas the Cu-BTC material is transformed into a crystalline phase which we could not directly identify. These MOFs did, however, preserve their crystallinity after 3 days contact time with the peroxide solution (even though their Langmuir surface area did decrease). In contrast, the UiO-67 and NH<sub>2</sub>-MIL-101 (Al) showed a complete degradation after only 3 days in the oxidative environment. The NH<sub>2</sub>-MIL-101 (Al) is converted into the thermodynamically more stable NH<sub>2</sub>-MIL-53 structure, whereas with the UiO-67, only the diffraction peaks of free linker 4,4'-diphenyldicarboxylic acid can be observed.





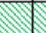

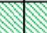

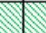

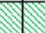
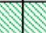

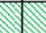
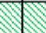

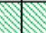
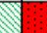
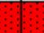

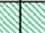
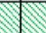
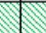







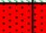



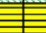



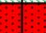
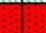
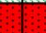

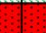
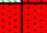
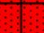
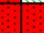
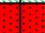
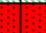
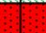
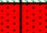
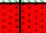















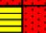



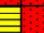

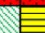





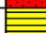








































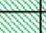
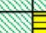
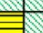


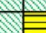



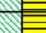
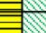


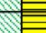
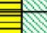
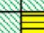
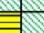
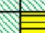

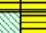

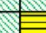






















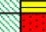



















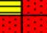


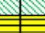
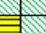
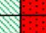


















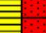



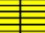




UiO-66 and NH<sub>2</sub>-UiO-66 show a remarkable stability in the peroxide solution, which is in contrast with the UiO-67. Even after 2 months exposure, no changes are observed in the XRPD pattern of the NH<sub>2</sub>-UiO-66 (see Appendix 1.5). However, where the Langmuir surface area of UiO-66 stayed unaltered, with the NH<sub>2</sub>-UiO-66 a significant decrease was observed (from 885 m<sup>2</sup>/g to 486 m<sup>2</sup>/g after 2 months).

Also for the MIL-53 (Al), a gradual decrease in the Langmuir surface area is noted in time (from 1531 m<sup>2</sup>/g, to 607 m<sup>2</sup>/g, and 241 m<sup>2</sup>/g, after respectively 3 days and 2 months), in addition to progressive structural transformation into a new crystalline phase. This phase was also observed after the hydrothermal treatment and exposure to acidic media, and could be assigned to free organic linker and  $\gamma$ -AlO(OH) [28]. A gradual degradation of the framework was also noted for the NH<sub>2</sub>-MIL-53. After 2 months in the H<sub>2</sub>O<sub>2</sub> solution, new diffraction peaks appear showing that the NH<sub>2</sub>-MIL-53 structure is modified.

## 5.4 Conclusions

In this work, we presented for the first time a systematic comparison of the stability of several metal-organic frameworks. In order to investigate these materials, not only the crystallinity before and after the tests was compared, but also the porosity. In the reports of many new MOF materials, some kinds of stability tests are proposed, yet in this work, all the materials were treated under the same conditions to allow a fair comparison. A complete overview of the results is provided in Table 5.5. For most of the MOFs under examination, i.e., MIL-101(Cr), NH<sub>2</sub>-MIL-101(Al), MIL-53(Al), NH<sub>2</sub>-MIL-53, UiO-66, NH<sub>2</sub>-UiO-66, UiO-67, ZIF-8, and Cu-BTC, the hydrothermal stability was confirmed. The chemical stability towards acids and bases was overall disappointing, especially after a 2 months exposure time, with a few notable exceptions. One example worth noting was MIL-101(Cr), that reached a higher internal surface area after an acid or alkaline washing step, proving to be an adequate purification method. The NH<sub>2</sub>-MIL-101(Al) structure, however, shows a very low stability, as it can be easily converted to the more thermodynamically stable NH<sub>2</sub>-MIL-53 framework. Very few of the examined MOFs showed a good stability in 5 wt. % H<sub>2</sub>O<sub>2</sub> solution. Only the UiO-66 and NH<sub>2</sub>-UiO-66 material showed no loss in crystallinity after exposure for 2 months. Furthermore, it was shown that it is important to not only consider the crystallinity to assess the stability of a material, but also the porosity features. Many materials which appeared to retain their crystallinity based on the XRPD analysis exhibit a significant decrease in internal surface area. Both analyses should be consistently applied to verify the stability of a material.

Table 5.5 Concluding overview on the stability (N<sub>2</sub> and XRD) of the examined MOFs in the various media.  the XRPD pattern and surface area are largely preserved,  the XRPD pattern and surface area are completely destroyed,  the XRPD pattern and surface area are partially decreased/degraded or transformed).

	3 days												2 months													
	pH=0		pH=4		pH=12		H <sub>2</sub> O <sub>2</sub>		H <sub>2</sub> O		air		pH=0		pH=4		pH=12		H <sub>2</sub> O <sub>2</sub>		H <sub>2</sub> O		air			
	XRD	N <sub>2</sub>	XRD	N <sub>2</sub>	XRD	N <sub>2</sub>	XRD	N <sub>2</sub>	XRD	N <sub>2</sub>	XRD	N <sub>2</sub>	XRD	N <sub>2</sub>	XRD	N <sub>2</sub>	XRD	N <sub>2</sub>	XRD	N <sub>2</sub>	XRD	N <sub>2</sub>	XRD	N <sub>2</sub>	XRD	N <sub>2</sub>
MIL-101 (Cr)																										
NH <sub>2</sub> -MIL-101 (Al)																										
MIL-53 (Al)																										
NH <sub>2</sub> -MIL-53		NP		NP		NP		NP		NP		NP		NP		NP		NP		NP		NP		NP		NP
UiO-66																										
NH <sub>2</sub> -UiO-66																										
UiO-67																										
CuBTC																										
ZIF-8																										

## REFERENCES

- [1] K. Leus, Y.Y. Liu, P. Van Der Voort, Metal-Organic Frameworks as Selective or Chiral Oxidation Catalysts, *Catal Rev*, 56 (2014) 1-56.
- [2] X.Z. Song, S.Y. Song, H.J. Zhang, Luminescent Lanthanide Metal-Organic Frameworks, *Struct Bond*, 163 (2015) 109-144.
- [3] B. Van de Voorde, B. Bueken, J. Denayer, D. De Vos, Adsorptive separation on metal-organic frameworks in the liquid phase, *Chem Soc Rev*, 43 (2014) 5766-5788.
- [4] J.Z. Gu, W.G. Lu, L. Jiang, H.C. Zhou, T.B. Lu, 3D porous metal-organic framework exhibiting selective adsorption of water over organic solvents, *Inorg Chem*, 46 (2007) 5835-5837.
- [5] P. Kussgens, M. Rose, I. Senkovska, H. Frode, A. Henschel, S. Siegle, S. Kaskel, Characterization of metal-organic frameworks by water adsorption, *Micropor Mesopor Mat*, 120 (2009) 325-330.
- [6] J.J. Low, A.I. Benin, P. Jakubczak, J.F. Abrahamian, S.A. Faheem, R.R. Willis, Virtual High Throughput Screening Confirmed Experimentally: Porous Coordination Polymer Hydration, *J Am Chem Soc*, 131 (2009) 15834-15842.
- [7] K. Tan, N. Nijem, P. Canepa, Q. Gong, J. Li, T. Thonhauser, Y.J. Chabal, Stability and Hydrolyzation of Metal Organic Frameworks with Paddle-Wheel SBUs upon Hydration, *Chem Mater*, 24 (2012) 3153-3167.
- [8] H.J. Choi, M. Dinca, A. Dailly, J.R. Long, Hydrogen storage in water-stable metal-organic frameworks incorporating 1,3-and 1,4-benzenedipyrazolate, *Energ Environ Sci*, 3 (2010) 117-123.
- [9] J. Ehrenmann, S.K. Henninger, C. Janiak, Water Adsorption Characteristics of MIL-101 for Heat-Transformation Applications of MOFs, *Eur J Inorg Chem*, (2011) 471-474.
- [10] G. Akiyama, R. Matsuda, S. Kitagawa, Highly Porous and Stable Coordination Polymers as Water Sorption Materials, *Chem Lett*, 39 (2010) 360-361.
- [11] D. Bazer-Bachi, L. Assie, V. Lecocq, B. Harbuzaru, V. Falk, Towards industrial use of metal-organic framework: Impact of shaping on the MOF properties, *Powder Technol*, 255 (2014) 52-59.
- [12] K.S. Park, Z. Ni, A.P. Cote, J.Y. Choi, R.D. Huang, F.J. Uribe-Romo, H.K. Chae, M. O'Keeffe, O.M. Yaghi, Exceptional chemical and thermal stability of zeolitic imidazolate frameworks, *P Natl Acad Sci USA*, 103 (2006) 10186-10191.
- [13] Y.K. Seo, J.W. Yoon, J.S. Lee, Y.K. Hwang, C.H. Jun, J.S. Chang, S. Wuttke, P. Bazin, A. Vimont, M. Daturi, S. Bourrelly, P.L. Llewellyn, P. Horcajada, C. Serre, G. Ferey, Energy-Efficient Dehumidification over Hierachically Porous Metal-Organic Frameworks as Advanced Water Adsorbents, *Adv Mater*, 24 (2012) 806-+.
- [14] J.E. Mondloch, M.J. Katz, N. Planas, D. Semrouni, L. Gagliardi, J.T. Hupp, O.K. Farha, Are Zr-6-based MOFs water stable? Linker hydrolysis vs. capillary-force-driven channel collapse, *Chem Commun*, 50 (2014) 8944-8946.
- [15] I.J. Kang, N.A. Khan, E. Haque, S.H. Jung, Chemical and Thermal Stability of Isotypic Metal-Organic Frameworks: Effect of Metal Ions, *Chem-Eur J*, 17 (2011) 6437-6442.
- [16] D.M. Jiang, A.D. Burrows, K.J. Edler, Size-controlled synthesis of MIL-101(Cr) nanoparticles with enhanced selectivity for CO<sub>2</sub> over N<sub>2</sub>, *Crystengcomm*, 13 (2011) 6916-6919.
- [17] M. Hartmann, M. Fischer, Amino-functionalized basic catalysts with MIL-101 structure, *Micropor Mesopor Mat*, 164 (2012) 38-43.

- [18] D.J. Tranchemontagne, J.R. Hunt, O.M. Yaghi, Room temperature synthesis of metal-organic frameworks: MOF-5, MOF-74, MOF-177, MOF-199, and IRMOF-0, *Tetrahedron*, 64 (2008) 8553-8557.
- [19] S. Biswas, P. Van der Voort, A General Strategy for the Synthesis of Functionalised UiO-66 Frameworks: Characterisation, Stability and CO<sub>2</sub> Adsorption Properties, *Eur J Inorg Chem*, (2013) 2154-2160.
- [20] M.J. Katz, Z.J. Brown, Y.J. Colon, P.W. Siu, K.A. Scheidt, R.Q. Snurr, J.T. Hupp, O.K. Farha, A facile synthesis of UiO-66, UiO-67 and their derivatives, *Chem Commun*, 49 (2013) 9449-9451.
- [21] T. Loiseau, C. Serre, C. Huguenard, G. Fink, F. Taulelle, M. Henry, T. Bataille, G. Ferey, A rationale for the large breathing of the porous aluminum terephthalate (MIL-53) upon hydration, *Chem-Eur J*, 10 (2004) 1373-1382.
- [22] T. Ahnfeldt, D. Gunzelmann, T. Loiseau, D. Hirsemann, J. Senker, G. Ferey, N. Stock, Synthesis and Modification of a Functionalized 3D Open-Framework Structure with MIL-53 Topology, *Inorg Chem*, 48 (2009) 3057-3064.
- [23] A.F. Gross, E. Sherman, J.J. Vajo, Aqueous room temperature synthesis of cobalt and zinc sodalite zeolitic imidizolate frameworks, *Dalton T*, 41 (2012) 5458-5460.
- [24] G. Ferey, C. Mellot-Draznieks, C. Serre, F. Millange, J. Dutour, S. Surble, I. Margiolaki, A chromium terephthalate-based solid with unusually large pore volumes and surface area, *Science*, 309 (2005) 2040-2042.
- [25] J.W. Ren, N.M. Musyoka, H.W. Langmi, T. Segakweng, B.C. North, M. Mathe, X.D. Kang, Modulated synthesis of chromium-based metal-organic framework (MIL-101) with enhanced hydrogen uptake, *Int J Hydrogen Energ*, 39 (2014) 12018-12023.
- [26] D.Y. Hong, Y.K. Hwang, C. Serre, G. Ferey, J.S. Chang, Porous Chromium Terephthalate MIL-101 with Coordinatively Unsaturated Sites: Surface Functionalization, Encapsulation, Sorption and Catalysis, *Adv Funct Mater*, 19 (2009) 1537-1552.
- [27] T. Wittmann, R. Siegel, N. Reimer, W. Milius, N. Stock, J. Senker, Enhancing the water stability of Al-MIL-101-NH<sub>2</sub> via postsynthetic modification, *Chemistry a European Journal*, 21 (2015) 314-323.
- [28] I. Bezverkhyy, G. Ortiz, G. Chaplais, C. Marichal, G. Weber, J.P. Bellat, MIL-53(Al) under reflux in water: Formation of gamma-AlO(OH) shell and H<sub>2</sub>BDC molecules intercalated into the pores, *Micropor Mesopor Mat*, 183 (2014) 156-161.
- [29] D.D. Zu, L. Lu, X.Q. Liu, D.Y. Zhang, L.B. Sun, Improving Hydrothermal Stability and Catalytic Activity of Metal-Organic Frameworks by Graphite Oxide Incorporation, *J Phys Chem C*, 118 (2014) 19910-19917.
- [30] D. Mustafa, E. Breynaert, S.R. Bajpe, J.A. Martens, C.E.A. Kirschhock, Stability improvement of Cu-3(BTC)(2) metal-organic frameworks under steaming conditions by encapsulation of a Keggin polyoxometalate, *Chem Commun*, 47 (2011) 8037-8039.
- [31] J.B. DeCoste, G.W. Peterson, H. Jasuja, T.G. Glover, Y.G. Huang, K.S. Walton, Stability and degradation mechanisms of metal-organic frameworks containing the Zr<sub>6</sub>O<sub>4</sub>(OH)<sub>4</sub> secondary building unit, *J Mater Chem A*, 1 (2013) 5642-5650.
- [32] Y.L. Hu, C.Y. Song, J. Liao, Z.L. Huang, G.K. Li, Water stable metal-organic framework packed microcolumn for online sorptive extraction and direct analysis of naproxen and its metabolite from urine sample, *J Chromatogr A*, 1294 (2013) 17-24.
- [33] X.K. Qian, B.L. Yadian, R.B. Wu, Y. Long, K. Zhou, B. Zhu, Y.Z. Huang, Structure stability of metal-organic framework MIL-53 (Al) in aqueous solutions, *Int J Hydrogen Energ*, 38 (2013) 16710-16715.
- [34] C. Prestipino, L. Regli, J.G. Vitillo, F. Bonino, A. Damin, C. Lamberti, A. Zecchina, P.L. Solari, K.O. Kongshaug, S. Bordiga, Local structure of framework Cu(II) in HKUST-1

metallorganic framework: Spectroscopic characterization upon activation and interaction with adsorbates, *Chem Mater*, 18 (2006) 1337-1346.

[35] J.B. DeCoste, G.W. Peterson, B.J. Schindler, K.L. Killops, M.A. Browe, J.J. Mahle, The effect of water adsorption on the structure of the carboxylate containing metal-organic frameworks Cu-BTC, Mg-MOF-74, and UiO-66, *J Mater Chem A*, 1 (2013) 11922-11932.

[36] M. Kandiah, M.H. Nilsen, S. Usseglio, S. Jakobsen, U. Olsbye, M. Tilset, C. Larabi, E.A. Quadrelli, F. Bonino, K.P. Lillerud, Synthesis and Stability of Tagged UiO-66 Zr-MOFs, *Chem Mater*, 22 (2010) 6632-6640.

[37] Q.Y. Yang, V. Guillermin, F. Ragon, A.D. Wiersum, P.L. Llewellyn, C.L. Zhong, T. Devic, C. Serre, G. Maurin, CH<sub>4</sub> storage and CO<sub>2</sub> capture in highly porous zirconium oxide based metal-organic frameworks, *Chem Commun*, 48 (2012) 9831-9833.

[38] C. Mottillo, T. Friscic, Carbon Dioxide Sensitivity of Zeolitic Imidazolate Frameworks, *Angew Chem Int Edit*, 53 (2014) 7471-7474.

[39] Z.Q. Bai, L.Y. Yuan, L. Zhu, Z.R. Liu, S.Q. Chu, L.R. Zheng, J. Zhang, Z.F. Chai, W.Q. Shi, Introduction of amino groups into acid-resistant MOFs for enhanced U(VI) sorption, *J Mater Chem A*, 3 (2015) 525-534.

[40] X.D. Zhao, D.H. Liu, H.L. Huang, W.J. Zhang, Q.Y. Yang, C.L. Zhong, The stability and defluoridation performance of MOFs in fluoride solutions, *Micropor Mesopor Mat*, 185 (2014) 72-78.



# 6 MOFs IN AQUEOUS ADSORPTION

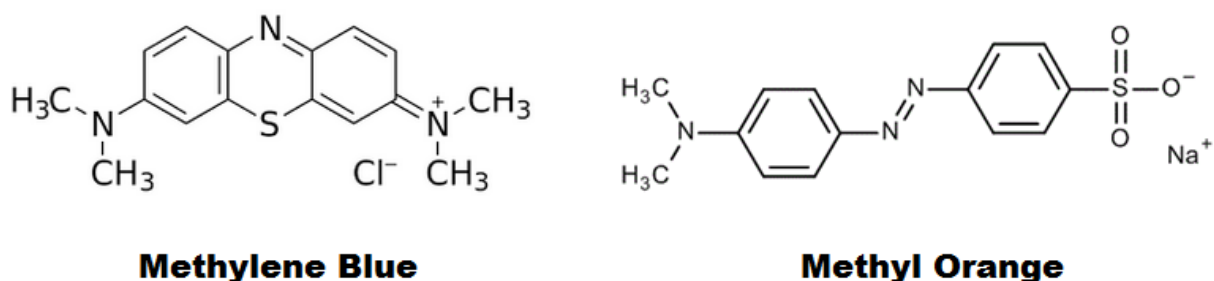
## 6.1 The search for promising MOF candidates

In this chapter, the current state of the art on MOF-based aqueous adsorbents is explored. The conclusions from previous chapters, regarding the general requirements for a good supporting material, are taken into account in order to help fully assess the potential of reported materials as good adsorbents. As the core of this work revolves around the adsorption of critical metals such as rare earths and uranium, special attention will be paid to the conditions wherein these elements are recovered from their aqueous sources. This means that research, dealing with adsorption in (often acidic) aqueous environments, full of competing metals, is of key interest. It is, however, equally important to discuss the organics removal with MOFs, as it can teach us valuable lessons on support choice and tailoring. Consequently, this chapter offers an overview on different important types of MOF-adsorbate interactions that have been used to develop selective adsorbents. This includes both inherent effects and interactions as a result of embedded functionalities. When necessary, strengths and flaws of the adsorbents are pointed out and a conclusion on their potential for long-term applications is drawn, supported with claims and/or evidence discussed in previous chapters.

## 6.2 Removal of Organic Components

Within the large scope of MOF-based applications, the field of aqueous adsorption is a rather recent one. This domain can roughly be split into two sections, i.e., adsorption of organic components, and adsorption of metal ions. The former has been given the most attention, as MOFs possess a lot of inherent characteristics that are particularly interesting for the removal of organics. These include specific pore structures, charge interactions between the adsorbent and

adsorbate, open metal sites<sup>1</sup>, or breathing<sup>2</sup> properties[1]. Common adsorbates of interest are harmful dyes, pharmaceuticals, herbicides, phenolics or other hydrocarbons[1-7]. A typical example is the removal of dyes such as methyl orange (MO), and methylene blue (MB) (Figure 6.1). Both are charged aromatic-based systems, therefore interaction with hybrid coordination polymers such as MOFs can be expected.



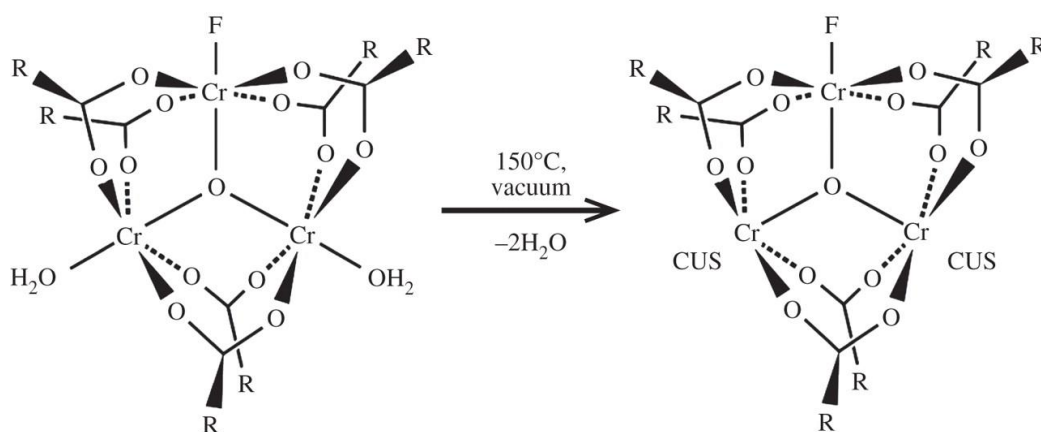
**Figure 6.1 Chemical structure of methylene blue and methyl orange.**

### 6.2.1 CUS-grafting

One of the first uses of MOFs as organic dye adsorbents was a study of Haque *et al.*, who investigated the use of two Cr-BDC type MOFs (MIL-53 and MIL-101) as potential MO adsorbents[3]. In addition, the performance of MIL-101 was tested pristinely, as well as functionalized with ethylenediamines. The functionalization was performed via grafting on the coordinatively unsaturated sites (CUS) of MIL-101's chromium clusters. Basically, the trimeric chromium(III) octahedral clusters of MIL-101 possess terminal water molecules, which are removable from the framework by vacuum treatment at 150 °C for 12 h, thus providing the CUS as Lewis acid sites in the structure, useful for surface functionalization[8] (Figure 6.2). Haque *et al.* used these CUS to graft ethylenediamine (ED) onto the structure (according to Hong *et al.*[8]), obtaining ED-MIL-101. Additionally, a protonated ethylenediamine on MIL-101 (PED-MIL-101) was obtained by acidification of EDMIL-101 with 0.1 M HCl solution (Figure 6.3).

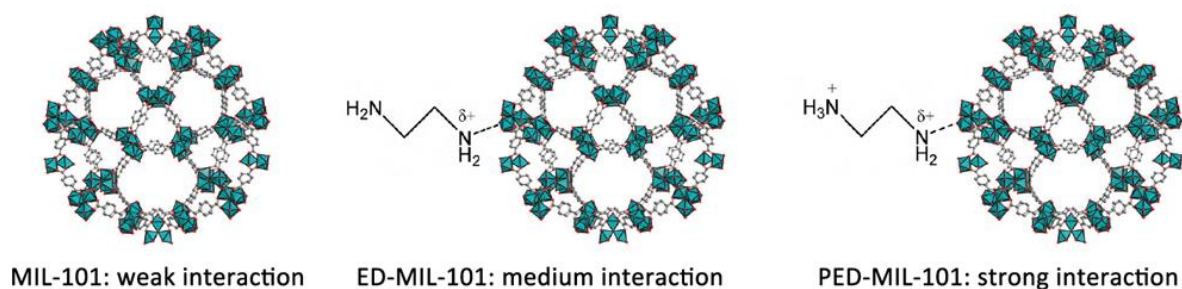
<sup>1</sup>During the MOF synthesis, the metal can coordinate to the organic linkers, but also to solvent molecules. Removal of such solvent molecules creates open/unsaturated metal sites inside the framework.

<sup>2</sup>Breathing of a MOF is the change in structure as a result of the adsorption/desorption of guest molecules, or the influence of temperature and/or pressure. Such flexible MOFs are able to expand or collapse their structure, resulting in different porosities, e.g., narrow-pore (NP), large-pore (LP)...



**Figure 6.2** Formation of coordinatively unsaturated chromium sites in the  $\text{Cr}_3\text{O}$ -carboxylate cluster of the MIL-101 structure. (Retrieved from [9])

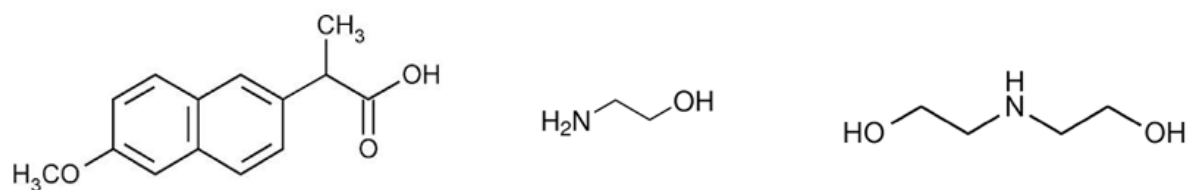
All tested materials (MIL-53, MIL-101, ED-MIL-101, and PED-MIL-101) were able to adsorb MO from aqueous solutions ( $\text{pH} = 5.4$ ) and their performances regarding MO uptake and adsorption kinetics were ranked as  $\text{MIL-53} < \text{MIL-101} < \text{ED-MIL-101} < \text{PED-MIL-101}$ . The difference between pristine MIL-53 and MIL-101 was attributed to the larger pore size of MIL-101, facilitating the adsorption of bulky MO. Charge effects play a key role in these kinds of adsorptions, which was demonstrated by the experiments (Figure 6.3). The pristine MOF metal clusters are weakly, positively charged, explaining their affinity for the negatively charged MO. By grafting ED on the CUS, a partially positive center is postulated to be created around the coordinating amine moiety, which has an increased affinity for MO. By protonating the ED, an additional charge is created on the dangling amine moiety, further increasing the interaction with MO. The best performing adsorbent of the series, PED-MIL-101, achieved a maximum uptake of about 200 mg MO/g ( $25^\circ\text{C}$ ), in approximately 2 hours, a very competitive result according to the authors. The uptake was approximately doubled compared to pristine MIL-101, and quadrupled compared to MIL-53. It is also important to consider the pH effect, which can influence the charge on the adsorbent. This was also observed by the authors, as increasing pHs resulted in a decreased charge (even deprotonation) of the PED-MIL-101, thereby limiting its performance.



**Figure 6.3** Illustration of the grafted diamine groups onto MIL-101 CUS. ED: ethylenediamines, PED: protonated ED. (Adapted from [3])

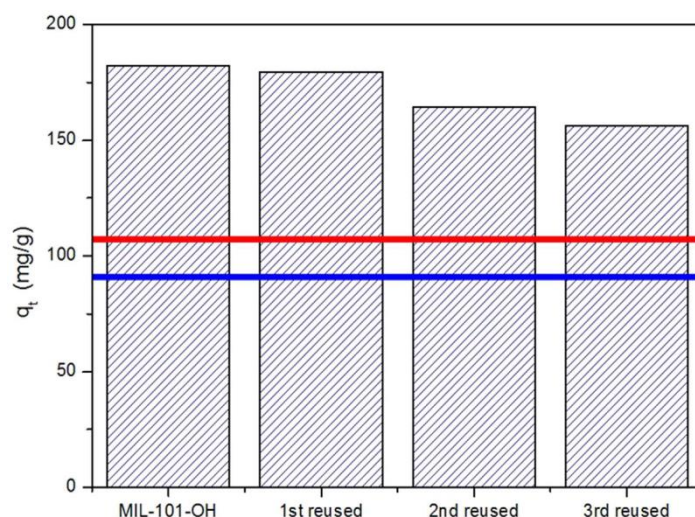
The grafting of functionalities, such as amines, on MOFs via the CUS is a widely applied technique, albeit mostly in non-aqueous applications (e.g., catalysis in organic media[10, 11], gas sorption[12]...). Nonetheless, several reports using this technique to obtain adsorbents for aqueous environment exist [3, 7, 13]. In the work of Haque *et al.*, the ED grafted MIL-101s are claimed to be stable reusable materials, as their MO uptake didn't change considerably over three adsorption runs (yet, a difference in kinetics was observed). Questions can be asked, however, on the effect of bringing CUS-functionalized MOFs into contact with liquid water. Especially for the MOFs containing hard Lewis acid metal clusters, such as Cr-MIL-101. These hard acids prefer coordination with hard bases, such as H<sub>2</sub>O. If the CUS grafting ligand has a (softer) nitrogen-based donating group, replacement by water molecules (aqueous environment) is plausible, especially on the long-term. This could severely flaw the performance of an adsorbent.

In the work of Seo *et al.*[7], MIL-101(Cr) is functionalized via its CUS (among various other functionalization methods) and used for the adsorption of pharmaceuticals, such as naproxen (Figure 6.4). Ethanolamine and diethanolamine were grafted onto dehydrated MIL-101 via their amine moiety, resulting in one or two dangling hydroxyl groups, respectively (Figure 6.4). These were used to adsorb naproxen via a postulated H-bonding mechanism.



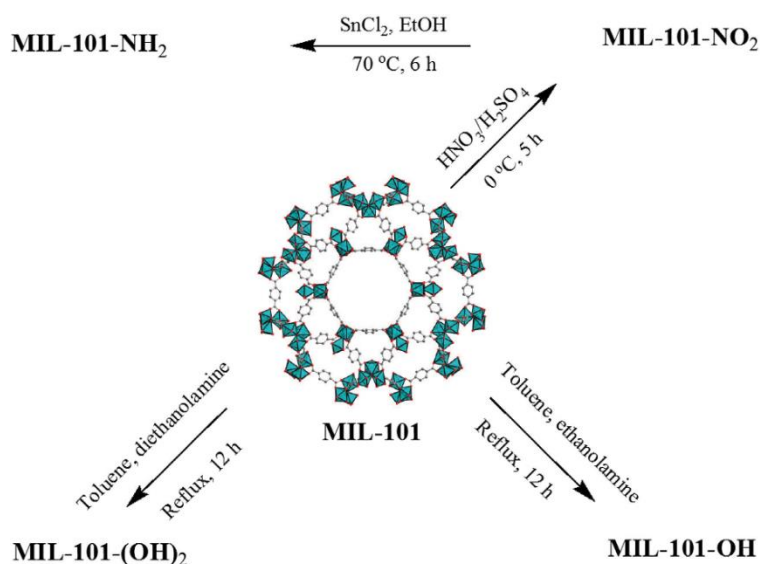
**Figure 6.4 Chemical structures of naproxen (left), ethanolamine (middle), and diethanolamine (right).**

While both materials (denoted MIL-101-OH and MIL-101-(OH)<sub>2</sub>) showed excellent performance in the adsorptive removal of naproxen from aqueous solutions (high uptakes; >130 mg/g, relatively rapid adsorption kinetics; ~4 h), there was a small but notable decrease in the performance over different adsorption cycles (Figure 6.5). As the authors tested and confirmed the high stability of the MIL-101 support, this decrease is probably due to gradual ligand leaching, as a result of competition with water molecules. Nonetheless, even after 4 cycles of 12 hours, the functionalized MOF adsorbent (MIL-101-OH) still outperforms its parent material and activated carbon by a lot. It will therefore depend on the type of application whether or not CUS-grafted adsorbents are suitable, but on the long-run a more thorough bond between support and ligand might be desired.



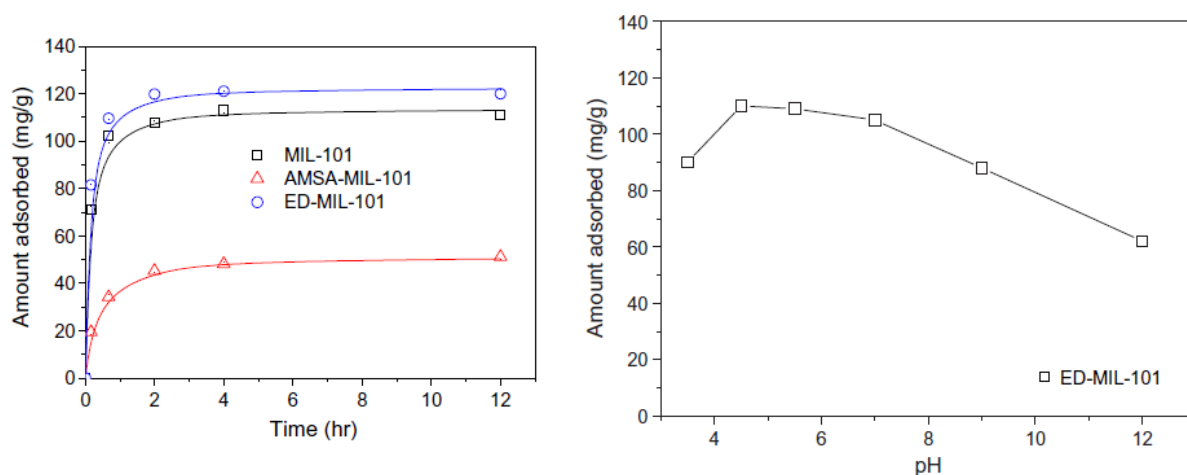
**Figure 6.5 Reusability of MIL-101-OH in the adsorption of naproxen over subsequent cycles. The red and blue horizontal lines show the adsorbed amount of naproxen over pristine MIL-101 and activated carbon, respectively. Adsorption time per cycle: 12 h, initial concentration of naproxen: 50 mg/L). (Retrieved from [7])**

Also in the work of Seo *et al.*[7], MIL-101(Cr) was functionalized via its aromatic rings. The MOF was nitrated by submerging it in an aqueous solution of nitric acid and sulfuric acid at 0 °C for several hours (according to [14]). The purified ‘MIL-101-NO<sub>2</sub>’ was then reduced to obtain primary amines on its aromatic rings, using SnCl<sub>2</sub>·2H<sub>2</sub>O in ethanol at 70 °C (also according to [14]). A schematic overview of the performed functionalizations (including CUS-grafting) is given in Figure 6.6. Both materials (MIL-101-NO<sub>2</sub> and –NH<sub>2</sub>) were tested in the naproxen adsorption, where it was observed that the amine-MIL-101 shows an increased uptake of naproxen compared to the pristine MIL-101, i.e., over 50 % increase on a surface area basis. The nitro version, however, barely did better than the pristine MOF, which the authors found somewhat surprising, as NO<sub>2</sub> is a polar group. Perhaps this is due to the fact that nitro groups are very strongly electron withdrawing, resulting in a strong negative charge around its oxygens. The naproxen (pK<sub>a</sub>: ~4.2 [7]) at pH 5.4 is nearly fully deprotonated and might therefore be repulsed by the nitro groups. The amine moieties of MIL-101-NH<sub>2</sub> do not experience this effect, as they are electron donating groups (as in towards the aromatic ring). The authors ascribe the affinity between naproxen and the amines to an acid-base interaction.



**Figure 6.6** Schematic overview of the different functionalization methods of MIL-101 by Seo *et al.* (Adapted from [7])

An earlier report by Hasan *et al.*[4], investigated the effect of grafting basic ( $-\text{NH}_2$ ) and acidic groups ( $-\text{SO}_3\text{H}$ ), respectively, onto MIL-101(Cr) via its CUS. It was found that the introduction of basic amine groups resulted in an increase of naproxen uptake (and the similar clofibric acid), compared to pristine MIL-101, while the sulfonated MOF performed a lot worse than its pristine counterpart (Figure 6.7, left). The authors claim that the introduction of basic functions, such as amines, on MIL-101, creates favorable acid-base interactions with the carboxyl groups of the naproxen/clofibric acid, while grafted acidic groups, such as the strongly acidic sulfonic acid, would counteract this interaction. The pH-effect is very important here. The maximum naproxen uptake with aminated MIL-101 was achieved at pH  $\sim 5$  (Figure 6.7, right). At higher pH levels, naproxen deprotonation ( $\text{pK}_a \sim 4.2$ ) begins to dominate, where the negative charge of the formed carboxylate on naproxen counteracts the interaction with the dangling amine moiety, which was indeed observed in the pH-dependency experiments. At lower pH levels, i.e., 4 or lower, the  $-\text{NH}_2$  group may be protonated, which results in a poor interaction with naproxen. In this study as well, it must be noted that a gradual decrease in adsorption performance was observed over different cycles. The ligands were both grafted via an amine moiety, i.e., ethylene diamine for the amine-MIL-101, and aminomethanesulfonic acid (AMSA) for the sulfonic-MIL-101. Gradual displacement of ligands by the competing water molecules is possibly the reason behind the decreasing performance.

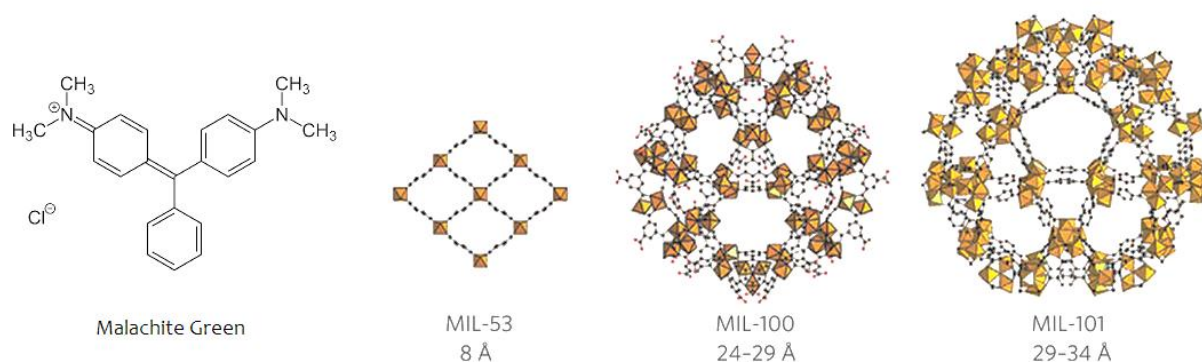


**Figure 6.7 (Left) Evolution of naproxen uptake over time on MIL-101(Cr) and its functionalizations (ED: ethylene diamine, AMSA: aminomethylsulfonic acid. (Right) pH-dependency plot of naproxen uptake by ED-MIL-101. (Retrieved from [4])**

### 6.2.2 Support charge effects

Another important effect of pH is its influence on the support, rather than just on the adsorbate. In a study of Huo *et al.*[5], three MOFs were tested in the aqueous adsorption of malachite green (MG), i.e., MIL-100(Fe), MIL-53, and MIL-101(Cr) (Figure 6.8). MIL-100 uses BTC linkers as struts, as opposed to the BDCs in MIL-53 and MIL-101. Amongst the three MOFs, MIL-53 performed the worst, which was attributed to its lower surface area ( $\sim 1000 \text{ m}^2/\text{g}$  BET) and lack of coordinating water molecules (at the MOF's metal clusters). Both MIL-100 and MIL-101 have coordinating  $\text{H}_2\text{O}$  molecules on their clusters, which can be replaced, thereby constituting as open metal sites. These active Lewis acid sites can coordinate with the Lewis base  $-\text{N}(\text{CH}_3)_2$  moieties from the malachite green. The authors also suggest an additional  $\pi$ - $\pi$  interaction between the benzene rings of the adsorbate and MIL-100's linkers. However, a striking difference was observed between MIL-100(Fe) and MIL-101(Cr). The latter, although having almost twice the BET surface area ( $\sim 1600 \text{ m}^2/\text{g}$  vs.  $\sim 2900 \text{ m}^2/\text{g}$ ), performed a lot worse. This was related to a pH effect on both MOF structures. In aqueous solutions of pH 10 or lower, the malachite green is a protonated cationic species. The authors observed that by increasing the pH, i.e., from 1 to 5, MIL-100 has an increasingly negative surface charge (as measured by zeta-potential analysis). Cationic MG can therefore be strongly adsorbed on the surface of MIL-100(Fe) via electrostatic interactions with the negatively charged MIL-100[5]. MIL-101(Cr), on the other hand, has a positive surface charge below pH 10 which causes repulsion of the cationic MG, resulting in a lower uptake.



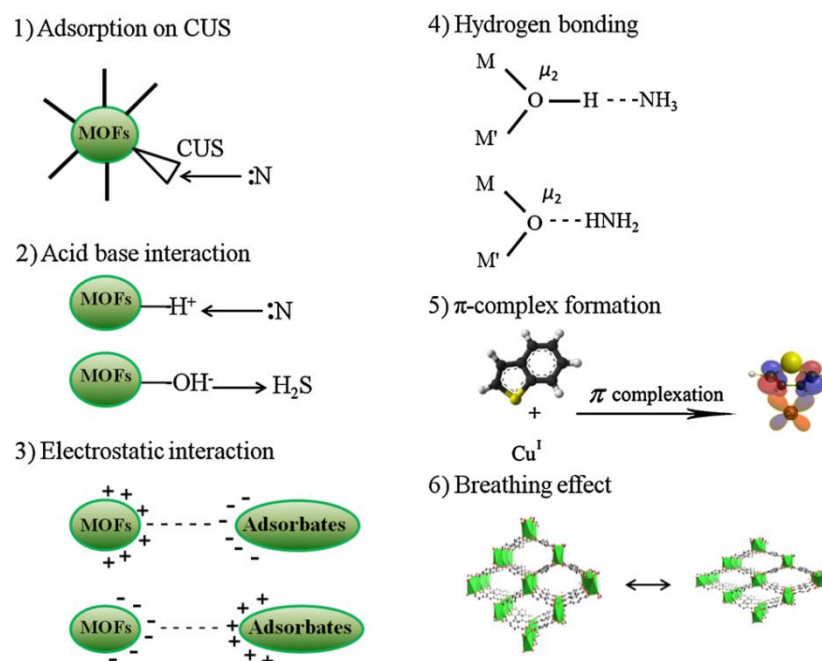


**Figure 6.8 Chemical Structure of Malachite Green. Structural representations of MIL-53, MIL-100, and MIL-101.**

This charge effect is very important, especially when the adsorbate of interest is charged as well. Similar to several organic compounds (MO, MB, MG...), ionic metal species carry a charge as well in aqueous solutions. Free metal cations, having a positive charge, could likely be hindered or repelled by a positively charged adsorbent. Anionic species, on the other hand, could experience a favorable interaction with the positively charged support. The pH of an aqueous environment is therefore an important parameter to consider in one's choice for a (MOF-based) adsorbent.

In the work of Khan *et al.*[1], a comprehensive overview is given on organics/inorganics removal from aqueous environments (and fuels), using MOF-based adsorbents. In addition, the most common interaction mechanisms between adsorbates and MOF adsorbents are discussed, as illustrated in Figure 6.9. The work of Wang *et al.*[15] also extensively reviews the applications of MOFs in water-based environments, including adsorption of organic compounds.





**Figure 6.9** Important mechanisms for the adsorption over MOFs. (Retrieved from [1])

### 6.3 Metal adsorption with MOFs

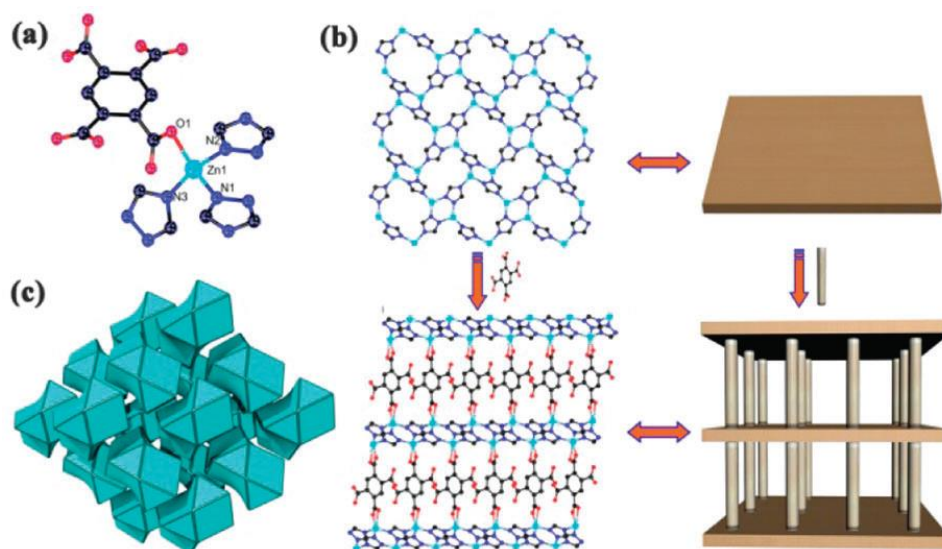
The recovery or removal of metallic species from an aqueous environment, using a metal-containing coordination polymer, might sound a bit contradictory. Especially since MOFs have the preconception of being unstable materials, some skepticism on this approach is not unexpected. It is, after all, the goal to remove certain species from their solution, rather than introducing new ones to it. It is therefore not surprising that the exploration of MOFs as metal adsorbents is a very recent field in the domain of MOF-based adsorption. Nonetheless, considerable advances have been made, of which an overview is given hereafter, structured by their different types of interaction.

#### 6.3.1 Inherent functionalities

Meng *et al.*[16] reported the solvothermal synthesis of a zinc-based 3D pillar-layer framework, denoted  $[\text{Zn}(\text{trz})(\text{H}_2\text{betc})_{0.5}]\cdot\text{DMF}$ , with uncoordinated carboxyl groups. The MOF was made up of 1,2,4-triazole (trz) and pyromellitic acid ( $\text{H}_4\text{betc}$ ) as ligands, and was used to selectively adsorb  $\text{Cu}^{2+}$  from  $\text{Co}^{2+}$  ions. The pillars of this framework are the pyromellitic acid units, of which half of the carboxyl groups are uncoordinated and serve as the metal adsorption sites (Figure 6.10). The zinc centers are coordinated to both the trz units (Zn-N bond) and the  $\text{H}_4\text{betc}$  units (Zn-O bond). The material is claimed to be exceptionally stable. Stability tests were performed in boiling methanol, ethanol, dimethylacetamide, dichloromethane, tetrahydrofuran, acetonitrile, hexane, and dimethyl sulfoxide for 12 h, where XRD analyses confirmed the structural stability of the framework. Open air exposure (2 weeks) showed similar results. Water stability was, however, only tested for 4 hours, after which no significant changes in XRD

pattern were observed. An extended exposure might be needed to fully assess this material's stability to water, especially since the Zn-O coordination bonds might face competition with water molecules. The material has been applied in a chromatographic column for separation of  $\text{Cu}^{2+}$  from  $\text{Co}^{2+}$  ions, using different solvents (DMF, MeOH,  $\text{H}_2\text{O}$ ). High selectivity (especially in water) was found for Cu over Co, which was attributed to a stronger chelating bond of copper with the carboxyl oxygens. Selectivity experiments in water with Cu, Co, and Ni resulted in a relative uptake of 0.163 % (Cu), 0.004 % (Co), and 0.016 % (Ni), based on zinc-content (weight-percentage). No recycling experiments were performed.

In any case, this is an interesting example of the development of a in-situ functionalized MOF, where the active sites are inherent to the structure, and no post-synthetic modification (PSM) is required. Yet, the carboxyl group is a rather general acidic adsorption site, and competition from other elements might be expected. It could serve, however, as a suitable anchoring point for other interesting ligands, when the adsorption of certain critical metals is desired.

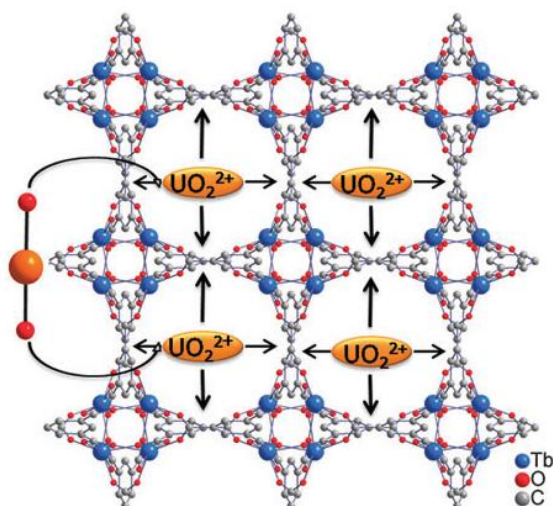


**Figure 6.10 (a) The coordination environment of the Zn(II) center; (b) the 2D layers pillared by the  $\text{H}_2\text{btc}$  ligand generate a 3D pillar-layer framework; (c) the (3,4)-connected augmented net as a natural tiling. (Retrieved from [16])**

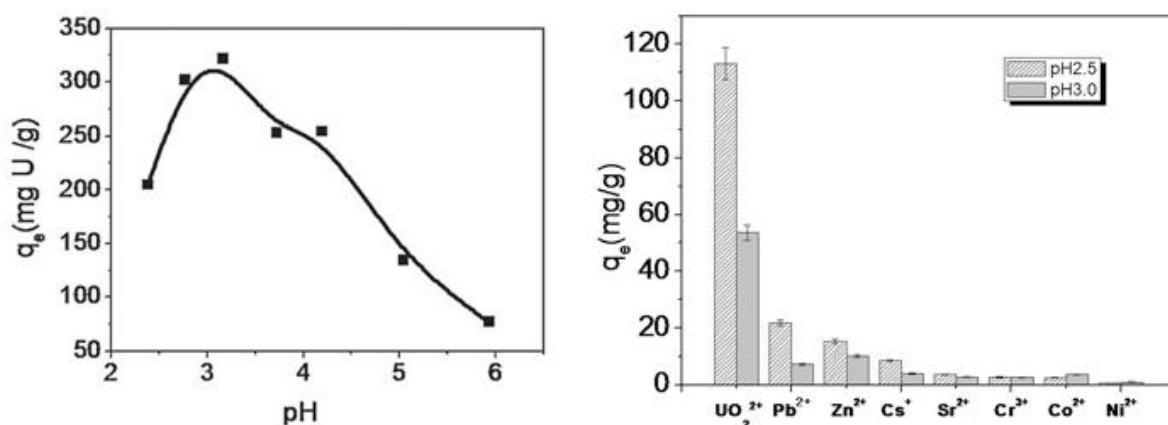
### 6.3.2 Aperture effects

Yang *et al.*[17] reported the use of MOF-76 to selectively adsorb uranium from aqueous solutions. MOF-76 is constructed by a rare earth central ion (Eu, Tb, Y...) and 1,3,5-benzenetricarboxylate (BTC) as linker. It has one-dimensional microporous channels, with an optimal aperture for the uranyl ion ( $\text{UO}_2^{2+}$ ) (Figure 6.11). It was found that MOF-76 was a very potent, yet highly pH-dependent U(VI) adsorbent. At pH 3 an optimal adsorption of ~300 mg U(VI)/g was achieved, which decreased as the pH increased. This was attributed to the fact that U(VI) speciation is also very pH dependent, and that at higher pH, larger hydroxylated uranium

species are formed (see Section 6.3.6). These larger species do not fit in the apertures of MOF-76. In addition, the authors suggest that a surface charge effect at higher pH might also play a role in the decreased uptake (Figure 6.12). Furthermore, the acidity of the environment had to be kept above pH 2, or partial framework collapse would occur. Selectivity experiments with competing elements  $\text{Pb}^{2+}$ ,  $\text{Zn}^{2+}$ ,  $\text{Cs}^+$ ,  $\text{Sr}^{2+}$ ,  $\text{Cr}^{3+}$ ,  $\text{Co}^{2+}$ , and  $\text{Ni}^{2+}$  (Figure 6.12) showed the high affinity for uranyl (especially at pH 2.5). The adsorbent could be regenerated with 0.1 M  $\text{Na}_2\text{CO}_3$  (desorption > 90%), which makes it a promising candidate for U(VI) preconcentration. A reusability study could give further insight in its potential.



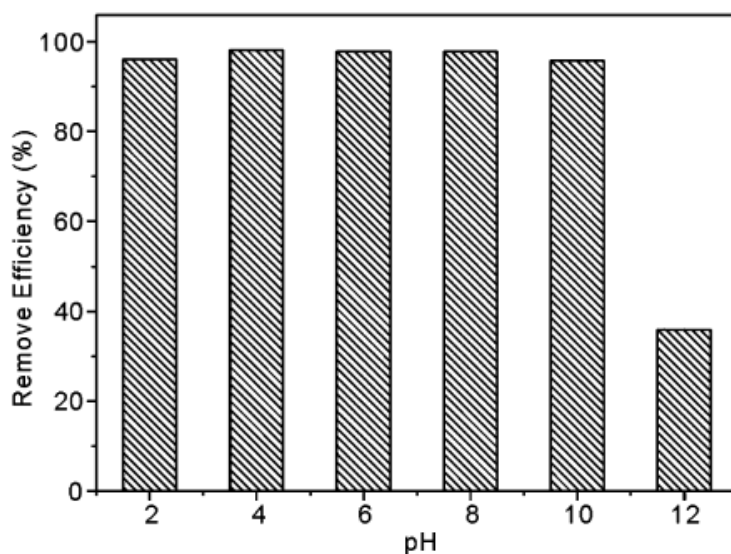
**Figure 6.11** Schematic of capture of  $\text{UO}_2^{2+}$  ions into the one-dimensional channels of MOF-76. (Retrieved from [17])



**Figure 6.12** (Left) Effect of solution pH on the U(VI) adsorption on the MOF-76 adsorbent.  $c_0(\text{U}) = 140 \text{ mg/L}$ ,  $m/V = 0.4 \text{ g/L}$ , and  $t = 5 \text{ h}$ . (Right) Competitive adsorption of coexisting ions by MOF-76. (Retrieved from [17])

### 6.3.3 Open metal sites

In a study of Zhu *et al.*[18], MIL-100(Fe) was used to adsorb As(V) from aqueous solutions. This approach was inspired by the high affinity between arsenic species and iron oxide (often applied as nanoparticles, due to their large surface-to-volume ratio, also embedded in MOFs for example[33]). A water-stable iron-based MOF with open-metal sites was therefore explored to investigate its possible affinity for arsenic(V). It was found that the MIL-100(Fe) showed an increased As(V) (from  $\text{Na}_3\text{AsO}_4$ ) adsorption capacity compared to  $\text{Fe}_2\text{O}_3$ -nanoparticles with a size of 50 nm, and commercial  $\text{Fe}_2\text{O}_3$  powders (size  $\sim 2\ \mu\text{m}$ ). The maximum adsorption capacities for each of the studied materials were 12.3, 6.4, and 1.1 mg/g, respectively (as calculated by the Langmuir model). When normalized to iron content, the capacities are 57.7, 9.1, and 1.6 mg/g Fe, respectively, which indicates that the effective adsorption sites in MIL-100(Fe) are nearly 6.5 times those of the iron oxide nanoparticles, and 37 times those of commercial iron oxide powders. In addition, fast kinetics were observed for the MOF adsorption (equilibrium  $< 10$  min), and the adsorbent appears to be suitable over a broad pH range (2 – 10). Above pH 10, however, a decreased uptake As(V) was observed (Figure 6.13), where the authors noted a gradual structure dissolution in (stronger) alkaline conditions (pH  $> 10$ ).



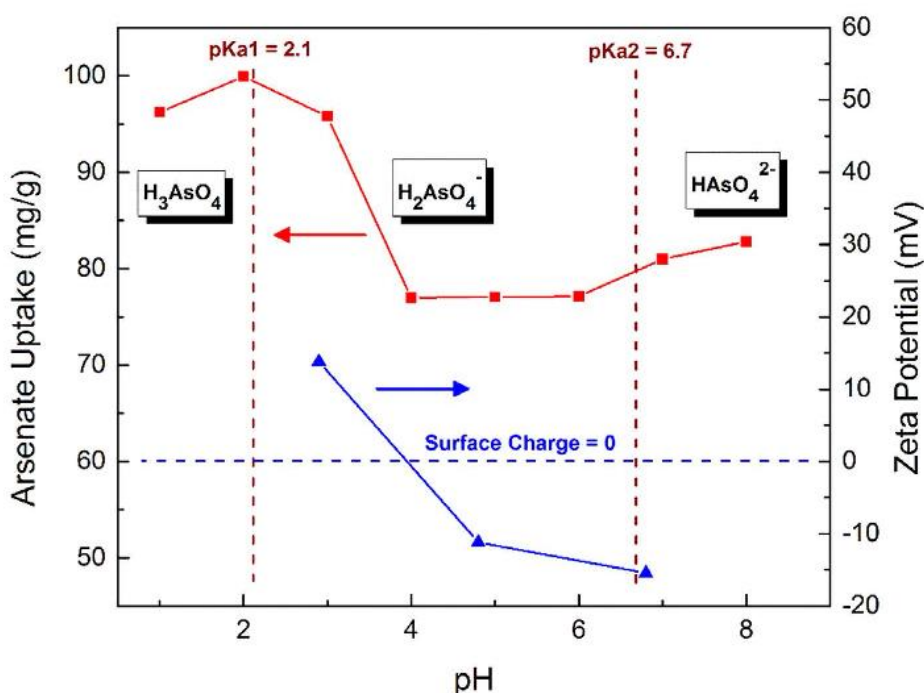
**Figure 6.13** Effect of pH on As(V) adsorption on MIL-100(Fe) ( $c_0(\text{As(V)})$ : 5 mg/L,  $m/V = 5.0$  g/L,  $T = 25\ ^\circ\text{C}$ ).

It must be noted that arsenic speciation is greatly depending on pH.  $\text{H}_2\text{AsO}_4^-$  dominates at acidic pH, which is less than pH  $\sim 6.9$ . At higher pH,  $\text{HAsO}_4^{2-}$  is dominant.  $\text{H}_3\text{AsO}_4$  and  $\text{AsO}_4^{3-}$  may be present in strong acid (less than pH 2.3) or base (higher than pH 11) conditions, respectively[19]. In the tested pH range of 2 – 10, it always carries a negative charge. In Section 6.2.2, it was mentioned that MIL-100(Fe) has got a negative surface charge in pH range 2 – 10 as well. This could possibly have a hindering effect on the adsorption of anionic arsenate

species, but could just as well be compensated by the strong interaction with the open iron sites of MIL-100. It would be interesting to compare this to a similar positively charged MOF. In addition, this research would benefit from a selectivity study to investigate the effect of competing anionic metal species on the adsorption process, e.g., chromates, selenates...

### 6.3.4 Combined interactions

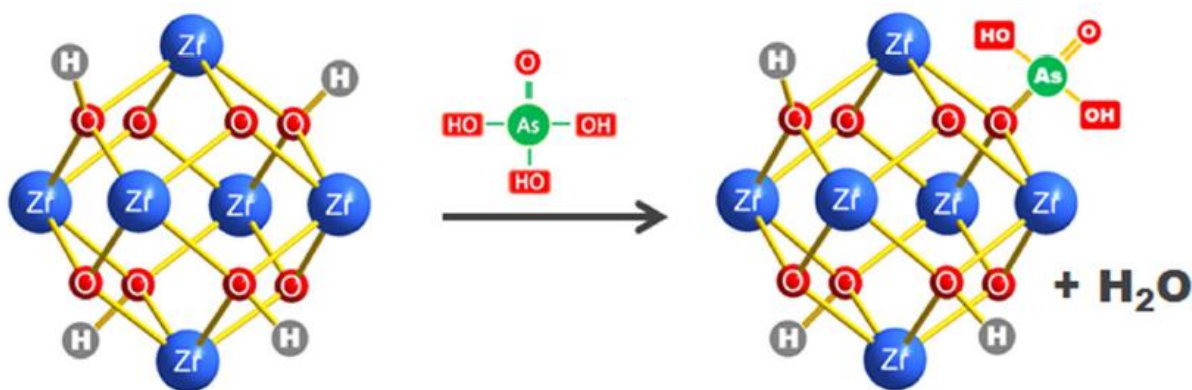
Another prominent example of arsenic removal with MOFs, is a study by Wang *et al.*[20], using the zirconium based UiO-66. This material achieves a staggering ~300 mg As(V)/g adsorption capacity at pH 2. The adsorbent was shown to be performant across a very broad pH range of 1 to 10. Similar to MIL-100(Fe) in the study of Zhu *et al.*[18] (*vide supra*), the UiO-66 also starts to decompose in pH levels above 10. In this work, the charge of the adsorbent and the arsenic species, as a function of pH, were taken into account, which showed that UiO-66 is positively charged below pH ~4, and negatively above it (Figure 6.14). The charge effect on the arsenic species was clearly visible. The authors suggested that electrostatic interaction plays a certain role in the adsorption process, e.g., at pH 3, anionic arsenate species could be effectively attracted to the positively charged adsorbents, which results in a better adsorption performance compared to when the pH is higher than 4.



**Figure 6.14** pH effect on arsenate speciation, adsorbent surface charge, and As(V) adsorption with UiO-66.  $C_0(\text{As(V)}) = 50 \text{ mg/L}$ ,  $m/V = 0.5 \text{ g/L}$ . (Retrieved from [20])

They also note, however, that electronic interaction is not the only parameter governing the adsorption, as below pH 2, the dominant arsenic species is neutral ( $\text{H}_3\text{AsO}_4$ ), yet a high uptake is achieved. It was found and confirmed that the hydroxyl groups on the Zr clusters (at the Zr-

O( $\mu_3$ )-Zr bridges) act as active sites for the arsenic. The authors propose an acid-base mechanism where the arsenate species, e.g.,  $\text{H}_3\text{AsO}_4$ , act as acids, binding to the hydroxyl groups in the Zr-clusters, after which the releasing protons and hydroxyl groups form water to maintain charge balance in the solution (Figure 6.15). In addition, they suggested that there might also be a partial exchange between MOF linkers (BDC) and arsenic species, but since the UiO-66 has a high degree of topological connectivity (see Chapter 4), this does not lead to structural disintegration, which was proven by XRD analyses.



**Figure 6.15** Proposed adsorption mechanism of arsenate onto UiO-66 through coordination at the Zr-O( $\mu_3$ )-Zr hydroxyl group. (Retrieved from [20])

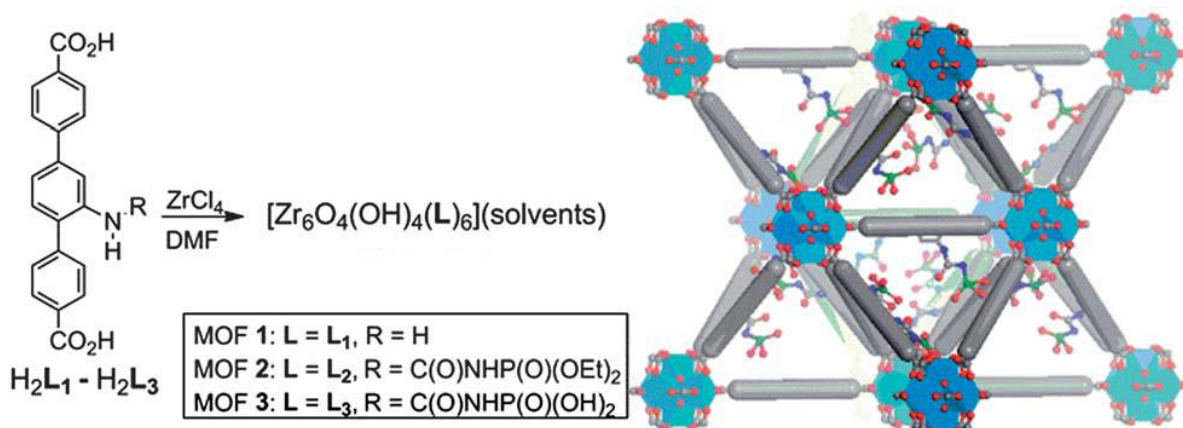
In addition to a high arsenic capacity, the presence of some common anions ( $\text{Cl}^-$ ,  $\text{NO}_3^-$ ,  $\text{CO}_3^{3-}$ ,  $\text{SO}_4^{2-}$ ) had little influence on the adsorption process (i.e., negligible competition). No other metallic species were tested, nor were regeneration and reuse. Although being very promising, a recyclability study might give more insight in the long term stability of this adsorbent. The work also offers a comprehensive comparison to other reported arsenic adsorbents, including other MOFs, such as MIL-53[21], and ZIF-8[22].

### 6.3.5 Pre-functionalized linkers

In the work of Carboni *et al.*[23], three MOFs, based on the UiO-68 topology, were investigated as potential uranium adsorbents. The UiO-68 is an isorecticular variant of UiO-66, using the extended p,p'-terphenyldicarboxylic acid (TPDC) as a linker, instead of BDC. In this research, modified TPDC linkers were used, namely amino-TPDC and diethoxyphosphorylurea-derived TPDC (Figure 6.16). The latter was prepared by condensation of amino-H<sub>2</sub>TPDC with commercially available diethoxyphosphinyl isocyanate. Both MOFs were then prepared by a solvothermal procedure in DMF, resulting in an amino-UiO-68 ("MOF 1"), and a diethoxyphosphorylurea-UiO-68 ("MOF 2"). A third material was obtained by deprotection of the diethoxyphosphorylurea-UiO-68, followed by hydrolysis with water. This yielded a UiO-68 with dihydroxyphosphorylurea groups, referred to as UiO-68-P(O)(OH)<sub>2</sub> ("MOF 3"). This

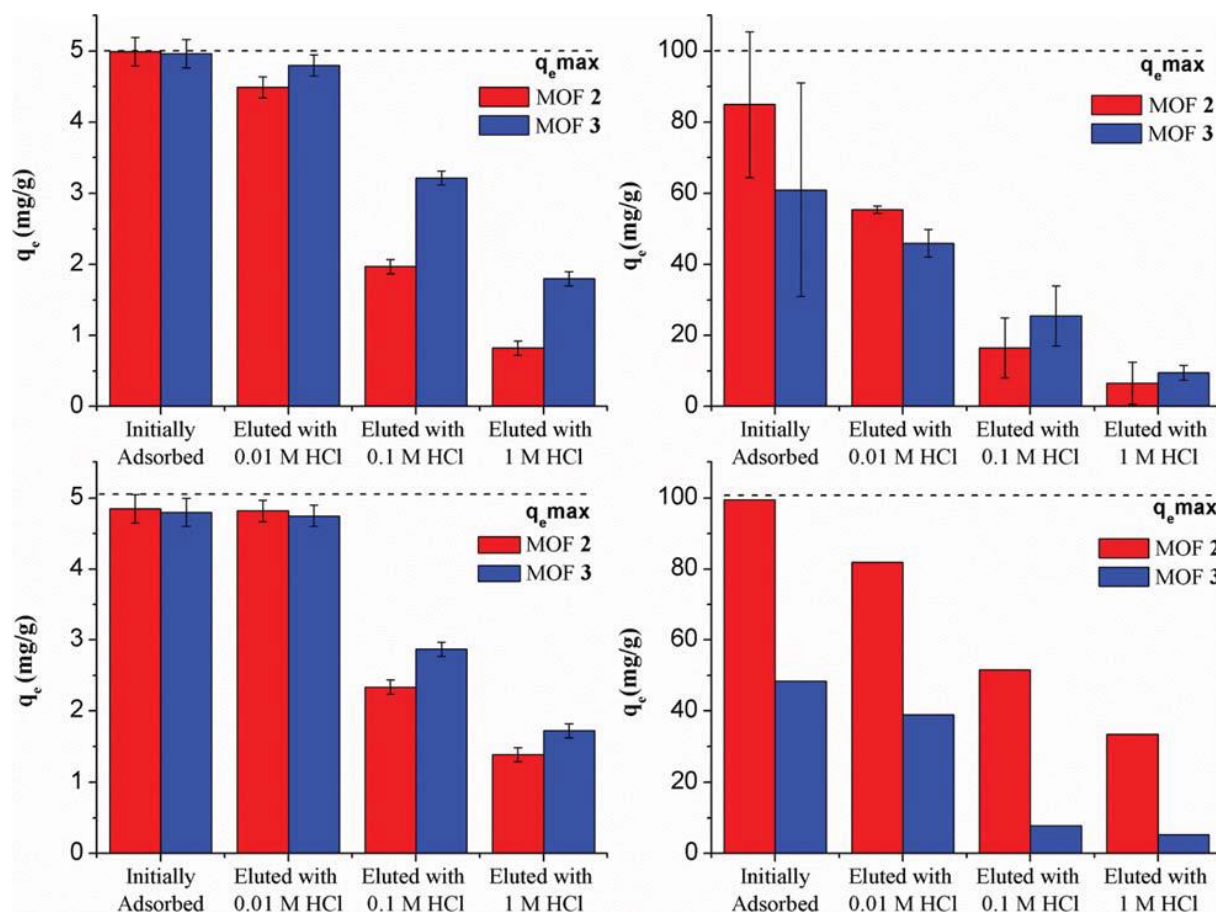


method of pre-functionalization is interesting as it affords precise loadings and facilitates investigation of sorption efficiency[23].



**Figure 6.16** Schematic showing the respective MOF (1-3) preparations, including a structural model of the new UiO-based MOF, displaying the readily accessible phosphorylurea groups. (Retrieved from [23])

The U(VI) sorption experiments were performed in water and simulated seawater at pH 2.5. The authors focused on seawater as they claim that novel sorbents are critically needed for the extraction of uranium from seawater, for nuclear fuel production. Uptakes of 217 mg U/g in water and 188 mg U/g in simulated seawater were obtained for MOF 2. MOF 3 achieved lower uptakes, i.e., 109 and 32 mg U/g in water and seawater, respectively. MOF 1 appeared to be inactive in the U(VI) adsorption. When the pH was increased from 2.5 to 5, respective saturation capacities of 152 and 104 mg U/g were obtained in water for MOF 2 and MOF 3. Regeneration was investigated by a washing procedure with aqueous HCl solutions (0.01 M, 0.1 M or 1 M). It was found that the uranium was rather strongly bound to the adsorbent, as acid stripping did not manage to fully regenerate the adsorbent. An effect of increased HCl concentration was clearly visible, however (Figure 6.17). Perhaps another stripping agent (e.g., nitric acid) could yield better results, but this was not investigated. The authors suggested that each uranyl ion is coordinating to two phosphorylurea ligands, via a monodentate bond with the phosphoryl oxygens. It was calculated that the ligands have an ideal orientation inside the MOF's tetrahedra, to form a suitable pocket for the uranyl ions. No additional recycling or selectivity studies were performed.



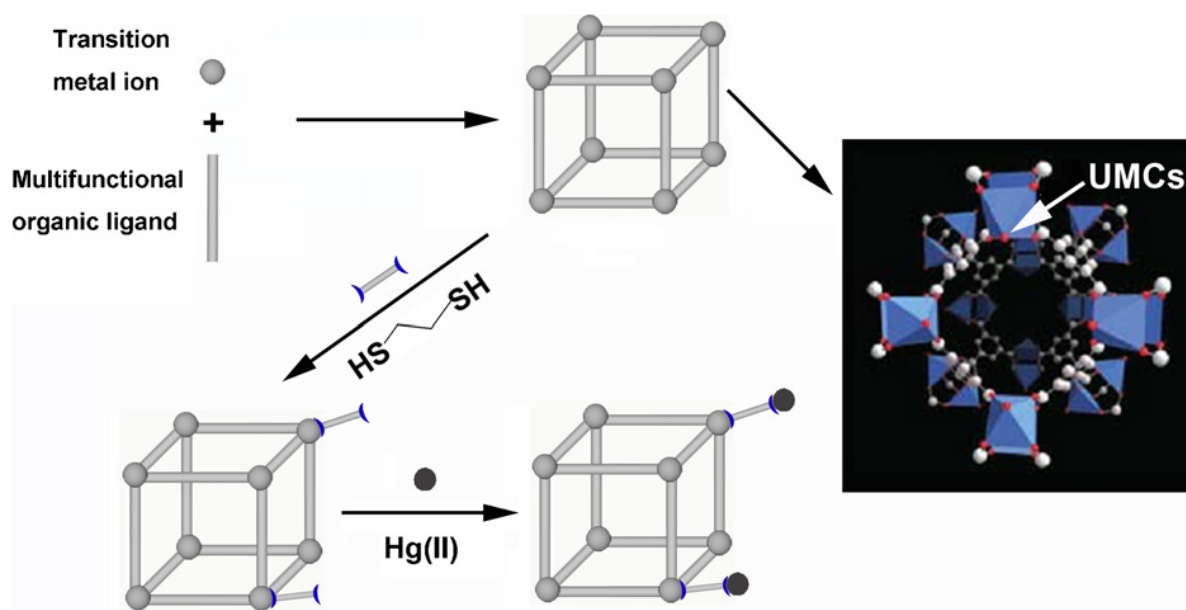
**Figure 6.17** Sorption and desorption of uranium with MOFs 2 and 3, with  $[U]_0 = 5 \text{ mg/L}$  and  $\text{pH} = 2.5$  in water (top left), and simulated seawater (bottom left), and with  $[U]_0 = 100 \text{ mg/L}$  at  $\text{pH} 2.5$  in simulated seawater, analysed by UV spectroscopy (top right) and ICP-MS (bottom right). (Retrieved from [23])

### 6.3.6 Post-synthetic modification

Ke *et al.*[24] modified the copper based HKUST-1 (Cu-BTC) with thiol groups in order to adsorb mercury ions. They used the MOF's unsaturated metal sites (CUS) to anchor dithiolglycol, which leaves one dangling thiol group available, while the other coordinates to the Cu centers (Figure 6.18). A preliminary adsorption experiment targeting  $\text{Hg}^{2+}$  ions in water was performed, resulting in an incredible uptake of  $714 \text{ mg Hg/g}$ . A control experiment, using pristine HKUST-1, showed zero uptake of mercury, proving that the thiol groups are the active sites in the adsorption. The adsorbent also showed great promise for  $\text{Hg}^{2+}$  trace removal, i.e., over 90 % removal from a 80 ppb mercury solution. No selectivity studies were performed. While thiol groups have a high affinity for  $\text{Hg}^{2+}$  ions[25] (cfr. HSAB), they might also have affinity for other competing (soft) metals. More importantly, it would be very interesting to investigate the stability of this material. In Chapters 4 and 5, it was shown that HKUST-1 shows a very poor resistance to aqueous environments. In this case, however, a lot of the coordinating water molecules on HKUST-1 have been replaced with dithiolglycol groups. A higher affinity



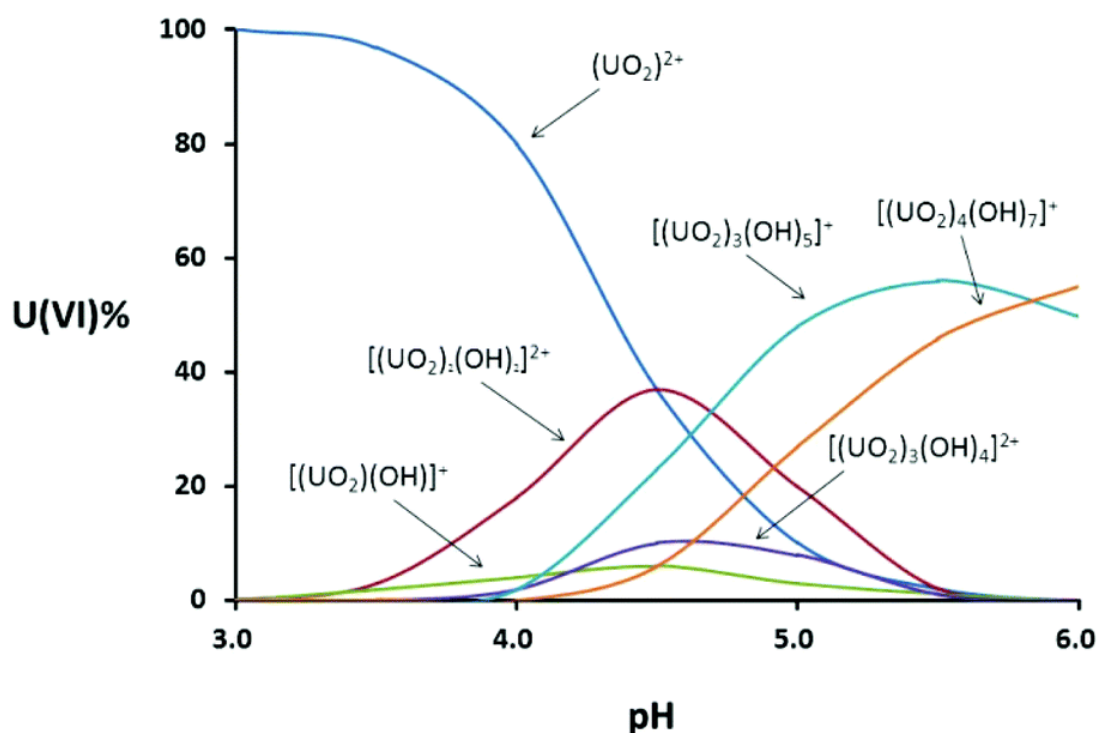
between the MOF's copper centers and the coordinating thiol groups could be expected (cfr. HSAB). An additional sterical effect from these ligands might perhaps partially hinder the coordination of water molecules to the copper centers, thereby delaying gradual disintegration. On the other hand, as the authors also noted, besides the adsorption itself, it may be challenging to recycle these MOF-type adsorbents after metal adsorption, because efficient regeneration often requires strong acidic conditions. It is therefore doubtful that this modified Cu-BTC MOF would survive such conditions. The authors clearly proved, however, that the introduction of a simple thiol-based ligand, can create a very efficient mercury adsorbent. If such a strategy would be applied on a highly stable MOF, it would certainly open up new avenues to the field of mercury removal from aqueous environments.



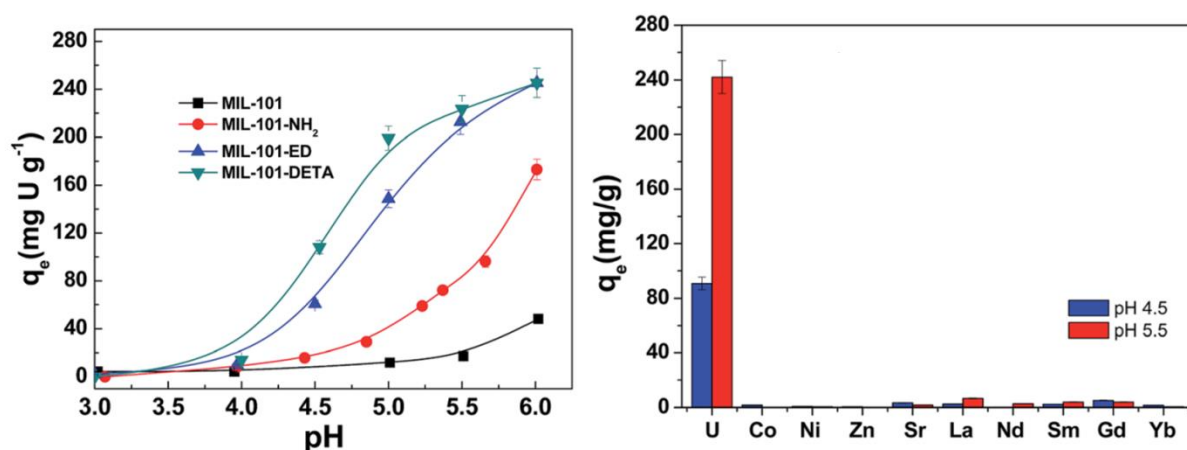
**Figure 6.18** Schematic illustration of the thiol-functionalization of MOFs through coordination bonding between one thiol group of dithioglycol and coordinatively unsaturated metal centers (UMCs) in MOFs. (Retrieved from [24])

Besides the right choice of MOF support, however, the type of post-synthetic modification (PSM) plays a critical role as well. This is illustrated by the work of Bai *et al.*[13], where the highly stable MIL-101(Cr) is functionalized with amine moieties, to obtain a uranium adsorbent. Bai *et al.* use different types of PSM methods, including a grafting procedure via the CUS (similar to the above mentioned work of Ke *et al.*). The amine ligands, respectively ethylenediamine (ED) and diethylenetriamine (DETA) were anchored on dehydrated MIL-101(Cr), resulting in MIL-101-ED, and MIL-101-DETA. In another PSM method, pristine MIL-101(Cr) was first nitrated into MIL-101-NO<sub>2</sub> and subsequently reduced to MIL-101-NH<sub>2</sub>, thereby creating primary amine groups on the aromatic rings (BDC) of MIL-101 (procedure explained in Section 6.2.1, and Figure 6.6).

It was found that MIL-101-DETA showed the highest adsorption capacity for U(VI) (350 mg/g), followed by MIL-101-ED (200 mg/g), and MIL-101-NH<sub>2</sub> (90 mg/g). The adsorption was also very pH-dependent, where higher pH levels resulted in a higher U(VI) uptake for all materials, due to the pH-dependent speciation of uranium in water[26] (Figure 6.19). At higher pHs (> 4), less uranium is present as uranyl ( $\text{UO}_2^{2+}$ ) and more hydroxylated species are formed, even multi-nuclear hydroxide species (i.e.,  $[(\text{UO}_2)_x(\text{OH})_y]^+$ ). It is obvious that when such species adsorb, the U(VI) uptake rises drastically compared to the adsorption of mononuclear species, such as uranyl at lower pHs (< 4). This is clearly visible in Figure 6.20. Even pristine MIL-101 shows interaction with these hydroxylated species, whereas at lower pHs, it is completely inactive. Below pH ~3.5, however, none of the materials adsorb any U(VI), which is integrally present as uranyl in such conditions. The authors suggested this has to do with the protonation of aminated species, which would repel the cationic uranyl.



**Figure 6.19** U(VI) species distribution as a function of pH at 25 °C. (Retrieved from [26])



**Figure 6.20 (Left)** Effect of pH on U(VI) sorption onto MIL-101, MIL-101-NH<sub>2</sub>, MIL-101-ED, and MIL-101-DETA;  $c_0 = 100$  mg/L,  $m/V = 0.4$  g/L,  $T = 25$  °C,  $t = 240$  min. **(Right)** Competitive sorption of coexistent ions by MIL-101-DETA at pH 5.5. The initial concentration of all metal ions was 0.5 mmol/L. (Adapted from [13])

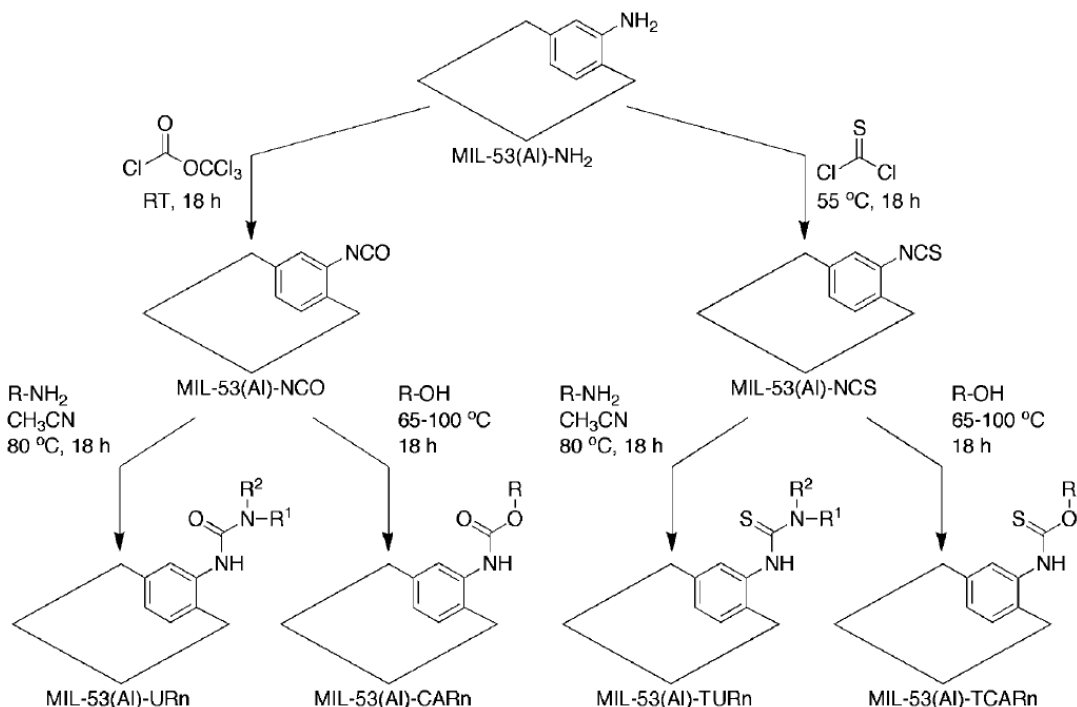
Selectivity experiments were carried out with MIL-101-DETA at pH 4.5 and 5.5 with competing cations Co<sup>2+</sup>, Ni<sup>2+</sup>, Zn<sup>2+</sup>, Sr<sup>2+</sup>, La<sup>3+</sup>, Nd<sup>3+</sup>, Sm<sup>3+</sup>, Gd<sup>3+</sup>, and Yb<sup>3+</sup> (Figure 6.20). A high affinity was observed for uranium at both pHs, with little to no uptake from the competing elements. The authors ascribe this to the favorable interaction between softer nitrogen donors and the actinide uranium. In addition, the adsorbed hydroxylated, multinuclear U(VI) species at higher pHs might be stabilized by hydrogen bonding with the amino groups. Additional work on exploring the intrinsic reasons for the selectivity of these amine-grafted MOFs is being performed by the authors.

In terms of recyclability, it was found out that the adsorbents could be readily regenerated by lowering the pH below 3, thereby effectively stripping all adsorbed uranium (>99 %) from the materials. It was shown that for MIL-101-NH<sub>2</sub> no remarkable decrease of adsorption capacity occurred after regeneration, whereas there is a ca. 30 % reduction of adsorption capacity for regenerated MIL-101-ED and MIL-101-DETA. MIL-101-NH<sub>2</sub> has its amine group directly anchored (covalently) on the aromatic rings of MIL-101. It is therefore not surprising that this material keeps its performance. As mentioned before in this chapter, CUS grafting might yield a less stable adsorbent, especially in acidic environments. This is also stated by the authors, who postulated that, as chromium is known to be a hard Lewis acid and thus prefers coordination with hard bases, such as H<sub>2</sub>O, some amine groups were replaced by water molecules in abundant amounts during the adsorption–desorption of U(VI).

If a very stable and reusable adsorbent is required, CUS grafting might not be the optimal path to pursue. Especially if a MOF's metal cluster prefers coordination to water molecules, i.e., hard acids such as Cr<sup>3+</sup>, Zr<sup>4+</sup>, Fe<sup>3+</sup>, it might be pointless to coordinate softer donors such as amines or

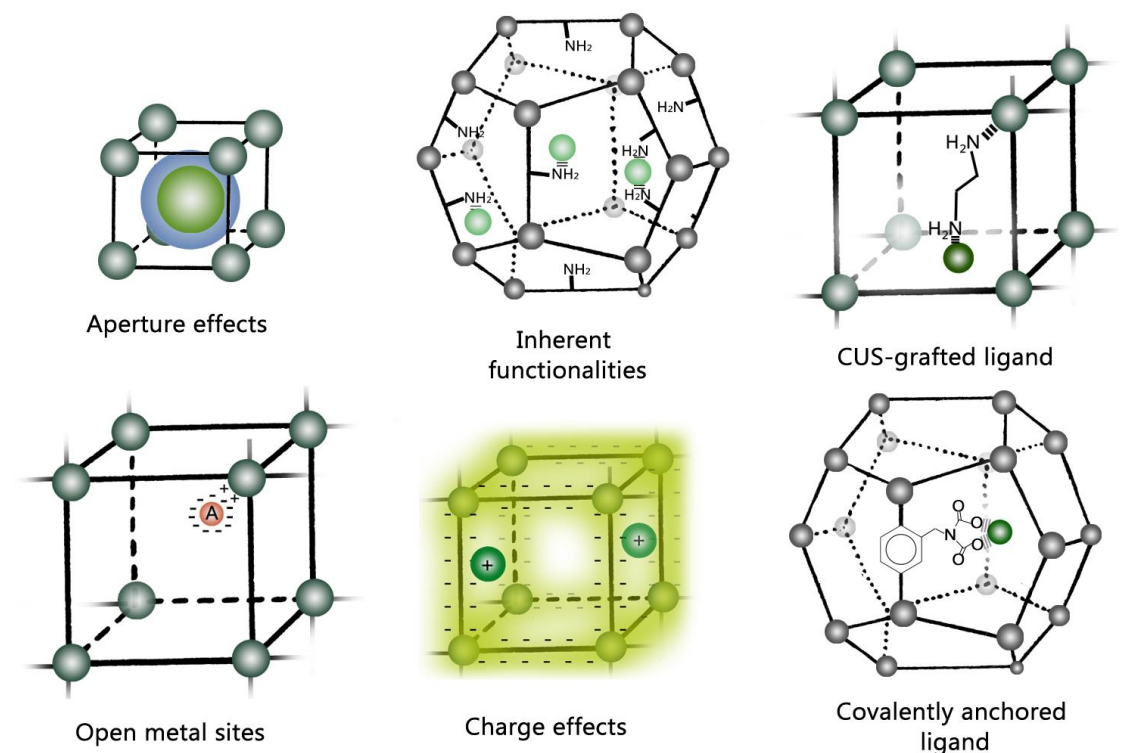
thiols to it. A covalent anchoring strategy seems to be a more interesting approach, where the MOF's linkers are functionalized (PSM) in one or more steps.

An example of the versatility of this approach is the work of Volkringer *et al.*[27]. They have used the  $\text{NH}_2\text{-MIL-53(Al)}$  as a starting support and discussed various kinds of PSM methods to obtain specific functions on this MOF. In the case of  $\text{NH}_2\text{-MIL-53(Al)}$ , an amine function is already present on the aromatic ring (from  $\text{NH}_2\text{-BDC}$ ), but such a function could be readily generated on other benzene-strut based MOFs, e.g.,  $\text{MIL-101-NH}_2$  in Bai *et al.*[13] or Seo *et al.*[7] (*vide supra*). Figure 6.21 gives an overview of these PSM strategies to obtain functional groups such as (thio)ureas, (thio)carbamates... The authors stressed that the choice of solvent is critical for these PSM methods, e.g., tetrahydrofuran was used in the first PSM step ( $-\text{NH}_2$  to  $-\text{NCO}$  or to  $-\text{NCS}$ ) with conversion of  $\sim 90\%$ , whereas no conversion was observed in other solvents tested, such as toluene, benzene, dimethyl sulfoxide, chloroform, dichloromethane, and acetonitrile. However, this is because  $\text{MIL-53(Al)}$  is a breathing MOF where the flexibility of the lattice may require the solvent to swell the framework to achieve efficient PSM. Also, the choice of MOF is very important, as some reactions (e.g., the reaction between amines and phosgene derivatives in tetrahydrofuran) could produce  $\text{HCl}$  as a byproduct. Hence, certain reactions performed with acid- (or moisture) sensitive MOFs could lead to immediate destruction of the materials.



**Figure 6.21** Strategy for the generation of MIL-53 presenting iso(thio)cyanate, (thio)carbamate, and (thio)urea functional groups. (Retrieved from [27])

An overview of the different interaction possibilities of MOFs (pristine or functionalized) with metallic adsorbates is presented in Figure 6.22.



**Figure 6.22** Different interaction types of MOFs (pristine/functionalized) with metallic species. (Green orbs: cationic adsorbate, Red orb: anionic adsorbate, Grey orbs: metal nodes of the MOF).

## 6.4 Concluding remarks

It is clear that MOFs possess a large spectrum of interaction types with various adsorbates, either pristinely or functionalized. The high number of MOFs that are available, permits us to make a rational choice on the optimal structure (porosity, cluster geometry, charge effects, functionalizability...), needed to interact specifically with certain species of our choice. The amount of different interaction types makes MOFs a very versatile materials class in adsorption, however, it could also be the source of several unwanted effects. For instance, if a MOF adsorbent has to be developed for the selective aqueous separation of certain cationic dyes from anionic ones, one way could be to graft a selective ligand with a negative charge (e.g., nitro groups), in order to have a favorable interaction with the positive dye. If, however, the chosen MOF contains metal clusters that are readily accessible by the dyes (e.g., open metal sites), an undesired interaction with the anionic dyes may occur, thereby diminishing the MOF's selective character. Similarly, if a MOF-based metal adsorbent is developed, the interaction could be hindered if the MOF has a very high positive surface charge. Furthermore, the pH-effect is a very important factor to consider when designing a MOF adsorbent. Not only does it influence

the material's charge, it can also influence anchored functionalities. If an amine-based MOF adsorbent for metal cations is developed, but the target environment is very acidic, then protonation of these amines could prevent interaction with the metal cations altogether.

Above all else, the adsorbent needs to be stable, and if functionalities are introduced, these need to be thoroughly linked to the support. Especially when highly selective, often expensive ligands are anchored, a gradually degrading material is not at all desired. Even if the initial results are very promising (high uptake, fast kinetics...), if after one adsorption and/or desorption run, the adsorbent structure is partially disintegrated, or a third of the functionalities are leached out, such a material is not suitable for (industrial) application.

## 6.5 Perspective: Shaping MOFs for industrial applications

More and more research is published on aqueous adsorption with MOF-based composites, in which a particular MOF is embedded within a specific matrix. Some reported matrices are polymers (fibres), carbon (graphite, activated carbon), silicon-rubber based membranes[2, 28-30]... While MOF-composites are not a part of this work, they are certainly worth exploring and possibly play a key role in the introduction of MOFs to a broader scope of industrial applications. Typical MOF morphology, i.e., fine powders, usually limits their application. For instance, material manipulation can be difficult, and column-based applications may experience back-pressure issues. A MOF-based composite could be the perfect solution for these problems, provided that the integration of the MOF in a matrix does not inhibit its performance. An additional advantage could be the enhanced stability of several MOFs, as a result of being thoroughly embedded in their matrix. An overview on the state of the art on MOF composites is presented in Zhu *et al.*[31]. Another possibility to improve the handling of MOFs is the preparation of MOF-based monoliths, beads or pellets. In a study by Hong *et al.*[32], MIL-101(Cr) monoliths were produced via paste extrusion, using bentonite clay as binder. The MIL-101 was mixed with the binder and water to form a paste, which was then matured at room temperature. The obtained paste is then extruded into monolith and subsequently dried and fired in a kiln, to form a strong, solid structure, which could be cut in pieces of appropriate size (Figure 6.22).



**Figure 6.23** Cross-sectional view of a fired MIL-101 (Cr) monolith. (Retrieved from [32])

## REFERENCES

- [1] N.A. Khan, Z. Hasan, S.H. Jhung, Adsorptive removal of hazardous materials using metal-organic frameworks (MOFs): A review, *J Hazard Mater*, 244 (2013) 444-456.
- [2] X.F. Chen, H. Zang, X. Wang, J.G. Cheng, R.S. Zhao, C.G. Cheng, X.Q. Lu, Metal-organic framework MIL-53(Al) as a solid-phase microextraction adsorbent for the determination of 16 polycyclic aromatic hydrocarbons in water samples by gas chromatography-tandem mass spectrometry, *Analyst*, 137 (2012) 5411-5419.
- [3] E. Haque, J.E. Lee, I.T. Jang, Y.K. Hwang, J.S. Chang, J. Jegal, S.H. Jhung, Adsorptive removal of methyl orange from aqueous solution with metal-organic frameworks, porous chromium-benzenedicarboxylates, *J Hazard Mater*, 181 (2010) 535-542.
- [4] Z. Hasan, E.J. Choi, S.H. Jhung, Adsorption of naproxen and clofibric acid over a metal-organic framework MIL-101 functionalized with acidic and basic groups, *Chem Eng J*, 219 (2013) 537-544.
- [5] S.H. Huo, X.P. Yan, Metal-organic framework MIL-100(Fe) for the adsorption of malachite green from aqueous solution, *J Mater Chem*, 22 (2012) 7449-7455.
- [6] M. Maes, S. Schouteden, L. Alaerts, D. Depla, D.E. De Vos, Extracting organic contaminants from water using the metal-organic framework CrIII(OH)[middle dot]{O2C-C6H4-CO2}, *Phys Chem Chem Phys*, 13 (2011) 5587-5589.
- [7] P.W. Seo, B.N. Bhadra, I. Ahmed, N.A. Khan, S.H. Jhung, Adsorptive Removal of Pharmaceuticals and Personal Care Products from Water with Functionalized Metal-organic Frameworks: Remarkable Adsorbents with Hydrogen-bonding Abilities, *Sci Rep-Uk*, 6 (2016).
- [8] D.Y. Hong, Y.K. Hwang, C. Serre, G. Ferey, J.S. Chang, Porous Chromium Terephthalate MIL-101 with Coordinatively Unsaturated Sites: Surface Functionalization, Encapsulation, Sorption and Catalysis, *Adv Funct Mater*, 19 (2009) 1537-1552.
- [9] N.V. Maksimchuk, O.V. Zalomaeva, I.Y. Skobelev, K.A. Kovalenko, V.P. Fedin, O.A. Kholdeeva, Metal-organic frameworks of the MIL-101 family as heterogeneous single-site catalysts, *P Roy Soc a-Math Phy*, 468 (2012) 2017-2034.
- [10] Y.K. Hwang, D.Y. Hong, J.S. Chang, S.H. Jhung, Y.K. Seo, J. Kim, A. Vimont, M. Daturi, C. Serre, G. Ferey, Amine grafting on coordinatively unsaturated metal centers of MOFs: Consequences for catalysis and metal encapsulation, *Angew Chem Int Edit*, 47 (2008) 4144-4148.
- [11] S.N. Kim, S.T. Yang, J. Kim, J.E. Park, W.S. Ahn, Post-synthesis functionalization of MIL-101 using diethylenetriamine: a study on adsorption and catalysis, *Crystengcomm*, 14 (2012) 4142-4147.
- [12] M. Anbia, V. Hoseini, Enhancement of CO<sub>2</sub> adsorption on nanoporous chromium terephthalate (MIL-101) by amine modification, *J Nat Gas Chem*, 21 (2012) 339-343.
- [13] Z.Q. Bai, L.Y. Yuan, L. Zhu, Z.R. Liu, S.Q. Chu, L.R. Zheng, J. Zhang, Z.F. Chai, W.Q. Shi, Introduction of amino groups into acid-resistant MOFs for enhanced U(VI) sorption, *J Mater Chem A*, 3 (2015) 525-534.
- [14] S. Bernt, V. Guillermin, C. Serre, N. Stock, Direct covalent post-synthetic chemical modification of Cr-MIL-101 using nitrating acid, *Chem Commun*, 47 (2011) 2838-2840.
- [15] C.H. Wang, X.L. Liu, N.K. Demir, J.P. Chen, K. Li, Applications of water stable metal-organic frameworks, *Chem Soc Rev*, 45 (2016) 5107-5134.
- [16] X. Meng, R.L. Zhong, X.Z. Song, S.Y. Song, Z.M. Hao, M. Zhu, S.N. Zhao, H.J. Zhang, A stable, pillar-layer metal-organic framework containing uncoordinated carboxyl groups for separation of transition metal ions, *Chem Commun*, 50 (2014) 6406-6408.



- [17] W. Yang, Z.Q. Bai, W.Q. Shi, L.Y. Yuan, T. Tian, Z.F. Chai, H. Wang, Z.M. Sun, MOF-76: from a luminescent probe to highly efficient U-VI sorption material, *Chem Commun*, 49 (2013) 10415-10417.
- [18] B.J. Zhu, X.Y. Yu, Y. Jia, F.M. Peng, B. Sun, M.Y. Zhang, T. Luo, J.H. Liu, X.J. Huang, Iron and 1,3,5-Benzenetricarboxylic Metal-Organic Coordination Polymers Prepared by Solvothermal Method and Their Application in Efficient As(V) Removal from Aqueous Solutions, *J Phys Chem C*, 116 (2012) 8601-8607.
- [19] D. Mohan, C.U. Pittman, Arsenic removal from water/wastewater using adsorbents - A critical review, *J Hazard Mater*, 142 (2007) 1-53.
- [20] C.H. Wang, X.L. Liu, J.P. Chen, K. Li, Superior removal of arsenic from water with zirconium metal-organic framework UiO-66, *Sci Rep-Uk*, 5 (2015).
- [21] T.A. Vu, G.H. Le, C.D. Dao, L.Q. Dang, K.T. Nguyen, Q.K. Nguyen, P.T. Dang, H.T.K. Tran, Q.T. Duong, T.V. Nguyen, G.D. Lee, Arsenic removal from aqueous solutions by adsorption using novel MIL-53(Fe) as a highly efficient adsorbent, *RSC Advances*, 5 (2015) 5261-5268.
- [22] M.P. Jian, B. Liu, G.S. Zhang, R.P. Liu, X.W. Zhang, Adsorptive removal of arsenic from aqueous solution by zeolitic imidazolate framework-8 (ZIF-8) nanoparticles, *Colloid Surface A*, 465 (2015) 67-76.
- [23] M. Carboni, C.W. Abney, S. Liu, W. Lin, Highly porous and stable metal-organic frameworks for uranium extraction, *Chem Sci*, 4 (2013) 2396-2402.
- [24] F. Ke, L.G. Qiu, Y.P. Yuan, F.M. Peng, X. Jiang, A.J. Xie, Y.H. Shen, J.F. Zhu, Thiol-functionalization of metal-organic framework by a facile coordination-based postsynthetic strategy and enhanced removal of Hg<sup>2+</sup> from water, *J Hazard Mater*, 196 (2011) 36-43.
- [25] S.X. Zhang, Y.Y. Zhang, J.S. Liu, Q. Xu, H.Q. Xiao, X.Y. Wang, H. Xu, J. Zhou, Thiol modified Fe<sub>3</sub>O<sub>4</sub>@SiO<sub>2</sub> as a robust, high effective, and recycling magnetic sorbent for mercury removal, *Chem Eng J*, 226 (2013) 30-38.
- [26] X. Gao, C. Wang, Z.F. Shi, J. Song, F.Y. Bai, J.X. Wang, Y.H. Xing, A family of uranyl-aromatic dicarboxylate (pht-, ipa-, tpa-) framework hybrid materials: photoluminescence, surface photovoltage and dye adsorption, *Dalton T*, 44 (2015) 11562-11571.
- [27] C. Volkringer, S.M. Cohen, Generating Reactive MILs: Isocyanate- and Isothiocyanate-Bearing MILs through Postsynthetic Modification, *Angew Chem Int Edit*, 49 (2010) 4644-4648.
- [28] F.N. Azad, M. Ghaedi, K. Dashtian, S. Hajati, V. Pezeshkpour, Ultrasonically assisted hydrothermal synthesis of activated carbon-HKUST-1-MOF hybrid for efficient simultaneous ultrasound-assisted removal of ternary organic dyes and antibacterial investigation: Taguchi optimization, *Ultrason Sonochem*, 31 (2016) 383-393.
- [29] L. Li, X.L. Liu, H.Y. Geng, B. Hu, G.W. Song, Z.S. Xu, A MOF/graphite oxide hybrid (MOF: HKUST-1) material for the adsorption of methylene blue from aqueous solution, *J Mater Chem A*, 1 (2013) 10292-10299.
- [30] X.L. Liu, H. Jin, Y.S. Li, H. Bux, Z.Y. Hu, Y.J. Ban, W.S. Yang, Metal-organic framework ZIF-8 nanocomposite membrane for efficient recovery of furfural via pervaporation and vapor permeation, *J Membrane Sci*, 428 (2013) 498-506.
- [31] Q.L. Zhu, Q. Xu, Metal-organic framework composites, *Chem Soc Rev*, 43 (2014) 5468-5512.
- [32] W.Y. Hong, S.P. Perera, A.D. Burrows, Manufacturing of metal-organic framework monoliths and their application in CO<sub>2</sub> adsorption, *Micropor Mesopor Mat*, 214 (2015) 149-155.
- [33] K. Folens, K. Leus, N. R. Nicomel, M. Meledina, S. Turner, G. Van Tendeloo, G. Du Laing, and P. Van Der Voort, Fe<sub>3</sub>O<sub>4</sub>@MIL-101 – A Selective and Regenerable Adsorbent for the Removal of As Species from Water. *Eur J Inorg Chem*, 27 (2016) 4395–4401.



# 7 FUNCTIONALIZED METAL-ORGANIC FRAMEWORK CMPO@MIL-101(Cr) AS A STABLE AND SELECTIVE RARE EARTH ADSORBENT

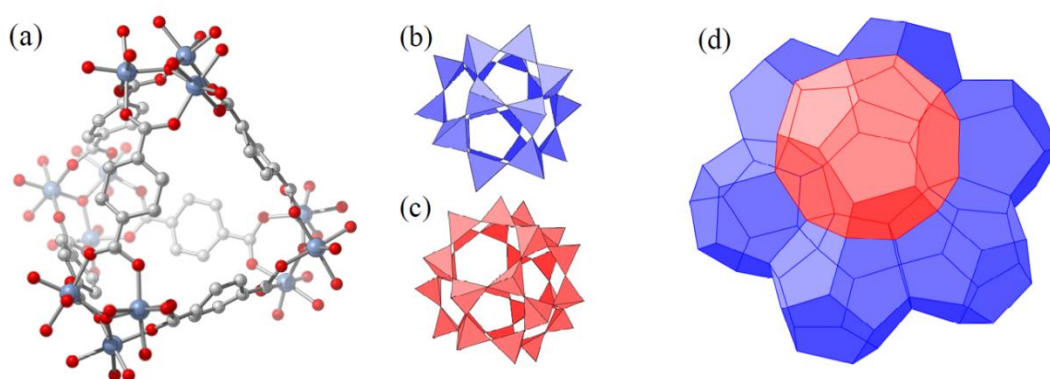
De Decker, J., De Clercq, J., Vermeir, P., and Van Der Voort, P. **Journal of Materials Science** 51 (2016) 5019-5026. **Contribution:** Synthesis, Characterization, Adsorption experiments.

## 7.1 Introduction

The rare earth elements (REEs) have an increasing importance to our modern society. They mainly consist of the fifteen lanthanides and are found in various high-tech applications. Particularly in the area of clean energy, many lanthanides (neodymium, dysprosium, europium,...) play a critical part in the design and operation of appliances and machinery such as hybrid and electrical vehicles, wind turbines, and lighting technology[1]. The demand for REEs is rapidly increasing, whereas the supply is rather limited[2]. In order to maintain a technologically sustainable future, it is of key importance to safeguard the availability of these valuable metals. An important way to help achieving this goal is to focus on the recycling of REEs. In this work we target a specific stage in the various phases of recycling processes: the recovery of rare earths from dilute aqueous solutions, suggesting the use of selective adsorption.

Over the past decade, metal-organic frameworks have gained a tremendous increase in attention in the field of (applied) nanoporous, crystalline materials research[3]. This interest is owed to their unique properties as hybrid materials, and has led to primary applications in energy storage[4, 5], catalysis[6-8], carbon dioxide capture[9, 10], adsorption/separation of hydrocarbons[11-13], magnetism[14],... A more recent field in the expanding scope of MOF research comprises applications in aqueous environment, more specifically in water treatment.

Although a lot of MOFs tend to be unstable in aqueous environment, a few of them have been proven more than suitable candidates for applications in water, serving as catalysts[15], and even as adsorbents for dyes and organic pollutants[16]. Comprehensive reviewing work on the application of MOFs (amongst other solids) as trace metal adsorbents (including water based systems) was performed by Hu *et al.*[17]. In this research, we use a very stable, highly porous metal-organic-framework, MIL-101(Cr), as a support in rare earth metal adsorption from acidic, aqueous solutions. MIL-101 is a mesoporous cage-type MOF, developed by Ferey in 2005[18]. Its three-dimensional framework consists of inorganic chromium-oxide clusters, interconnected by terephthalate linkers, which leads to the formation of highly ordered cages of super tetrahedral (Figure 7.1). The abundance of aromatic linkers in the structure makes the MOF particularly easy to post-functionalize. The MIL-101(Cr) is a highly porous MOF and the mesoporous cages are large enough to enable the incorporation of large molecules. Moreover, it shows excellent resistance to acidic, aqueous media and belongs to the most stable mesoporous MOFs to date[19, 20] (Appendix 2.1 and 2.2). MIL-101(Cr) is therefore a promising candidate as a support in (acidic) aqueous adsorption processes.

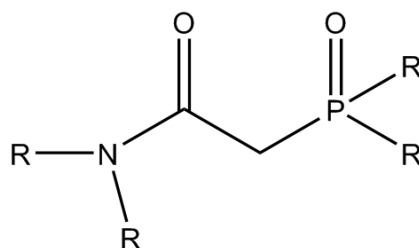


**Figure 7.1 (a) MIL-101 super tetrahedron. (b resp. c) Small and large super cage. (d) MIL-101 structure (MTN zeotype).**

When it comes to the removal/recovery of specific molecules or ions from dilute solutions, adsorption is a very efficient and cost-effective method. Because it is a heterogeneous process, adsorbent separation and reuse are a lot more facile compared to its homogeneous counterpart. When designing an adsorbent for REEs, two major aspects come into play: adsorbent stability and selective targeting. Stability of the adsorbent is required on two levels, namely the stability

of the supporting material and of the linkage between support and active sites. Both have to survive the applied acidic conditions during REE adsorption experiments to prevent leaching and structure degradation. Selective targeting of rare earth cations is established by using specific functional groups and immobilizing them into the structure. These selective ligands need to interact preferentially with the REEs and neglect any interfering cations (transition metals, alkali metals...) as much as possible.

In order to select a ligand with a high affinity towards lanthanide complexation, one has to look at the chemistry of these metals. Lanthanides form trivalent cations and, as a result, are rather hard Lewis acids. Conforming the HSAB concept, the incorporation of a series of hard Lewis bases into a ligand structure can yield a selective environment for lanthanide complexation. Moreover, it has been found that combining different classes of donor moieties into the same ligand (chelate), can result in a synergistic effect on the selectivity of the ligand, as if both donors enhance each other's affinity towards the lanthanide cation[21-23]. Especially the combination of amides (O-donor) and carbonyl groups seems to result in synergistic chelates for lanthanide complexation[24]. A prominent example of this combination is the carbamoylmethylphosphine oxide (CMPO) type ligand (Figure 7.2). These chelating ligands appear to be very selective lanthanide complexants, with a very low affinity for competing transition- or alkali metals [25].



**Figure 7.2 Carbamoylmethylphosphine oxide (CMPO) ligand structure.**

By immobilizing these ligands onto a proper support, a heterogeneous system can be synthesized able to perform as a selective adsorbent for rare earth metals. Several REE-selective adsorbents have been reported in literature. Many of those are based on porous silicas as a support material, combined with alkyl-silane chemistry to embed the proper functionalities. Fryxell *et al.* have immobilized several REE-selective ligands onto mesoporous MCM-41 silica and successfully obtained selective lanthanide adsorbents[24]. Kleitz *et al.* made use of mesoporous silica (KIT-6) to embed diglycolamide moieties (DGA) to selectively recover lanthanides from a variety of metals[26].

In this research, we aimed to apply the stable MIL-101(Cr) metal-organic-framework as a promising support for uses in selective REE adsorption. The MOF was functionalized into an adsorbent, resistant to leaching, by step-wise anchoring of CMPO ligands onto the support. We have avoided using siloxane chemistry, as it is found that these bonds are prone to cleaving in

the presence of (acidic) water [27]. This novel adsorbent was used in adsorption experiments in order to recover europium from aqueous solutions as a proof of concept. In addition, selectivity experiments were conducted to determine the affinity of the adsorbent between REEs (Eu, Y) and transition metals (Zn). These three target metals were selected as they are found in end-of-life products, such as fluorescent lamps, TVs and PC screens.

## 7.2 Experimental Section

### 7.2.1 Chemicals

Europium standard solution (1,000 ppm  $\text{Eu}^{3+}$  in dil. nitric acid) was purchased from VWR Chemicals.  $\text{Eu}(\text{NO}_3)_3 \cdot 6\text{H}_2\text{O}$  (99.9%) was purchased from Alfa Aesar. Yttrium standard solution (1,000 ppm  $\text{Y}^{3+}$  in dil. nitric acid),  $\text{Y}(\text{NO}_3)_3 \cdot 6\text{H}_2\text{O}$  (99.8%),  $\text{Zn}(\text{NO}_3)_2 \cdot 6\text{H}_2\text{O}$  (98%) and all remaining chemicals were purchased from Sigma Aldrich.

### 7.2.2 Synthesis of MIL-101(Cr)

MIL-101(Cr) was synthesized, using an adaptation of Jiang *et al.* [28]. In a random order, terephthalic acid (4 mmol) and  $\text{Cr}(\text{NO}_3)_3 \cdot 9\text{H}_2\text{O}$  (4 mmol) were added to deionized water (20 mL). The obtained suspension was poured into a Teflon-lined autoclave and heated to 210 °C for eight hours (2 hours warm-up) under autogenous pressure. When cooled down to room temperature, the obtained mixture was filtered and the green MIL-101 was collected and rinsed thoroughly with dimethylformamide (DMF) and HCl solution (1M) to remove from any leftover reagents. Samples were vacuum dried for 24 hours at 120 °C prior to functionalization.

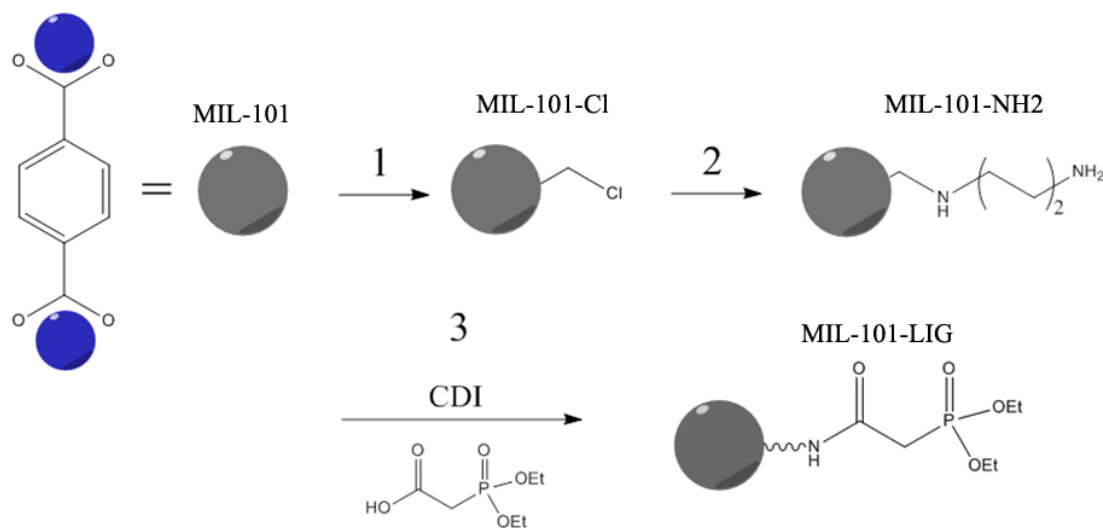
### 7.2.3 CMPO-functionalization of MIL-101(Cr)

The three-step functionalization process of the MIL-101 is shown in Figure 7.3. At first, a chloromethylation was performed in order to obtain a suitable anchoring point for subsequent functionalization. 1 gram of MIL-101(Cr) was suspended in 70 mL of nitromethane, based on the recipe by Goesten *et al.* [29]. Subsequently, 1.9 g of  $\text{AlCl}_3 \cdot 6\text{H}_2\text{O}$  was added together with 0.7 g of methoxyacetyl chloride (by syringe). The mixture was stirred for 10 hours at 100 °C. Afterwards, the solid material was recovered by filtration and rinsed thoroughly with water, nitromethane, and acetone. The sample was vacuum dried for 24 hours at 120 °C.

In a second step, the chloromethylated MIL-101 (1 g) was added, together with 1,4-diaminobutane (2.2 g), to 70 mL of DMF. The mixture was stirred at 80 °C under inert atmosphere for 24 hours. The material was recovered through filtration, thoroughly rinsed with DMF and acetone, and vacuum dried for 24 hours at 120 °C prior to elemental analysis.

In step three, the primary amine groups of the aminated MIL-101 are coupled with carboxylic end-groups of diethylphosphonoacetic acid, thus forming the amide link of the CMPO-ligand.

500 mg of amine-functionalized MIL-101 is added to 25 mL of anhydrous DMF. In a separate flask, 3 mmol diethylphosphonoacetic acid is dissolved in anhydrous DMF at room temperature (argon atmosphere). To this solution, carbonyldiimidazole (CDI) is added (equimolar: 3 mmol) and the mixture is stirred moderately[24].



**Figure 7.3 Stepwise anchoring of CMPO on MIL-101(Cr). MIL-101: pristine MOF, -Cl: Chloromethylated, -NH<sub>2</sub>: Aminated, MIL-101-LIG: completed CMPO on MIL-101.**

CDI is an often used coupling agent for the synthesis of peptides. It requires anhydrous conditions[30]. The mechanism of the initial coupling of CDI with carboxyl groups leads to the formation of CO<sub>2</sub>, which can be seen escaping from the solution. After about 15 minutes, the CO<sub>2</sub> formation ceases and the stirring is stopped. Subsequently, the mixture containing the aminated MOF in DMF is added to the mixture holding the phosphonoacetic acid. The suspension is then stirred for 12 hours at room temperature. The functionalized MOF is recovered through filtration and rinsed with DMF, water, and acetone. Afterwards, the material is vacuum dried for 24 hours at 120 °C.

#### 7.2.4 Characterization Techniques

The materials obtained in this research were characterized on their composition, morphology and surface chemistry, using following characterization techniques: N<sub>2</sub> gas sorption experiments were performed at 77 K using a Belsorp-mini II gas analyzer. Samples were pre-dried at 120°C under vacuum. The Langmuir method was used to calculate the specific surface area. Total pore volumes were estimated at p/p<sub>0</sub> = 0.98. DRIFTS-spectra were measured on a Nicolet 6700 FTIR spectrometer (Thermo-Scientific) with MCT detector. Analyses were performed at 120 °C under vacuum. X-ray fluorescence (XRF) spectroscopy measurements were performed using an energy-dispersive Rigaku NexCG spectrometer. CHNS elemental analysis was performed on a

Flash 2000 (Thermo-Scientific). X-ray diffraction analyses (powder) were performed using an ARL X'tra diffractometer (Thermo-Scientific).

### 7.2.5 Adsorption experiments

Single cation europium adsorption tests were performed by weighing a desired amount of adsorbent (50 mg) and adding it to 50 ml of aqueous  $\text{Eu}^{3+}$ -solutions of different concentrations (liquid/solid ratio (L/S): 1000 mL/g, arbitrarily chosen) in glass vials (w/ plastic lids) to determine the adsorption isotherm. The obtained isotherm is then fitted to the Langmuir (and Freundlich) model. The pH of the initial solutions was set to  $4.00 \pm 0.05$  by adding aqueous HCl solution. The vials were shaken at constant temperature in a thermostatic shaking device (Infors HT Multitron standard, Analys, 25 °C, 200 rpm) for 24 hours to ensure equilibrium. After filtration through a 0.45  $\mu\text{m}$  PET syringe filter, the filtrates were analyzed by means of ICP-AES (IRIS Intrepid II XSP). Each test was performed in duplicate. Selectivity tests in the presence of yttrium and zinc were performed in an analogue way with concentrations of 50 ppm for each metal and an L/S ratio of 400 mL/g (lower L/S ratio because of the combined high concentration of the three metals (150 ppm), which will directly saturate the adsorbent. By lowering the L/S, a more reliable concentration difference can be measured). The solutions were made by dissolving the respective metal nitrates in deionized water and adjusting the pH to  $5.00 \pm 0.05$  w/ HCl (aq.). This pH is low enough to prevent hydrolysis of the lanthanides, and high enough to prevent ligand protonation, i.e., pH >2 [24]). Zinc and europium/yttrium concentrations of the filtrates were analyzed by means of Flame-AAS (Varian SpectrAA 220FS) and ICP-AES respectively. Kinetic experiments were carried out with a 50 ppm  $\text{Eu}^{3+}$  solution at pH  $4.0 \pm 0.05$ . 250 mg of adsorbent was suspended in 250 mL of solution. The suspension was magnetically stirred at 1000 rpm rotation speed. Periodical sampling (0 – 24 hours) was performed with a syringe, fitted with a 0.45  $\mu\text{m}$  PET filter. The filtrates were analyzed by means of ICP-AES.

The equilibrium adsorption capacity  $q_e$  of the metals (mg/g) is calculated using the following expression:

$$q_e = \frac{C_0 - C_e}{m} \cdot V$$

with  $C_0$  and  $C_e$  the initial and equilibrium metal concentrations (mg/L) in the solution respectively,  $V$  the solution volume (L) and  $m$  the adsorbent mass (g).

The affinity of the adsorbent for a specific metal can be represented by the distribution coefficient  $K_d$  (mL/g), which is a mass-based partition coefficient between the solid- and liquid phase:

$$K_d = \frac{C_0 - C_e}{C_e} \cdot \frac{V}{m}$$

To further assess the preference of an adsorbent towards a specific metal, the separation factor is often used, being the ratio of the distribution coefficients of the respective metals:

$$SF_{a/b} = \frac{K_{d,a}}{K_{d,b}}$$

## 7.3 Results and Discussion

### 7.3.1 Material characterization

During the different stages of the functionalization process (Figure 7.3), the MIL-101 is properly characterized with: (1) N<sub>2</sub> sorption measurements; (2) DRIFTS-analyses; (3) CHNS analyses to quantify the nitrogen content; (4) XRF-measurements to quantify the phosphorous content (and thereby estimate the ligand loading); (5) XRD measurements to assess the stability of the material in each step. Table 7.1 gives a quantitative overview of the stepwise functionalization procedure, based on CHN- and XRF-results, as well as the numeric evolution of Langmuir surface area and total pore volume.

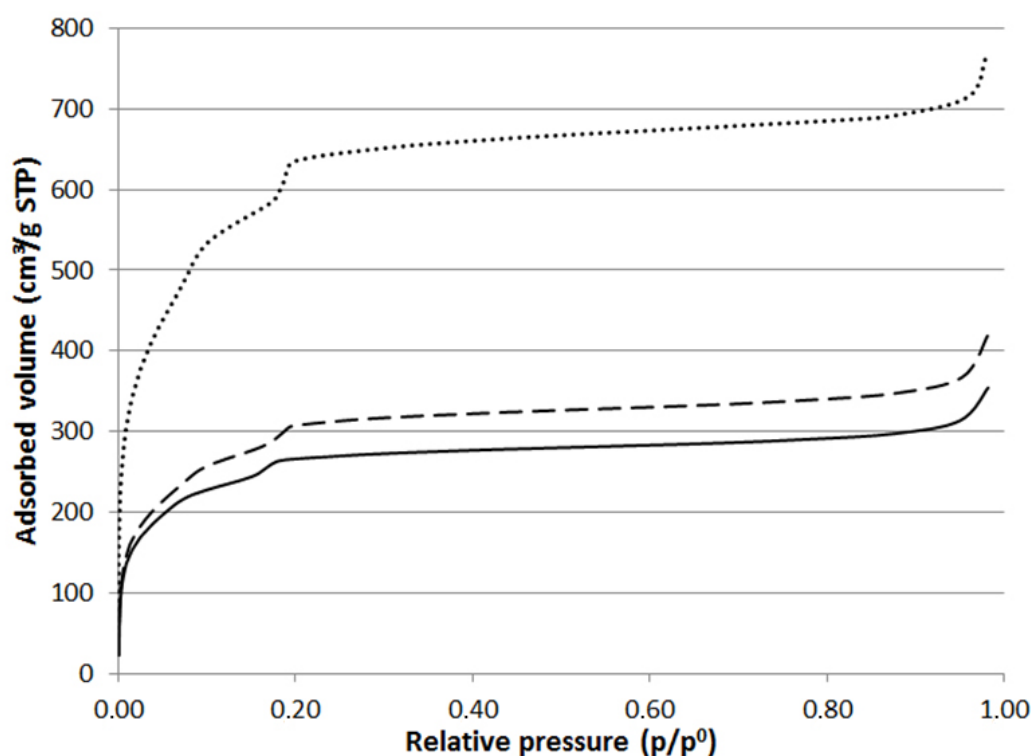
**Table 7.1 Quantitative overview of the MIL-101(Cr) functionalization**

	S <sub>Langmuir</sub> (m <sup>2</sup> /g)	V <sub>p</sub> (cm <sup>3</sup> /g)	Wt.% N	mmol diamine/g	Wt.% P	mmol CMPO/g
MIL-101	3105	1.36	0.39%	-	ND	-
MIL-101- Cl <sup>(1)</sup>	3063	1.35	0.29%	-	ND	-
MIL-101- NH <sub>2</sub>	1696	0.85	5.20%	1.8	ND	-
MIL-101- LIG	1390	0.57	4.42% <sup>(2)</sup>	1.5 <sup>(2)</sup>	1.55%	0.5

(1) Chlorine analyses were omitted as they proved to be unreliable since the MOF's counter ions influence the result considerably. (2) The apparent small reduction in nitrogen content is due to the weight increase after finalizing the CMPO ligand. ND: Not Detected.

Table 7.1 shows that the specific surface area of the MOF, as well as its pore volume gradually decreases throughout the functionalization process. This is also shown in Figure 7.4. Starting out at S<sub>Langmuir</sub>: 3000 ± 200 m<sup>2</sup>/g (throughout different batches), the MIL-101 decreases in specific surface area upon each step due to anchored species that fill up the cages and increase the weight of the material. The decrease of total pore volume confirms these findings. The isotherm of the chloromethylated MIL-101 (MIL-101-Cl) practically overlaps the original MIL-101 isotherm and was therefore omitted from Figure 7.4 for clarity reasons. Desorption isotherms were omitted as well, as they completely overlap the adsorption isotherms. The

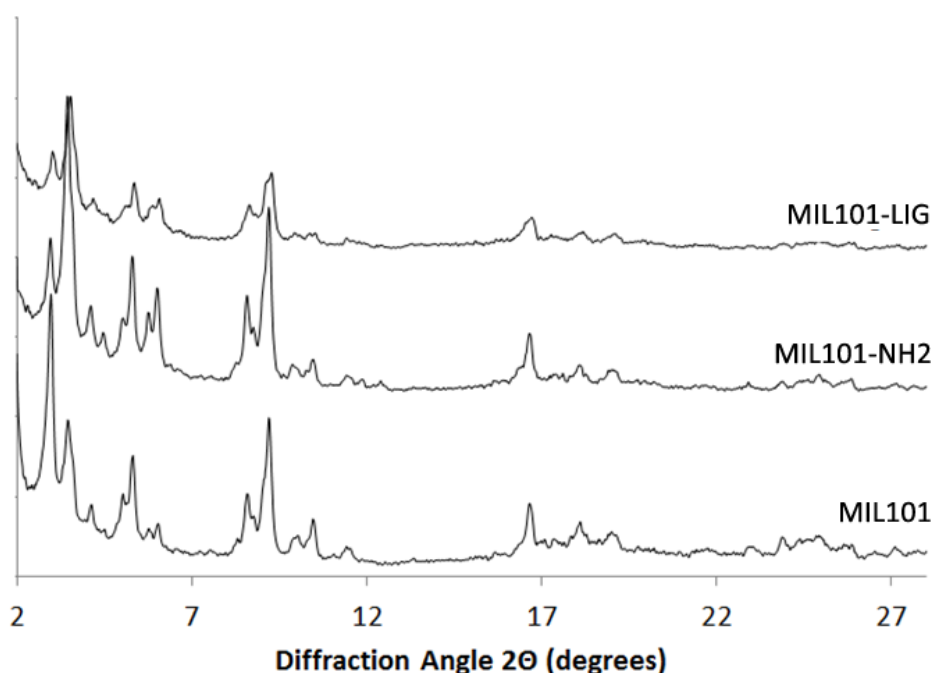
amination of the material with diaminobutane (MIL-101-NH<sub>2</sub>) appears to have the largest effect on the specific surface area and pore volume. The final anchoring step results in a less pronounced decrease in specific surface area and pore volume (MIL-101-LIG). This could be due to a combination of differences in ligand flexibility and interaction with the nitrogen, but above all the fact that not all free amine groups have reacted into the full CMPO ligand. The characteristic shape of the isotherms already indicates indirectly that the support withstands the reaction conditions, and maintains its ordered porous structure. The MIL-101 isotherm can in general be interpreted as a Type I isotherm, however, small capillary condensation steps can be discerned at relative pressures of  $P/P^0 \sim 0.1$  and at  $P/P^0 \sim 0.2$ [18]. These originate from the two mesoporous cages (2.9 and 3.4 nm). The experimental mesopore sizes of the pristine MIL-101(Cr) were calculated at 2.4 and 3.0 nm, respectively, which is in agreement with literature [33]. Throughout the functionalization process, a slight shift can be noticed in the capillary condensation steps towards lower relative pressures. This indicates a decrease in mesopore size. After complete ligand anchoring, we observed this shift for the large cage size to smaller diameters (3.00 to 2.76 nm), however, information about the smaller cage size could not be discerned properly from the pore size distribution plot, perhaps because its diameter decreased to the (near) micropore range. These data, as well as desorption plots, are provided in Appendix 2.3 and 2.4.



**Figure 7.4** Nitrogen adsorption isotherm of the unfunctionalized MIL-101 (•), aminated MIL-101 (--) and finalized ligand MIL-101 (—).

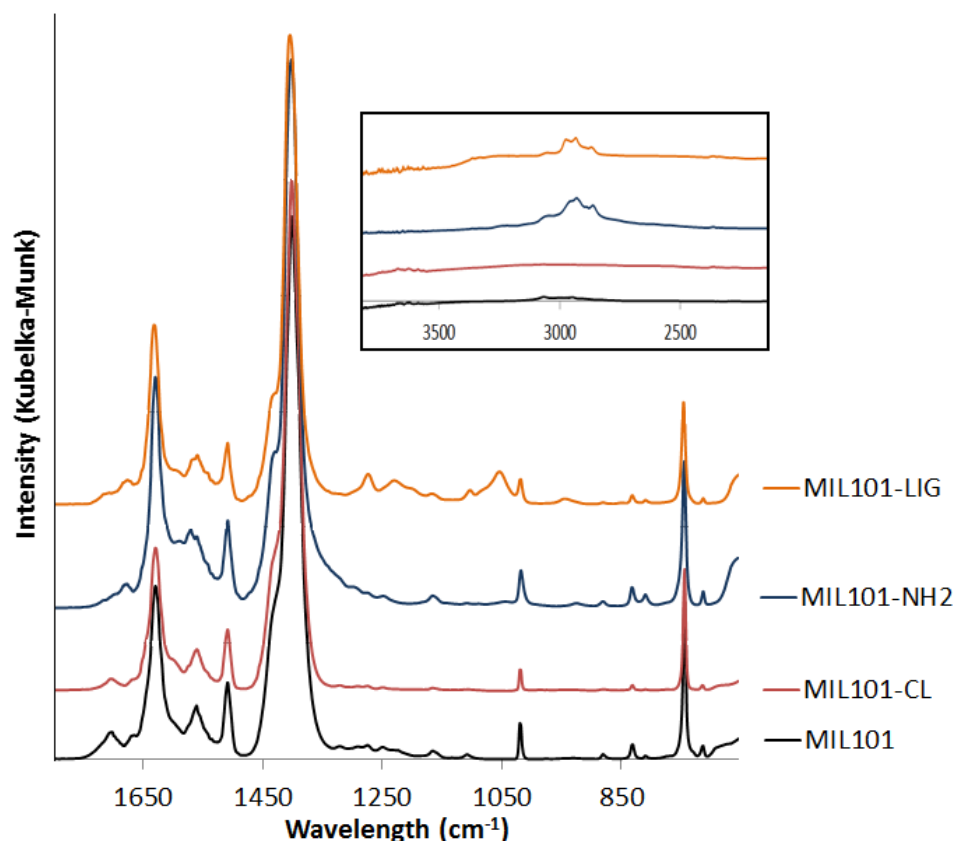


Figure 7.5 shows the powder-XRD patterns of the MOF throughout the functionalization procedure. The characteristic reflections of the MIL-101 are well preserved after each reaction step and no new reflections arise, which further confirms that the MIL-101 perfectly maintains its structure throughout the functionalization process, without formation of new crystalline phases.



**Figure 7.5 Powder XRD patterns of the (un)functionalized materials.**

In the DRIFTS spectra (Figure 7.6), aliphatic CH stretches can be observed between  $2850 - 3000\text{ cm}^{-1}$  (inset), which confirms the presence of diaminobutane in the aminated sample and the final adsorbent. An indication of amine groups is visible near  $1550$  and  $1650\text{ cm}^{-1}$ , corresponding to primary- $\text{NH}_2$  scissoring. These do not appear as isolated peaks but partially overlap with vibrations originating from the MIL-101 structure. In the spectrum of the finalized adsorbent, vibrations are visible at  $1040\text{ cm}^{-1}$  and in the region between  $1200$  and  $1260\text{ cm}^{-1}$ . These indicate the P-OR ester and the phosphine oxides or phosphonates vibrations, respectively. Presence of other characteristic peaks could not be proven unambiguously due to overlap with the MIL-101 structural vibrations and possible low loading. Through CHNS analysis, it was found that the sample contained approx. 5 wt.% additional nitrogen after the amination step (Table 7.1), corresponding to  $1.8 \pm 0.11$  mmol diaminobutane per gram. XRF-analysis showed a phosphorous-loading of  $0.5 \pm 0.15$  mmol P/g throughout different batches (Table 1). This leads to a functionalization grade of  $\sim 12\%$  of complete CMPO ligands based on the present aromatic rings in the MIL-101 structure.



**Figure 7.6** DRIFTS spectra of each step in the functionalization. Inset: zoom on the aliphatic stretch region.

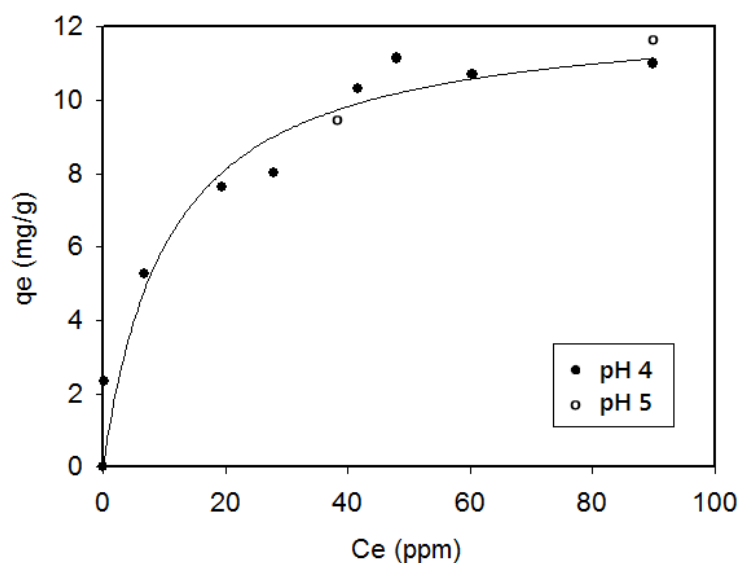
### 7.3.2 Adsorbent stability

In order to assess the material's stability in the adsorption media, post-contact XRD and XRF measurements have been performed, after filtration of the solid material and subsequent rinsing with distilled water and acetone, followed by vacuum drying at 120°C for 24 hours. XRD showed no loss of crystallinity, showing that the functionalized MOF perfectly survives the various applied conditions during the experiments (HCl (aq), pH 0 – 5). XRF was used to calculate the ligand loading via phosphorous content. Leaching was typically in the order of 5% (e.g. reduction 0.4 mmol P/g to 0.38 mmol P after 24 hours, showing that these ligands are strongly bonded to the support. Additionally, nitrogen sorption experiments were carried out to further investigate the structural stability of the adsorbent after contact with acidic europium solution. The results are shown in Appendix 2.5 and 2.6. As can be seen, the characteristic MIL-101 isotherm shape is retained, proving the stability of the adsorbent.

### 7.3.3 Sorption Isotherm

The europium adsorption isotherm is shown in Figure 7.7. A continuous increase of Eu(III) adsorption with increasing initial europium concentrations was observed. The adsorption isotherm has a good correlation to the Langmuir model ( $R^2 > 95\%$ ) and a maximum adsorption

capacity ( $q_{\max}$ ) of 12.46 mg Eu/g (or 0.082 mmol Eu/g) was calculated. The Langmuir model is appropriate as it concerns metal adsorption through complexation. A fit to the Freundlich model yielded a good correlation ( $R^2 > 95\%$ ) as well (results not shown), however, seems less probable due to the reason stated above. In addition, the adsorption capacity of the chloromethylated and aminated MIL-101 was measured as well, by saturating the materials with a 100 ppm  $\text{Eu}^{3+}$  solution (L/s: 1000 mL/g, pH 4, 24 hrs). The chloromethylated and aminated MIL-101s adsorbed no Eu(III), which confirms that only the fully intact CMPO ligands are active in the Eu adsorption and that the MIL-101 support itself has no europium uptake. As a preliminary pH-influence experiment, two isotherm points were tested a pH 5 instead of 4 ( $C_0$  50 ppm, resp. 100 ppm) and are shown in Figure 7.7 as well. These points were not included in the model fitting. No significant difference in equilibrium uptake was observed. Drawing a comparison to results from literature is not straightforward as the experiments are often completely different in method or adsorbent characteristics (structure, porosity, ligand type and loading,...). Pietrelli *et al.* investigated the sorption behavior of a CMPO loaded silica phase for europium in extraction chromatography[31]. The material contained 1.2 mmol CMPO/g and was used in an equilibrium study in 3 M  $\text{HNO}_3$ . The calculated maximum uptake through the Langmuir model was 0.206 mmol Eu/g (31 mg Eu/g) or a standardized capacity of 26 mg Eu per mmol of ligands. In our case, a calculated uptake of 12.46 mg Eu/g with 0.5 mmol CMPO/g corresponds to 25 mg Eu per 1 mmol CMPO, which is nearly the same. As mentioned before, also Fryxell *et al.* used CMPO loaded silica (SAMMS) in europium adsorption experiments, but their scope was mainly focused on maximum removal of trace concentrations ( $\leq 2$  ppm) and no europium isotherms were reported to our knowledge.



**Figure 7.7** Eu(III) adsorption isotherm w/ Langmuir fit (•) of the CMPO functionalized MIL-101 (average values of duplicates). pH = 4, L/s = 1000 mL/g, T = 25 °C. pH 5 influence check (◦).

### 7.3.4 Selectivity experiments

Table 7.2 shows the selectivity results with CMPO@MIL-101, using both distribution coefficients ( $K_d$ ) and separation factors (SF) to assess the performance. We opted to work in ~100 ppm conditions, as to simulate real life aqueous streams conditions, e.g., waste streams from solvent extractions. However, in such saturated solutions (in our case 150 ppm total metal concentration),  $K_d$  values are lower, as a fraction of the present metals in solution already occupies all available adsorption sites. This can give a distorted view on the selectivity of the material. In this case, separation factors are a more tangible quantity to represent the selectivity performance. Nonetheless, both parameters are presented in Table 7.2.

The CMPO functionalized MOF has a high affinity for europium ( $K_d$ : 149 mL/g), a much lower affinity for yttrium ( $K_d$ : 48 mL/g), and a very low affinity for zinc ( $K_d$ : 17 mL/g). In terms of selectivity, this means that the adsorbent has got a considerable selectivity between the REEs europium and yttrium ( $SF_{Eu/Y}$ : 3.2) and a high preference for europium over the transition metal zinc ( $SF_{Eu/Zn}$ : 8.5).

**Table 7.2 Selectivity results of CMPO@MIL-101(Cr), ( $C_0_{Eu} = C_0_Y = C_0_{Zn} \approx 50$  ppm, pH = 5,  $t = 24$  hrs,  $L/S = 400$  mL/g,  $T = 25$  °C).**

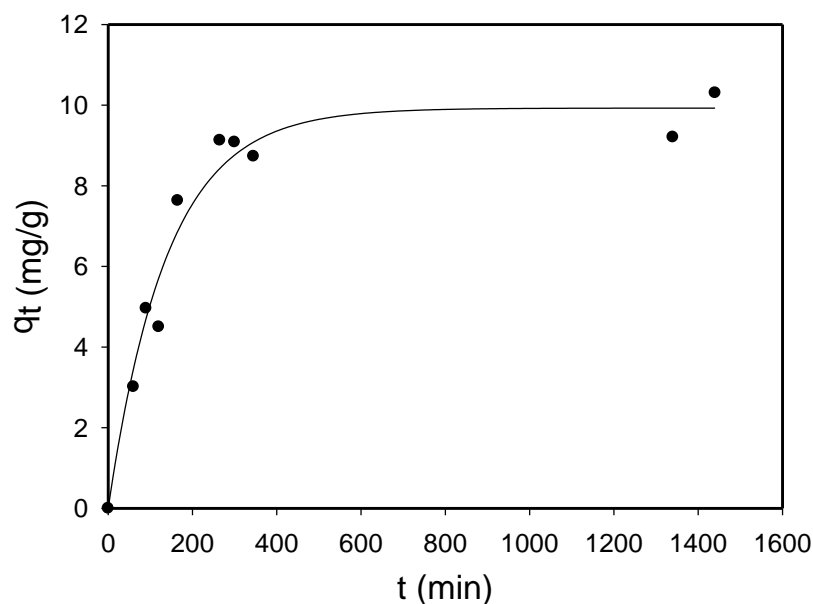
x	$K_d$ (mL/g)	$SF_{Eu/x}$
Eu	149	-
Y	48	3.2
Zn	17	8.5

### 7.3.5 Sorption Kinetics

The uptake kinetics for Eu(III) at room temperature (25°C) for CMPO@MIL-101(Cr) are presented in Figure 7.8. Adsorption equilibrium is achieved within 5 hours. Given the high initial concentration[32], the Lagergren pseudo-first-order kinetics model was fitted to the experimental data ( $R^2$ : 96.5%), which is given as:

$$\frac{dq}{dt} = k(q_e - q_t)$$

Where  $q_t$  is the adsorption capacity at time  $t$  (mg/g), and  $k$  is pseudo-first-order rate constant ( $\text{min}^{-1}$ ). A  $q_e$  of 9.93 mg/g was found ( $k$ :  $0.0071 \text{ min}^{-1}$ ), which is in line with the values obtained from the Eu isotherm.



**Figure 7.8** Eu(III) adsorption kinetics with CMPO@MIL-101(Cr) ( $C_0 = 50$  ppm, pH = 4, L/S = 1000 mL/g, T = 25 °C).

## 7.4 Conclusion

We have demonstrated that the metal-organic-framework MIL-101(Cr) is an excellent candidate for applications in aqueous adsorption. The material possesses all the required characteristics of a good supporting material (stability, porosity, functionalizability, hydrophilicity) for uses in pH 4 – 5 acidic water. Carbamoylmethylphosphine oxide type ligands (CMPO) were successfully anchored in a stepwise, covalent manner onto the MOF matrix, with a yield of  $0.5 \pm 0.15$  mmol/g. Acidic aqueous solutions did not influence the matrix in any way, and minimal ligand leaching was observed. As a proof of concept, the novel material was used in the adsorption of the rare earth element europium from acidic aqueous solutions (pH 4 – 5). An equilibrium study was performed yielding an isotherm that correlates well to the Langmuir model, suggesting a theoretical maximum uptake of 12.45 mg Eu/g. Selectivity tests of europium in the presence of yttrium and zinc showed a high separation factor for Eu over Zn ( $SF_{Eu/Zn}$ : 8.5) and even a considerable separation between Eu and Y ( $SF_{Eu/Y}$ : 3.2). Kinetic experiments for europium showed that equilibrium is reached within 5 hours. This shows that the MIL-101(Cr) is a suitable candidate as a support in the field of liquid adsorption, as it can be readily functionalized with rare earth selective ligands and used as a REE adsorbent in acidic (pH 4 – 5) aqueous environment.

## REFERENCES

- [1] E. Alonso, A.M. Sherman, T.J. Wallington, M.P. Everson, F.R. Field, R. Roth, R.E. Kirchain, Evaluating Rare Earth Element Availability: A Case with Revolutionary Demand from Clean Technologies, *Environ Sci Technol*, 46 (2012) 4684-4684.
- [2] A. Jordens, Y.P. Cheng, K.E. Waters, A review of the beneficiation of rare earth element bearing minerals, *Miner Eng*, 41 (2013) 97-114.
- [3] P. Falcaro, R. Ricco, C.M. Doherty, K. Liang, A.J. Hill, M.J. Styles, MOF positioning technology and device fabrication, *Chem Soc Rev*, 43 (2014) 5513-5560.
- [4] G. Ferey, M. Latroche, C. Serre, F. Millange, T. Loiseau, A. Percheron-Guegan, Hydrogen adsorption in the nanoporous metal-benzenedicarboxylate  $M(OH)(O_2C-C_6H_4-CO_2)$  ( $M = Al^{3+}, Cr^{3+}$ ), MIL-53, *Chem Commun*, (2003) 2976-2977.
- [5] J.L.C. Rowsell, E.C. Spencer, J. Eckert, J.A.K. Howard, O.M. Yaghi, Gas adsorption sites in a large-pore metal-organic framework, *Science*, 309 (2005) 1350-1354.
- [6] S. Bhattacharjee, D.A. Yang, W.S. Ahn, A new heterogeneous catalyst for epoxidation of alkenes via one-step post-functionalization of IRMOF-3 with a manganese(II) acetylacetonate complex, *Chem Commun*, 47 (2011) 3637-3639.
- [7] J. Gascon, U. Aktay, M.D. Hernandez-Alonso, G.P.M. van Klink, F. Kapteijn, Amino-based metal-organic frameworks as stable, highly active basic catalysts, *J Catal*, 261 (2009) 75-87.
- [8] J. Lee, O.K. Farha, J. Roberts, K.A. Scheidt, S.T. Nguyen, J.T. Hupp, Metal-organic framework materials as catalysts, *Chem Soc Rev*, 38 (2009) 1450-1459.
- [9] R. Kitaura, K. Seki, G. Akiyama, S. Kitagawa, Porous coordination-polymer crystals with gated channels specific for supercritical gases, *Angew Chem Int Edit*, 42 (2003) 428-431.
- [10] D.A. Yang, H.Y. Cho, J. Kim, S.T. Yang, W.S. Ahn, CO<sub>2</sub> capture and conversion using Mg-MOF-74 prepared by a sonochemical method, *Energ Environ Sci*, 5 (2012) 6465-6473.
- [11] E. Haque, J.W. Jun, S.H. Jung, Adsorptive removal of methyl orange and methylene blue from aqueous solution with a metal-organic framework material, iron terephthalate (MOF-235), *J Hazard Mater*, 185 (2011) 507-511.
- [12] E. Haque, N.A. Khan, J.E. Lee, S.H. Jung, Facile Purification of Porous Metal Terephthalates with Ultrasonic Treatment in the Presence of Amides, *Chem-Eur J*, 15 (2009) 11730-11736.
- [13] S.H. Jung, J.H. Lee, J.W. Yoon, C. Serre, G. Ferey, J.S. Chang, Microwave synthesis of chromium terephthalate MIL-101 and its benzene sorption ability, *Adv Mater*, 19 (2007) 121.
- [14] S.M. Humphrey, P.T. Wood, Multiple areas of magnetic bistability in the topological ferrimagnet  $[Co_3(NC_5H_3(CO_2)_2)_2(\mu_3-OH)_2(OH_2)_2]$ , *J Am Chem Soc*, 126 (2004) 13236-13237.
- [15] A. Dhakshinamoorthy, A.M. Asiri, H. Garcia, Catalysis by metal-organic frameworks in water, *Chem Commun*, 50 (2014) 12800-12814.
- [16] N.A. Khan, Z. Hasan, S.H. Jung, Adsorptive removal of hazardous materials using metal-organic frameworks (MOFs): A review, *J Hazard Mater*, 244 (2013) 444-456.
- [17] B. Hu, M. He, B.B. Chen, Nanometer-sized materials for solid-phase extraction of trace elements, *Anal Bioanal Chem*, 407 (2015) 2685-2710.
- [18] G. Ferey, A chromium terephthalate-based solid with unusually large pore volumes and surface area (vol 309, pg 2040, 2005), *Science*, 310 (2005) 1119-1119.
- [19] R.B. Ferreira, P.M. Scheetz, A.L.B. Formiga, Synthesis of amine-tagged metal-organic frameworks isostructural to MIL-101(Cr), *RSC Advances*, 3 (2013) 10181-10184.

- [20] S. Bernt, V. Guillermin, C. Serre, N. Stock, Direct covalent post-synthetic chemical modification of Cr-MIL-101 using nitrating acid, *Chem Commun*, 47 (2011) 2838-2840.
- [21] E.P. Horwitz, R. Chiarizia, M.L. Dietz, DIPEX: A new extraction chromatographic material for the separation and preconcentration of actinides from aqueous solution, *React Funct Polym*, 33 (1997) 25-36.
- [22] M.L.P. Reddy, J.R.B. Bharathi, S. Peter, T.R. Ramamohan, Synergistic extraction of rare earths with bis(2,4,4-trimethylpentyl) dithiophosphinic acid and trialkyl phosphine oxide, *Talanta*, 50 (1999) 79-85.
- [23] Y. Masuda, Y.W. Zhang, C.H. Yan, B.G. Li, Studies on the extraction and separation of lanthanide ions with a synergistic extraction system combined with 1,4,10,13-tetrathia-7,16-diazacyclooctadecane and lauric acid, *Talanta*, 46 (1998) 203-213.
- [24] G.E. Fryxell, H. Wu, Y.H. Lin, W.J. Shaw, J.C. Birnbaum, J.C. Linehan, Z.M. Nie, K. Kemner, S. Kelly, Lanthanide selective sorbents: self-assembled monolayers on mesoporous supports (SAMMS), *J Mater Chem*, 14 (2004) 3356-3363.
- [25] B. Lambert, V. Jacques, A. Shivanyuk, S. Matthews, A. Tunay, M. Baaden, G. Wipff, V. Bohmer, J.F. Desreux, Calix[4]arenes as Selective Extracting Agents. An NMR Dynamic and Conformational Investigation of the Lanthanide(III) and Thorium(IV) Complexes, *Inorg Chem*, 39 (2000) 2033 - 2041.
- [26] J. Florek, F. Chalifour, D. Larivière, F. Kleitz, Nanostructured Hybrid Materials for the Selective Recovery and Enrichment of Rare Earth Elements, *Adv Funct Mater*, 24 (2014) 2668–2676.
- [27] M. Cypryk, Y. Apeloig, Mechanism of the Acid-Catalyzed Si-O Bond Cleavage in Siloxanes and Siloxanols. A Theoretical Study, *Organometallics*, 21 (2002) 2165 - 2175.
- [28] D.M. Jiang, A.D. Burrows, K.J. Edler, Size-controlled synthesis of MIL-101(Cr) nanoparticles with enhanced selectivity for CO<sub>2</sub> over N<sub>2</sub>, *Crystengcomm*, 13 (2011) 6916-6919.
- [29] M.G. Goesten, K.B.S.S. Gupta, E.V. Ramos-Fernandez, H. Khajavi, J. Gascon, F. Kapteijn, Chloromethylation as a functionalisation pathway for metal-organic frameworks, *Crystengcomm*, 14 (2012) 4109-4111.
- [30] J. Podlech, *Synthesis of Peptides and Peptidomimetics* 4ed., Thieme, Stuttgart, 2001.
- [31] L. Pietrelli, A. Salluzzo, F. Troiani, Sorption of Europium and Actinides by Means of Octyl(Phenyl)-N,N-Diisobutyl Carbamoylmethyl Phosphine Oxide (Cmpo) Loaded on Silica, *J Radioan Nucl Ch Ar*, 141 (1990) 107-115.
- [32] S. Azizian, Kinetic models of sorption: a theoretical analysis, *J Colloid Interf Sci*, 276 (2004) 47-52.
- [33] X. Zhou, W. Huang, J. Shi, Z. Zhao, Q. Xia, Y. Li, H. Wang, and Z. Li, A novel MOF/graphene oxide composite GrO@MIL-101 with high adsorption capacity for acetone, *J Mater Chem A*, 2 (2014) 4722-4730.





# 8 CMPO-FUNCTIONALIZED MIL-101(Cr) AS HIGHLY SELECTIVE URANIUM ADSORBENT

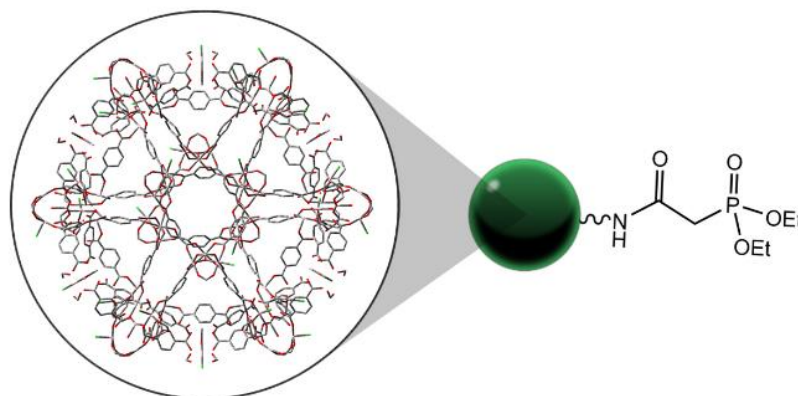
De Decker, J., Rochette, J., De Clercq, J., Florek, J., and Van Der Voort, P. **Analytical Chemistry** (2017) In press. **Contribution:** Synthesis, Characterization.

## 8.1 Introduction

Continuous development of innovative technologies, such as hybrid cars, wind turbines, fiber-optics, lighting devices, flat-screens TVs or fuel cells, created growing demand for rare earth elements (REE)[1]. Predominantly, the more valuable heavy elements (HREE) are a critical resource (*i.e.*, HREE, from gadolinium to lutetium). The ion-adsorption clays, found in southern China, are the main source for heavy rare earths production in the world[2, 3]. These clay deposits are mined by open pit methods and frequently require no ore beneficiation. Simple leaching processes, using monovalent sulfate or chloride salt solutions at ambient temperature, can produce a high grade rare earth oxide (REO) product[4]. The adsorption clays, however, often contain small amounts of uranium and thorium oxides (ppm level), for which no radiation measures are taken, due to their low concentration[2, 3]. In the conventional rare earth ores, such as xenotime, there is a considerable amount of uranium present (up to 5 % oxides[5]) which is deemed high enough to invest in uranium recovery as a by-product for uses in nuclear

fuel[2]. Ores such as monazite can contain up to 16 % uranium oxides and 20 % thorium oxides[5]. Therefore, a combination of several aspects, such as reduced radio-toxicity to the environment, potentially higher grade of the REO product or the increasing demand for uranium in the nuclear industry can justify a selective uranium and/or thorium recovery method in the processing of ion-adsorption clays. As the concentration is typically at ppm levels, selective adsorption might be an ideal solution to recover the metals, whether it is applied to pre-treat the leachate solutions and purify them from these radioactive elements, or to manage the generated waste streams (after selective rare earth recovery). Furthermore, selective U/Th adsorbents could also be suitable for deployment in various aqueous environments, such as contaminated waters, waste streams from solvent extraction processes, or even in the primary uranium recovery from unconventional orebodies (*e.g.*, phosphorites, lignite, seawater)[6].

Metal-organic frameworks (MOFs) are used in an ever-increasing scope of applications, ranging from the traditional fields of gas sorption[7, 8] and catalysis[9, 10], to new applications in water-based technologies[11]. Several of these porous coordination polymers were found to be highly stable in variety of aqueous environments (acidic, alkaline), both on short and long-term[12]. Among various MOF-types, MIL-101(Cr) is a mesoporous cage-type MOF with particular high stability in the aqueous solutions[12, 13]. In addition, this material can be readily functionalized and has already been demonstrated as an efficient metal adsorbent[14, 15]. Due to its large mesoporous cages, chelating bulky ligands can be grafted onto the framework, in order to tailor the adsorption affinity towards specific metal ions. A carbamoylmethylphosphine oxide ligand type (CMPO) has already been covalently immobilized onto the MIL-101(Cr) structure via a three-step method[15]. As a proof of concept, the material, called CMPO@MIL-101(Cr) (Figure 8.1) was used to selectively adsorb the REEs europium and yttrium, from zinc in aqueous solutions. The adsorbent displayed a preferable selective uptake of europium over zinc, and to some extent, over yttrium as well. In the present work, we subjected the CMPO@MIL-101(Cr) to a detailed adsorption study to verify its performance in the selective separation of uranium from REEs, as these CMPO-type ligands are often used for selective uranium recovery[16-18]. In addition, adsorption kinetics were investigated and the optimal regeneration conditions were determined through column setup conditions.



**Figure 8.1** CMPO@MIL-101(Cr) with the magnified MIL-101 cage structure.

## 8.2 Materials and Methods

**Synthesis and Characterization.** The synthesis of CMPO@MIL-101(Cr) was performed according to De Decker *et al.*[15]. Nitrogen sorption experiments were conducted at  $-196\text{ }^{\circ}\text{C}$  (77 K) using a Belsorp-mini II gas analyzer. Samples were pre-dried at  $120\text{ }^{\circ}\text{C}$  under vacuum. The Langmuir method was used to calculate the specific surface area. Total pore volumes were estimated at  $p/p_0 = 0.98$ . Ligand loading estimation was performed via phosphorus analysis by energy-dispersive X-ray fluorescence spectrometry (Rigaku NexCG).

**Selectivity experiments.** Solutions of REEs (Y, La, Ce, Pr, Nd, Sm, Eu, Gd, Tb, Dy, Ho, Er, Tm, Yb, Lu) and U, Th in  $\text{HNO}_3$  ( $\text{pH} = 4$ ) were prepared from the standard solutions (Plasma, Cal, SCP Science), in order to obtain final metal concentrations of  $500\text{ }\mu\text{g/L}$  for each element tested. The same procedure was used to obtain a solution with respective metal concentrations of  $10\text{ mg/L}$ . The liquid/solid ratio was fixed to  $500\text{ mL/g}$  (L/S). The samples ( $10\text{ mg}$ ) were stirred in an orbital shaker for  $30\text{ min}$  at room temperature ( $25\text{ }^{\circ}\text{C}$ ) and subsequently the supernatant was filtered through a  $0.2\text{ }\mu\text{m}$  syringe filter. The equilibrium time for all experiments was selected based on our previous studies[19-21]. All experiments were performed in triplicate and the average values are reported. The initial and final metal concentrations in solution were determined by ICP-OES measurements (Perkin Elmer, Optima 3000).

**Kinetic Experiments.** Kinetic experiments were performed with three different initial U(VI) concentrations ( $50$ ,  $100$ , and  $150\text{ mg/L}$ , respectively). Six different contact times were considered ( $1$ ,  $3$ ,  $5$ ,  $10$ ,  $20$ ,  $30\text{ minutes}$ ), with an individual vial for each contact time. Experimental conditions ( $\text{pH}$ , shaking, L/S ratio, temperature, filtration) were kept identical to the selectivity experiment conditions. The initial and final metal concentrations in solution were determined by ICP-OES (Perkin Elmer, Optima 3000).

**Adsorbent reusability experiments.** All studies were performed in column setup, using a 2 mL column cartridge with an inner diameter of 8 mm (Eichrom Technologies, USA). The column was packed using the slurry packing technique described in Lebed *et al.* (peristaltic pump Minipuls 3, Gilson, USA)[21]. In each experiment 10 mg of adsorbent was loaded into the column and conditioned with HNO<sub>3</sub> at a specific pH. All solutions were passed through the column at a nominal flow rate of 1 mL/min and the collected fractions were analyzed by ICP-OES (Perkin Elmer, Optima 3000). Each test was performed in triplicate and the average values are reported. In a typical experiment, the adsorbent was conditioned with 10 mL HNO<sub>3</sub> solution at pH 4 and both adsorption and desorption took place at pH 4. In the adsorption phase, 15 mL of uranium solution (100 mg/L, pH 4) was passed through the column and collected in fractions. The uranium loaded on the adsorbent was then eluted from the column with 15 mL of 0.1 M ammonium oxalate solution at pH 4. Afterwards, the column was reconditioned with 10 mL nitric acid (pH 4). The above mentioned loading/regeneration cycle was repeated four additional times. Experiments in pH 2 with 0.1 and 1 M oxalate solution were performed in analogue fashion.

### 8.3 Results and Discussion

The material characteristics of the synthesized CMPO@MIL-101 are summarized in Table 1. The obtained ligand loading lies in line with the reported loading range (*i.e.*,  $0.5 \pm 0.15$  mmol CMPO/g)[15]. The adsorbent was subjected to a comprehensive selectivity study, where the affinity towards U(VI) over various rare earth metals and thorium was investigated (Figure 8.2). The adsorption performance for a specific cation was evaluated in terms of  $K_d$  values. The  $K_d$  expresses the distribution coefficient, which is calculated by the following expression[14, 15, 19, 22]:

$$K_d = \frac{C_0 - C_e}{C_e} \cdot \frac{V}{m}$$

Where  $C_0$  and  $C_e$  are the initial and final metal concentrations in solution (mg/L), respectively, and  $V$  and  $m$  are the solution volume (mL) and adsorbent mass (mg), respectively.

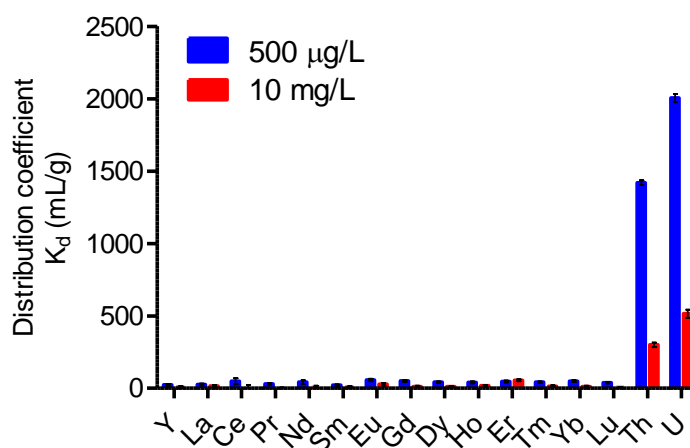
A significant selectivity towards uranium is observed, with  $K_d$  values over 2000 mL/g. A high affinity for thorium ( $K_d > 1400$  mL/g) was observed as well. In this multi-element solution, the rare earths are a lot less favored by the adsorbent (REE  $K_d < 60$  mL/g) when in competition with U/Th (Appendix 3.1).

**Table 8.1 Characterization results of CMPO@MIL-101(Cr) by N<sub>2</sub>-physisorption and XRF.**

	Surface area <sup>a</sup> (m <sup>2</sup> /g)	Pore Volume (cm <sup>3</sup> /g)	Phosphorous content (wt. %)	CMPO loading (mmol/g)
CMPO@MIL-101(Cr)	1237	0.51	1.7	0.54

<sup>a</sup> Langmuir model

As expected, when the initial metal concentration is increased from 500 µg/L to 10 mg/L, the  $K_d$  values for almost all competing elements decrease. Nonetheless, a similar selectivity pattern between the elements is obtained, indicating that the adsorbent has a high preference for uranium, as well as thorium, over competing elements. The reported moderate differentiation between europium and yttrium[15], is observed in these experiments as well. Selectivity experiments with the pristine MIL-101(Cr) were carried out as well (Appendix 3.2). It was found that the unfunctionalized material loses its selectivity for uranium, however, interestingly enough; the MIL-101 appeared to be quite active for thorium adsorption. This phenomenon could be further investigated in future work. Nonetheless, this experiment confirms that only after CMPO anchoring, the material becomes a selective adsorbent for uranium.

**Figure 8.2 Selectivity results of CMPO@MIL-101(Cr). Zoom on the competing elements: Appendix 3.1).**

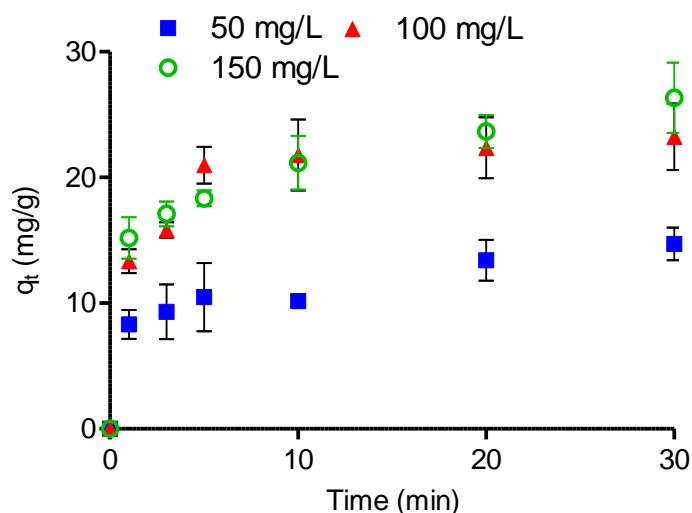
The kinetics of uranium adsorption with CMPO@MIL-101(Cr) were investigated with three different initial U(VI) concentrations (*i.e.*, 50, 100, 150 mg/L) (Figure 8.3). Within the first five minutes, a high initial uptake rate is observed in all three cases. Afterwards, the adsorption gradually increases. The high initial adsorption rate makes the adsorbent suitable for uses in adsorption column setups[23]. The effect of the initial concentration on the adsorption is also

apparent. Where there is a clear uptake difference ( $q_t$ , mg/g) after 30 minutes between initial U(VI) concentrations of 50 and 100 mg/L, the kinetic profiles of 100 mg/L and 150 mg/L are closer to each other. The former indicates that the initial U(VI) concentration serves as an important driving force in overcoming the mass transfer resistance of U(VI) between the aqueous and solid phase, where a higher concentration gradient leads to an increased interaction between U(VI) ions and the free adsorption sites[24]. At initial U(VI) concentrations of 100 mg/L, it appears that the maximum adsorption capacity is achieved, *i.e.*, the plateau of the adsorption isotherm might have been reached, since an increase in initial concentration (+50%) does not significantly influence the U(VI) uptake. The gradual increase in uptake after the initial high adsorption rate (first few minutes), might be explained by gradual physisorption of a small fraction of hydroxylated uranium species (which are present at pH 4 or higher) on the MIL.101 scaffold, as described by Krestou *et al.*[27] and Bai *et al.*[14] (also see Chapter 9).

Because of the fast adsorption kinetics of CMPO@MIL-101(Cr), a comprehensive adsorption/desorption study was performed in a column setup. Ammonium oxalate solution was chosen as a regenerant owing to its strong chelating properties[25]. Five adsorption/desorption cycles were performed, using 0.1 M oxalate solution at pH 4 as stripping agent. A consistent full desorption was observed in each cycle (Figure 8.4). Furthermore, the regeneration with the oxalate solution at pH 2 was investigated as well. At this pH, a 0.1 M oxalate solution was not able to desorb all uranium, with an increasing uranium fraction remaining on the adsorbent (Appendix 3.3). This can be expected since the oxalate species at pH 2 are present mostly in their protonated form (*i.e.*, as bioxalate [ $\text{HC}_2\text{O}_4^-$ ]), whereas at pH 4 the oxalate is deprotonated and better stripping ability is expected[26] (Appendix 3.4). When increasing the molarity of the oxalate solution at this pH, from 0.1 M to 1 M, high regeneration percentages are once again achieved (>95 %) (Appendix 3.5). Nevertheless, the regeneration at pH 4 with 0.1 M oxalate solution is preferable since a lower concentration is already sufficient to obtain 100 % regeneration throughout each cycle.

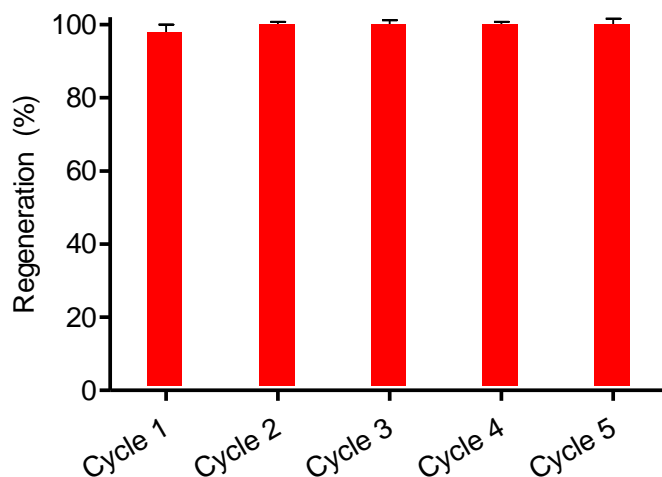
To confirm the stability of CMPO@MIL.101(Cr) after U column extraction studies in acidic pH, characterizations of the used material were performed. The PXRD results show that the adsorbent greatly maintains its crystalline structure throughout the adsorption/desorption process in acidic pH (Appendix 3.6). FTIR analysis qualitatively confirms the presence of the organic CMPO ligand, both before and after the adsorption studies (Appendix 3.7). A slight increase in Langmuir specific surface area and pore volume was noticed after the 5-cycle column experiment (Appendix 3.8), which could indicate some ligand leaching. To confirm this, TGA and powder XRF analyses were performed to, respectively; verify the impact of the MOF functionalization and subsequent adsorption studies on its characteristic decomposition pattern, and to quantify possible leaching. TGA results (Appendix 3.9) showed that the anchored ligand provided an additional stability to the material, with framework collapse taking

place at much higher temperatures. The adsorbent after use in the column experiments still showed increased stability compared to the pristine MOF, albeit less pronounced than the fresh adsorbent, confirming the presumption of ligand leaching. XRF analyses (Appendix 3.8) confirmed a ~15 wt. % loss of ligands after the 5-cycle column experiment. Other stripping agents than oxalate, e.g., dilute mineral acids, could be explored in the future to verify their impact on this leaching.



**Figure 8.3 Experimental kinetic profiles for U(VI) adsorption with CMPO@MIL-101(Cr) using three different uranium concentrations.**

We have studied the use of CMPO@MIL-101(Cr) as an efficient uranium adsorbent in aqueous, acidic environment. The MOF based material, which consists of covalently anchored carbamoylmethylphosphine oxide (CMPO) type ligands onto the MIL-101 structure, shows a high selectivity for both uranium ( $K_d > 2000$  mL/g) and thorium ( $K_d > 1400$  mL/g) over various rare earths (REE  $K_d < 60$  mL/g). Fast adsorption kinetics were observed both in batch setup as well as under dynamic flow conditions (column setup). Column conditions were also used for a comprehensive reusability study, in which uranium was first adsorbed at ppm levels, followed by complete regeneration with oxalate solution. Optimal conditions were achieved at pH 4, using 0.1 M oxalate solution, leading to a minimum of five consistent adsorption/desorption cycles. These combined adsorption results suggest that CMPO@MIL-101(Cr) is a suitable material for selective low-concentration recovery (ppm range) of uranium and/or thorium from various aqueous environments, such as contaminated waters, waste streams from solvent extraction processes, or even in the processing of REE-rich adsorption clays.



**Figure 8.4** Regeneration results per cycle for CMPO@MIL-101, using 0.1 M oxalate solution (pH 4) via column setup.

## REFERENCES

- [1] Rare Earths Industry - Technological, Economic, and Environmental Implications, Elsevier, 2016.
- [2] Z.W. Zhu, Y. Pranolo, C.Y. Cheng, Separation of uranium and thorium from rare earths for rare earth production - A review, *Miner Eng*, 77 (2015) 185-196.
- [3] S. Maes, W.-Q. Zhuang, K. Rabaey, L. Alvarez-Cohen, T. Hennebel, Concomitant leaching and electrochemical extraction of Rare Earth Elements from monazite, *Environ Sci Technol*, 51 (2017) 1654–1661.
- [4] V.G. Papangelakis, G. Moldoveanu, Recovery of Rare Earth Element from Clay Minerals, in: *ERES2014: 1st European Rare Earth Resources Conference*, Milos, Greece, 2014.
- [5] A. Jordens, Y.P. Cheng, K.E. Waters, A review of the beneficiation of rare earth element bearing minerals, *Miner Eng*, 41 (2013) 97-114.
- [6] Committee on Uranium Mining in Virginia, Committee on Earth Resources, Board on Earth Sciences and Resources, Division on Earth and Life Studies, National Research Council Uranium Occurrences, Resources, and Markets, in: *Uranium Mining in Virginia*, The National Academy Press, Washington, D.C., 2012.
- [7] J.R. Li, R.J. Kuppler, H.C. Zhou, Selective gas adsorption and separation in metal-organic frameworks, *Chem Soc Rev*, 38 (2009) 1477-1504.
- [8] J.R. Li, Y.G. Ma, M.C. McCarthy, J. Sculley, J.M. Yu, H.K. Jeong, P.B. Balbuena, H.C. Zhou, Carbon dioxide capture-related gas adsorption and separation in metal-organic frameworks, *Coord Chem Rev*, 255 (2011) 1791-1823.
- [9] J. Lee, O.K. Farha, J. Roberts, K.A. Scheidt, S.T. Nguyen, J.T. Hupp, Metal-organic framework materials as catalysts, *Chem Soc Rev*, 38 (2009) 1450-1459.
- [10] J.W. Liu, L.F. Chen, H. Cui, J.Y. Zhang, L. Zhang, C.Y. Su, Applications of metal-organic frameworks in heterogeneous supramolecular catalysis, *Chem Soc Rev*, 43 (2014) 6011-6061.
- [11] J. Canivet, A. Fateeva, Y.M. Guo, B. Coasne, D. Farrusseng, Water adsorption in MOFs: fundamentals and applications, *Chem Soc Rev*, 43 (2014) 5594-5617.



- [12] K. Leus, T. Bogaerts, J. De Decker, H. Depauw, K. Hendrickx, H. Vrielinck, V. Van Speybroeck, P. Van Der Voort, Systematic study of the chemical and hydrothermal stability of selected "stable" Metal Organic Frameworks, *Micropor Mesopor Mat*, 226 (2016) 110-116.
- [13] N.C. Burtch, H. Jasuja, K.S. Walton, Water Stability and Adsorption in Metal-Organic Frameworks, *Chem Rev*, 114 (2014) 10575-10612.
- [14] Z.Q. Bai, L.Y. Yuan, L. Zhu, Z.R. Liu, S.Q. Chu, L.R. Zheng, J. Zhang, Z.F. Chai, W.Q. Shi, Introduction of amino groups into acid-resistant MOFs for enhanced U(VI) sorption, *J Mater Chem A*, 3 (2015) 525-534.
- [15] J. De Decker, J. De Clercq, P. Vermeir, P. Van Der Voort, Functionalized metal-organic-framework CMPO@MIL-101(Cr) as a stable and selective rare earth adsorbent, *J Mater Sci*, 51 (2016) 5019-5026.
- [16] Ion Exchange and Solvent Extraction: A Series of Advances, CRC Press, Florida, USA, 2009.
- [17] J. Florek, S. Giret, E. Juere, D. Lariviere, F. Kleitz, Functionalization of mesoporous materials for lanthanide and actinide extraction, *Dalton T*, 45 (2016) 14832-14854.
- [18] F.W. Lewis, M.J. Hudson, L.M. Harwood, Development of Highly Selective Ligands for Separations of Actinides from Lanthanides in the Nuclear Fuel Cycle, *Synlett*, (2011) 2609-2632.
- [19] J. Florek, F. Chalifour, F. Bilodeau, D. Lariviere, F. Kleitz, Nanostructured Hybrid Materials for the Selective Recovery and Enrichment of Rare Earth Elements, *Adv Funct Mater*, 24 (2014) 2668-2676.
- [20] J. Florek, A. Mushtaq, D. Lariviere, G. Cantin, F.-G. Fontaine, F. Kleitz, Selective recovery of rare earth elements using chelating ligands grafted on mesoporous surfaces, *RSC Advances*, 5 (2015) 103782-103789.
- [21] P.J. Lebed, J.D. Savoie, J. Florek, F. Bilodeau, D. Lariviere, F. Kleitz, Large Pore Mesoporous Organosilica-Phosphonate Hybrids as Highly Efficient and Regenerable Sorbents for Uranium Sequestration, *Chem Mater*, 24 (2012) 4166-4176.
- [22] D. Xu, X.L. Tan, C.L. Chen, X.K. Wang, Adsorption of Pb(II) from aqueous solution to MX-80 bentonite: Effect of pH, ionic strength, foreign ions and temperature, *Appl Clay Sci*, 41 (2008) 37-46.
- [23] L.S. Djokic, R. Pantovic, N. Stavretovic, R. Igc, Origin of Arsenic in Drinking Waters in the West Backa District of Serbia, in: M. Václavíková, K. Vitale, G.P. Gallios, L. Ivaničová (Eds.) *Water Treatment Technologies for the Removal of High-Toxicity Pollutants*, Springer Science, 2010, pp. 41-50.
- [24] X.T. Zhang, X.M. Wang, Adsorption and Desorption of Nickel(II) Ions from Aqueous Solution by a Lignocellulose/Montmorillonite Nanocomposite, *Plos One*, 10 (2015) 1-21.
- [25] W. Hummel, G. Anderegg, L. Rao, I. Puigdomènech, O. Toshiyama, Discussion of Data Selection for Oxalate Compounds and Complexes in: M. Illemassène, J. Perrone (Eds.) *Chemical Thermodynamics*, Elsevier, Amsterdam, The Netherlands, 2005.
- [26] J. Schijf, R.H. Byrne, Stability constants for mono- and dioxalato-complexes of Y and the REE, potentially important species in groundwaters and surface freshwaters, *Geochim Cosmochim Acta*, 65 (2001) 1037-1046.
- [27] A. Krestou, D. Panias, Uranium (VI) speciation diagrams in the  $\text{UO}_2^{2+}/\text{CO}_3^{2-}/\text{H}_2\text{O}$  systems at 25 °C, *Eur J Miner Process Environ Prot*, 4 (2004) 113-129.



# 9 SHIP-IN-A-BOTTLE CMPO IN MIL-101(CR) FOR SELECTIVE URANIUM RECOVERY FROM AQUEOUS STREAMS THROUGH ADSORPTION

De Decker, J., Folens, K., De Clercq, J., Meledina, M., Van Tendeloo, G., Du Laing, G., and Van Der Voort, P. **Journal of Hazardous Materials** 335 (2017) 1 - 9. **Contribution:** Synthesis, Characterization, Adsorption experiments.

## 9.1 Introduction

According to the International Energy Outlook Reference case (IEO2016), the total world energy consumption is projected to increase by 48% between 2012 and 2040. With renewables as the number one fastest-growing energy source, nuclear power occupies second place with a projected annual consumption increase of 2.3%. Even though the consumption of non-fossil fuels is expected to grow faster than consumption of fossil fuels, the latter will still account for 78% of the energy use in 2040[1]. Meanwhile, the world has to deal with environmental threats

caused by anthropogenic polluting emissions. Nuclear energy provides a significant part of the energy (electricity) demand, combined with a reduction in polluting emissions. Uranium fuel will remain to play a key role in energy production, with the rise of next generation light water reactors, which are expected to dominate the world market in the first half of the 21<sup>st</sup> century[2]. However, as the demand for nuclear fuel rises, equal effort should be made to close the nuclear fuel cycles (recyclability) or to optimize current processes with clear and effective waste management strategies. At the 2012 level of uranium requirements, currently identified resources (2013) are sufficient for over 120 years of supply for the global nuclear power fleet (5.9 million tons in the <USD 130/kg U category)[3]. This calls for uranium extraction and recovery from sources other than the conventional orebodies. Unconventional resources (where uranium is present as a by-product or as traces) include phosphate rocks, non-ferrous ores, carbonatite, black shale, lignite, and seawater[3-5]. With the proper (economically feasible) techniques at hand, these secondary resources could become viable orebodies.

For example, uranium occurs in all types of phosphate rocks with varying concentrations[6]. These rocks are usually leached with acids, as part of the production process of fertilizers, which eventually leads to uranium containing aqueous solutions that constitute as a secondary uranium source[7-9]. The uranium content of both the phosphate rocks, as well as the obtained leachates, lies in the ppm range[5, 9]. In addition to uranium, many other ppm-level impurities, such as Pb, Ni, Cu and Mn may be present[5]. Therefore, selective uranium recovery is necessary and currently, solvent extraction processes and precipitations techniques are typically applied (industrially) to achieve these kinds of selective separations[8, 9]. Despite their effectiveness, however, these conventional techniques usually suffer from economical and/or environmental limitations, due to the labor-intensiveness and high usage of chemicals that are inherent to the respective techniques[9-11].

In addition to being a key raw material for nuclear energy, uranium also causes a long-term potential environmental hazard because of its long half-life and high radio-toxicity[12-14]. In the case of rare earth mining, uranium is often present in the minerals via lattice substitution, resulting in radiation issues in rare earth processing[15]. Also in ion-adsorption clays, mainly found in China, there is a considerable amount of uranium present (ppm range). These clays are rich in yttrium and heavy rare earths (HREE), and are the main source for the world's HREE production. No measures are taken in controlling the uranium radiation due to its low concentrations in the clays[15]. An appropriate method to selectively separate the uranium from these valuable rare earths is therefore desired.

These are but a few examples of uranium-containing sources that would benefit from recovery techniques optimized for low concentrated, aqueous streams. Selective adsorption is an ideal technique to recover specific species from such dilute solutions. Adsorbents are readily tunable to preference and the added value of easy separation and reuse makes them perfect candidates

for this field of metal recovery. Novel adsorbents are therefore of high interest, not only to extract uranium from secondary orebodies for nuclear fuel production, but also for the removal of these toxic radionuclides from waste streams and acid mine drainage[4, 11, 16-18]. Metal-organic frameworks (MOFs) could play a big role in the development of new water-applicable adsorbents. This class of porous coordination polymers consist of highly uniform networks of inorganic metal centers (ions or clusters), bridged with polytopic organic ligands as linkers. By varying these metal centers and/or linkers, a vast amount of different MOFs can be synthesized, each with its specific physicochemical properties, including water-stable MOFs [19]. Due to this remarkable versatility, MOFs have already been applied in a broad range of research fields, such as gas storage and separation[20-23], catalysis[24, 25], separation of chemicals[26, 27], drug delivery[28, 29], magnetism[30], luminescence[31]... When dealing with aqueous metal adsorption, the conditions are often very demanding, and additional stability in acidic and/or alkaline media is required[19]. Several types of MOFs meet these criteria, such as MOF-76, (NH<sub>2</sub>-)UiO-66, NH<sub>2</sub>-MIL-53, MIL-101(Cr)...[32, 33], which often show remarkable stability even during long-term exposure to these conditions. Recently, it was reported that MOFs could be applied as potential uranium adsorbents, e.g., Zn-MOF-74, Ln-MOF-76, UiO-68, and MIL-101(Cr) have been functionalized (Zn-MOF-74, UiO-68, MIL-101) or used pristinely (Ln-MOF-76) to recover uranium from aqueous environment[32, 34-36].

In this work, we have selected MIL-101(Cr) as a highly stable, mesoporous host for the embedment of N,N-Diisobutyl-2-(octylphenylphosphoryl)acetamide (CMPO), a sterically demanding, commercially available ligand known for its high affinity with U(VI). The mesoporous zeotypic MIL-101 cages with diameters of ca. 29 and 34 Å are ideal to enclose the CMPO, while the microporous cage-apertures (12 – 16 Å) are small enough to contain it, yet large enough to facilitate the transportation of metal cations through the pore network. CMPO is often used as a highly efficient (co-)extractant for actinides and lanthanides in solvent extraction processes, such as the trans-uranium extraction process (TRUEX)[37, 38]. The CMPO ligand was embedded in the MIL-101 host, through the bottle-around-the-ship approach, in which the host is formed in-situ around the CMPO. This approach is cost- and time effective, when compared to conventional adsorbent synthesis where the host is pre-synthesized, followed by a single or multistep post-functionalization. The obtained materials were properly characterized by X-ray diffraction (XRD), nitrogen adsorption, FT-IR spectrometry, X-ray fluorescence spectrometry and a combination of ADF-STEM (annular dark field scanning transmission electron microscopy) and EDX (energy dispersive X-ray) spectroscopy. An extensive U(VI) centered adsorption study was performed, including equilibrium experiments, kinetics, selectivity, pH-influence, regeneration, and reuse, to investigate the viability of this novel material as a selective, reusable uranium adsorbent.

## 9.2 Experimental

### 9.2.1 Chemicals and Reagents

Single-element standard solutions (1000 mg/L) for ICP-OES analysis were obtained from Chem-Lab, Belgium. Uranium(VI) standard solution (10000 mg/L in 1% HNO<sub>3</sub>) was obtained from J.T.Baker, The Netherlands, and was used for adsorption experiments. N,N-Diisobutyl-2-octylphenylphosphoryl acetamide (CMPO) was obtained from Carbosynth Ltd, United Kingdom. CdSO<sub>4</sub> · 2 H<sub>2</sub>O and Al<sub>2</sub>(SO<sub>4</sub>)<sub>3</sub> · 18 H<sub>2</sub>O were obtained from Chem-Lab, Belgium, and CoSO<sub>4</sub> · 7 H<sub>2</sub>O, CuSO<sub>4</sub> · 5 H<sub>2</sub>O, MnSO<sub>4</sub> · H<sub>2</sub>O, and ZnSO<sub>4</sub> · 7 H<sub>2</sub>O from Merck, United States. NiSO<sub>4</sub> · 6 H<sub>2</sub>O and PbSO<sub>4</sub> were obtained from UCB, Belgium. All remaining chemicals were obtained from Sigma Aldrich, Belgium. All chemicals were used as received, without further purification.

### 9.2.2 Synthesis of Ship-in-a-Bottle CMPO in MIL-101(Cr)

N,N-Diisobutyl-2-(octylphenylphosphoryl)acetamide (CMPO, MW: 407.6 g/mol, 0.16 mmol) was ground into a fine powder with mortar and pestle and added to a Teflon-lined autoclave containing 20 mL of deionized water. Terephthalic acid (4 mmol) and Cr(NO<sub>3</sub>)<sub>3</sub> · 9H<sub>2</sub>O (4 mmol) were added to this suspension (according to [39]). The autoclave was heated to 210 °C for 8 hours (2 hours warm-up) under autogenous pressure. After cooling to room temperature, the product was filtered off and washed thoroughly with 1 M HCl solution (at RT) and dimethylformamide (DMF) at 60°C respectively (overnight), in order to purify the material from leftover and/or clogged reagents. The material was once again filtered off and rinsed with acetone, followed by vacuum drying at 120 °C for 24 hours.

### 9.2.3 Characterization techniques

Different characterization techniques were applied to map the materials' morphology, surface chemistry and composition. Nitrogen sorption experiments were conducted at 77 K using a Belsorp-mini II gas analyzer. Samples were vacuum dried at 120 °C before measurements. Specific surface areas were calculated using the Langmuir and BET method. Pore volumes were estimated at  $p/p_0 = 0.90$ . FTIR (DRIFTS) spectra were recorded on a Nicolet 6700 FTIR spectrometer (Thermo-Scientific) equipped with MCT detector (Analyses performed at 120 °C under vacuum). X-ray fluorescence (XRF) spectroscopy was used to quantify the phosphorous content of the material. The XRF measurements were performed using an energy-dispersive Rigaku NexCG spectrometer. X-ray diffraction analyses (powder) were performed using an ARL X'tra diffractometer (Thermo-Scientific). ADF-STEM and EDX spectroscopy analyses were performed, using a FEI Tecnai Osiris electron microscope operated at 200 kV, equipped

with a ChemiSTEM system, to analyze the dispersion of phosphorous throughout the chromium-rich MIL-101(Cr) environment.

### 9.2.4 Stability

The stability of the adsorbent was verified by exposure to pH 0 (either 1 M HCl or 1 M HNO<sub>3</sub>). 100 mg of adsorbent was magnetically stirred in 50 mL of the respective acid solution for 48 hours. Afterwards, the solids were filtered off, rinsed with distilled water and acetone, followed by vacuum drying at 120 °C. XRD and XRF solid analyses were used to verify the material stability and leaching behavior.

### 9.2.5 Adsorption Experiments

The adsorbent was subjected to a series of adsorption experiments, including equilibrium, selectivity, kinetics, pH-dependency, regeneration and reuse experiments. These were carried out in batch setup at room temperature (25 °C). The U(VI) equilibrium experiment was performed with varying initial concentrations (from a 1000 mg/L U(VI) solution, 2% HNO<sub>3</sub>). The pH of the initial solutions was set to either 3.0 ± 0.1 or 4.0 ± 0.1 by adding aqueous NaOH solution (0.1 M), followed by short sonication. These two pH levels were chosen since uranium speciation is very pH dependent in this pH-range. The tests were performed in cylindrical plastic tubes, using 10 mg of adsorbent per 10 mL of solution (L/S: 1000 mL/g). The tubes were shaken for 24 hours to ensure equilibrium, using a GFL 3015 orbital shaking device at 200 rpm. Each test was performed in duplicate and the average values are reported. After filtration, using 0.45 µm PET syringe filters, the filtrates (and initial solutions) were analyzed with ICP–OES (Vista MPX, Varian). All solutions were acidified with HNO<sub>3</sub> prior to ICP-OES analysis.

The equilibrium metal adsorption capacity  $q_e$  (mg/g) is calculated using the following equation:

$$q_e = \frac{C_0 - C_e}{m} \cdot V$$

where  $C_0$  and  $C_e$  are the initial and equilibrium metal concentrations (mg/L) in the solution respectively,  $V$  is the solution volume (L) and  $m$  equals the adsorbent mass (g).

The experimental data was fitted to the Langmuir and Freundlich model, which are given respectively by the following equations:

$$q_e = \frac{q_{max} \cdot K_L \cdot C_e}{1 + K_L \cdot C_e}$$

$$q_e = K_F \cdot C_e^{1/n}$$

where  $K_L$  (L/mg) and  $K_F$  (mg/g.(mg/L)<sup>1/n</sup>) are the respective Langmuir and Freundlich constants,  $q_{max}$  is the maximum adsorption capacity (mg/g), and  $n$  is a constant related to surface heterogeneity.

Selectivity experiments were conducted on a multi-element solution containing Eu(III), Gd(III), Nd(III), Y(III), U(VI), Al(III), Cd(II), Co(II), Cu(II), Mn(II), Ni(II), Pb(II), and Zn(II). The concentration of each metal was ~1 mg/L. Both the adsorbent as well as the pristine MIL-101 were tested in this experiment. The conditions were kept identical to the equilibrium study (L/S: 1000 mL/g and pH 4.0) and samples were filtered and analyzed in the same manner. Each test was performed in triplicate and the average values are reported.

The affinity of the adsorbent for a specific metal is expressed by the distribution coefficient  $K_d$  (mL/g), calculated by the following equation:

$$K_d = \frac{C_0 - C_e}{C_e} \cdot \frac{V}{m}$$

To account for analysis inaccuracies  $K_d$  values between -30 and +30 are reported as  $K_d = 0$  mL/g. The original data, including standard deviations are shown in Appendix 4.1.

Kinetic experiments were performed with an initial U(VI) concentration of 30 mg/L (L/S: 1000 mL/g) at pH 3.0. Seven different contact times were considered (5 min, 30 min, 60 min, 120 min, 360 min, 1320 min, and 1440 min). Each test was performed in duplicate and the average values are reported. The experimental data was fitted to both pseudo-first and pseudo-second-order kinetic models, which are given respectively by the following equations (non-linear form):

$$q_t = q_e(1 - e^{-k_1 \cdot t})$$

$$q_t = \frac{q_e^2 \cdot k_2 \cdot t}{1 + k_2 q_e t}$$

where  $q_t$  is the amount of adsorbed metal at time  $t$  (mg/g),  $k_1$  and  $k_2$  are the respective rate constants of the Lagergren pseudo-first-order model (L/min) and the pseudo-second-order model (g/mg/min).

pH-dependency experiments were performed, in order to get information about: (1) the practical operating pH-range of the adsorbent, (2) the pH level at which the MOF matrix no longer interacts with the adsorbate, (3) the pH level at which regeneration experiments could be performed. The influence of pH on the adsorption was investigated by performing experiments at three different pH levels: 0.5, 3.0, and 6.0, with an initial U(VI) solution of 30 mg/L adjusted with either aq. NaOH (0.1 M) or aq. HNO<sub>3</sub> (0.1 M) to the desired pH level, followed by short sonication. The adsorption experiment was performed analogously to the equilibrium experiments.

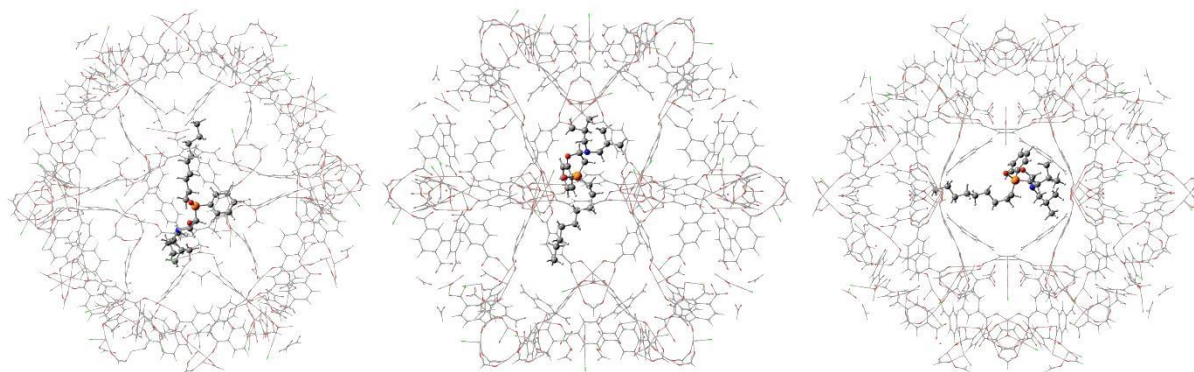


Regeneration and reusability experiments were performed by initially saturating the adsorbent with a 100 ppm U(VI) solution at pH 4 (setup similarly to the equilibrium experiments). Afterwards, the solids were filtered off from the suspension and dried under vacuum, whilst the filtrate was analyzed for its uranium concentration. Regeneration was then performed using 0.1 M HNO<sub>3</sub>, by shaking at 200 rpm for 24 hours at 25 °C (L/S: 1000 mL/g). The solids were filtered off and dried once again, and the filtrate was analyzed for its uranium content. This comprises one cycle. A total of three cycles was performed.

## 9.3 Results and discussion

### 9.3.1 Ship-in-a-bottle adsorbent

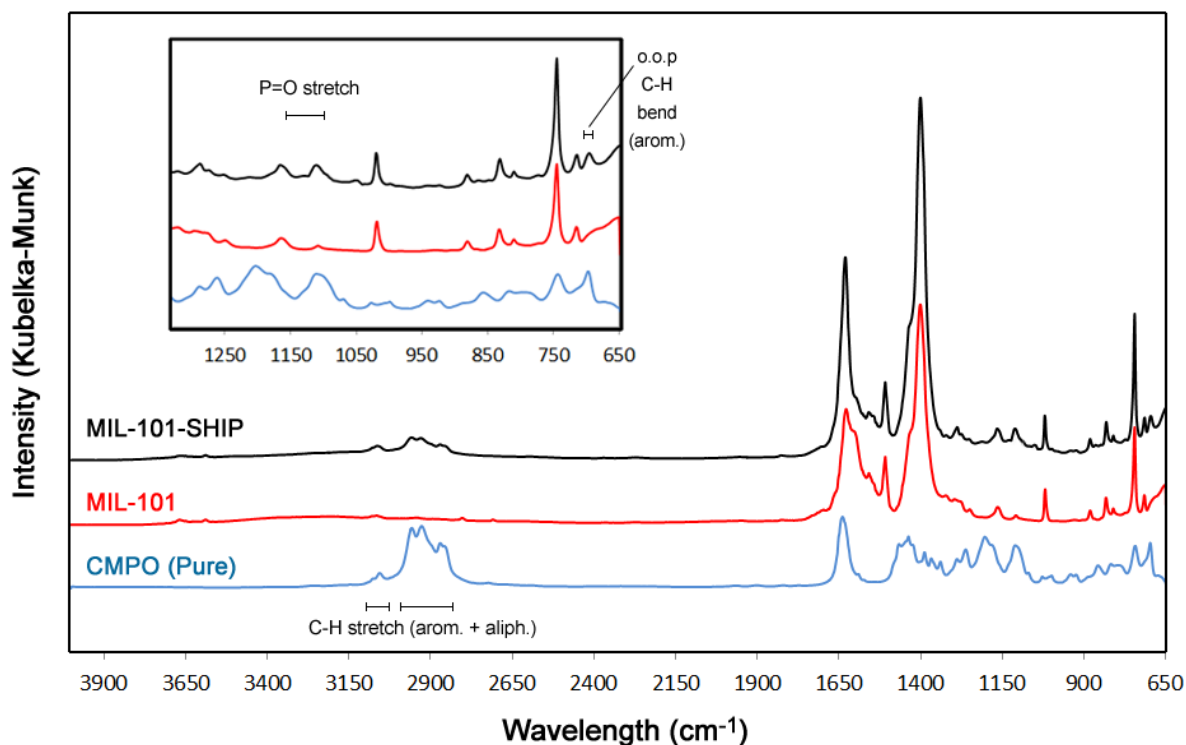
The CMPO-containing MIL-101 was synthesized through a so-called “bottle-around-the-ship” approach, in which the adsorbent matrix is formed around a molecule of interest. Ideally, this molecule is then trapped in the system, but can still act freely and unhindered within the pores of the host, hence the name of this approach. A ship-in-a-bottle system is a perfect compromise between homogeneous and heterogeneous analogues. The effectiveness of a free homogeneous ligand or other moiety (catalytic complex, biomolecule...) is combined with the advantages of heterogeneous systems (easy separation and reuse). The way several frameworks of MOFs are built up makes them very interesting for this kind of systems, and already several reports have been published where MOFs are used as matrices for ship-in-a-bottle catalyst systems[40-46]. To our knowledge, MOFs have not yet been applied as ship-in-a-bottle matrix for adsorbents. In this work, MIL-101(Cr) was selected as matrix, owing to its unique characteristics. This particular MOF is both mesoporous and a cage-type MOF (as mentioned above), and is therefore suitable to encapsulate rather bulky molecules (chelating ligands), which are often used as selective complexants. The cage structure itself is made up of microporous windows (12 – 16 Å), which can prevent such bulky moieties from leaving the cages (Figure 9.1). In addition, MIL-101(Cr) is one of the few mesoporous MOFs possessing an excellent stability in both acidic as alkaline aqueous environments (short- and long term)[33, 47, 48]. All these qualities make the MIL-101(Cr) a perfect candidate for uses in aqueous adsorption environments and as a host for the “bottle-around-the-ship” approach.



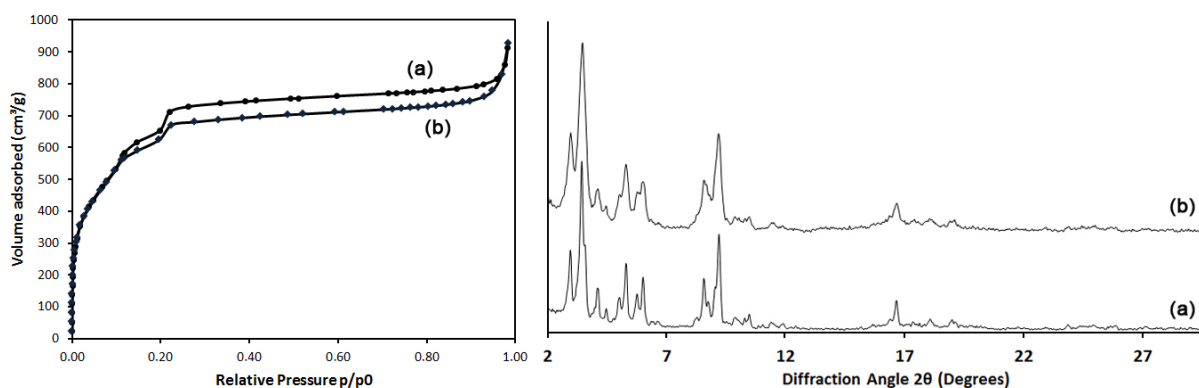
**Figure 9.1 Visualization of a CMPO molecule trapped in an individual MIL-101(Cr) cage. Three different angles of the cage are represented. The CMPO ligand is visualized in the ball-stick manner, whereas the MIL-101 cage is represented as a wireframe, for clarity reasons. (High-resolution images are provided in Appendix 4.2)**

### 9.3.2 Material characterization

Figure 9.2 shows the DRIFTS spectra of the pristine MIL-101(Cr) and the ship-in-a-bottle CMPO in MIL-101, hereafter called MIL-101-Ship. By comparing both spectra to the included pure CMPO spectrum, the presence of CMPO in the structure can be successfully confirmed. A clear indication of aliphatic and aromatic C-H stretches in the MIL-101-Ship spectrum is visible around  $2850 - 3000\text{ cm}^{-1}$  and  $3010 - 3050\text{ cm}^{-1}$  respectively. Phosphine oxide (P=O) stretching vibrations are observed around  $1100\text{ cm}^{-1}$  and an additional aromatic C-H out-of-plane bending vibration is visible as well around  $690\text{ cm}^{-1}$ . Other characteristic vibrations of the CMPO are not clearly discernible due to either the overlap with vibrations inherent to MIL-101, or because of the limited ligand loading in the material. Figure 9.3 shows the  $\text{N}_2$ -sorption isotherms and XRD diffractograms for MIL-101 and MIL-101-Ship. In both of the nitrogen adsorption isotherms, the characteristic MIL-101 isotherm shape can be recognized, which indirectly confirms that the addition of CMPO to the synthetic mixture did not prevent the hydrothermal formation of MIL-101. This is further confirmed by XRD where the MIL-101 crystallography is clearly observed in both patterns. Table 9.1 shows the specific surface areas and pore volumes, as well as phosphorous content (wt. %) as detected by XRF. The calculated CMPO loading (mmol/g) is added as well.



**Figure 9.2** DRIFTS spectra of the pristine MIL-101(Cr), the MIL-101-Ship and pure CMPO. (Inset: zoom on the 650 – 1300  $\text{cm}^{-1}$  region).



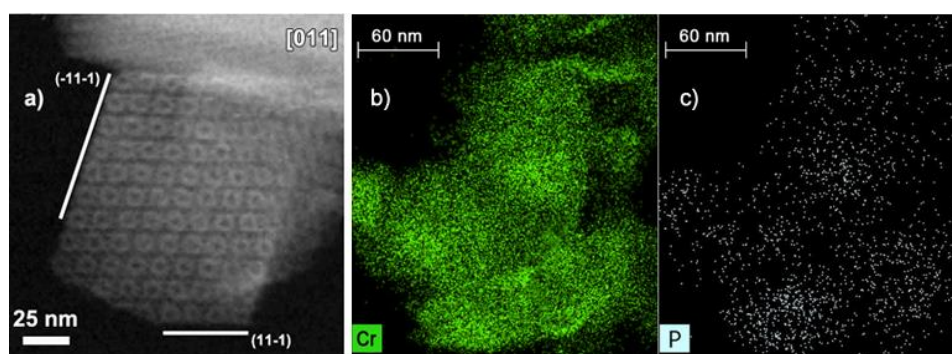
**Figure 9.3** Nitrogen adsorption isotherms (left) and X-ray diffraction patterns (right) of pristine MIL-101(Cr) (a) and MIL-101-Ship (b).

**Table 9.1 Numerical N<sub>2</sub>-adsorption data and loading calculations of MIL-101(Cr) and MIL-101-Ship.**

	Specific Surface Area - Langmuir (m <sup>2</sup> /g)	Specific Surface Area - BET (m <sup>2</sup> /g)	Pore volume V <sub>p</sub> (mL/g)	P content (wt. %)	CMPO loading (mmol/g)
MIL-101(Cr)	3400-3500	2500-2600	1.29	-	-
MIL-101-Ship	3200	2365	1.15	0.28 ± 0.03	0.09 ± 0.01*

\*for reference: MIL-101 contains ~0.14mmol cages/g when pore volume = 1.3 mL/g

A small reduction in Langmuir surface area (as well as BET surface area and pore volume) is observed in the MIL-101-Ship, which can indicate the loading of the CMPO ligand inside the MOF. This reduction correlates well to the rather low CMPO loading. Via phosphorous XRF analysis, a loading of ~0.3 wt.% P was found, correlating to ~0.1 mmol CMPO/g. In addition to these powder analyses, the phosphorous-chromium ratio was calculated based on EDX data, demonstrating an average phosphorous loading of 0.12 mmol P/g, which is in good agreement with the initial XRF analysis. ADF-STEM and EDX imaging was applied to observe the MIL-101-Ship structure and P dispersion, respectively. Highly crystalline particles with the typical MIL-101 truncated octahedron morphology and preferential {111} faceting are present. Phosphorous is found to be well dispersed throughout the material (Figure 9.4).



**Figure 9.4 (a)** ADF-STEM image of a MIL-101 crystalline particle recorded along the [011] zone axis. (b,c) chromium (green) and phosphorous (white) EDX mapping, showing well dispersed P throughout the Cr-rich environment. Additional ADF-STEM images can be found in Appendix 4.3.

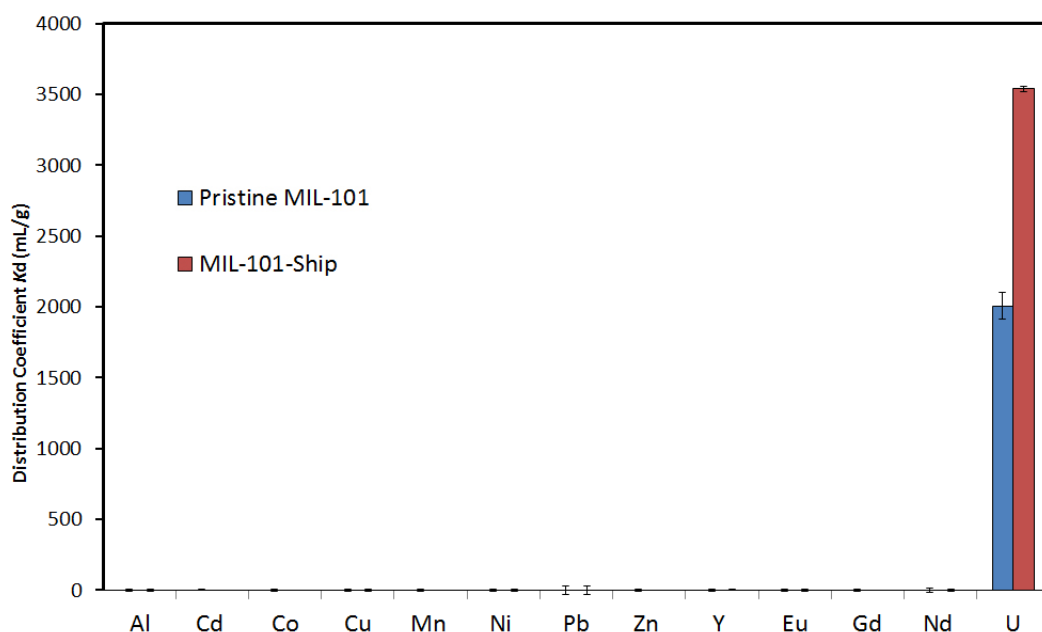
### 9.3.3 Adsorbent Stability

An important requirement for adsorbents (and heterogeneous systems in general) is material stability. In the case of aqueous metal adsorption, a water-stable adsorbent is required, preferably with a high resistance to acidic conditions (adsorption/regeneration). In order to assess the MIL-101-Ship's resistance to these conditions, stability experiments were conducted in 1 M HCl and 1 M HNO<sub>3</sub>. Based on XRD (Appendix 4.4), the adsorbent shows a perfect resistance to both acidic conditions. This was already confirmed by Van Der Voort et al. for HCl[33]. Through XRF (phosphorous content analysis) it was found that no CMPO leached out during the acid treatments, which confirms that the CMPO is trapped within the cages of the MIL-101.

### 9.3.4 Adsorption Studies

#### *Selectivity*

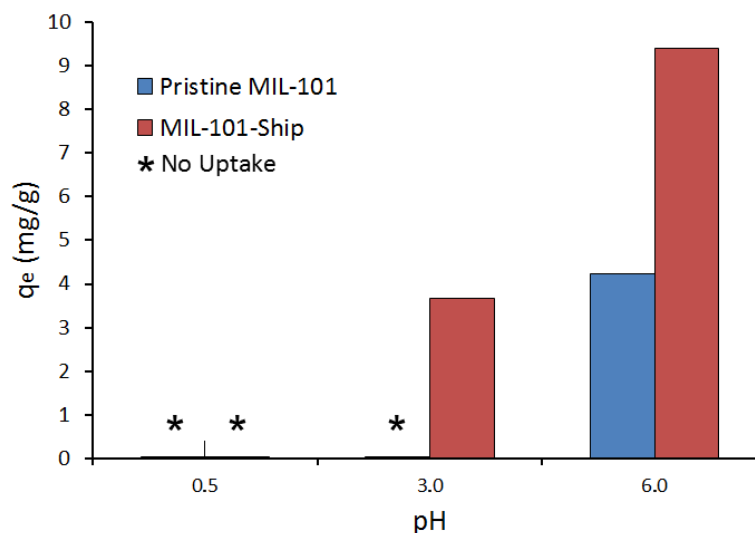
Adsorption of U(VI) in the presence of various competing ions was performed with the MIL-101-Ship adsorbent and the pristine MIL-101, and evaluated in terms of the *K<sub>d</sub>* values (Figure 9.5). MIL-101-Ship shows a very high selectivity towards uranium, with nearly no uptake of the competing ions, which include both REEs (Eu, Gd, Nd, Y) as other cations (Al, Cd, Co, Cu, Mn, Ni, Pb, Zn). Appendix 4.1 zooms in on the competing metals. It appears that the pristine MIL-101(Cr) possesses some affinity for U(VI) as well. We believe this is due to the presence of various hydroxylated uranium species ( $[(\text{UO}_2)_x(\text{OH})_y]^{2x-y}$ ), next to the dominant uranyl ( $\text{UO}_2^{2+}$ ) species, at pH levels of ~ 4 and above. These hydroxylated species could weakly adsorb on the MIL-101 metal-oxide clusters. As the pH increases (> 4), more hydroxylated species are present instead of uranyl[49] and the interaction with MIL-101 increases, according to Bai *et al.*[35], who postulated that the multi-nuclear hydroxide complexes of U(VI) may be favored by the MIL-101.



**Figure 9.5** Distribution coefficients ( $K_d$ ) for the MIL-101-Ship (red) and pristine MIL-101 (blue), provided with standard deviations (error bars).  $C_0(M) = 1 \text{ mg/L}$  each, pH: 4.0, L/S: 1000 mL/g,  $T = 25^\circ\text{C}$ ,  $t = 24 \text{ hrs}$ .

#### *pH-dependency*

The results are visualized in Figure 9.6. At pH 6, both materials are active, with an increased uptake observed for MIL-101-Ship. At this pH level, hydroxylated uranium species are dominant, which might explain the affinity with the matrix (as mentioned above). At pH 3, U(VI) is entirely present as uranyl ( $\text{UO}_2^{2+}$ ) and no interaction with the matrix should be expected. Indeed, only MIL-101-Ship adsorbs U(VI), whereas the pristine MIL-101 shows no uptake at all, which is a direct confirmation of the activity of CMPO within the cages of the MOF. At pH 0.5, none of the materials are active in the adsorption of U(VI). This result is interesting with respect to regeneration of the adsorbent, where a low pH could be used to effectively desorb the uranium.



**Figure 9.6** U(VI) adsorption capacity in function of the pH for MIL-101-Ship (red) and the pristine MIL-101 (blue).  $C_0(\text{U}) = 30 \text{ mg/L}$ ,  $L/S: 1000 \text{ mL/g}$ ,  $T = 25 \text{ }^\circ\text{C}$ ,  $t = 24 \text{ hrs}$ .

#### *Equilibrium study*

A U(VI) equilibrium study on MIL-101-Ship was performed at two pH levels (3.0 and 4.0), as the uranium speciation at both pH levels might result in different adsorption characteristics. A continuous increase of U(VI) adsorption at both pH levels was observed with increasing initial uranium concentrations. The experimental data was fitted to the Langmuir and Freundlich models, both of which are frequently used to describe the adsorption mechanism of metals onto heterogeneous systems[50, 51]. Table 9.2 gives an overview of the obtained adsorption parameters for each model at the respective pH level. At pH 3, a good correlation is found with both models, however, regardless the comparable correlation coefficient ( $R^2$ ), the Langmuir model is deemed more suitable as it concerns metal adsorption through complexation with the CMPO ligand. This was also demonstrated by the pH-dependency study. The calculated maximum adsorption capacity via the Langmuir model is 5.32 mg U/g at pH 3. At pH 4, an increased U(VI) uptake was observed, which is again in line with the results for the pH dependency experiments. Both the Langmuir and Freundlich models have a similar high correlation, but selecting either of these is not straightforward, since at pH 4 a fraction of the uranium is present as  $\text{UO}_2\text{OH}^+$  which can interact with the framework. Besides, adsorption of multinuclear uranyl hydroxide complexes would lead to a substantial increase in uranium uptake. Nonetheless, as most of the uranium at pH 4 is present as uranyl, the Langmuir model was used to estimate the maximum adsorption capacity at ~28 mg U/g. The Langmuir isotherms for both pH 3 and pH 4 are plotted in Figure 9.7. Both the Langmuir and Freundlich isotherms can be found in Appendix 4.5.

**Table 9.2 Adsorption parameters of U(VI) on MIL-101-Ship at pH 3 and pH 4, fitted to Langmuir and Freundlich models.**

	Langmuir			Freundlich		
	$q_{\max}$ (mg/g)	$K_L$ (L/mg)	$R^2$	n	$K_F$ (mg/g (L/mg) $^{1/n}$ )	$R^2$
pH 3	5.32	0.0215	0.9760	2.05	0.3833	0.9771
pH 4	27.99	0.0066	0.9833	1.43	0.4503	0.9894

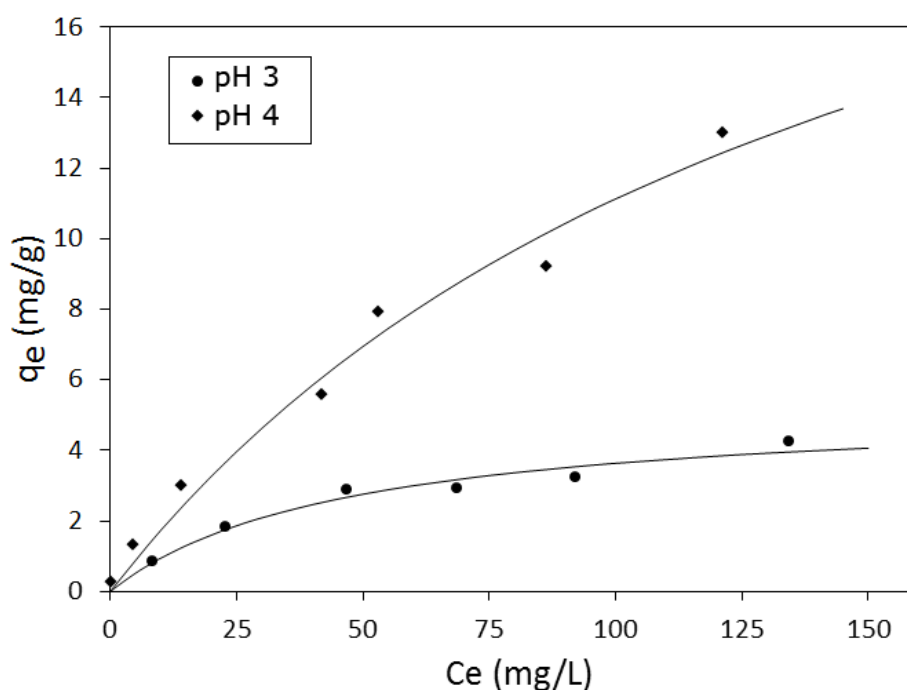
**Figure 9.7 U(VI) adsorption isotherm for MIL-101-Ship, fitted to the Langmuir model. pH: 3.0 and 4.0, L/S: 1000 mL/g, T = 25 °C, t = 24 hrs. Average value of duplicates.**

Table 9.3 gives an overview of the MIL-101-Ship adsorption performance, compared to other reported MOF-based U(VI) adsorbents. On a pure capacity basis, our MIL-101-Ship does not surpass these reported adsorbents. This is mainly due to the limited amount of cages per gram in MIL-101 (0.14 mmol cages/g for a pore volume of 1.3 mL/g), which determines the amount of ligand which can be loaded into the structure. At ~0.09 mmol CMPO/g, we obtain a ~65 % theoretical filling ratio (assuming on average 1:1 ligand:cage). If each of these ligands were able to coordinate with one uranyl ion (which is generally the reported stoichiometry[34, 52]), the theoretical maximum uptake would be ~24 mg U(VI)/g (framework affinity and multinuclear complex coordination left aside). By normalizing the U(VI) adsorption to an active site basis (mg U(VI)/mmol active site), the MIL-101-Ship becomes competitive with the other reported



adsorbents, and future work on improving the ligand loading could increase the uptake performance even further. Moreover, MIL-101-Ship excels at its zero-leaching behavior and high affinity for U(VI) with almost no competitive metal uptake.

**Table 9.3 Overview of reported MOF-based U(VI) adsorbents and their adsorption performance, compared to MIL-101-Ship.**

Adsorbent	Saturation capacity (mg/g)	pH	Active sites (mmol/g)	Capacity /Active site (mg/m mol)	Ligand Leaching (1 run)	Selectivity for U(VI)	Reference
MIL-101-Ship	5.32	3.0	0.09	59	0%	Highly over Al, Cd, Co, Cu, Mn, Ni, Pb, Zn, Y, Eu, Gd, Nd	This work
	27.99	4.0	0.09	310			
MIL-101-NH <sub>2</sub>	90	5.5	1.63	55	0%	NM	[35]
MIL-101-ED*	200	5.5	1.28	156	30%*	Highly over Co, Ni, Zn, Sr, La, Nd, Sa, Yb	[35]
MIL-101-DETA*	350	5.5	0.72	486	30%*	Highly over Co, Ni, Zn, Sr, La, Nd, Sa, Yb	[35]
MOF-76	300	3.0	-	-	-	Highly over Sr, Cs, Cr, Co, Ni. Medium over Pb, Zn	[32]
UiO-68-P(O)(OEt) <sub>2</sub>	217	2.5	ligand:linker 1:1	-	NM	NM	[34]
Zn(H <sub>3</sub> BTC)(L).(H <sub>2</sub> O) <sub>2</sub>	115	2.0	NM**	-	-	NM	[53]
Zn-MOF-74 w/ Coumarin (11.7 wt%)	360	4.0	0.8	450	NM	NM	[36]

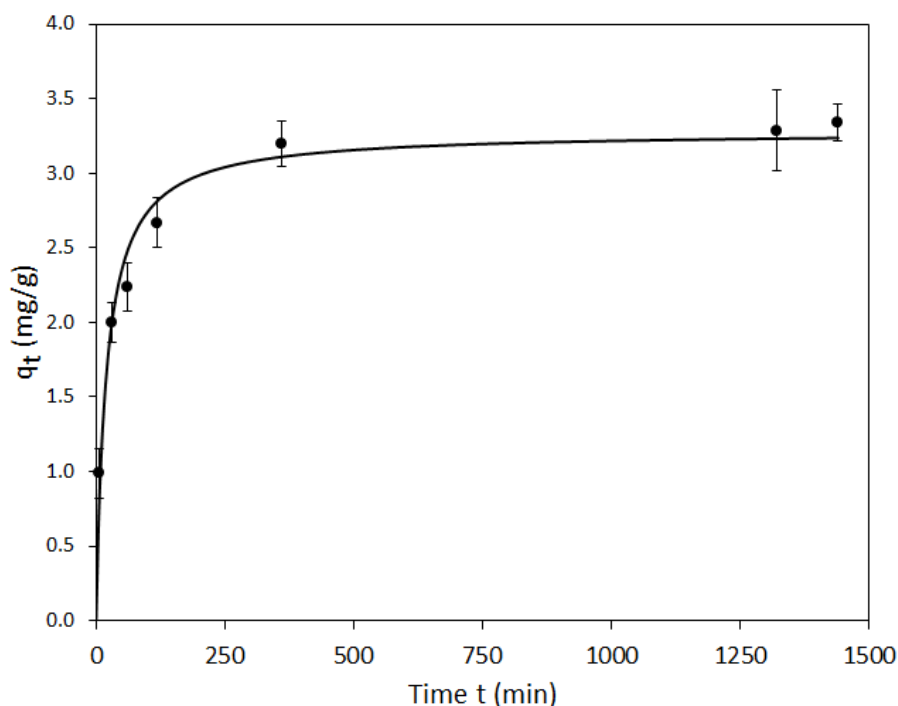
ED: ethylenediamine, DETA: diethylenetriamine, H<sub>3</sub>BTC: 1,3,5-benzenetricarboxylic acid, L: N4,N4'-di(pyridin-4-yl) biphenyl-4,4'-dicarboxamide), \*: grafting via coordinatively unsaturated sites (CUS), \*\*: ligands embedded in MOF structure, NM: not mentioned.

### Kinetics

To evaluate the adsorption rate of U(VI) by the MIL-101-Ship, a series of identical adsorption tests were conducted with varying contact times (five minutes to 24 hours). The experiment was performed at pH 3.0, in order to obtain adsorption solely by the CMPO and avoid matrix interaction (see pH dependency). The experimental data was fitted to two kinetic models, namely the pseudo-first and pseudo-second-order model (Table 9.4). The best fit, namely pseudo-second-order, was plotted in Figure 9.8. Both fits are also provided in Appendix 4.6. The pseudo-second order model indicates that the rate-limiting step is the surface adsorption that involves chemisorption, in which the removal of adsorbate from a solution is a result of physicochemical interactions between both phases[54]. The adsorption kinetics of U(VI) and other metal cations on ligand-functionalized adsorbents have often been described with pseudo-second-order kinetics[35, 55-57]. From this model, it can be calculated that after 375 minutes, over 95 % of the maximum U(VI) uptake is achieved and the adsorption gradually equilibrates. Within the first hour, 75 % uptake is achieved. In practical applications, a sorbent with fast kinetics but smaller maximum uptake is often preferred over high uptakes and slow kinetics, and thus, the obtained kinetic profile is suitable for uses in adsorption column setups (dynamic conditions)[58].

**Table 9.4 Parameters of the pseudo-first-order and pseudo-second-order kinetic models for adsorption of U(VI) on MIL-101-Ship.  $C_0$ : 30 mg/L, pH: 3.0, L/S: 1000 mL/g,  $T = 25$  °C.**

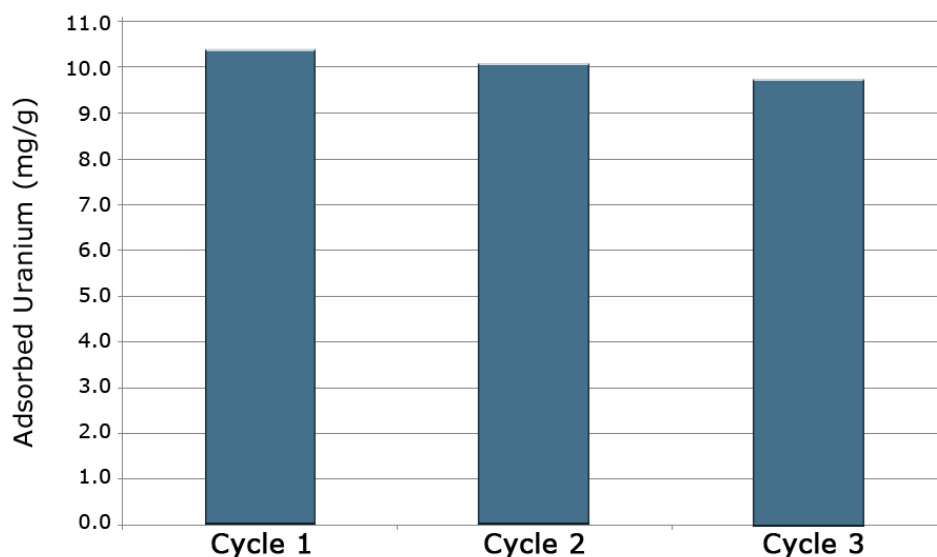
Pseudo-first-order model			Pseudo-second-order model		
$q_e$ (mg/g)	$k_1$ (L/min)	$R^2$	$q_e$ (calc) (mg/g)	$k_2$ (g/mg/min)	$R^2$
3.05	0.0308	0.935	3.23	0.016	0.975



**Figure 9.8** Adsorption kinetics of U(VI) on MIL-101-Ship, fitted to the pseudo-second-order kinetic model.  $C_0(\text{U}) = 30 \text{ mg/L}$ ,  $\text{L/S: } 1000 \text{ mL/g}$ ,  $T = 25^\circ\text{C}$ ,  $\text{pH} = 3$ . Average value of duplicates.

#### *Regeneration and Reuse*

Nitric acid (0.1 M) was used as regenerant, as a result of the pH dependency experiments. The results are plotted in Figure 9.9. Stripping efficiencies of ~98% are obtained. A total of three complete cycles was performed. A constant uptake of about 10 mg U/g is observed, only slightly decreasing throughout the cycles. As three batch adsorption/desorption cycles comprise over 140 hours of turbulent contact with the acidic aqueous environment, additional XRD and XRF solid analyses were performed to investigate the adsorbent's resistance to this long-term exposure. The MIL-101 structure was found to remain perfectly intact, according to XRD, and the loss of CMPO was nearly negligible (<5%), confirming the remarkable stability of the adsorbent.



**Figure 9.9 Reusability results for MIL-101-Ship over three consecutive cycles, using 0.1 M  $\text{HNO}_3$  as regenerant. L/S: 1000 mL/g,  $T = 25^\circ\text{C}$ , adsorption  $\text{pH} = 4.0$ .**

## 9.4 Conclusion

We have reported the innovative combination of a highly water-stable MOF with selective chelating ligands, through a facile, cost-effective ship-in-a-bottle synthetic approach, yielding an effective adsorbent for uranium recovery from aqueous environments. The adsorbent consists of N,N-Diisobutyl-2-(octylphenylphosphoryl)acetamide (CMPO) trapped inside the cages of the MIL-101(Cr), making it an ideal compromise between homogeneous and heterogeneous systems. The synthesis comprises a one-step procedure and yields a leaching-free material with a loading of 0.09 mmol CMPO/g. The adsorption performance for U(VI) was investigated through an extensive adsorption study, including selectivity experiments, pH-dependency, equilibrium, kinetics, regeneration, and reuse. A very high selectivity was obtained for U(VI), with almost no uptake from competing metals, including rare earths and transition metals. The maximum adsorption capacity was calculated via the Langmuir model at 5.32 mg U/g (pH 3) and 27.99 mg U/g (pH 4). Kinetic experiments show that 75 % of the maximum uptake is achieved within the first hour of adsorption, after which the adsorption gradually equilibrates. Furthermore, the adsorbent can be effectively regenerated using 0.1 M  $\text{HNO}_3$ , and used for at least three cycles of uranium adsorption/desorption. It can therefore be concluded that the ship-in-a-bottle CMPO in MIL-101 system may be an efficient and feasible adsorbent for U(VI) recovery from aqueous environments, for instance as an effective uranium sequester in rare earth rich clay leachates or waste streams in phosphate rock processing. These streams are often neutralized to slightly acidic pH (4 - 5) in order to precipitate elements such as iron and thorium[15]. This is a suitable environment for our adsorbent to purify the obtained leachate from uranium. Besides, a selective adsorbent could be an ideal end-of-line technique to further increase the uranium recovery rate in industrial processes using solvent extractions.

## REFERENCES

- [1] International Energy Outlook 2016, U.S.E.I. Administration, Washington, DC 20585 (2016).
- [2] M. Salvatores, G. Palmiotti, Radioactive waste partitioning and transmutation within advanced fuel cycles: Achievements and challenges, *Prog Part Nucl Phys*, 66 (2011) 144-166.
- [3] Uranium 2014: Resources, Production and Demand, (2014).
- [4] J. Kim, C. Tsouris, R.T. Mayes, Y. Oyola, T. Saito, C.J. Janke, S. Dai, E. Schneider, D. Sachde, Recovery of Uranium from Seawater: A Review of Current Status and Future Research Needs, *Separ Sci Technol*, 48 (2013) 367-387.
- [5] E.H.Y. AbowSlama, E. Ebraheem, A.K. Sam, Precipitation and purification of uranium from rock phosphate, *J Radioanal Nucl Ch*, 299 (2014) 815-818.
- [6] F. Habashi, Correlation between the uranium content of marine phosphates and other rock constituents, *Econ Geol*, 57 (1962) 1081 - 1084.
- [7] M.J. Lottering, L. Lorenzen, N.S. Phala, J.T. Smit, G.A.C. Schalkwyk, Mineralogy and uranium leaching response of low grade South African ores, *Miner Eng*, 21 (2008) 16-22.
- [8] [www.world-nuclear.org/info/phosphates\\_inf124.html](http://www.world-nuclear.org/info/phosphates_inf124.html) (Accessed in
- [9] M. Walters, T. Baroody, W. Berry, Technologies for Uranium Recovery from Phosphoric Acid in: AIChE Central Florida Section, Florida, 2008.
- [10] M.A. Maheswari, M.S. Subramanian, AXAD-16-3,4-dihydroxy benzoyl methyl phosphonic acid: a selective preconcentrator for U and Th from acidic waste streams and environmental samples, *React Funct Polym*, 62 (2005) 105-114.
- [11] J. Veliscek-Carolan, Separation of actinides from spent nuclear fuel: A review, *J Hazard Mater*, 318 (2016) 266-281.
- [12] M.C. Okeji, K.K. Agwu, F.U. Idigo, Assessment of Natural Radioactivity in Phosphate Ore, Phosphogypsum and Soil Samples Around a Phosphate Fertilizer Plant in Nigeria, *B Environ Contam Tox*, 89 (2012) 1078-1081.
- [13] S. Bachmaf, B.J. Merkel, Sorption of uranium(VI) at the clay mineral-water interface, *Environ Earth Sci*, 63 (2011) 925-934.
- [14] Y. Feng, H. Jiang, S. Li, J. Wang, X. Jing, Y. Wang, M. Chen, Metal-organic frameworks HKUST-1 for liquid-phase adsorption of uranium, *Colloid Surface A*, 431 (2013) 87-92.
- [15] Z. Zhu, Y. Pranolo, C.Y. Cheng, Separation of uranium and thorium from rare earths for rare earth production - A review, *Miner Eng*, 77 (2015) 185-196.
- [16] M.R.L. Nascimento, O. Fatibello-Filho, L.A. Teixeira, Recovery of uranium from acid mine drainage waters by ion exchange, *Miner Process Extr Metall Rev*, 25 (2004) 129 - 142.
- [17] A.C. Quieroz Ladeira, C.R. Goncalves, Influence of anionic species on uranium separation from acid mine water using strong base resins, *J Hazard Mater*, 148 (2007) 499-504.
- [18] A. Mellah, S. Chegrouche, M. Barkat, The removal of uranium(VI) from aqueous solutions onto activated carbon: Kinetic and thermodynamic investigations, *J Colloid Interf Sci*, 296 (2006) 434-441.
- [19] J. Canivet, A. Fateeva, Y.M. Guo, B. Coasne, D. Farrusseng, Water adsorption in MOFs: fundamentals and applications, *Chem Soc Rev*, 43 (2014) 5594-5617.
- [20] J.R. Li, R.J. Kuppler, H.C. Zhou, Selective gas adsorption and separation in metal-organic frameworks, *Chem Soc Rev*, 38 (2009) 1477-1504.

- [21] J.R. Li, Y.G. Ma, M.C. McCarthy, J. Sculley, J.M. Yu, H.K. Jeong, P.B. Balbuena, H.C. Zhou, Carbon dioxide capture-related gas adsorption and separation in metal-organic frameworks, *Coord Chem Rev*, 255 (2011) 1791-1823.
- [22] J. Liu, P.K. Thallapally, B.P. McGrail, D.R. Brown, J. Liu, Progress in adsorption-based CO<sub>2</sub> capture by metal-organic frameworks, *Chem Soc Rev*, 41 (2012) 2308-2322.
- [23] M.P. Suh, H.J. Park, T.K. Prasad, D.W. Lim, Hydrogen Storage in Metal-Organic Frameworks, *Chem Rev*, 112 (2012) 782-835.
- [24] J. Lee, O.K. Farha, J. Roberts, K.A. Scheidt, S.T. Nguyen, J.T. Hupp, Metal-organic framework materials as catalysts, *Chem Soc Rev*, 38 (2009) 1450-1459.
- [25] J.W. Liu, L.F. Chen, H. Cui, J.Y. Zhang, L. Zhang, C.Y. Su, Applications of metal-organic frameworks in heterogeneous supramolecular catalysis, *Chem Soc Rev*, 43 (2014) 6011-6061.
- [26] B. Chen, S. Xiang, G. Qian, Metal-Organic Frameworks with Functional Pores for Recognition of Small Molecules, *Accounts Chem Res*, 43 (2010) 1115-1124.
- [27] J.R. Li, J. Sculley, H.C. Zhou, Metal-Organic Frameworks for Separations, *Chem Rev*, 112 (2012) 869-932.
- [28] R.C. Huxford, J. Della Rocca, W. Lin, Metal-organic frameworks as potential drug carriers, *Curr Opin Chem Biol*, 14 (2010) 262-268.
- [29] P. Horcajada, R. Gref, T. Baati, P.K. Allan, G. Maurin, P. Couvreur, G. Ferey, R.E. Morris, C. Serre, Metal-Organic Frameworks in Biomedicine, *Chem Rev*, 112 (2012) 1232-1268.
- [30] M. Kurmoo, Magnetic metal-organic frameworks, *Chem Soc Rev*, 38 (2009) 1353-1379.
- [31] J. Rocha, L.D. Carlos, F.A. Almeida Paz, D. Ananias, Luminescent multifunctional lanthanides-based metal-organic frameworks, *Chem Soc Rev*, 40 (2011) 926-940.
- [32] W. Yang, Z.Q. Bai, W.Q. Shi, L.Y. Yuan, T. Tian, Z.F. Chai, H. Wang, Z.M. Sun, MOF-76: from a luminescent probe to highly efficient U-VI sorption material, *Chem Commun*, 49 (2013) 10415-10417.
- [33] K. Leus, T. Bogaerts, J. De Decker, H. Depauw, K. Hendrickx, H. Vrielinck, V. Van Speybroeck, P. Van Der Voort, Systematic study of the chemical and hydrothermal stability of selected "stable" Metal Organic Frameworks, *Micropor Mesopor Mat*, 226 (2016) 110-116.
- [34] M. Carboni, C.W. Abney, S. Liu, W. Lin, Highly porous and stable metal-organic frameworks for uranium extraction, *Chem Sci*, 4 (2013) 2396-2402.
- [35] Z.Q. Bai, L.Y. Yuan, L. Zhu, Z.R. Liu, S.Q. Chu, L.R. Zheng, J. Zhang, Z.F. Chai, W.Q. Shi, Introduction of amino groups into acid-resistant MOFs for enhanced U(VI) sorption, *J Mater Chem A*, 3 (2015) 525-534.
- [36] L. Zhang, L.L. Wang, L.L. Gong, X.F. Feng, M.B. Luo, F. Luo, Coumarin-modified microporous-mesoporous Zn-MOF-74 showing ultra-high uptake capacity and photo-switched storage/release of U-VI ions, *J Hazard Mater*, 311 (2016) 30-36.
- [37] F.W. Lewis, M.J. Hudson, L.M. Harwood, Development of Highly Selective Ligands for Separations of Actinides from Lanthanides in the Nuclear Fuel Cycle, *Synlett*, (2011) 2609-2632.
- [38] Ion Exchange and Solvent Extraction: A Series of Advances, CRC Press, Florida, USA, 2009.
- [39] D.M. Jiang, A.D. Burrows, K.J. Edler, Size-controlled synthesis of MIL-101(Cr) nanoparticles with enhanced selectivity for CO<sub>2</sub> over N<sub>2</sub>, *Crystengcomm*, 13 (2011) 6916-6919.
- [40] T. Bogaerts, A. Van Yperen-De Deyne, Y.Y. Liu, F. Lynen, V. Van Speybroeck, P. Van Der Voort, Mn-salen@MIL101(Al): a heterogeneous, enantioselective catalyst synthesized using a 'bottle around the ship' approach, *Chem Commun*, 49 (2013) 8021-8023.

- [41] R. Fazaeli, H. Aliyan, M. Moghadam, M. Masoudinia, Nano-rod catalysts: Building MOF bottles (MIL-101 family as heterogeneous single-site catalysts) around vanadium oxide ships, *J Mol Catal a-Chem*, 374 (2013) 46-52.
- [42] J. Juan-Alcaniz, J. Gascon, F. Kapteijn, Metal-organic frameworks as scaffolds for the encapsulation of active species: state of the art and future perspectives, *J Mater Chem*, 22 (2012) 10102-10118.
- [43] J. Juan-Alcaniz, E.V. Ramos-Fernandez, U. Lafont, J. Gascon, F. Kapteijn, Building MOF bottles around phosphotungstic acid ships: One-pot synthesis of bi-functional polyoxometalate-MIL-101 catalysts, *J Catal*, 269 (2010) 229-241.
- [44] J.C. Jiang, O.M. Yaghi, Bronsted Acidity in Metal-Organic Frameworks, *Chem Rev*, 115 (2015) 6966-6997.
- [45] M. Yoshizawa, J.K. Klosterman, M. Fujita, Functional Molecular Flasks: New Properties and Reactions within Discrete, Self-Assembled Hosts, *Angew Chem Int Edit*, 48 (2009) 3418-3438.
- [46] M.H. Alkordi, Y.L. Liu, R.W. Larsen, J.F. Eubank, M. Eddaoudi, Zeolite-like metal-organic frameworks as platforms for applications: On metalloporphyrin-based catalysts, *J Am Chem Soc*, 130 (2008) 12639-12641.
- [47] S. Bernt, V. Guillerme, C. Serre, N. Stock, Direct covalent post-synthetic chemical modification of Cr-MIL-101 using nitrating acid, *Chem Commun*, 47 (2011) 2838-2840.
- [48] R.B. Ferreira, P.M. Scheetz, A.L.B. Formiga, Synthesis of amine-tagged metal-organic frameworks isostructural to MIL-101(Cr), *RSC Advances*, 3 (2013) 10181-10184.
- [49] Q.H. Fan, L.M. Hao, C.L. Wang, Z. Zheng, C.L. Liu, W.S. Wu, The adsorption behavior of U(VI) on granite, *Environ Sci-Proc Imp*, 16 (2014) 534-541.
- [50] J. Febrianto, A.N. Kosasih, J. Sunarso, Y.H. Ju, N. Indraswati, S. Ismadji, Equilibrium and kinetic studies in adsorption of heavy metals using biosorbent: A summary of recent studies, *J Hazard Mater*, 162 (2009) 616-645.
- [51] K. Folens, K. Leus, N.R. Nicomel, M. Meledina, S. Turner, G. Van Tendeloo, G. Du Laing, P. Van Der Voort, Fe<sub>3</sub>O<sub>4</sub>@MIL-101 – A Selective and Regenerable Adsorbent for the Removal of As Species from Water, *Eur J Inorg Chem*, 2016 (2016) 4395-4401.
- [52] A. Sengupta, M.S. Murali, S.K. Thulasidas, P.K. Mohapatra, Solvent system containing CMPO as the extractant in a diluent mixture containing n-dodecane and isodecanol for actinide partitioning runs, *Hydrometallurgy*, 147 (2014) 228-233.
- [53] L.L. Wang, F. Luo, L.L. Dang, J.Q. Li, X.L. Wu, S.J. Liu, M.B. Luo, Ultrafast high-performance extraction of uranium from seawater without pretreatment using an acylamide- and carboxyl-functionalized metal-organic framework, *J Mater Chem A*, 3 (2015) 13724-13730.
- [54] D. Robati, Pseudo-second-order kinetic equations for modeling adsorption systems for removal of lead ions using multi-walled carbon nanotube, *Journal of Nanostructure in Chemistry*, 3 (2013) 1-6.
- [55] A.M. Donia, A.A. Atia, E.M.M. Moussa, A.M. El-Sherif, M.O. Abd El-Magied, Removal of uranium(VI) from aqueous solutions using glycidyl methacrylate chelating resins, *Hydrometallurgy*, 95 (2009) 183-189.
- [56] Y.S. Ho, Review of second-order models for adsorption systems, *J Hazard Mater*, 136 (2006) 681-689.
- [57] Y. Liu, L. Yuan, Y. Yuan, J. Lan, Z. Li, Y. Feng, Y. Zhao, Z. Chai, W. Shi, A high efficient sorption of U(VI) from aqueous solution using amino-functionalized SBA-15, *J Radioanal Nucl Ch*, 292 (2012) 803-810.

[58] L.S. Djokic, R. Pantovic, N. Stavretovic, R. Igic, Origin of Arsenic in Drinking Waters in the West Backa District of Serbia, in: M. Václavíková, K. Vitale, G.P. Gallios, L. Ivaničová (Eds.) *Water Treatment Technologies for the Removal of High-Toxity Pollutants*, Springer Science, 2010, pp. 41-50.



# 10 COMPARISON OF THE DEVELOPED ADSORBENTS

Throughout this work, two different approaches were pursued to functionalize the MIL-101(Cr) framework with CMPO ligands, and ultimately obtain REE and/or uranyl selective adsorbents. This chapter is intended to compare both adsorbents to each other, based on their characteristics and performance. In addition, an attempt is made to correlate their performance to the theoretical principles that were described throughout this work.

MIL-101(Cr) was functionalized with CMPO via a stepwise covalent anchoring route (cfr. Chapter 7 and 8), and via a one-step *in-situ* encapsulation approach (cfr. Chapter 9). Table 10.1 offers a direct comparison in terms of material characteristics. In further discussion, the adsorbents are respectively referred to as ‘anchoring approach’ and ‘encapsulation approach’.

## 10.1 Ligand loading

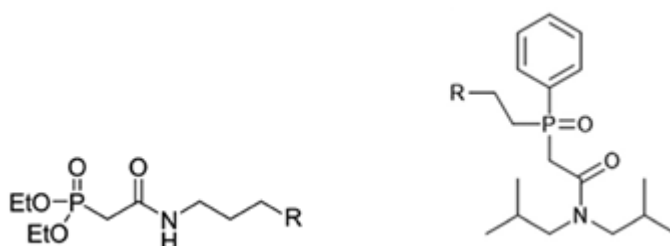
The major point of difference between the two adsorbents is their ligand loading (with a direct effect on the obtained porosity). The anchoring approach contains about 5 - 6 times the amount of CMPO ligands compared to the encapsulation approach. When a numerical ratio is calculated, based on the amount of ligands that are present, and the available cages inside MIL-101, it is found that the anchoring approach obtains a ratio of ~3.5 ligands per cage, while the encapsulation leads to ~0.65 ligands per cage. In order to explain the significant difference in loading, one must look at the way these ligands are present inside the cages. In the anchoring approach, the ligands are physically attached to the aromatic units (benzene-dicarboxylate linkers) of MIL-101. As there are ~4.2 mmol/g of such aromatic units present in the structure, they offer a lot of anchoring points for functionalization. As a result, the ~0.5 mmol CMPO/g leads to a ~12 % functionalization rate based on these aromatic units.

**Table 10.1 Overview of the material characteristics for both developed adsorbents.**

CMPO/MIL-101(Cr) Adsorbent	Langmuir surface area (m <sup>2</sup> /g)	Pore Volume (ml/g)	CMPO loading (mmol/g)	Ratio CMPO ligands per cage*
Covalently anchored (Chapter 7, Chapter 8)**	1313 ±108	0.54±0.04	0.5±0.15	~3.5 : 1
Ship-in-a-bottle (Chapter 9)	3200	1.15	0.09± 0.01	~0.65 : 1

\*Ratio based on 0.14mmol cages/g for MIL-101(Cr). \*\*Average values based on the reported results from Chapter 7 and 8.

In the encapsulation approach, no MIL-101 anchoring points are used for the functionalization, and the CMPO ligand is simply confined in the cages. The amount of cages per gram is thereby the limiting factor to achieve a certain loading. For a MIL-101(Cr) with a pristine pore volume of ~1.3 mL/g (as measured by N<sub>2</sub>-sorption analysis), the amount of cages is ~0.14 mmol/g. In addition, the CMPO used in this approach is different from the one in the anchoring approach (Figure 10.1). For the encapsulation approach, a bulky, sterically demanding CMPO was selected to prevent escape from the cage. Possibly, the combination of a limited amount of cages per gram, and the sterically demanding CMPO resulted in a lower tendency to confine one or more CMPO ligands in a cage. Nonetheless, by investigating synthesis conditions (time, temperature, reagents...) a loading optimizing could possibly be achieved.

**Figure 10.1 Difference between the CMPO ligands used in the anchoring approach (left) and encapsulation approach (right).**

## 10.2 Selectivity

Table 10.2 gives a comparison of the metal adsorption performances of both adsorbents. The preliminary work on europium adsorption with the anchored approach (Chapter 7) counts more as a proof of concept for MOF-based metal adsorbents (i.e., verify its viability). More elaborate experiments are required to obtain a thorough picture of this materials performance for selective rare earth recovery (both vs. other metals and within the lanthanide series itself). Nonetheless, from the work in Chapter 7 it was observed that the selectivity between Eu (+ Y) and Zn was significant. This correctly follows the expectations for the CMPO ligand being recommended for selective rare earth coordination, as was described in Chapter 3. The small preference for Eu over Y is not so easy to explain, as also became clear in Chapter 3. In terms of ionic size,  $\text{Eu}^{3+}$  (~95-100 pm) is, on average, larger than  $\text{Y}^{3+}$  (~90-95 pm); but this is highly dependent on coordination mode (see [1]). When only looking at electrostatic interaction of the metal and the CMPO, one would expect  $\text{Y}^{3+}$ , which has a higher charge density than  $\text{Eu}^{3+}$ , to be more attracted towards the hard bases of CMPO. On the other hand, it was also described in Chapter 3 that the intraligand repulsions increase as the ions get smaller, thereby hindering the interaction with such smaller ions. Additional factors like counter ions and/or solvent molecules have a significant influence on the first coordination sphere, and thus the overall coordination behavior. It turns out that in this material, the combined parameters of influence result in a slight preference for Eu over Y. Nonetheless, as mentioned, an elaborate selectivity experiment, including more lanthanides, could provide more information on the adsorption behavior of the anchored approach, and possible patterns in selectivity might be deduced.

When this adsorbent (anchored approach) is subjected to a selectivity experiment including uranium (Chapter 8), the selectivity completely shifts towards this actinide. We learned from Chapter 3 that the CMPO is both effective for uranyl and lanthanide coordination, and that for basic CMPO, i.e. without the influence of substituents, the selectivity was quite comparable between both. Once again, it is difficult to provide definitive reasoning for the observed large difference in selectivity. Perhaps we have to broaden our focus from the performance of one ligand to the effect of various ligands in the metal's coordination sphere (as also described in Chapter 3). From Table 10.1, we learn that the anchored approach yields ~3.5 ligands per cage. Although this is significantly higher than the encapsulated approach (~0.65 ligands per cage), it is still too low for it to be considered a dense network of ligands onto a surface, such as is, for instance, the case with the SAMMS approach on porous silicas (> 1.5 ligands/nm<sup>2</sup>) [2] (see also Chapter 3). From the work of Binnemans *et al.* [3], it was suggested that the ligand density (chelates) greatly influences the selectivity. An increase of density resulted in the materials being more selective towards smaller lanthanides, while a lower density favored the larger ions.

**Table 10.2 Overview of developed adsorbents and their adsorption performance.**

CMPO/MIL-101(Cr) Adsorbent	Saturation capacity (mg/g)	pH	Active Sites (mmol/g)	Selectivity	Regeneration (%)	Equilibrium time	Ligand leaching
Anchoring Approach (Chapter 7, Chapter 8)	12.46 (Eu)	4	$0.5 \pm 0.15$	Highly over Zn, slightly over Y	Not tested	~5 hrs (~75% in 3.5 hrs)*	Not tested
	~ 25 (U)	4		Highly over REEs	100 % (0.1 M oxalate)	30 mins (~75% in 10 min)*	~15 % after 5 cycles
Ship-in-a-bottle (Chapter 9)	5.32 (U)	3	$0.09 \pm 0.01$	Highly over Al, Cd, Co, Cu, Mn, Ni, Pb, Zn, Y, Eu, Gd, Nd	~98 % (0.1 M HNO <sub>3</sub> )	~6hrs (~75% in 1 hr)*	0 % (after 1 cycle)
	27.99 (U)	4					<5 % (after 3 cycles)

\*Achieved % of the maximum adsorption capacity.

The reason for this was attributed to an effect on the ligands conformation (or *bite*), influenced by the amount of steric hindrance of the ligands (i.e., crowding). This was also described in Chapter 3, albeit because of the influence of ligand substituents. Nonetheless, it is once more confirmed that steric effects play a major role in metal selectivity.

Perhaps because of the low density of CMPO ligands inside the cages of MIL-101, the effective coordination stoichiometry is 1:1 (cation:ligand) and the CMPO ligands can be regarded as isolated from each other. As a consequence, the ligand might prefer coordination to the larger uranyl cation. Additionally, it was mentioned that the two O<sub>yl</sub>-bonds in uranyl are very strong (Chapter 3). It might be less favorable for such an ion to be complexated by a dense network of (surface-organized) CMPOs, compared to a solvated lanthanide cation, where all solvent molecules or counter ions in its first coordination sphere are more readily exchanged with donor atoms from the CMPO. The uranyl oxygens could cause some steric hindrance with the organized CMPOs (densely anchored to a surface). This might also explain why the CMPO-calixarene setups, described in Chapter 3, show preference for lanthanides (cfr. Table 3.3: Eu(III) > U(VI)). An isolated CMPO ligand could be favorable for selective uranyl coordination, as it is suggested that a stable U(VI)-CMPO adduct is already possible at 1:1 stoichiometry, especially in nitrate rich aqueous environments [4].

The high selectivity for U(VI) over competing elements was also observed in the encapsulated approach (Chapter 9). In this approach, the more sterically demanding CMPO was used (Figure 10.1, right). Similar reasons could be suggested for the observed selectivity difference. The low loading suggests 1:1 stoichiometry, which might favor the uranyl ions. Although, this ligand is more mobile as opposed to the anchored approach, the presence of bulky substituents on CMPO will result in a highly specific *bite* size of the ligand.

## 10.1 Capacity and Kinetics

The anchored approach results in an adsorption capacity (Table 10.2) of ~12.5 mg/g for europium (Chapter 7) and ~25 mg/g (based on the kinetic experiments) for uranium (Chapter 8). On a mmol/g basis, the results are closer together (uranium being a lot heavier than europium), although uranium uptake (0.105 mmol/g) is still higher than europium's (0.083 mmol/g). In terms of equilibrium time, there is a large difference for both metals. While it takes about 5 hours to achieve equilibrium for Eu(III), only about 30 minutes are needed for U(VI). As the adsorbents are identical in both experiments, this effect must be related to the way europium, respectively uranyl, interacts with the ligands. Perhaps because of the nearly isolated CMPO species in the cages, the 1:1 cation:CMPO adducts are more readily formed in the case of uranyl, compared to Eu(III), resulting in faster kinetics. This is but a mere suggestion of course. Alternatively, the adsorption tests in Chapter 7 (Eu) were performed in HCl-acidified solutions, whereas the ones in Chapter 8 (U) in nitric acid-based solutions. Based on the role of counter

ions, described in Chapter 3, the steric influence of nitrate ions from  $\text{HNO}_3$  in the first coordination sphere might provoke quicker exchange for CMPO donors, as opposed to the chlorine ions of  $\text{HCl}$ . Additional experiments on the influence of the used acid-type could give more insight in this matter. The difference in kinetics between uranyl and europium will most definitely have an effect on the selectivity as well. If it takes 5 hours to reach equilibrium for Eu, it is easy to understand that after 30 minutes, the quickly adsorbed uranyl results in a high Eu/U selectivity. It would be interesting to also test the selectivity after 5 hours of contact, when Eu has equilibrated as well. Finally, it must be noted that the kinetic setups in Chapter 7 and 8 differ quite a lot. Where the europium experiments made use of a one-pot setup with periodical sampling, the uranium setup used individual vials per concentration test. Also, the used liquid and solid amounts were different in each setup. The experimental conditions might have had a (partial) impact on the results. In order to unambiguously assess the differences, an identical approach is desired.

The encapsulation approach (Chapter 9) achieves a maximum adsorption capacity of  $\sim 28$  mg U/g (obtained at pH 4). Higher uptakes would be possible by increasing the pH, but that would result in the formation of multinuclear hydroxylated uranium species, which would drastically increase the uptake, but also lead to interaction of these species with the MOF framework itself (as described in Chapter 9). pH 4 is therefore a good indication of the optimal ligands performance with mononuclear uranyles. The kinetic results for this approach show an equilibrium time of  $\sim 6$  hours. This is quite long, and rather surprising when compared to the results in Chapter 8 (30 min). In both cases, uranyl adsorption is considered; therefore similar uptake kinetics could be expected. A possible answer for these low uptake kinetics is perhaps found when comparing both CMPO ligands to each other (Figure 10.1). In the anchored approach, the dangling CMPO ligands, with their amide and phosphonate parts, are quite hydrophilic in nature. If one looks at the bulky CMPO ligand, used in the encapsulated approach; the presence of the aromatic rings and long aliphatic chains introduces some hydrophobicity around the ligand. This could perhaps hinder the migration of solvated uranyl complexes towards the donor atoms of the CMPO, thereby significantly delaying the uptake kinetics.

## 10.2 Reusability

The proof of concept study with the anchored approach (Chapter 7) did not include a regeneration and reuse part. In the uranium-oriented study with this material (Chapter 8), it was found that efficient stripping could be achieved (100 %) when using dilute oxalate solution as regenerant. Nonetheless, it was already mentioned in Chapter 8 that this type of stripping agent is perhaps not the best choice for the regeneration of a MOF-based adsorbent. The chelating properties of the oxalate might affect the coordination bonds between MIL-101's chromium

metals and its carboxylate linkers, possibly leading to gradual structure degradation and a loss in activity. Eventhough the ligand leaching was about 15 wt. % after 5 full adsorption/desorption cycles, it would still be desirable to investigate alternative stripping agents, such as mineral acids.

In the encapsulation approach, it is shown that effective stripping (~98 %) can be achieved by using dilute nitric acid. The combination of the pH effect (protonation of CMPO) and the good coordinating properties of nitrate ions with uranyl, suggest an excellent regenerant. Moreover, the ligand leaching was found to be of a very low level, i.e., 0 wt. % after 1 full adsorption/desorption cycle, and less than 5 wt. % after 3 full cycles (which in these experiments corresponds to over 140 hours of turbulent contact with the acidic aqueous environment). It would, however, be interesting to see the effect of HCl as a possible regenerant, for reasons stated earlier (effect counter ions).

## REFERENCES

- [1]: Database of Ionic Radii. <http://abulafia.mt.ic.ac.uk/shannon/ptable.php> (Accessed in May 2017).
- [2]: G.E. Fryxell, H. Wu, Y.H. Lin, W.J. Shaw, J.C. Birnbaum, J.C. Linehan, Z.M. Nie, K. Kemner, S. Kelly, Lanthanide selective sorbents: self-assembled monolayers on mesoporous supports (SAMMS), *J Mater Chem*, 14 (2004) 3356-3363.
- [3]: D. Dupont, W. Brullot, M. Bloemen, T. Verbiest, K. Binnemans. Selective Uptake of Rare Earths from Aqueous Solutions by EDTA-Functionalized Magnetic and Nonmagnetic Nanoparticles, *ACS Appl. Mater. Interfaces*, 6 (2014) 4980–4988.
- [4]: J. Florek, S. Giret, E. Juere, D. Lariviere, F. Kleitz, Functionalization of mesoporous materials for lanthanide and actinide extraction, *Dalton Trans*, 45 (2016) 14832-14854 and references therein.





# 11 CONCLUSIONS AND OUTLOOK

In this work, the prospect of using metal-organic frameworks in the field of aqueous-phase metal adsorption was investigated. It has become clear throughout these chapters that there is a dire need for stable, selective adsorbents for the recovery or removal of all kinds of species. Especially with respect to critical metals, such as rare earths, or radiotoxic elements like uranium, the necessity for a technology that can treat low-concentration aqueous streams is high. Before commencing an experimental study on the application of MOFs as aqueous-phase adsorbents, it was highly important to be able to judge these materials on their water stability. MOFs have the prejudice of being water-unstable and indeed, apparently many of them are not suitable at all for moist conditions, let alone water itself. The question could therefore be raised on why anyone would investigate their potential in metal adsorption, a field where aqueous, often acidic conditions are a standard environment.

It is because MOFs have several advantages over other commonly applied materials, that they are worth exploring. Their incredible surface areas and porosity, simple syntheses, high amount of different structures, no inactive bulk material and versatile properties make them objects of intensive research... Based on the stability studies described in this work (theoretical and practical), a few MOFs have emerged with a high permanent stability in water (MIL-101(Cr), NH<sub>2</sub>-MIL-53, UiO-66, UiO-67). Some of these even permanently withstand moderate acidic conditions (MIL-101(Cr), NH<sub>2</sub>-MIL-53, UiO-66), while MIL-101(Cr) and UiO-66 are even perfectly resistant to highly acidic conditions (pH 0). Several of the other tested MOFs also show proper stability to these conditions (3 days exposure), yet not permanently. It will therefore depend on the application whether or not a certain MOF is suitable.

For this work, a highly acid stable MOF was required for the incorporation of selective ligands for the recovery of critical metals, such as REEs or uranium. As these selective ligands often tend to be chelating, bulky molecules, a large pore material was desired. MIL-101(Cr) was selected as an ideal candidate, due to its mesoporous cages, and ready functionalizability, on top of the proven high permanent stability. The sterically demanding CMPO-type ligand was then introduced into this MOF via two different routes. The first conventional route consisted of stepwise covalent build-up of the CMPO onto the aromatic units of the MOF. While this approach was successful, questions could be raised on the design of this material. First, the MOF has to be synthesized, followed by a three-step anchoring method. For industrial applications, a more facile and cost-effective approach might be desired. As a result, the encapsulation approach was investigated. This approach confined CMPO ligands in-situ during the MOF synthesis, thereby trapping them in its cages. Consequently, the CMPO is present in MIL-101 as a ship in a bottle. This one-step strategy sounds a lot more attractive than a multistep functionalization method. Moreover, such a ship-in-a-bottle approach is a perfect compromise between heterogeneous and homogeneous systems, where the CMPO can act freely inside the pores, yet remains confined within the cages of MIL-101.

It has, above all, become clear from the adsorption studies that both developed adsorbents show a high stability in the applied conditions. Therefore, the main goal was achieved, i.e., creating an adsorbent suitable for repetitive application in metal adsorption processes. This applies to both support stability and functionality preservation. Secondly, the incorporated ligands have proven to be active in the adsorption of the targeted species. In our case, the CMPO showed its high affinity for uranium, and the study in absence of uranium also pointed out affinity for rare earths (cfr. Eu and Y from Zn). Therefore, incorporating these ligands did not hinder their performance. Thirdly, both adsorbents are readily regenerable, which means the adsorbed species can be recovered and the adsorbent can be reused in additional cycles.

There is room for improvement, however. When comparing our adsorbents to the state of the art (e.g., Table 3.1, Table 9.3), the metal capacity is often a limiting factor. Several reported MOF-based adsorbents show uptakes that well exceed our own. Yet, it is confirmed that this is due to the currently limited loading of ligands. This is a parameter that can be investigated and optimized, while potential problems with stability or selectivity would be inherent to the material, thus requiring a new adsorbent design. It has been shown in this work that some of the reported MOF adsorbents with incredible capacities will face difficulties in real life applications, due to either structural instability or weakness of the support-functionality linkage. These phenomena are often not investigated or simply omitted from the work, but they are of key importance in order to properly assess the potential of an adsorbent.

In my opinion, several of these MOFs show a lot of promise for applications in aqueous adsorption processes. We can optimize them on a structural basis, e.g., perfect their porosity,

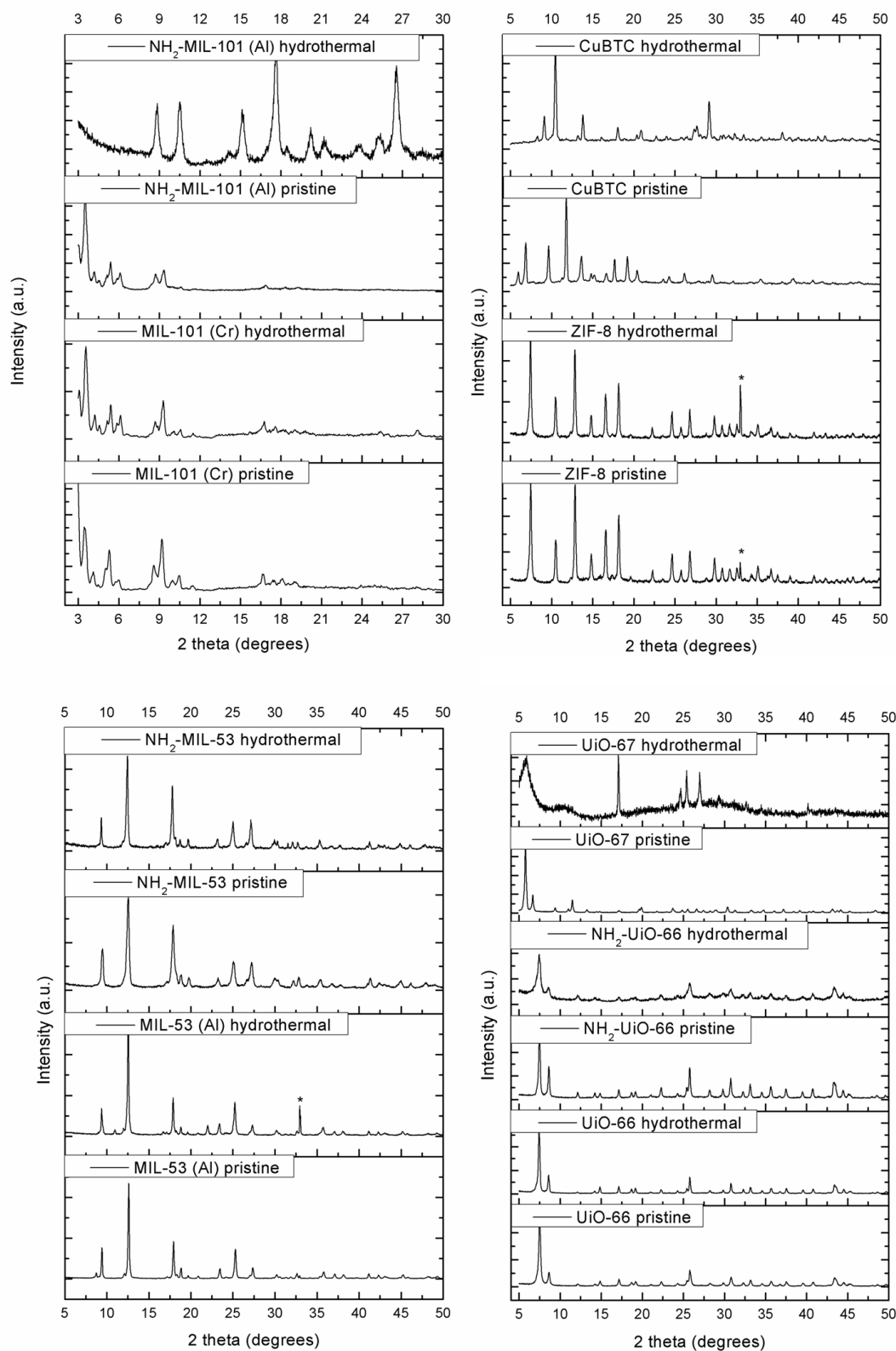
influence their charge effects, and we can tailor their properties by modification, either in-situ or post-synthetic. With the help of theoretical (and practical) insights in their stability, novel highly stable MOFs can be designed through a rational approach.

Does this make MOFs the pinnacle of metal adsorbents? Probably not. They have a lot of advantages, but the concept of a metal-containing coordination polymer, to recover metallic species from an aqueous environment will probably often raise suspicion. For organics removal, on the other hand, they are perfect candidates, and often don't even need to be post-modified to have the desired selectivity. There isn't one class of porous materials that offers this kind of versatility in terms of structures and interactions than the metal-organic frameworks, which is ideal for the adsorption of a large scope of different organic compounds

This does not mean that metal adsorption is out of the question, though. As stated, some frameworks are definitely worth exploring deeper, and this work clearly shows their potential. However, as a class of porous materials (i.e., MOFs as such) they might face competition from alternative material classes, such as the more recent, but similar covalent-organic frameworks (COFs), which do not use metals in their structure, and show great promise in terms of porosity, stability, and functionalizability. In any case, a great deal of exciting research lies hidden in the world of these porous frameworks, whether they are hybrid or purely organic.

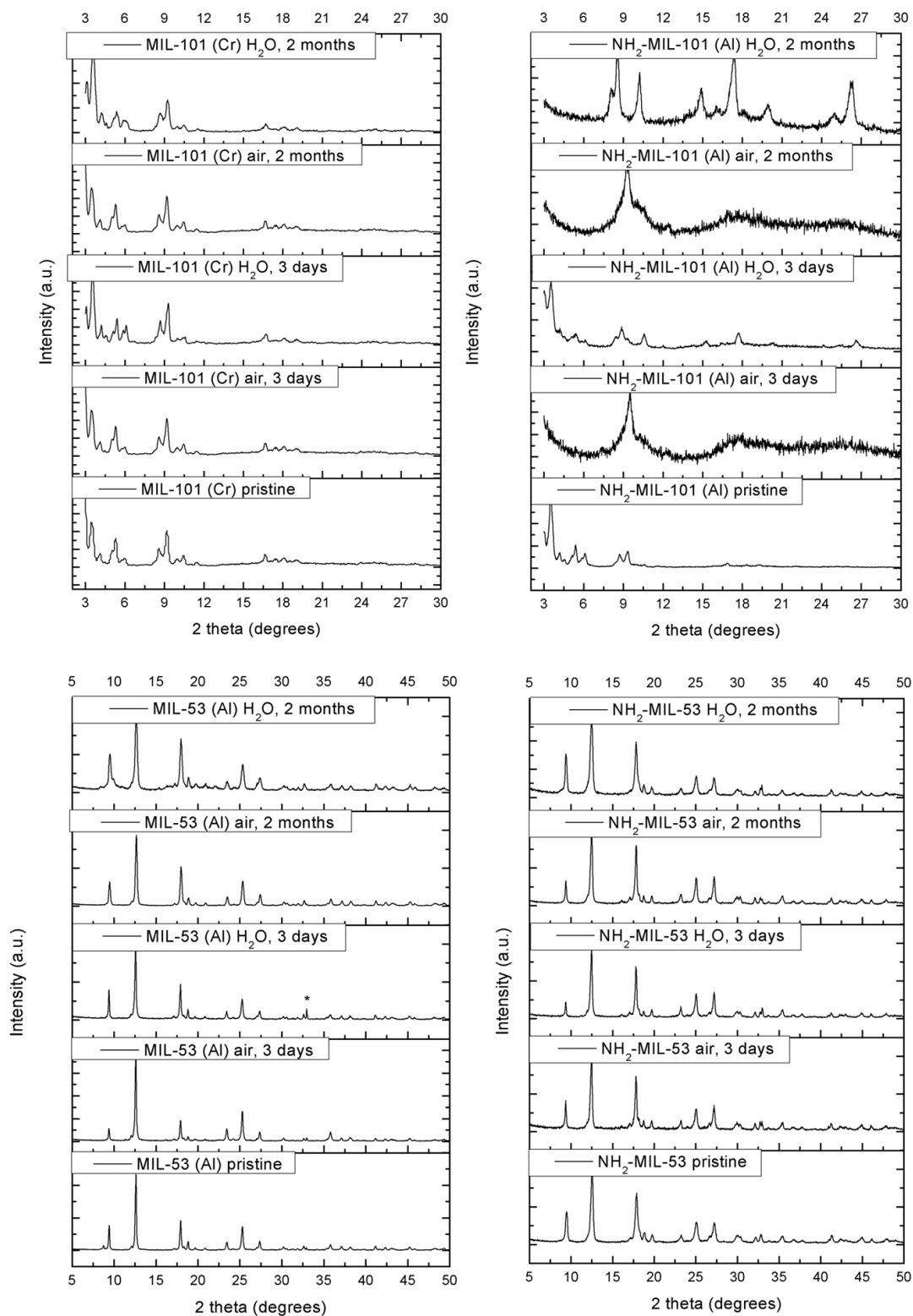


# 12 APPENDICES

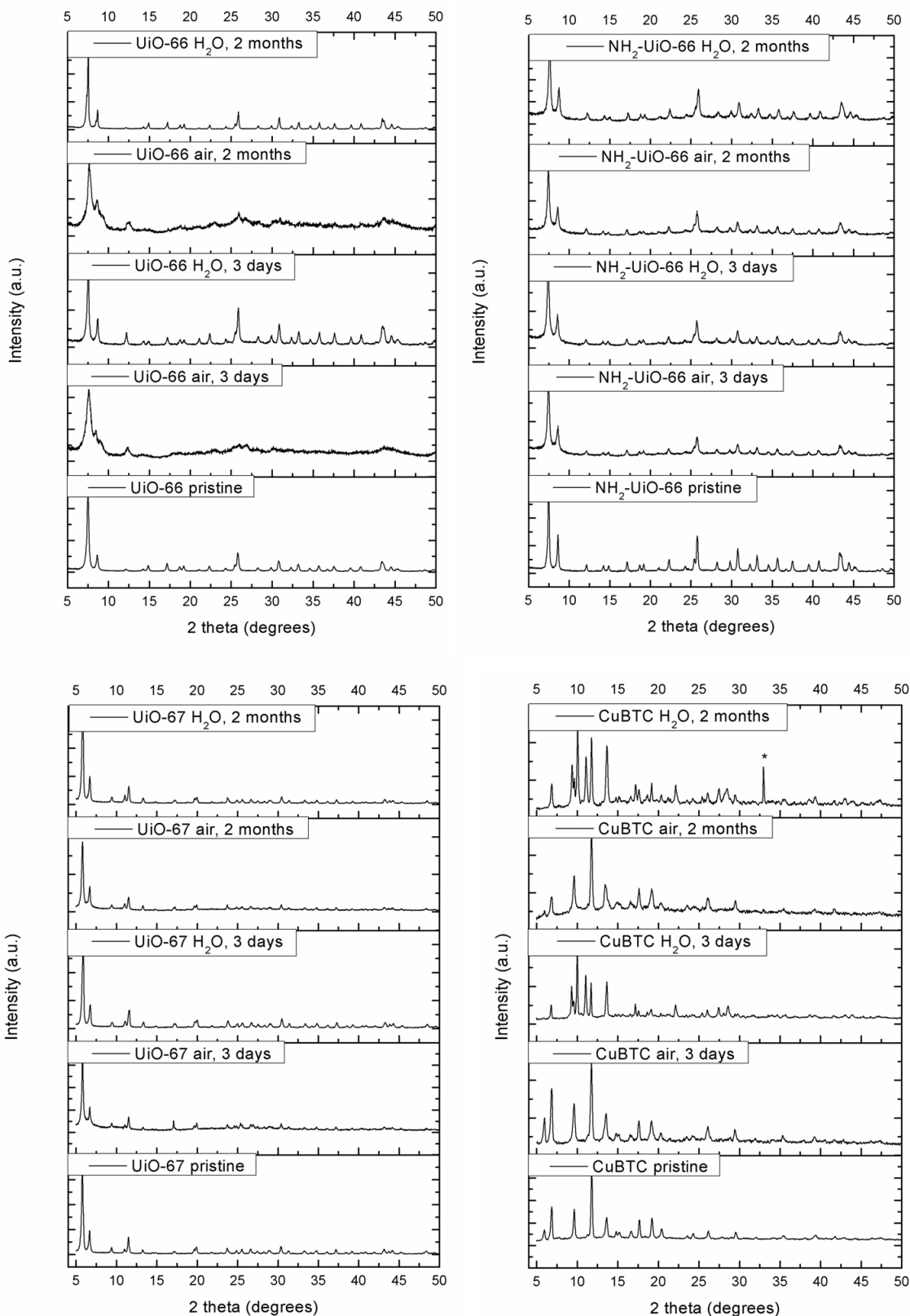


Appendix 1.1 XRPD patterns of all pristine MOF materials and after the hydrothermal treatment

(\*is from the sample holder at an angle of 32.9°).

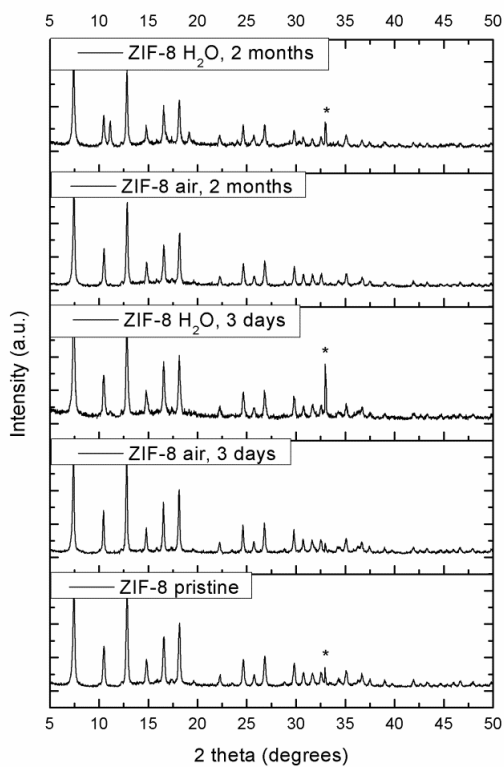


Appendix 1.2 (A) XRPD patterns of all pristine MOF materials and after exposure to water or air for 3 days to 2 months (\*is from the sample holder at an angle of 32.9°). (1/3)

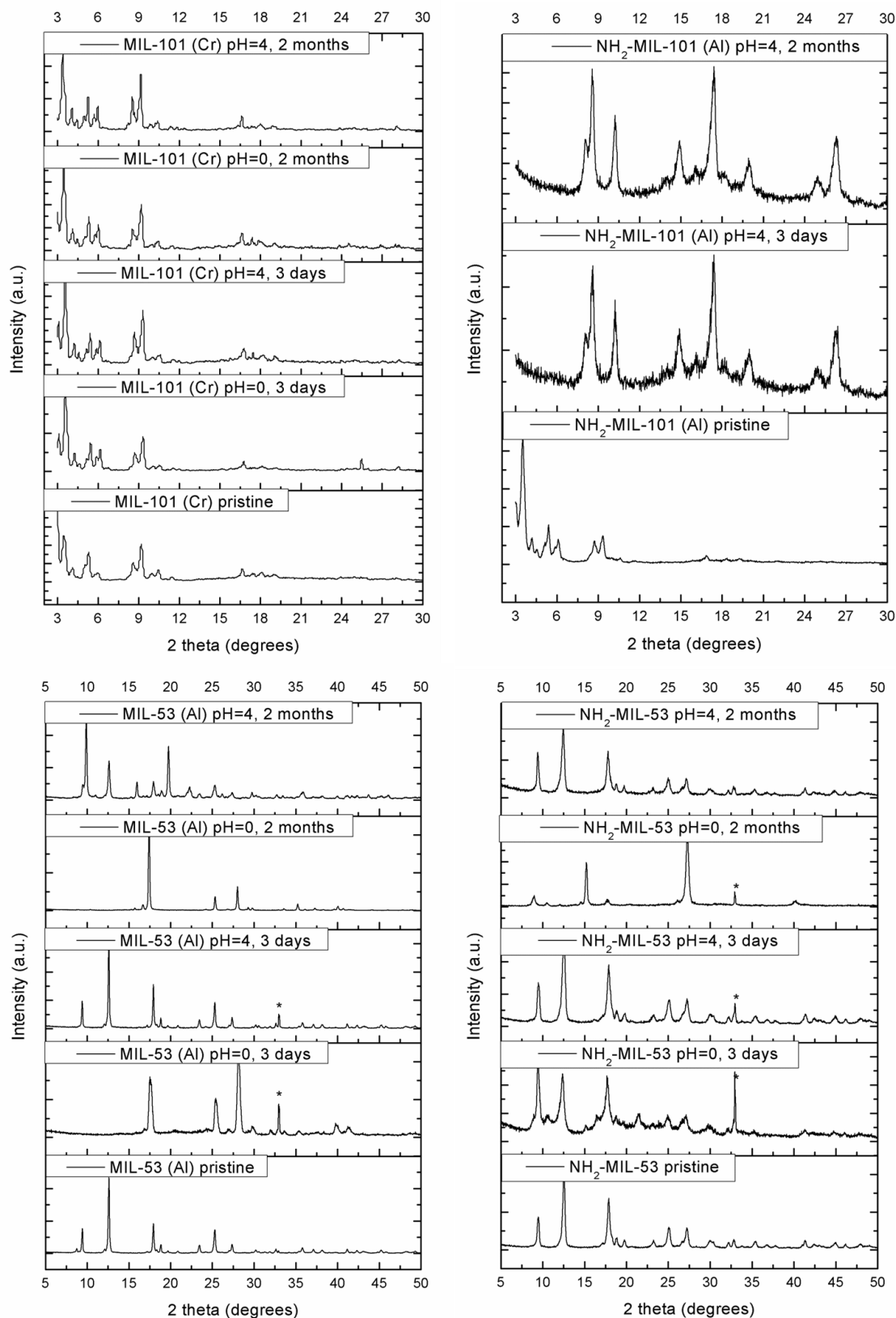


Appendix 1.2 XRPD patterns of all pristine MOF materials and after exposure to water or air for 3 days to 2 months (\*is from the sample holder at an angle of 32.9°). (2/3)

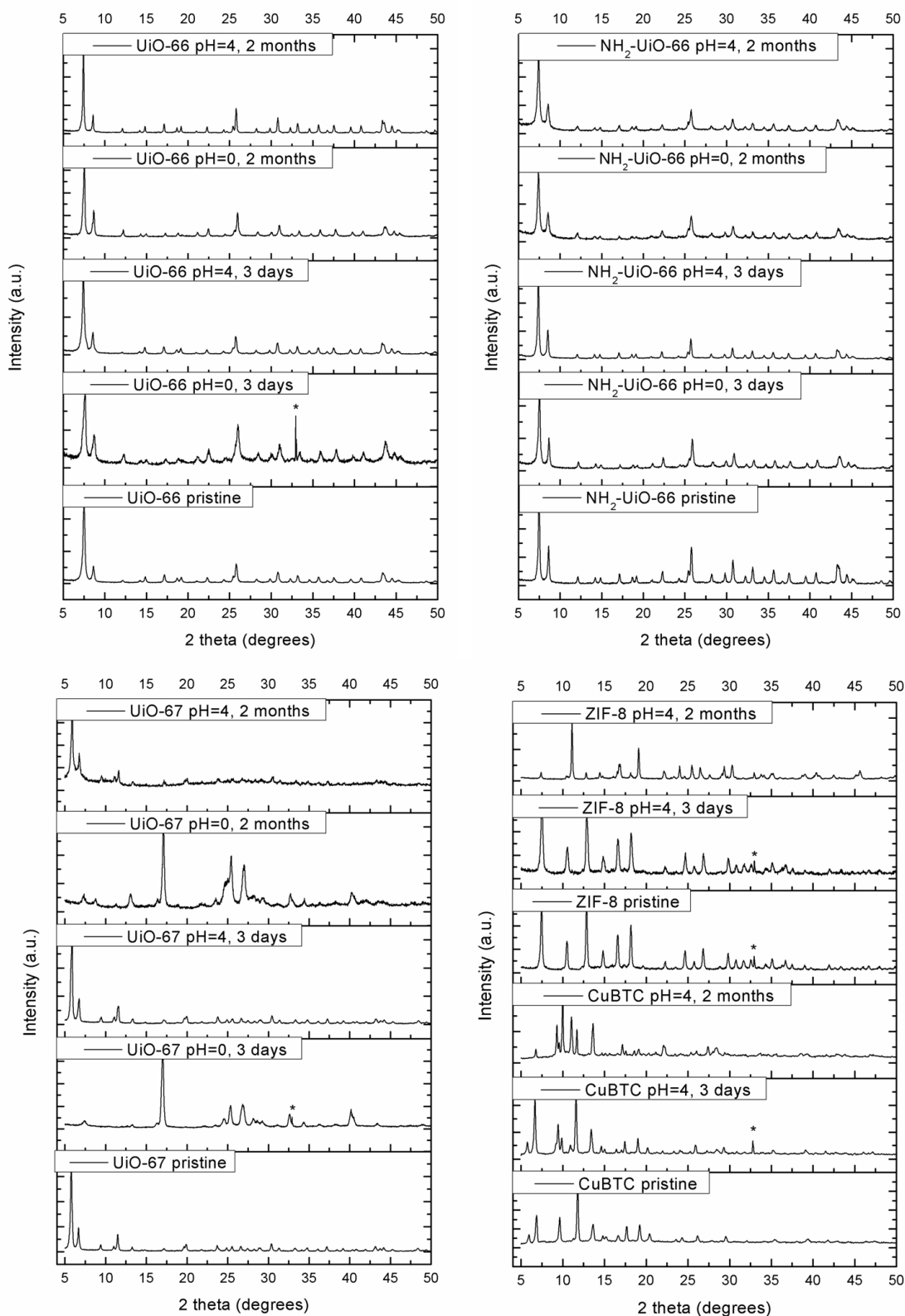




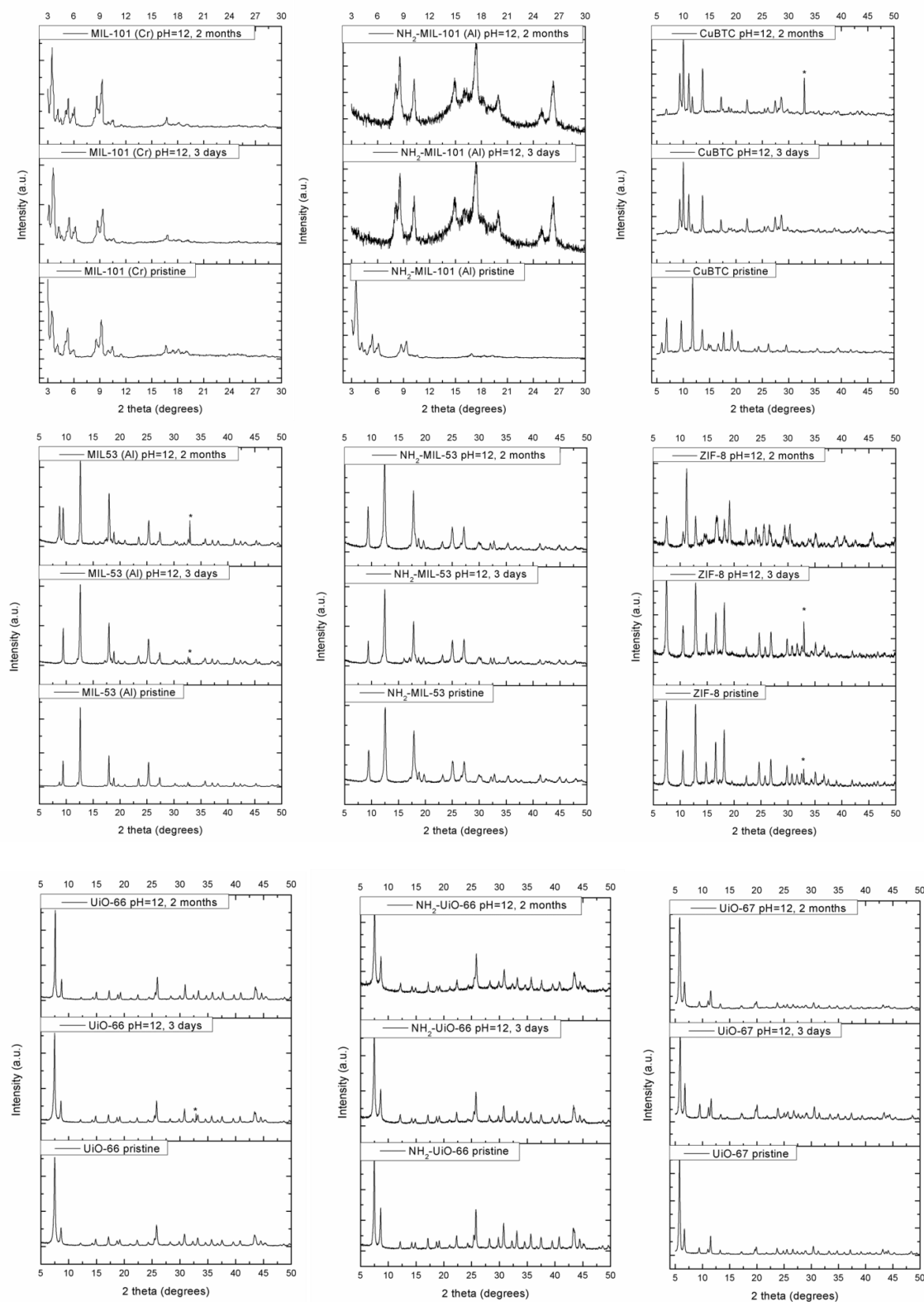
Appendix 1.2 XRPD patterns of all pristine MOF materials and after exposure to water or air for 3 days to 2 months (\*is from the sample holder at an angle of  $32.9^\circ$ ). (3/3)



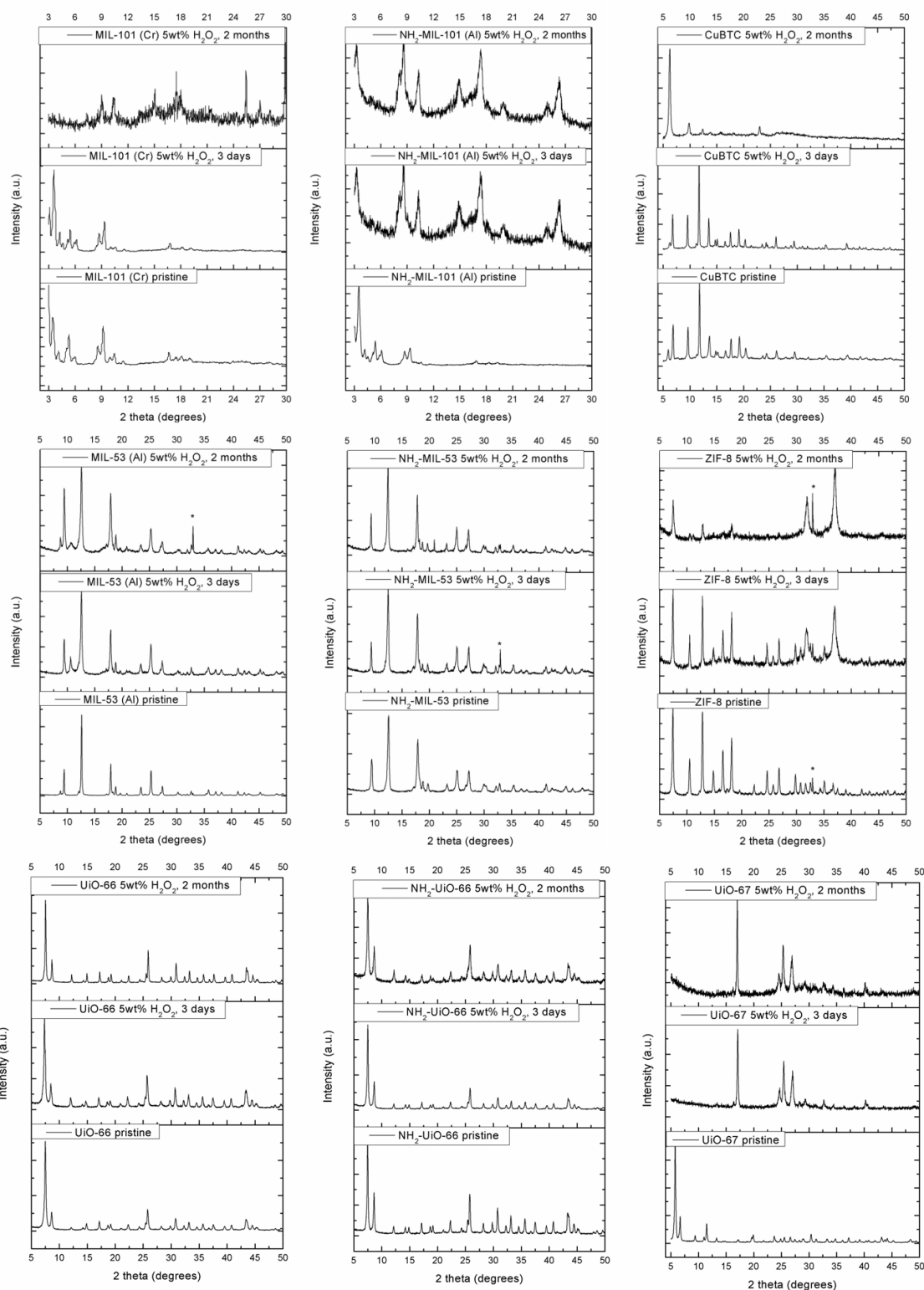
Appendix 1.3 XRPD patterns of all pristine MOF materials and after exposure to acidic conditions (pH=0 and pH=4) for 3 days to 2 months (\*is from the sample holder at an angle of 32.9°). (1/2)



Appendix 1.3 (B) XRPD patterns of all pristine MOF materials and after exposure to acidic conditions (pH=0 and pH=4) for 3 days to 2 months (\*is from the sample holder at an angle of 32.9°). (2/2)

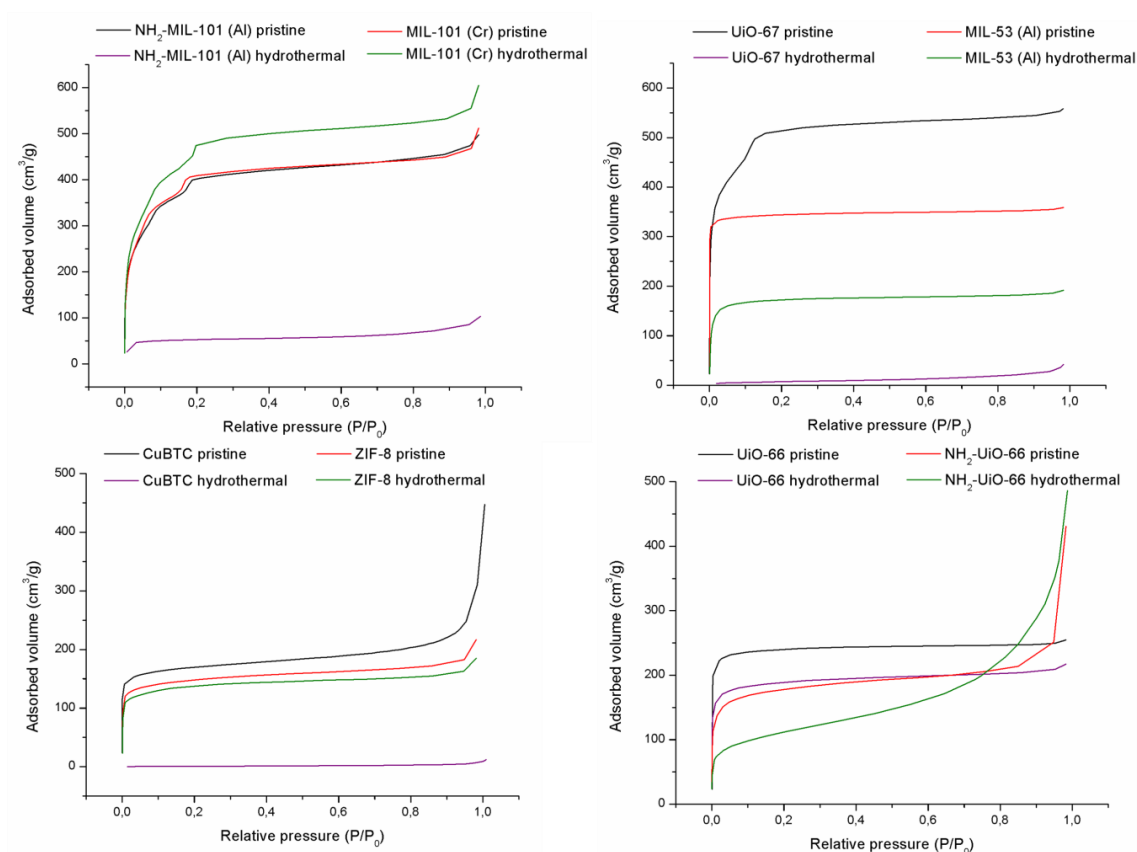


Appendix 1.4 XRPD patterns of all pristine MOF materials and after exposure to basic conditions (pH=12) for 3 days to 2 months (\*is due from the sample holder at an angle of 32.9°).

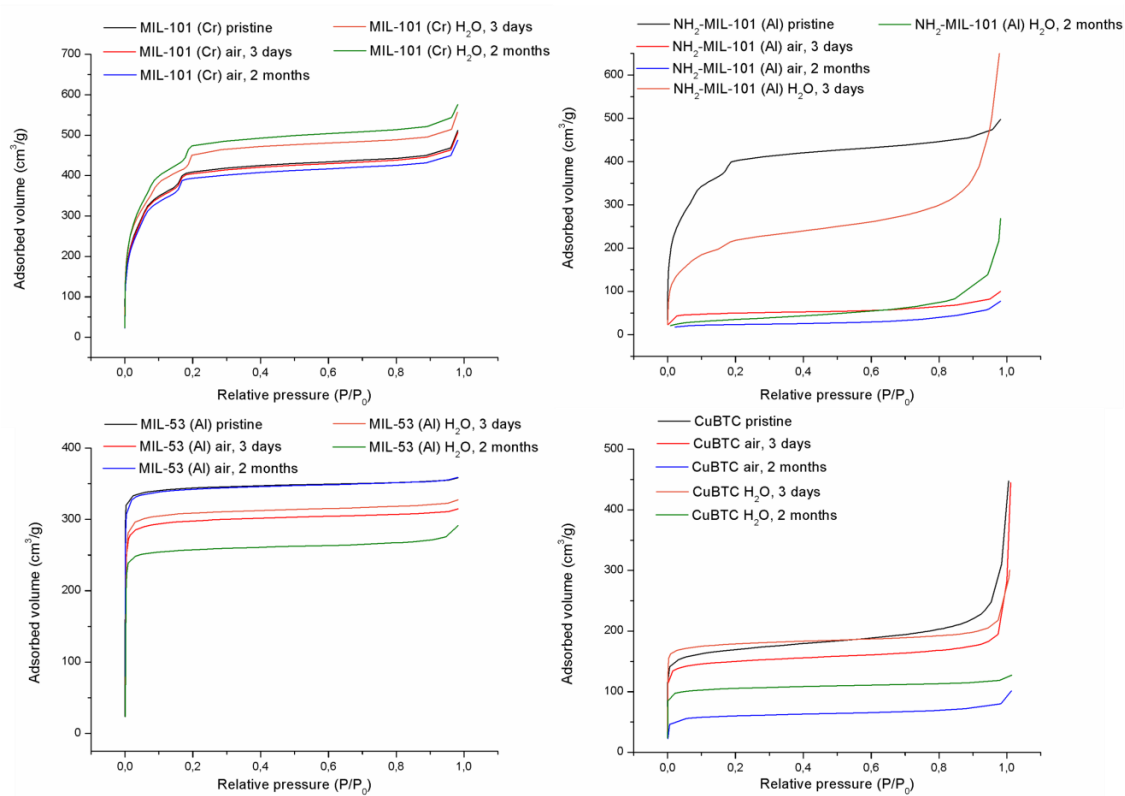


Appendix 1.5 XRPD patterns of all pristine MOF materials and after exposure to oxidative conditions (5 wt.%  $H_2O_2$ ) for 3 days to 2 months (\*is from the sample holder at an angle of 32.9°).

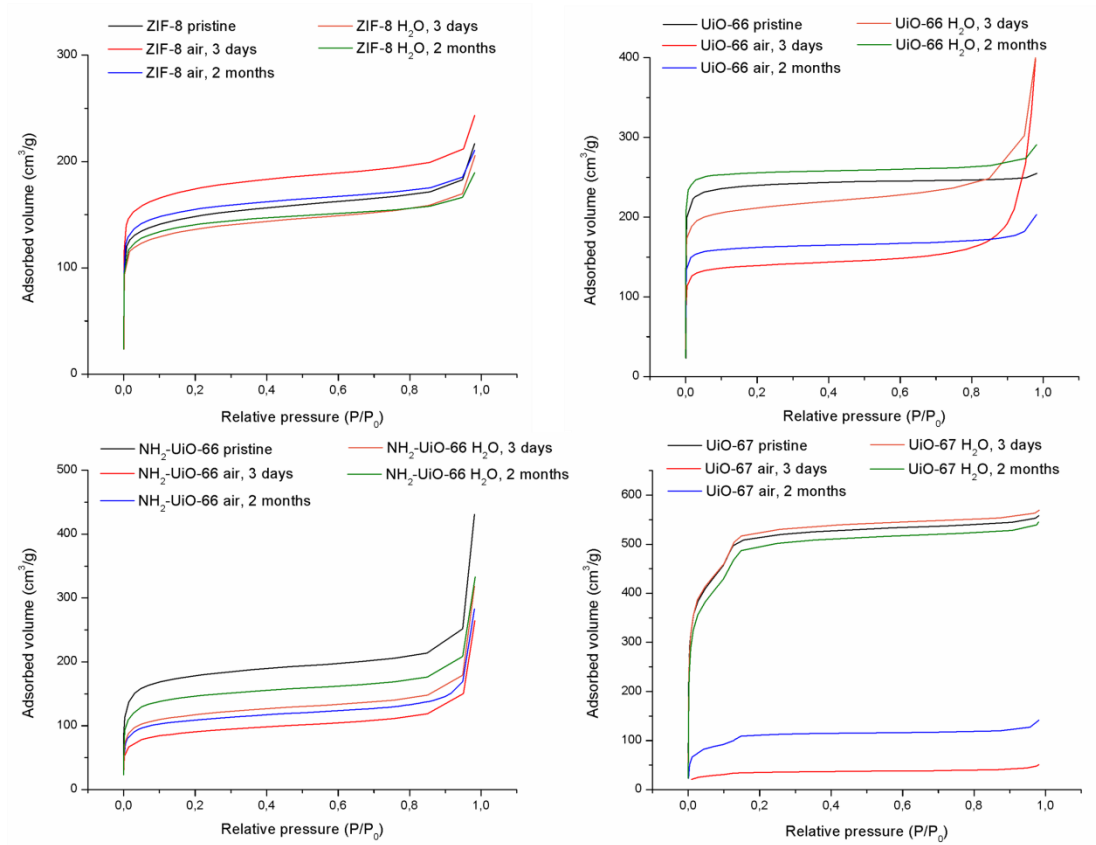
## Functionalized Metal-Organic Frameworks as Selective Metal Adsorbents



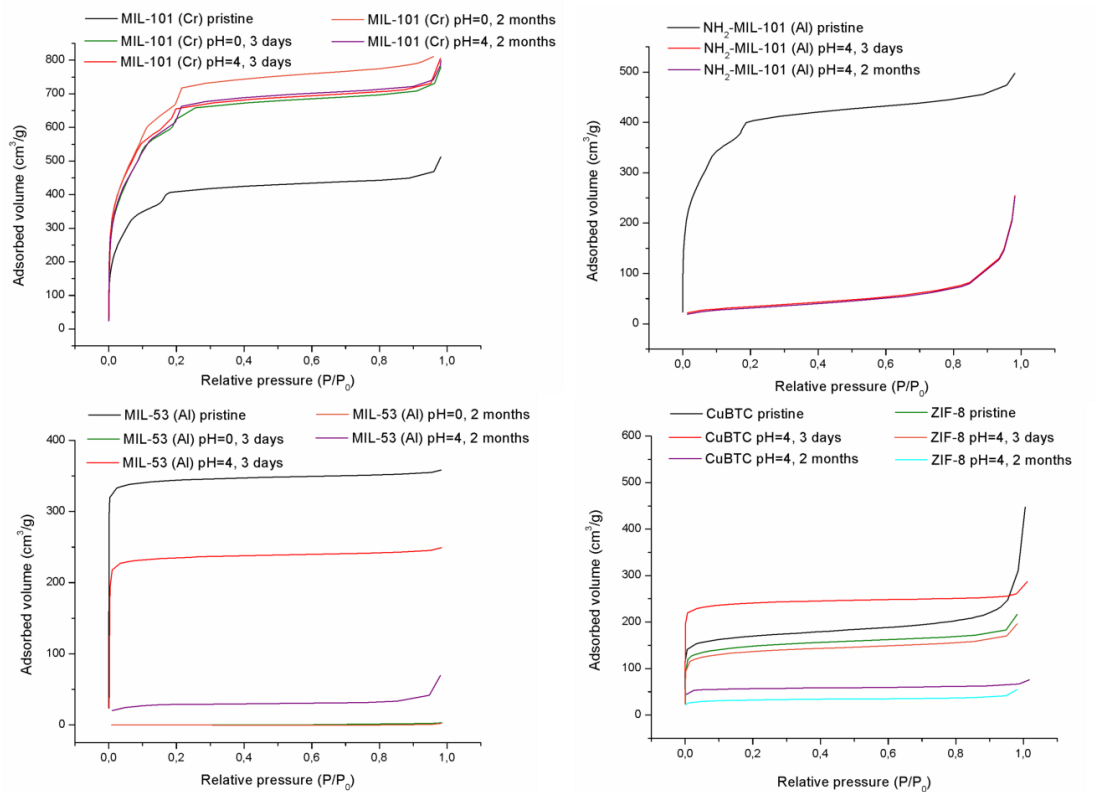
Appendix 1.6 Nitrogen adsorption isotherms of all pristine MOF materials and after the hydrothermal treatment.



Appendix 1.7 Nitrogen adsorption isotherms of all pristine MOF materials and after exposure to water or air for 3 days to 2 months. (1/2)

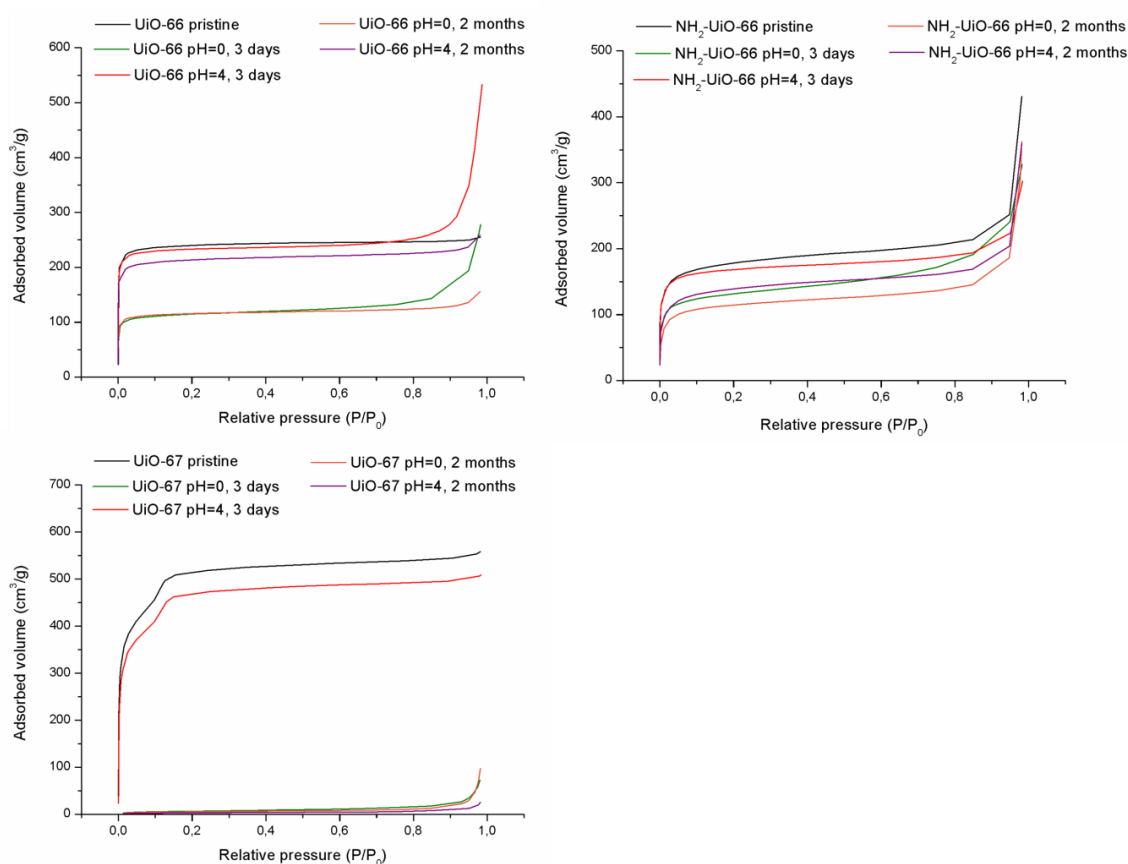


Appendix 1.7 Nitrogen adsorption isotherms of all pristine MOF materials and after exposure to water or air for 3 days to 2 months. (2/2)

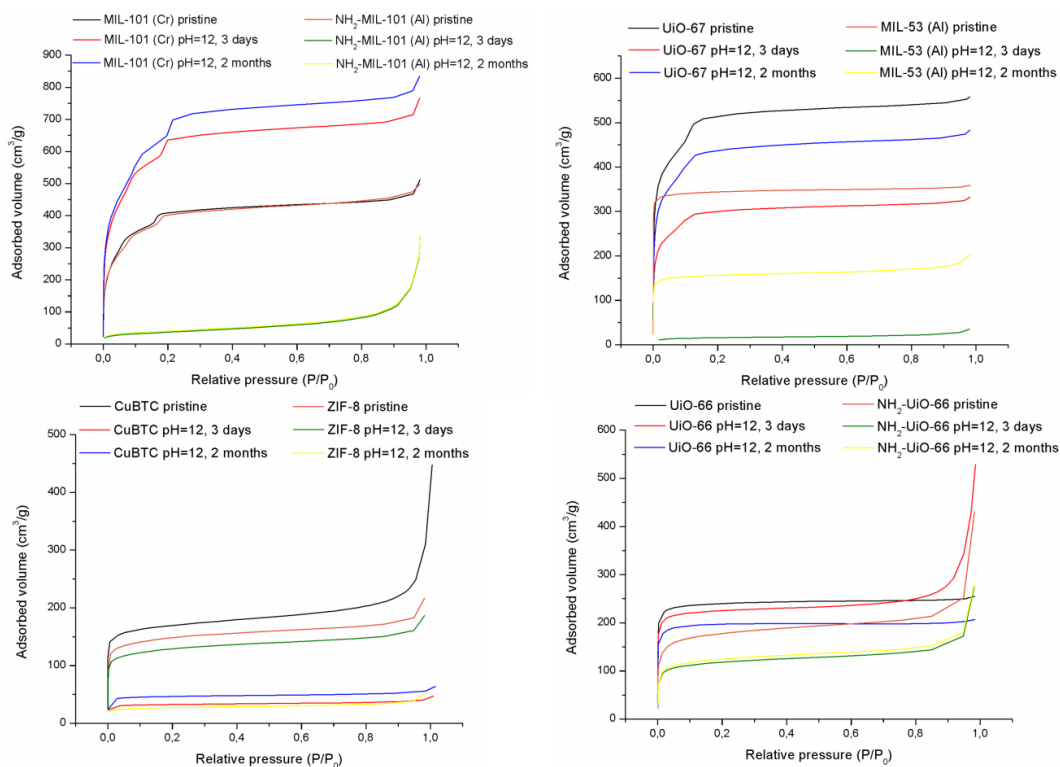


Appendix 1.8 Nitrogen adsorption isotherms of all pristine MOF materials and after exposure to acidic conditions (pH=0 and pH=4) for 3 days to 2 months. (1/2)

## Functionalized Metal-Organic Frameworks as Selective Metal Adsorbents

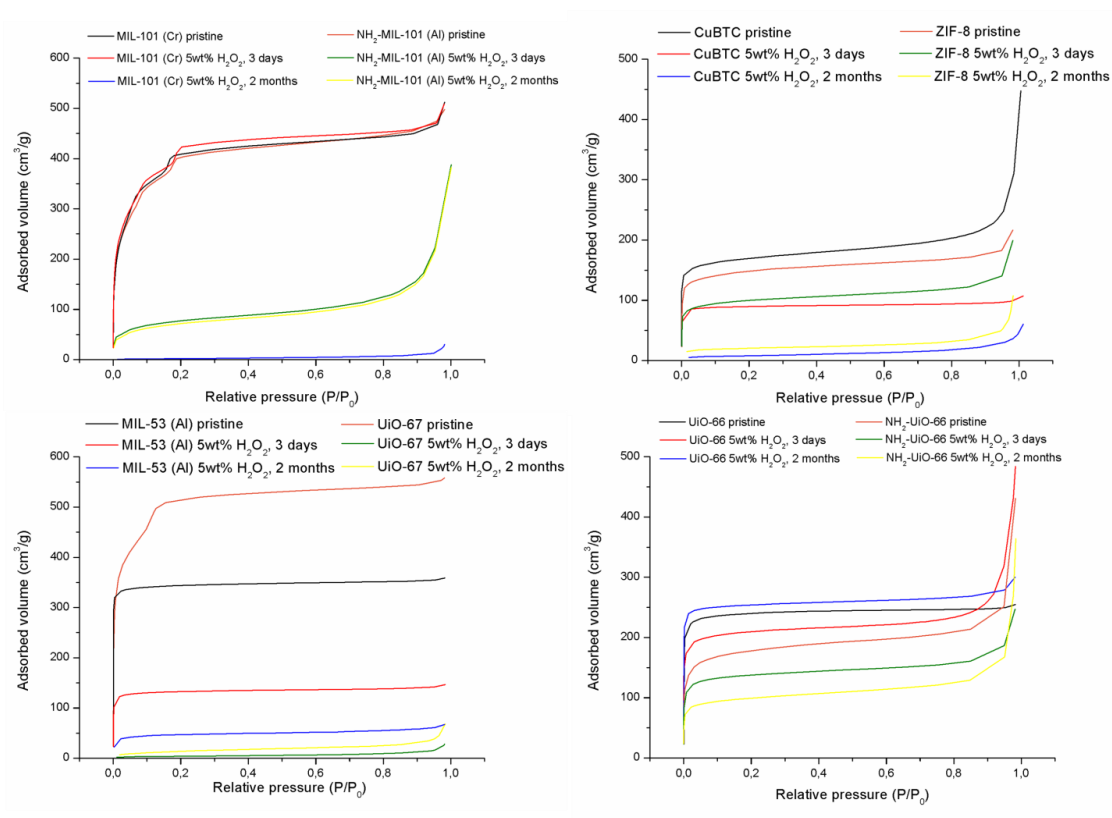


Appendix 1.8 Nitrogen adsorption isotherms of all pristine MOF materials and after exposure to acidic conditions (pH=0 and pH=4) for 3 days to 2 months. (2/2)



Appendix 1.9 Nitrogen adsorption isotherms all pristine MOF materials and after exposure to basic conditions (pH=12) for 3 days to 2 months.



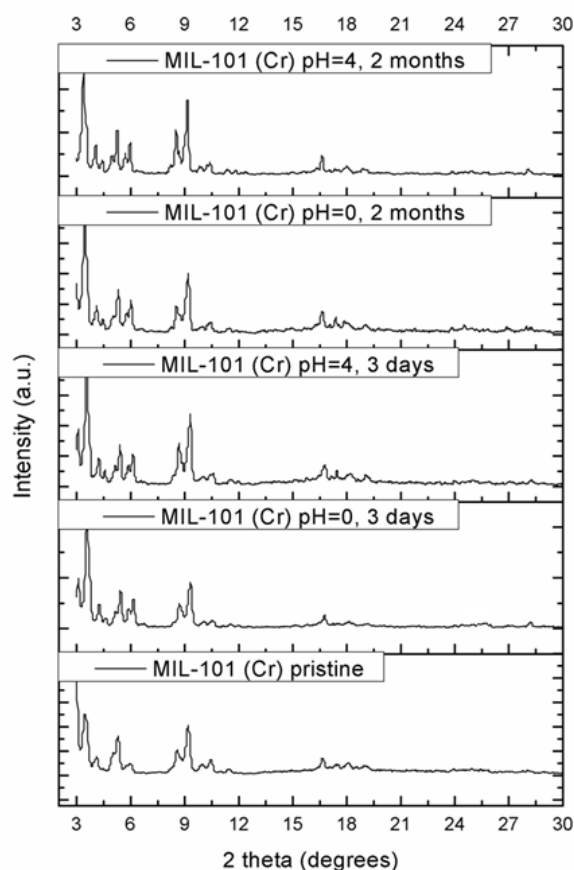


Appendix 1.10 Nitrogen adsorption isotherms of all pristine MOF materials and after exposure to oxidative conditions (5 wt% H<sub>2</sub>O<sub>2</sub>) for 3 days to 2 months.

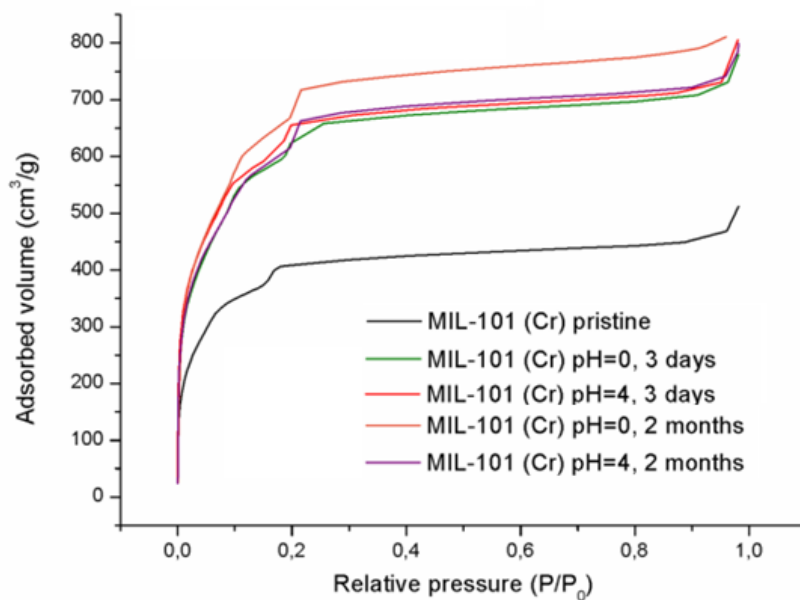
Appendices 1.1 to 1.10 are part of “Systematic study of the chemical and hydrothermal stability of selected “stable” Metal Organic Frameworks” (Chapter 5), as supporting information.

The electronic version of this supporting information (including higher resolution images) can be consulted online at: <http://www.sciencedirect.com/science/article/pii/S1387181115007209>

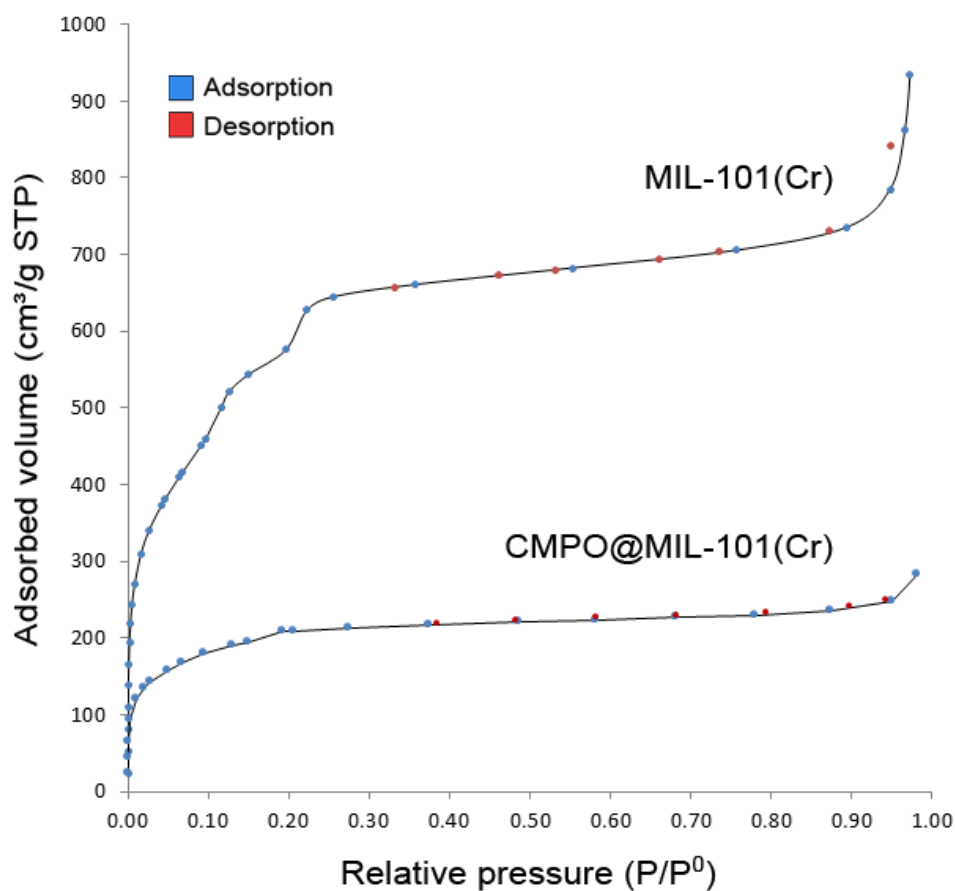




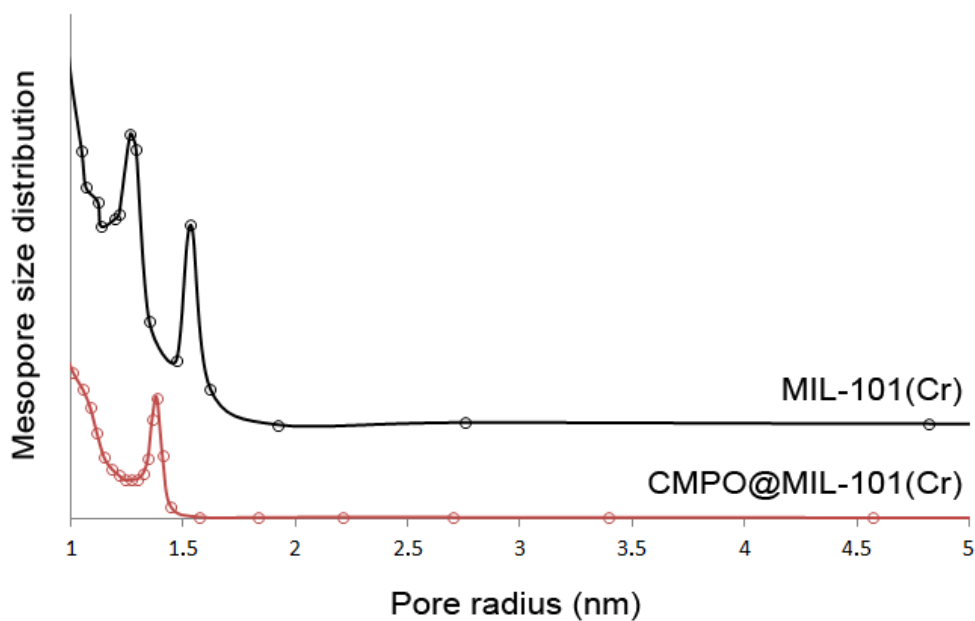
Appendix 2.1 PXRD overview of MIL-101(Cr) contact tests with HCl (pH 4 and pH 0).



Appendix 2.2 N<sub>2</sub>-sorption isotherms of MIL-101(Cr) before and after exposure to HCl solutions (pH 4, pH 0) at varying contact times.



Appendix 2.3 Nitrogen adsorption/desorption isotherms before and after CMPO functionalization of MIL-101(Cr).

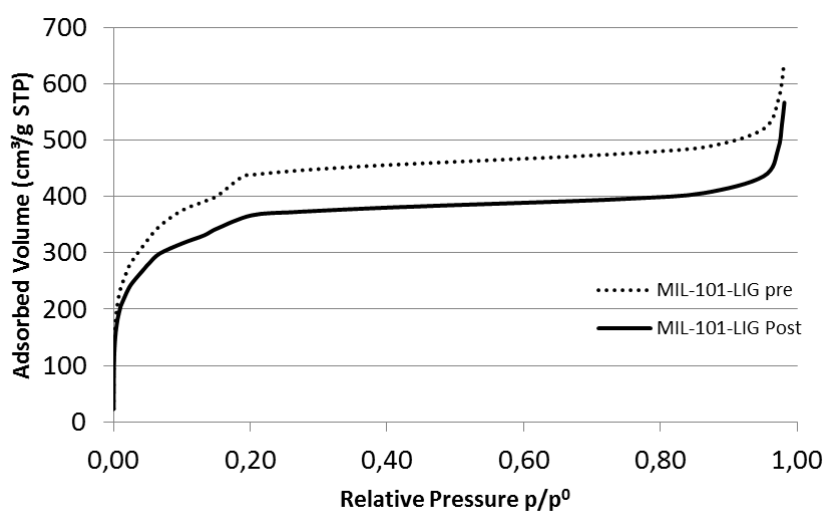


Appendix 2.4 Poresize distribution before and after CMPO functionalization of MIL-101(Cr).

Appendix 2.5 Nitrogen adsorption results pre-/post-adsorption experiment ( $C_0(\text{Eu})$ : 100 ppm, pH 4.00, 25 °C, 24 hrs).

	$S_{\text{Langmuir}} \text{ (m}^2/\text{g)}$	$V_p \text{ (cm}^3/\text{g)}$
MIL-101-LIG Pre	2151	0.97
MIL-101-LIG Post	1780	0.87

Note that these experiments were conducted on a different batch of CMPO@MIL-101(Cr) than reported in the main manuscript. This batch started out with highly purified MIL-101 at a Langmuir surface area of ~4000 m<sup>2</sup>/g. As can be seen from the results and isotherms, the adsorbent perfectly survives the applied conditions. The small drop in surface area and pore volume is due to the adsorbed europium, which increases the specific weight of the material and most probably influences the adsorption behavior of nitrogen.

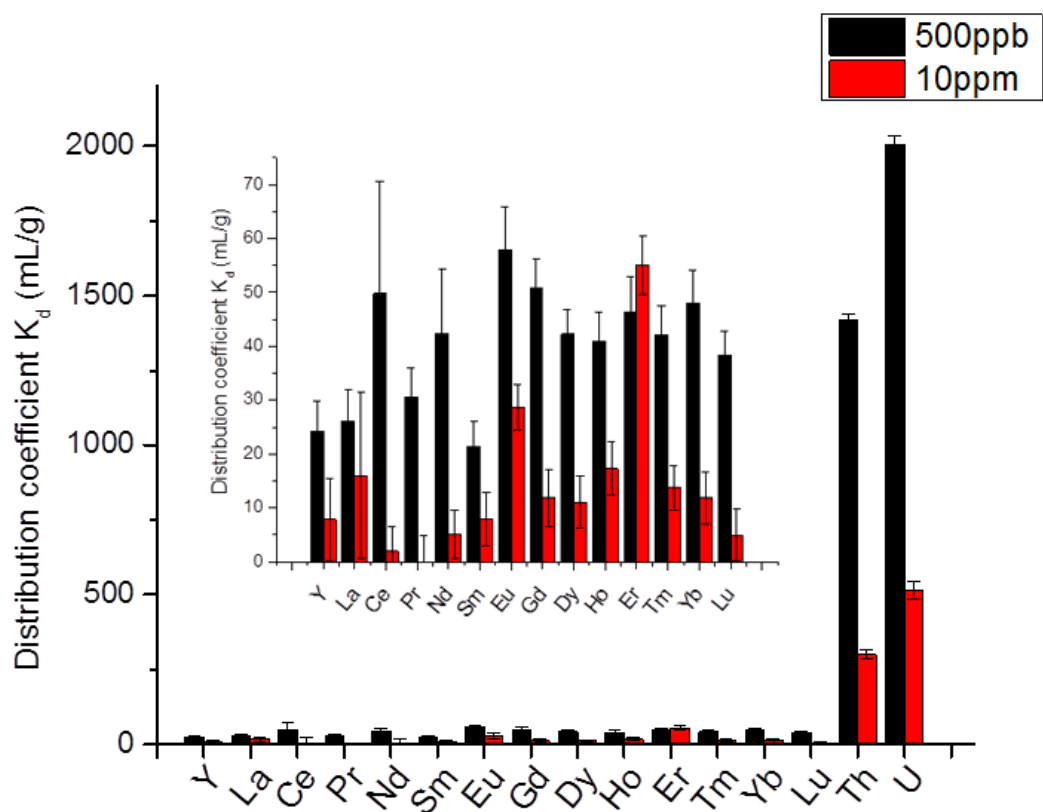


Appendix 2.6 Nitrogen adsorption isotherms pre-/post-adsorption experiment ( $C_0(\text{Eu})$ : 100 ppm, pH 4.00, 25 °C, 24 hrs).

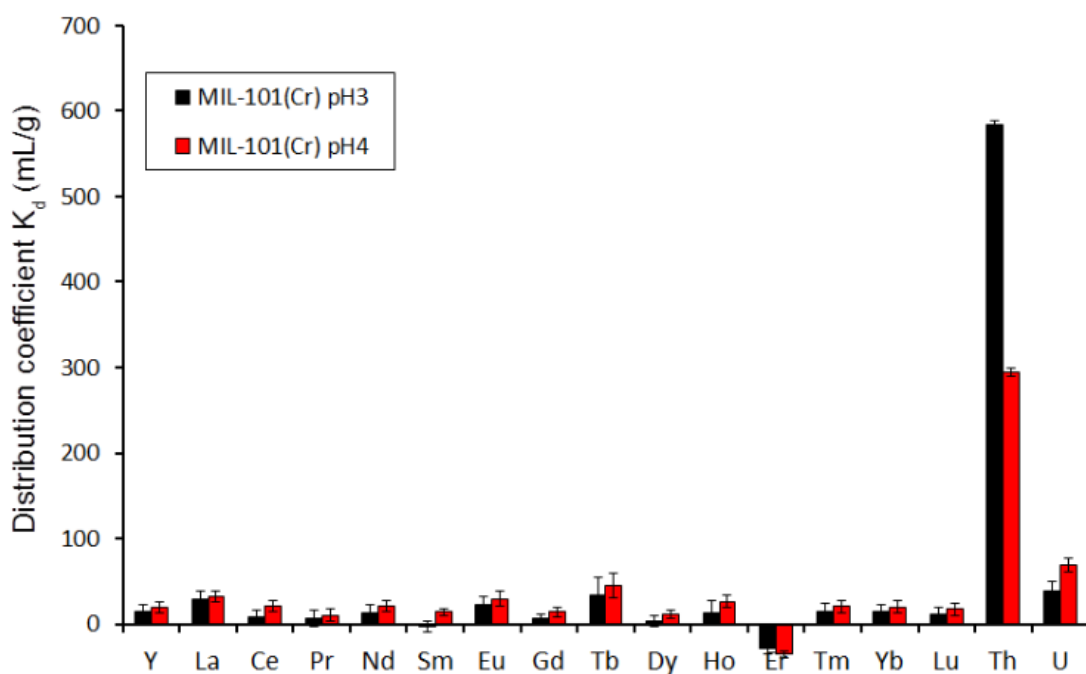
Appendices 2.1 to 2.6 (excl. 2.3 and 2.4) are part of “Functionalized metal-organic-framework CMPO@MIL-101 (Cr) as a stable and selective rare earth adsorbent” (Chapter 7), as supporting information.

The electronic version of this supporting information (including higher resolution images) can be consulted online at: <http://link.springer.com/article/10.1007/s10853-016-9807-9>

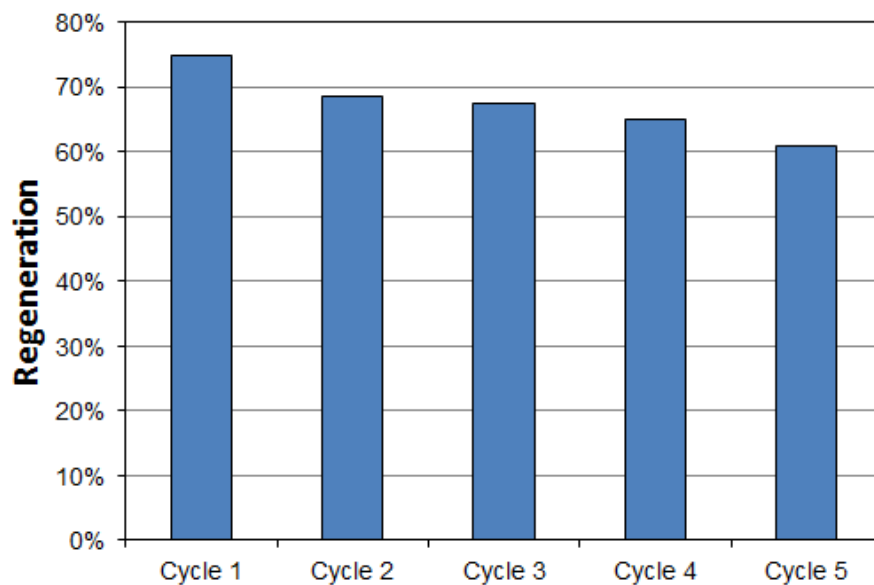




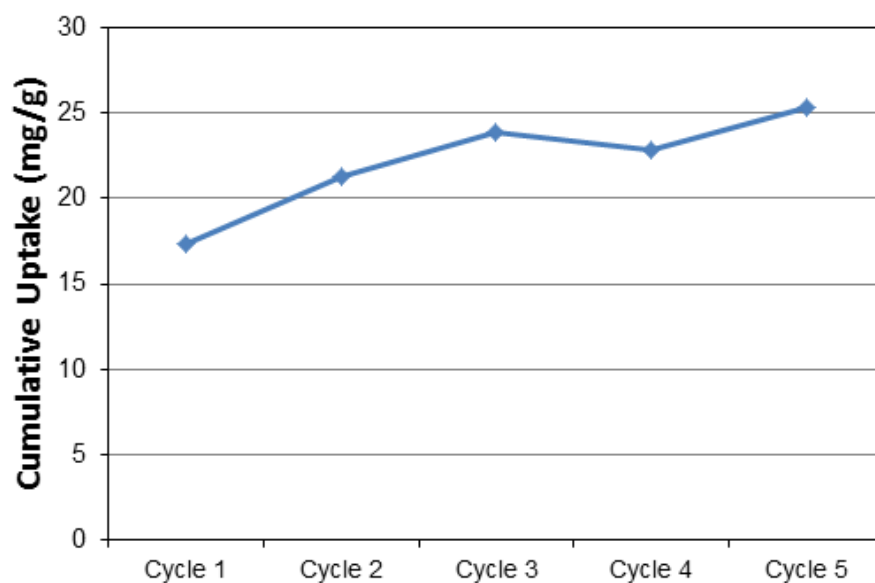
Appendix 3.1 Selectivity results of CMPO@MIL-101(Cr). Zoom on the competing REE elements included. (ppm = mg/L, ppb =  $\mu$ g/L)



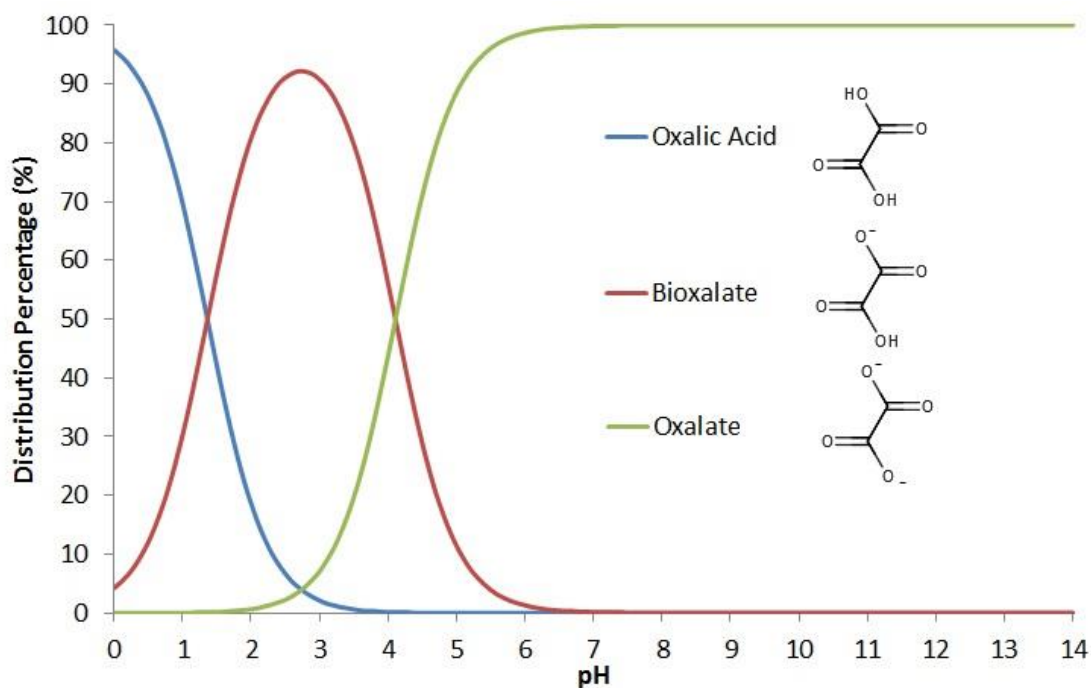
Appendix 3.2 Selectivity results of pure MIL-101(Cr) at pH 3 and pH 4.  $C_0$ : 10 mg/L.



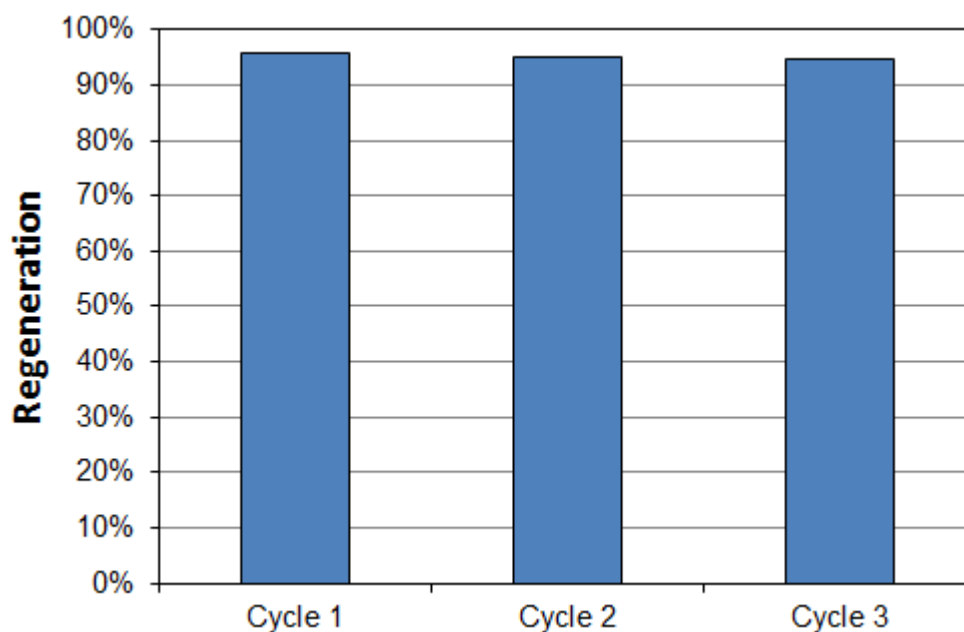
Appendix 3.3 Uranium regeneration results for CMPO@MIL-101 using 0.1 M oxalate solution (pH 2) via column setup. (1/2)



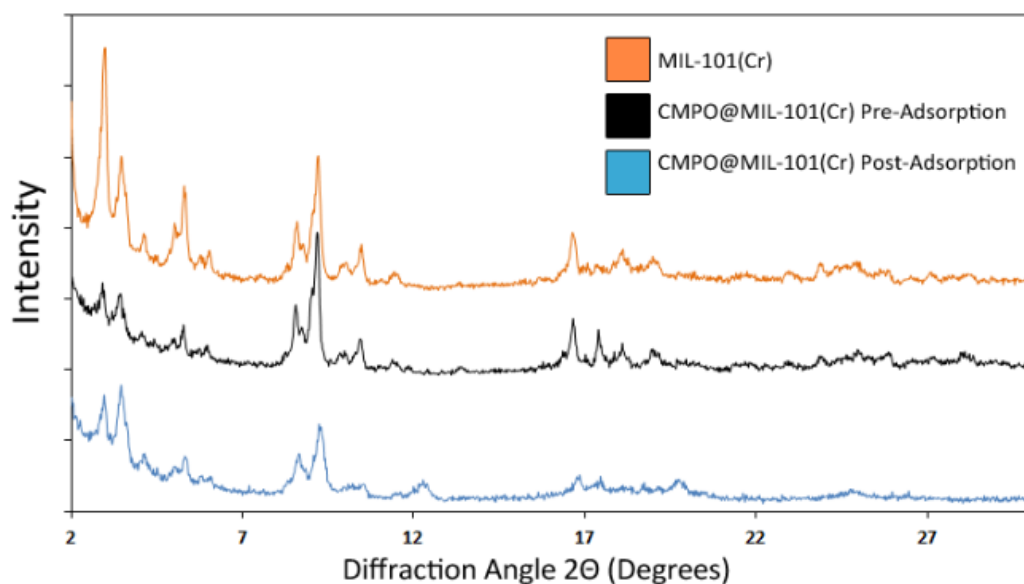
Appendix 3.3 Cumulative uranium uptake over five consecutive adsorption/desorption cycles with 0.1 M oxalate solution (pH 2) as stripping agent. (Experimental conditions in Chapter 8). (2/2)



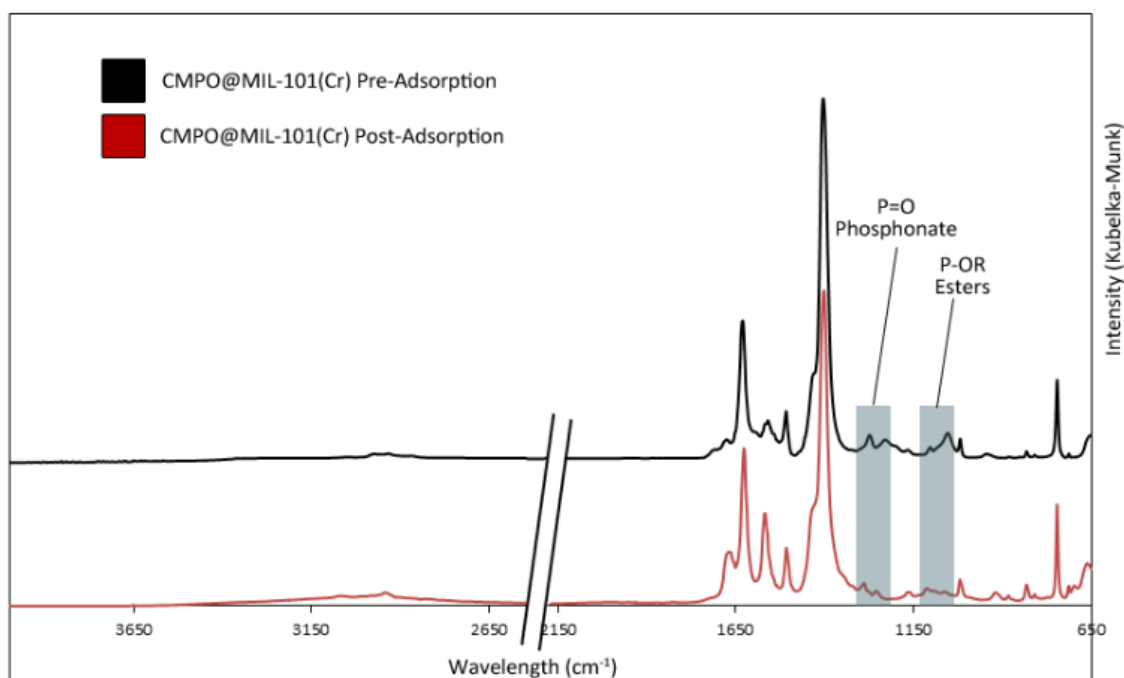
Appendix 3.4 Speciation diagram for the oxalate system in water as a function of pH. The y-axis gives the fraction of each species present.



Appendix 3.5 Uranium regeneration results for CMPO@MIL-101 using an increased 1 M oxalate solution (pH 2) via column setup. (Experimental conditions in Chapter 8).



Appendix 3.6 Powder X-ray Diffraction comparison of pristine MIL-101(Cr) (orange) and CMPO@MIL-101(Cr) pre-(black) and post-adsorption/desorption experiments (blue).

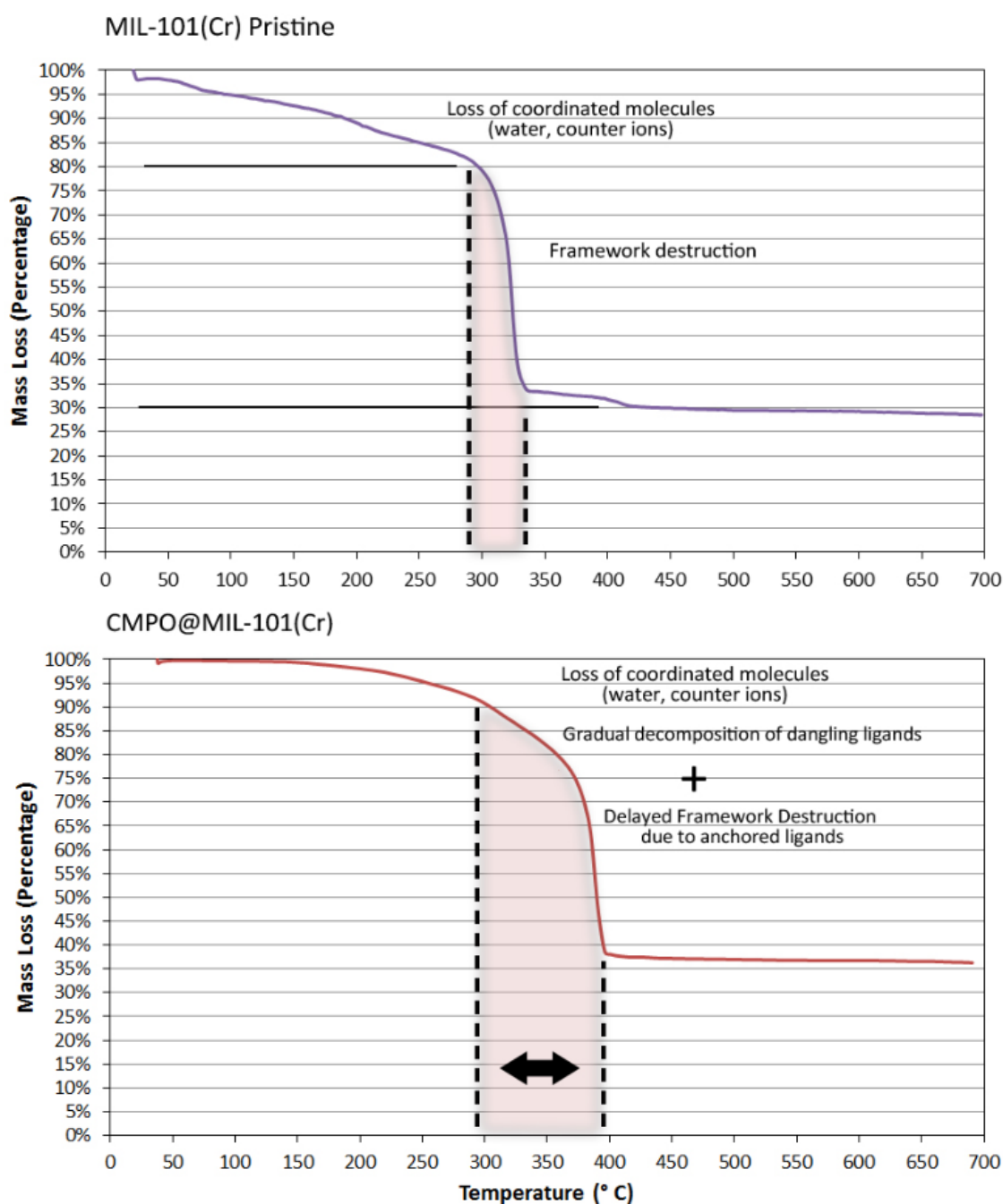


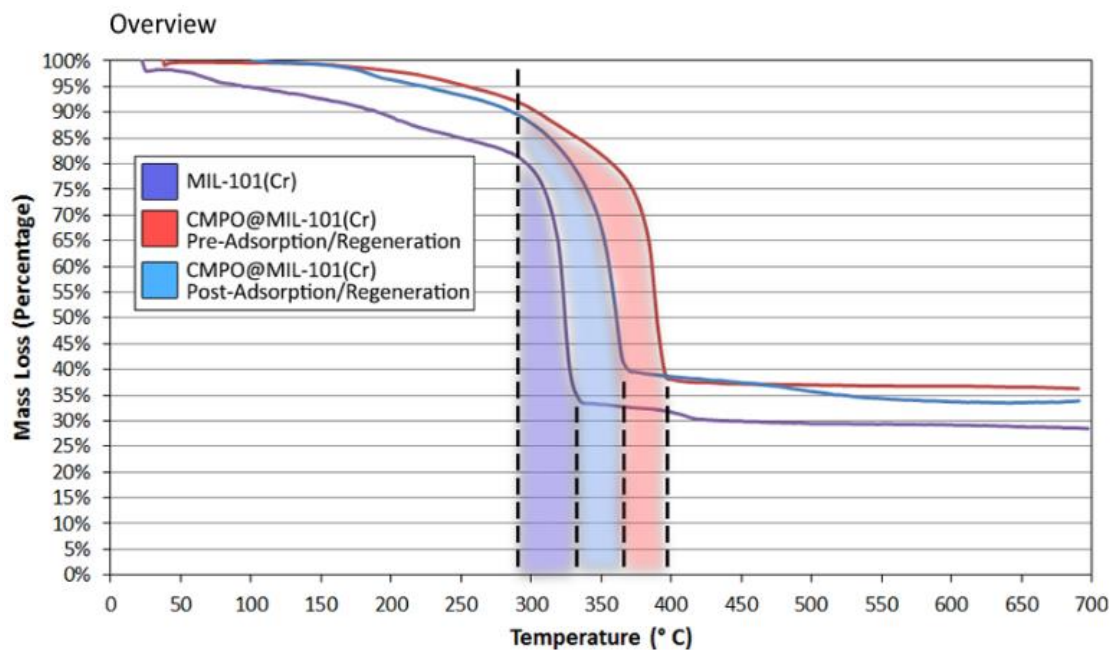
Appendix 3.7 FTIR comparison (DRIFTS) of CMPO@MIL-101(Cr) pre-(black) and post-adsorption/desorption experiments (red). The zone of interest (i.e., corresponding to ligand vibrations) is highlighted and annotated.



<b>CMPO@MIL-101(Cr)</b>	$S_L^a$ (m <sup>2</sup> /g)	$S_{BET}^b$ (m <sup>2</sup> /g)	Pore Volume (cm <sup>3</sup> /g)	Leaching (wt. %) <sup>c</sup>
Prior adsorption studies	1336	1014	0.59	-
Post adsorption studies	1780	1310	0.68	15 %
<sup>a</sup> Langmuir model. <sup>b</sup> Calculated between $p/p_0$ 0.05 – 0.3. <sup>c</sup> As determined by XRF.				

Appendix 3.8 Numerical N<sub>2</sub>-adsorption data and leaching analysis for CMPO@MIL-101(Cr) prior/post column adsorption studies.



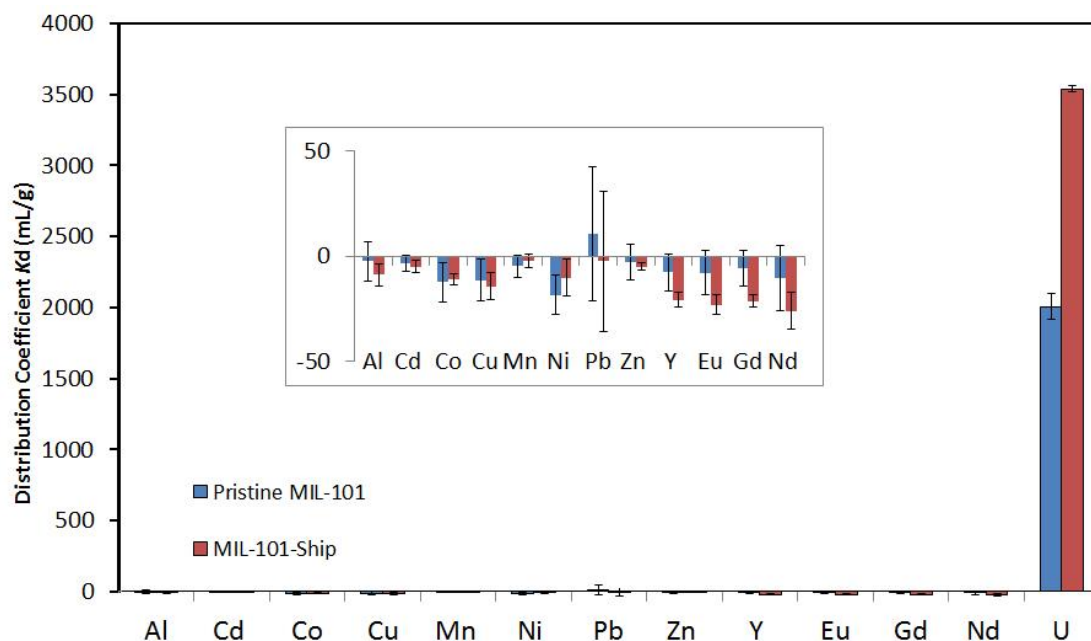


Appendix 3.9 Comparison of Thermogravimetric analysis results of CMPO@MIL-101(Cr), pre- (red) and post-adsorption/desorption experiments (blue).

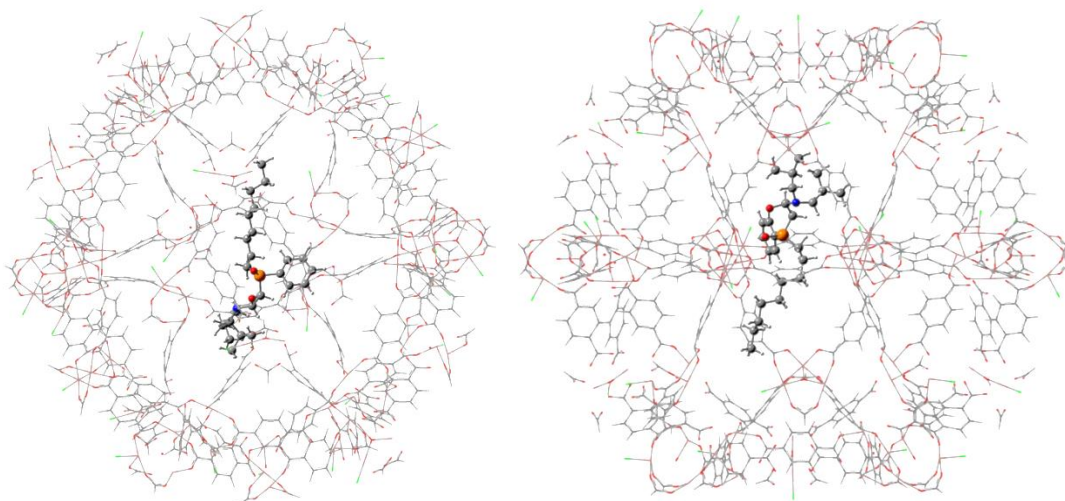
Appendices 3.1 to 3.9 are part of “Carbamoylmethylphosphine oxide-functionalized MIL-101(Cr) as highly selective uranium adsorbent” (Chapter 8), as supporting information.

The electronic version of this supporting information (including higher resolution images) can be consulted online at: <http://pubs.acs.org/doi/abs/10.1021/acs.analchem.7b00821>

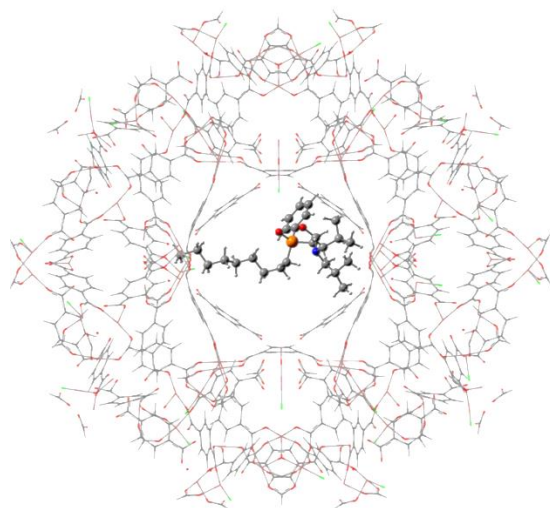




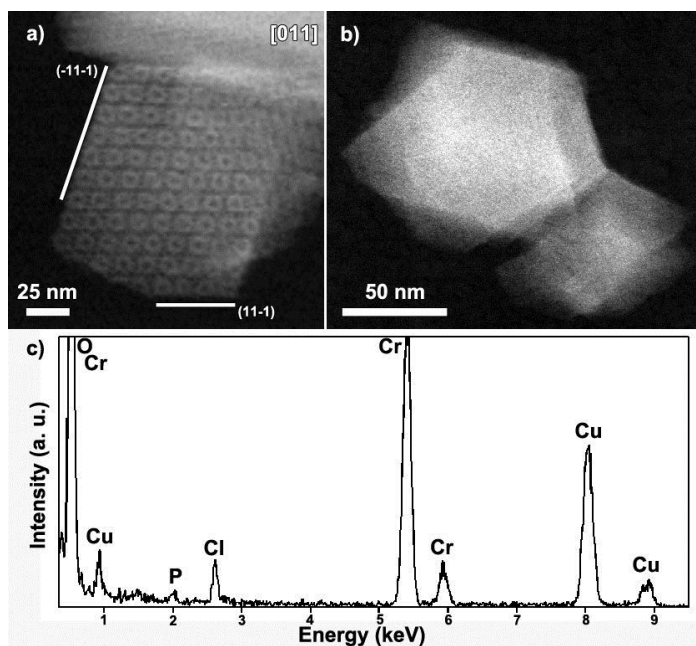
Appendix 4.1 Distribution coefficients ( $K_d$ ) for the MIL-101-Ship (red) and pristine MIL-101 (blue), provided with standard deviations (error bars).  $C_0(M) = 1$  mg/L each, L/S: 1000 mL/g,  $T = 25$  °C,  $t = 24$  hrs. Zoom on competing elements (inset). Negative values due to analysis inaccuracies.



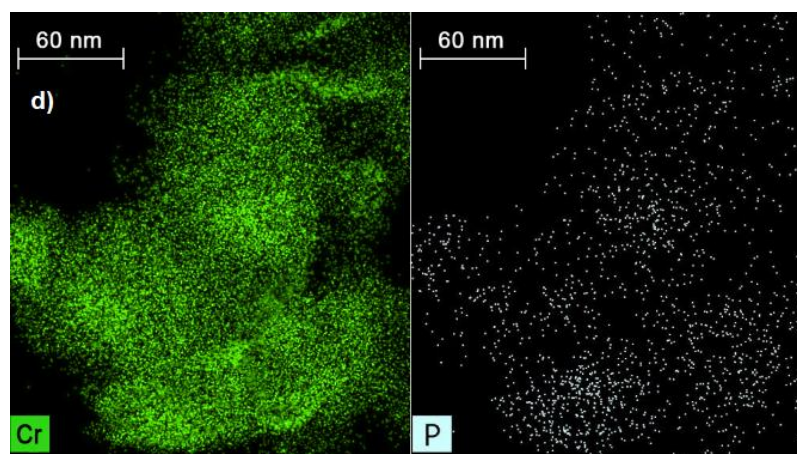
Appendix 4.2 Illustration of a CMPO molecule trapped in an individual MIL-101(Cr) cage. Different angles of the cage are represented. The CMPO ligand is visualized in the ball-stick manner, whereas the MIL-101 cage is represented as a wireframe, for clarity reasons. (1/2)



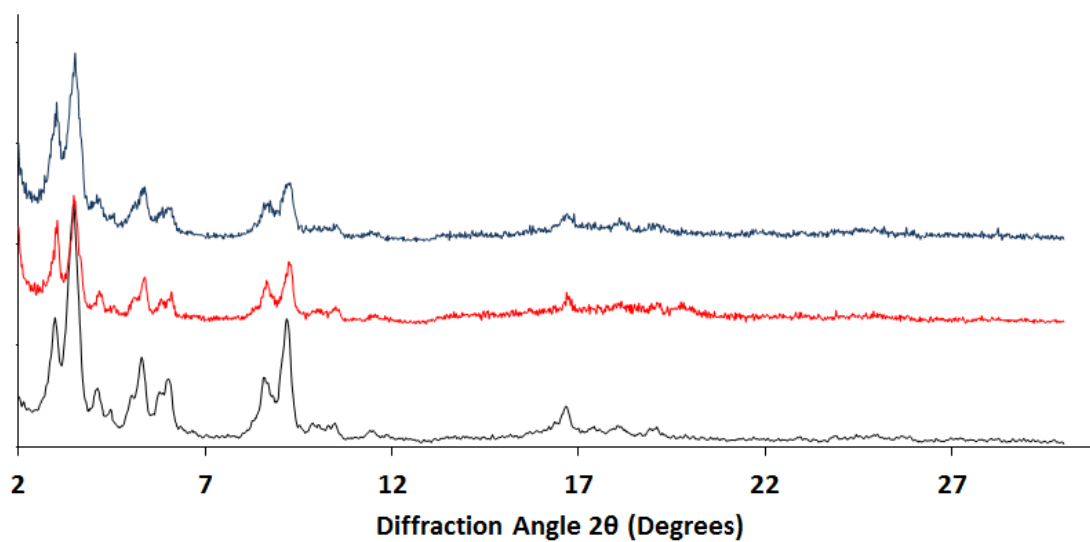
Appendix 4.2 Illustration of a CMPO molecule trapped in an individual MIL-101(Cr) cage. Different angles of the cage are represented. The CMPO ligand is visualized in the ball-stick manner, whereas the MIL-101 cage is represented as a wireframe, for clarity reasons. (2/2)



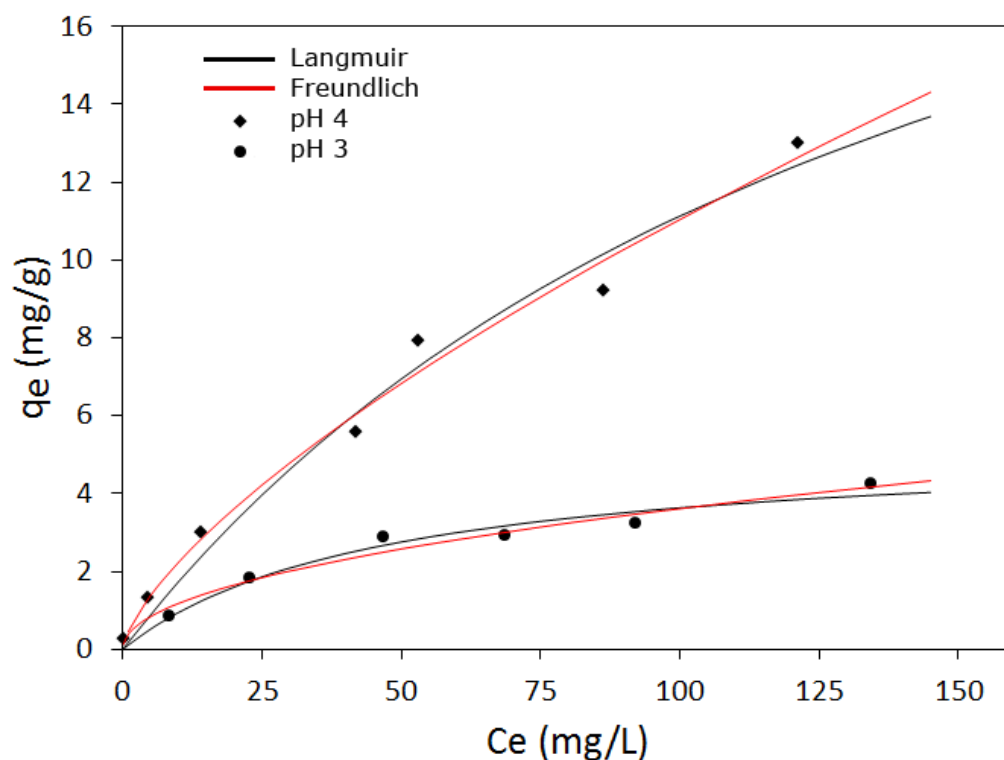
Appendix 4.3 a) ADF-STEM image of a MIL-101 crystalline particle recorded along the [011] zone axis b) ADF-STEM overview showing the region of EDX acquisition together with the c) EDX spectrum showing a clear P signal. (1/2)



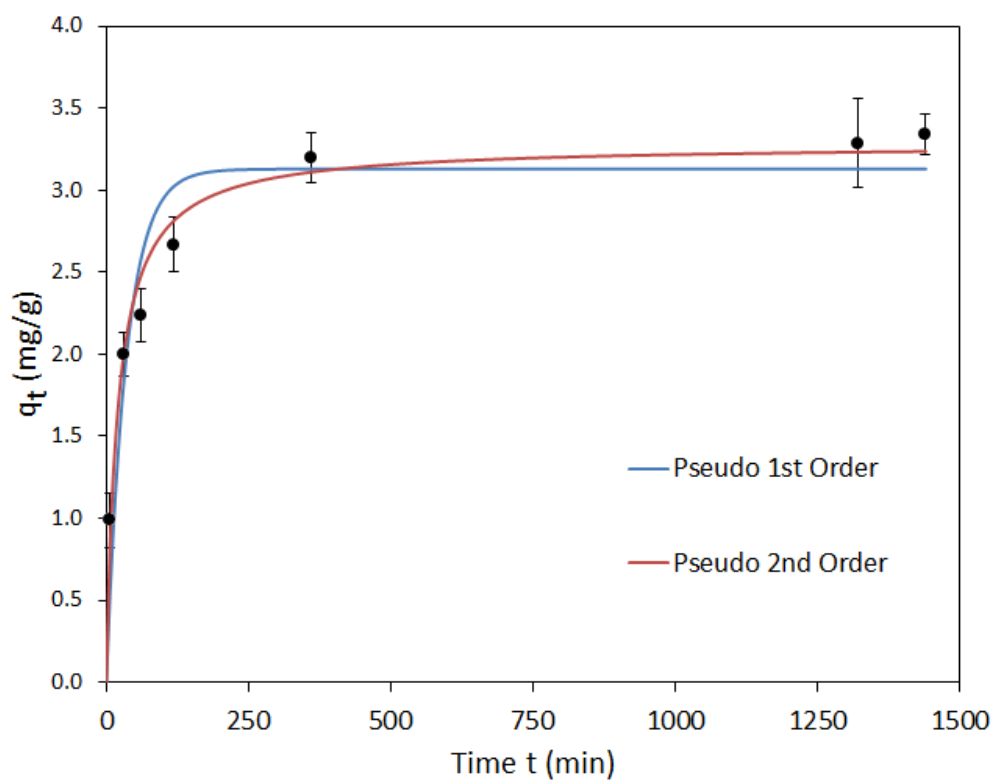
Appendix 4.3 d) chromium (green) and phosphorous (white) EDX mapping, showing well dispersed P. (2/2)



Appendix 4.4 X-ray diffraction patterns of MIL-101-Ship as synthesized (black) and after acid treatment with 1 M HCl (red), and 1 M HNO<sub>3</sub> (blue).



Appendix 4.5 U(VI) adsorption isotherm for MIL-101-Ship, fitted to the Langmuir and Freundlich model. pH: 3.0 and pH: 4.0, L/S: 1000 mL/g,  $T = 25\text{ }^{\circ}\text{C}$ ,  $t = 24$  hrs. Average value of duplicates.



Appendix 4.6 Adsorption kinetics of U(VI) on MIL-101-Ship, fitted to the pseudo-first (black) and pseudo-second-order (red) kinetic model.  $C_0(\text{U}) = 30\text{ mg/L}$ , L/S: 1000 mL/g,  $T = 25\text{ }^{\circ}\text{C}$ , pH = 3. Average value of duplicates.

Appendices 4.1 to 4.6 are part of “Ship-in-a-bottle CMPO in MIL-101(Cr) for selective uranium recovery from aqueous streams through adsorption” (Chapter 8), as supporting information.

The electronic version of this supporting information (including higher resolution images) can be consulted online at: <http://www.sciencedirect.com/science/article/pii/S0304389417302716>

